The Dissertation Committee for Ritika Kundu Certifies that this is the approved version of the following dissertation:

BALANCING RHEOLOGY AND FILTRATION: A NOVEL APPROACH FOR OPTIMIZING SUSPENSION FLOW AND SUSTAINABILITY IN GRANULAR MEDIA

Committee:

Chadi S. El Mohtar, Supervisor

Robert B. Gilbert

Jorge G. Zornberg

Masa Prodanovic

Marc A. Hesse

BALANCING RHEOLOGY AND FILTRATION: A NOVEL APPROACH FOR OPTIMIZING SUSPENSION FLOW AND SUSTAINABILITY IN GRANULAR MEDIA

by

Ritika Kundu, B.TECH.; M.TECH.

Dissertation

Presented to the Faculty of the Graduate School of

The University of Texas at Austin

in Partial Fulfillment

of the Requirements

for the Degree of

Doctor of Philosophy

The University of Texas at Austin

May 2017

Dedication

To the most caring parents

Gayatri Devi and Kuldeep Singh Sangroya,

Urmila Devi and Daya Singh Kundu

To the most loving husband

Sandeep Kundu

To the most supporting siblings

Neha and Rahul

ACKNOWLEDGEMENT

It is my pleasure to acknowledge the roles of several individuals for completion of my Ph.D. research

Firstly, I would like to express my sincere gratitude to my advisor Dr. Chadi S. El Mohtar for the continuous support of my Ph.D. study and related research, for his patience, motivation, and immense knowledge. His guidance helped me in all the time of research and writing of this thesis. I could not have imagined having a better advisor and mentor for my Ph.D. study. Dr. El. Mohtar's skillful guidance, innovative ideas and stoic patience are greatly appreciated. Besides my advisor, I would like to express my deep appreciation to the rest of my thesis committee: Dr. Robert B. Gilbert, Dr. Jorge G. Zornberg, and Dr. Masa Prodanovic and Dr. Marc A. Hesse, for their insightful comments and encouragement, but also for the hard question which incented me to widen my research from various perspectives.

I thank my colleagues Hamza Jaffal for the stimulating discussions, and helping me out with legalities when I was not in Austin, and for all the fun we have had in the last four years. Also I thank my friends, Rohit Jagdale; Neha Nogia; Rahul Verma; Akur Kumar; Ankur Bhambotta; Kapil Sharma; and Gurpreet Kaur to support me and keep me sane throughout my time at UT Austin.

Finally, I would like to thank my family: my parents (Mrs. Gayatri Devi, Dr. Kuldeep Singh, Mrs. Urmila Devi and Mr. Daya Singh Kundu) and to my brother (Rahul Sangroya); sister-in-law (Sunesh Sangroya) and sister (Neha Sungroya) for their patience, continuous love and support throughout the course of this dissertation. I would not be writing this without my mother's dedication and belief that I can achieve anything I want. Last but not least, I would like to express my deep and sincere gratitude to my loving, supporting, encouraging and patient husband Sandeep Kundu for his continued and unfailing love, understanding underpins my persistence in the graduate career and makes the completion of this dissertation possible.

Ritika Kundu

May 2017

Balancing Rheology and Filtration: A Novel Approach for Optimizing Suspension Flow and Sustainability in Granular Media

Publication No. _____.

Ritika Kundu, PhD.

The University of Texas at Austin, 2017

Supervisor: Chadi S. El. Mohtar

A significant amount of research (at laboratory scale) has been performed in recent years on the use of chemical and suspension grouts for ground improvement, however; field implementation has always been hindered by the in-situ soil heterogeneity and discontinuities. In the field, there are many practices of grouting such as compaction grouting, jet grouting and permeation grouting; the exquisiteness of permeation grouting is that it can be performed without disturbing the existing facilities in close vicinity. However, permeation grouting of granular soils in the field face two main challenges: how to maximize the penetration depth of grout propagation in sands and how to control flow and ensure the stability of grouts in gravels. Consultants and site engineers design grouting work mostly based on their experiences and some empirical correlations. These empirical correlations are mainly based on particle size of grout and soil, and in some cases, include

pressure, yield stress, and concentration of suspensions. Even when these correlations indicate that a soil can be penetrated by a specific grouting material, there is little information about the maximum injection depth, appropriate grout mixture or allowable injection pressure.

The flow of suspension grouts through porous media is a very complex phenomenon owing to the diversity of the mechanisms involved. It is controlled by the rheology of the suspensions and its filtration as it flows through the porous media. Filtration is the process of particles being filtered from a suspension grout by soil grains leading to the simultaneous change in the physical properties of porous media and the grout with permeation. The rheology of a grout is dependent on the grout mix as well as the flow rate and size of voids in the porous media, all of which change with time and space as filtrations occurs.

The objective of this study is to investigate the grout flow through porous media by balancing its rheological and filtration properties. Rheological properties of non-Newtonian suspension grouts were determined for a better understanding of its flow behavior through porous media. The rheology of thicker suspension was modified using additives to lower its initial viscosity and get better permeation. One dimensional constant flux permeations tests were performed to determine the effect of different parameters (such as bentonite concentration, injection flow rate, the percentage of additives, apparent viscosity, and grain size) on filtration and ultimately, groutability and permeation depth.

A simple laboratory test was introduced to study the filtration behavior of clay and cement suspensions permeating through porous media. The filtration function and permeability reduction function were determined to simulate the flow of suspension grout through the granular soil. The proposed filtration model predicts the permeation depth and

the distribution of suspension particles along the permeation length to evaluate the performance of the grouted specimen. The rate of particle deposition depends on the rheology and concentration of grout, particle size and shape of suspended particle, grain size distribution of porous media, and physio-chemical interaction of grout with the porous medium through which it is flowing. The novelty of the newly proposed model is that it accounts for the changes in the rheology of grout and the porosity and permeability of the porous medium as a function of the deposition of particles, none of which has been considered in the past.

Another research focus is to evaluate the homogeneity of prepared sand specimens in the laboratory. The distribution of local void ratio is more pertinent to the mechanical and hydraulic properties of the soil than a single average value for the whole specimen. A simple method is proposed and evaluated to determine the spatial variability of pore space within the soil specimen. The new method composes of a simple experimental water flushing sequence that can be performed on specimens assembled in most existing geotechnical testing setups. For the specimens tested in this study, it was found that local porosity can be off by up to 10 percent to the average porosity of the whole specimen (despite special care being taken to produce unifrom specimens).

The final research focus in this dissertation is the development of a simple, inexpensive and quick method, to characterize the unsaturated hydraulic properties of sandy soils. This method combines a multistage constant flux water flushing experimentation with inverse modeling using Hydrus 1D to obtain the unsaturated hydraulic properties of a soil. The unsaturated hydraulic properties obtained from the proposed method were comparable to those obtained using conventional hanging column test without the need for any specialized equipment. Additionally, the new method covers a wider range of soils as can

be seen by the results obtained on a uniform sand with a very lower suction that is couldn't be tested using the hanging column test.

List of Contents

List of Figures

List of Tables

CHAPTER 1 INTRODUCTION

1.1 Problem Statement

Grouting is an important ground improvement method for underground construction and foundation engineering. It is the process in which fluid flows through rock cavities and soil pores to decrease the permeability and improve the shear strength of porous media. Grouting has wide application in modern civil engineering such as:

- reduce the uplift pressure on levees/dams and prevent erosion of soil from its foundation soils.
- reduce the permeability of a formation to control the under seepage and loss of water.
- fix pre-stressed rock anchors.
- lift and erect the tilted structures to grade
- fill the voids between rock and tunnel lining (Contact grouting)
- provide the structural stability by increasing the shear strength of material under foundation of heavy structure and reduce the settlement (Consolidation grouting)
- repair and seal cracks/joints in a structure by injecting the cracks/seams between them with grout as in concrete dam or arch dam.

Grouting has nearly 200 years of history. In 1802, inventor of injection technique, Charles Berjing was engaged in the Harbor of Dieppe committee. Water had eroded the soil under the shallow

foundation of the tide sluices built on gravel material, and heavy undercurrents endangered the safety of the structures. Plastic clay was injected into holes by blows of a heavy hammer onto piston until clay filled all the gaps between foundation slab and the underground. This was the first successful application of injection grouting technique in foundation engineering. Beaudemoulin (1839) described another application of grouting to reinforce the foundation of the bridge at Tours by pouring a slurry of mortar mix into voids through injection holes until they were filled. P.W. Barlow obtained a patent for the construction of tunnels in 1864 using the shielding method in which cement grout was injected to form the lining. Further developments and a wider range of applications of grouting emerged in the construction of mining shafts to protect the excavations from groundwater infiltration. Grouting for dam foundation was applied as remedial measures to prevent excessive seepage, especially in the USA. Systematic improvement of grouting techniques started with the injection of foundation rock at Hoover Dam on Colorado River in the USA.

The consultants and site engineer design the grouting work based on the experiences from their previous jobs and knowledge of local geology. Even if they know that the soil can be penetrated in principle by a specific grouting material, they have limited information on the maximum injection depth, appropriate grout mixture or allowable injection pressure except for some empirical correlations based on particle size (of grout and soil), and in some cases, pressure, yield stress and concentration of suspensions. Lapwood (1911) mentioned that grouting is the last possibility in the design of dam foundation and other measures should be considered to prevent seepage because grouting was based on guesses only. Gourley (1922) also concluded from a detailed study of hydro projects where a large volume of grouting was involved that this option should be revised to reduce the cost and delay in construction of dams without sacrificing tightness

and safety. Therefore, there is need to understand and engineer the grouting process for more stable and reliable field applications.

The flow of chemical grouts and some cement based suspensions through homogenous porous media has been researched in the last few decades. These studies ranged from studying contamination transport through groundwater flow, grouting for controlling hydraulic conductivity and liquefaction to surface flooding of sediments to create secondary hydraulic barriers. These researchers were, for the most part, more focused on the improved mechanical/hydraulic properties in the presence of the grout rather than the permeation process itself. The work focusing on the permeation process is mostly limited to chemical grouting, especially Colloidal Silica; however, the mechanisms of flow, filtration and viscous behavior of chemical grouts are different from that of the suspensions. The limited work done on suspension grouts (mostly cement based) has focused only on flow through homogenous porous media and did not consider the effect of filtration on the grout rheology and porous media properties. In fact, the characterization of suspensions in civil engineering applications used, with few exceptions, experimental methods that are more appropriate for Newtonian fluids and does not account for the complex viscoelastic behavior of suspensions.

The flow of suspensions through porous media is a very complex phenomenon owing to the diversity of the mechanisms involved. The flow of particulate or suspension grout through a porous media is controlled by filtration, which is the process of particles being filtered from a suspension grout by soil grains, leading to retarding grout flow. Due to this phenomenon, the size of the pore space gradually decreases, increasing hydrodynamic resistance and gradually causing clogging of the flow path. For permeation grouting, the sealing effect of suspension grouting flow on the

porous media governs the extent of grout propagation. Liquid-solid separation by filtration can occur either by solid accumulation at the entry point at the surface of a porous medium or through retention inside a porous bed. In the first case, a filter cake builds up at the entry point, and it creates a very low permeability layer with small void spaces that prevents the suspended particles in the grout from penetrating into the soil. In the second case, the suspension flows through the porous medium but the porous medium retains some of the particles that leads to a decrease in its permeability and reduction in suspension concentration flowing forward. The retention mechanism depends on various factors such as: size, concentration, shape and surface properties of grout particles (Eriksson et al., 2000, Abichou et al., 2002, Dupla et al., 2004); grain and pore size distribution, shape and surface properties of formation; rheology of grout (Eriksson et al., 2000); and interstitial velocity and physiochemical properties. Many researchers (Bell, 1993; Burwell, 1958; Incecik and Ceren, 1995; Yoon and El Mohtar, 2013) have developed empirical models to describe/predict suspension flow in porous media, with different models including some subset of the parameters above. However, to better predict the success of the grouting process, it is important to understand the filtration mechanism thoroughly, including its impact on the rheology of the grout as well as the properties of the porous medium.

1.2 Research Objectives

The research objective of this dissertation is to bridge the gap between current state of knowledge on lab scale and field application by: (1) understanding the effects of the rheological and filtration properties of suspensions on their flow through granular media; (2) developing models to better predict the groutability and injection depth; (3) engineering “smart” grouts for site-specific application by balancing its rheological and filtration properties; and (4) studying the grouts’

stability in the pores against groundwater flow. These objectives will be achieved through an integrated experimental and numerical program which includes:

- Rheological tests to determine the properties of the suspensions used (such as yield stress, apparent viscosity, shear rate effects, storage and loss moduli). These properties will be used to understand the flow behavior of the suspensions and will be incorporated in the proposed numerical models.

- 1-D constant flux permeation tests on 2 feet sand columns to determine the impact of different factors (such as bentonite concentration, injection flow rate, the percentage of SPP additives, apparent viscosity, and grain size) on groutability and permeation depth.

- The analytical, empirical relationship for pressure buildup at injection point during constant flux permeation test.

- 1-D constant flux permeation tests on 1.5inch sand column to determine the dynamic behavior of filtration coefficient. The filtration and permeability reduction functions are determined from these tests and later used to explain and model the filtration mechanism mathematically.

- Numerical modeling to define the flow of suspension grout through granular soil incorporating the change in rheology of grout and pore space of granular soil as a function of particle deposition (filtration).

- Inexpensive and easy to perform sand column test to determine the unsaturated hydraulic conductivity parameters and evaluation of heterogeneity of prepared sand column for permeation tests.

1.3 Organization of chapters

This dissertation is organized in nine main chapters. Following this introduction, a detailed review of the literature in presented in Chapter 2.

The literature review chapter (**Chapter 2**) is divided into five parts: (a) background on the determination of unsaturated hydraulic properties of sand; (b) literature on the rheological properties of grout material (bentonite and cement) and their structure in aqueous media; (c) discussion on the history and field applications of permeation grouting with detailed information on groutability; and (d) summary of existing description of filtration mechanisms and available mathematical filtration models.

In Chapter 3, a new inexpensive and simple to use method (the SEM method) is proposed to determine the unsaturated hydraulic properties of sand. Sand columns are flushed with water from bottom to top at constant flux rate while the pressure buildup at the bottom is measured using a pressure transducer. The recorded pressure data is used to determine the unsaturated hydraulic properties of sand using inverse modeling technique. The results of SEM method are compared with the conventional hanging column test.

In **Chapter 4,** a simple methodology is introduced to determine the spatial variability of pore space within the soil column before performing any laboratory experiment. In the testing stage, water is flushed through specimen from bottom to top under constant flux, and the change in pressure is

recorded at the injection point using a pressure transducer. This conceptual framework for this method is based on the relationship between the change in pressure, change in waterfront elevation and total volume filled under constant flux to determine the distribution of void ratio within along the height of a specimen.

Chapter 5 focuses on the permeation of bentonite suspension through granular soils. First, it covers the rheological properties of bentonite suspensions focusing on the effect of SPP on yield stress, apparent viscosity, and the time-dependent behavior. The effect of shear rate on the rheology of suspension is presented for the stress ramp testing method. Second, this chapter includes the results of constant flux 1D permeation tests, which are presented as the pressure buildup at injection point and bentonite-content profile along the sand column. The parameters affecting the groutability and permeation depth (such as bentonite concentration, injection flow rate, the percentage of SPP additives, apparent viscosity, and grain size) are investigated. and an empirical equation is fit to the pressure-time curve obtained from the constant flux permeation tests. The constants of the empirical equation are determined and defined as a function of apparent viscosity, flow rate and grain size ratio (d_{10}/D_{95}) where d_{10} is the grain size of sand and D_{95} is the particle size of bentonite.

Chapter 6 presents the experimental tests to evaluate and compare the performance of two microfine cement types, and the effect of two commonly used additives with cement grouts are discussed. Rheology and stability of the different grout mixes are presented. Constant flow permeation tests using 2-foot long rigid wall permeameter are explained, followed by measurements of the unconfined compressive strength of the grouted sand as a function of the

distance from the injection point. The results from laboratory tests are analyzed to evaluate the performance of different grout mixes and the quality of the end product in each case.

In **Chapter 7**, seven filtration models are explained with different filtration coefficients and solid deposition empirical relationships to determine the model which appropriately defines the filtration mechanism of bentonite suspension through the granular soil. One of the seven filtration models uses the filtration function and permeability function determined experimentally in Chapter 6. Filtration coefficient and formation damage parameters are determined using the experimentally obtained pressure-time curve by inverse modeling technique. Validation of best-suited filtration model is evaluated be comparing the bentonite content profile along the height of the sand column determined numerically and that obtained experimentally from the post-permeation analysis of sand columns.

Chapter 8 introduces the filtration tests to determine the essential elementary filtration parameters which was later used in mathematical modeling to simulate the suspension flow and estimate the permeation grouting performance numerically. The filtration function, i.e., the relationship of filtration coefficient with the concentration of previously deposited particles is determined by evaluating the temporal variation of effluent concentration. The permeability reduction, i.e., the relationship of reduced permeability with changed porosity and volume of deposited particles is calculated from the recorded injection pressure using Darcy's law.

The main conclusion drawn from the analyses of results are presented in **Chapter 9** with the recommendation for scope of future research.

CHAPTER 2 LITERATURE REVIEW

2.1 Introduction

This chapter is divided into four major parts: 1) general background on the unsaturated hydraulic conductivity of granular soil 2) literature review on the heterogeneity in the sand specimen preparation in the laboratory 3) technical background on permeation grouting and 4) description of the numerical software and mathematical optimization technique used in this dissertation. The first part focuses on the different methods to determine the unsaturated hydraulic conductivity of granular soil in the laboratory and on site. The second presents the literature on various techniques to prepare the sand specimen in the laboratory and an evaluation of sand specimen homogeneity. The third part describes the theoretical and experimental issues associated with permeation grouting of bentonite and cement based grout, such as rheology and structural kinetics of bentonite and cement suspensions and the filtration mechanism and groutability of granular soil deposits.

2.2 Unsaturated hydraulic conductivity of granular soil

There are various geotechnical and geoenvironmental engineering problems where unsaturated soils are encountered. Volume change, shear strength, and seepage analyses all require an understanding of the matric suction in the ground. Soil suction is one of the most important parameters for assessing the practical applications of unsaturated soil mechanics because it describes the moisture stress condition of unsaturated soils. The laboratory measurements of

suction can be very useful for evaluating the quality of the samples and estimating the in situ effective stress.

The concept of suction was initially developed by soil physicists in the early 1900's. Total suction consists of two components: matric and osmotic suction. The matric suction is defined as the pressure exerted by dry soil on the surrounding soil to equalize the moisture content. The osmotic suction is the negative gauge pressure to which a pool of pure water subjected to be in equilibrium with a pool containing a solution identical in composition with soil water through semipermeable.

SWCC is a relationship between suction and volumetric moisture content (or gravimetric moisture content or degree of saturation) in the active pore space of material. It defines soil's ability to store and release water. In the last few decades, many researchers have developed various direct and indirect suction measurement techniques to determine the unsaturated hydraulic properties of soil in the laboratory. Direct measurement techniques include axis-transition technique (Tempe pressure cell), a tensiometer and suction probes; whereas indirect suction measurement techniques include: time domain reflectometry (TDR), in-contact filter paper, thermal conductivity sensor (TCS), and thermocouple psychrometer techniques.

2.2.1 Direct Measurement of soil suction

The matrix suction is the difference between air pressure and pore-water pressure and can be determined by the direct measurement of negative pore pressure. The direct measurement of matric suction can be determined by direct measurement of negative pore pressure which is

measured by the difference in water and air phase through the ceramic cup or disk. The maximum matric suction value depends on the air entry value of ceramic disk.

(a) Suction probe

Ridley and Burland (1993) explained the function of a suction probe for measuring matric suction of soil to be based on the principal of the equilibrium between the pore-water pressure in the soil and in the water compartment. The matric suction is the difference between the pore air pressure and the pore-water pressure (ua– uw), where the pore-water pressure (uw) is measured using the suction probe and applied air pressure (ua) is known. A suction probe has the ability to measure a broad range of soil suctions (i.e. up to 1500 kPa). The maximum limit of matric suction that can be measured is ruled by the air-entry value of the ceramic disk used. The limitation of this method is the cavitation and air diffusion through the ceramic head during the suction measurement.

(b) Tensiometer

Tensiometers are used to measure the negative pore pressure of soil. Tensiometers consist of a small ceramic cup attached to burette filled with deaired water which is connected to a pressure measuring device. Ensuring saturation of the ceramic cup and tube is essential for accurate pore pressure reading. Having air in the sensor results in bad or less negative measurement of the pore water pressure for the following reasons (a) air comes out of the water as pore pressure decreases (b) air in soil can easily diffuse through ceramic material.

(c) Axis translation technique

Hilf (1956) developed a null type, axis translation technique as a means of avoiding the cavitation problem. First, an unsaturated soil specimen was placed in the pressure vessel. Then, a pore pressure probe consisting of a needle with a saturated, porous ceramic tip was inserted into the soil. Soon after the probe was inserted, the movement of water in the measuring system towards the sample was slowed, and equilibrium was reached. The pore pressure was subtracted from the air pressure in the vessel to calculate matric suction. According to Hilf (1956), the procedure simply translated the origin of reference for the pore-water pressure measurement from the saturated atmospheric condition to the final air pressure value; hence the term 'axis translation.' Triaxial testing equipment has also been adopted to the axis translation technique by Bishop and Donald (1961), Biggs and Coffey (1969) and Fredlund (1973). The range of axis translation technique is limited by two factors, namely, the maximum air pressure which can be imposed on the experiment system and the air entry value of the ceramic disk. Axis translation technique is valid provided all of the gas voids are interconnected. Pore-water containing occluded (i.e., non-interconnected) air bubbles renders the pore fluid highly compressible. Another drawback is the long equilibrium time associated with this technique, which could lead to air diffusion.

2.2.2 Indirect measurement of matric suction

The indirect measurement of matric suction is generally performed by a conventional porous sensor made of a special material (e.g., filter paper, fiberglass, gypsum, nylon, sintered glass, clay ceramics, and metal). The measurement is performed by equilibrating the porous sensor

with the matric suction in the soil. Therefore, the water content of the porous sensor represents the magnitude of matric suction of the soil.

(a) Time domain reflectometry

Topp et al. (1980) proposed a time domain reflectometry technique for measuring the volumetric water content of soil by measuring the apparent dielectric constant of the soil. A soil water characteristic curve is required to relate the volumetric moisture content to matric suction. The advantage of this technique is that reliable measurement of moisture content can be conducted within short time duration (Benson and Bosscher, 1999). The limitation of the TDR technique is that it requires a sophisticated electronic device and that it measures the matric suction using the SWCC of the soil tested. Hence, the accuracy of TDR depends on the precise determination of the SWCC of the soil tested.

(b) Electrical conductivity sensors

The working principle behind the use of electrical conductivity sensors is the relationship between the electrical conductivity and moisture content of porous media. The electrical conductivity sensor consists of a porous block and two concentric electrodes embedded inside the block. The electrical conductivity sensor measures the electrical conductivity of the porous block. As the moisture content of porous block decreases the electrical conductivity increases. The limitation of an electrical conductivity sensor is that it has a long equilibration time in a rapidly changing moisture environment (Aitchison and Richards, 1965). Additionally, the sensitivity of the electrical conductivity sensor becomes very low when the matric suction exceeds 300 kPa.

These shortcomings have led to a diminished use of electrical conductivity sensors for matric suction measurement, even in the agricultural industry (Skinner *et al.*, 1997).

(c) Thermal conductivity sensor

Shawand Baver (1939) proposed using thermal conductivity sensors (TCS) to measure suction. TCS consist of a porous ceramic block containing a temperature sensing element and a miniature heater. The measurement of matric suction is made by inserting the sensor into the soil and allowing the water to flow through the porous block and the soil. Eventually, the water content of the porous media comes into equilibrium with the water content of the soil. The amount of water in the porous block affects the rate of heat dissipation within the block, which can be measured indirectly by measuring the heat dissipation within the block. Thermal conductivity sensors have been used in the laboratory as well as in the field (Fredlund and Wong 1989; Oloo and Fredlund 1995; O'Kane *et al.* 1998; Marjerison *et al.* 2001; Nichol *et al.* 2003). TCS has the ability to measure suction over a wide range. The low strength and poor durability of the ceramic tip; the poor stability of electrical signal and the inaccuracy particularly in high ranges of suction are some limitations of thermal conductivity sensors.

(d) Flow experiments

Various researchers used flow experiments accompanied with inverse modeling techniques to determine SWCC for sandy soils, either through one-step flow (Gardner, 1958) or multistep flow (Eching et al., 1993; van Dam et al., 1994) testing. Parameter identification by inverse modeling has evolved in the last few decades. One such improvement is that measured flow data,

water content or suction during testing, is used to determine the unsaturated hydraulic properties by inverse simulation (Ahmed et al., 2014; Zardav at al., 2011). The first usage of the inverse method in the field of unsaturated water flow was reported in the early 80's by Zackmann et al. (1982) and Dane and Hruska (1982). Yeh et al. (1996) and Zhang and Yeh (1997) developed an inverse method in which a successive linear estimator (SLE) was used to include the nonlinear relationship between the hydraulic parameters and the hydraulic heads. This technique was validated both in the laboratory, using sandbox experiments (Liu et al., 2002, 2007), and in the field (Straface et al., 2007; Cardiff et al., 2009). Durner et al., (1999) reported that the inflow/outflow experiments provide sufficient information to uniquely identify the parameters of the retention function and the unsaturated conductivity function by inverse modeling.

2.2.3 Soil water-Characteristic curve (SWCC)

Soil water characteristic curve (SWCC) is the relationship between the water content and the soil water potential. This characteristic curve is unique to different types of soil (Figure 2-1).

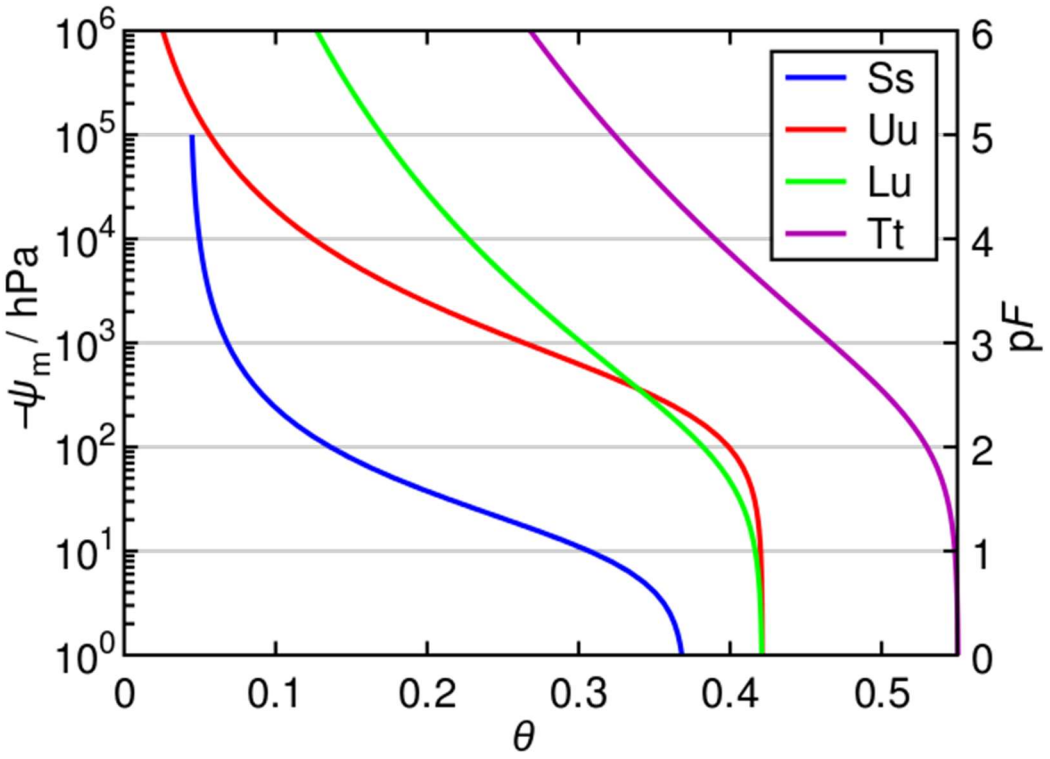

Figure 2-1: Water retention curve of sand (Ss), clay loam (Uu), clay (Lu) and peat (Tt)

ref: https://www.wikiwand.com/en/Water_retention_curve

Water movement in the partially rigid saturated sand is described by a modified form of Richard's equation (2-1) using the assumption that the air phase plays an insignificant role in the liquid flow process.

$$\frac{\partial \theta}{\partial t} = \frac{\partial}{\partial x}\left[K\left(\frac{\partial h}{\partial x} + cos\alpha\right)\right] - S \qquad (2\text{-}1)$$

Where h is the water pressure head [L], θ is the volumetric water content [L^3L^{-3}], t is time [T], x is the spatial coordinate [L] (positive upwards). S is the sink term [$L^3L^{-3}T^1$], α is the angle between the flow direction and the vertical axis and K is the unsaturated hydraulic conductivity function [LT^{-1}].

The SWRC is indispensable when studying water flow processes and modeling water and solute movement through an unsaturated soil. Empirical formulas are widely used to describe SWRC, and the Van Genuchten (VG) equation is appropriate to almost all soil textures. However, four independent parameters need to be determined to use the Van Genuchten equation.

The soil hydraulic function proposed by Van Genuchten (1980) is used because its inversions are better for characterizing sand than other functions (Schapp et al., 2003). Van Genuchten (1980) used the pore size distribution model of Mualem (1976) to obtain a predictive equation for the unsaturated hydraulic conductivity function in terms of soil water retention parameters. The expressions of Van Genuchten (1980) are given by:

$$S_e = \frac{\theta - \theta_r}{\theta_s - \theta_r} \tag{2-2}$$

$$\theta(h) = \begin{cases} \theta_r + \dfrac{\theta_s - \theta_r}{[1 + |\alpha h|^n]^m} & h < 0 \\ \theta_s & h \geq 0 \end{cases} \tag{2-3}$$

$$K(h) = K_s S_e{}^{l}[1 - \left(1 - S_e{}^{\frac{1}{m}}\right)^{m}]^2 \quad (2\text{-}4)$$

$$m = 1 - 1/n \quad (2\text{-}5)$$

The above equations contain five independent parameters: θ_r and θ_s are the residual and saturated volumetric water contents, respectively; α is a scaling parameter inversely proportional to the pore diameter; n is a shape parameter of the soil water characteristic curve which is directly proportional to pore size distribution, and K_s is the saturated hydraulic conductivity. The pore connectivity parameter *l* in the hydraulic conductivity function (Equation 2-4) is set to a value of 0.5 (Mualem, 1976).

2.3 Heterogeneity of sand column

The void ratio is a critical factor for various engineering properties. In most cases, this is referred as a single average value for the whole specimen. However, the local void ratio distribution is more relevant to soil behaviors. For instance, the drained or undrained behavior of cohesionless soil is dominated by the loosest or the densest portion of void distribution (Frost and Jang 2000) and the same soils with identical void ratios demonstrate different liquefaction potentials (Lee et al., 1999). The distribution of local void ratio is an important parameter which affects the geotechnical properties (shear strength, hydraulic conductivity, etc.) of granular material.

Many researchers rely on preparing a reconstituted specimen of the cohesionless soil for laboratory testing. Various methods like dry pluviation, wet pluviation, slurry deposition, vibration or moist tamping have been developed to obtain a homogenous reconstituted sample in the laboratory. Ibrahim and Kagawa (1991) examined the effect of the specimen preparation on the void ratio of sand and found that the dry pluviation tended to produce a more significant deviation of local void ratios than wet tamping for samples prepared at the same relative density. The fabrics resulting from different specimen preparation methods have shown a significant effect on the static and dynamic behavior of granular material (Ladd, 1974; Muililis et al., 1977; Oda, 1972). Specimens reconstituted in the laboratory are characterized by relative density; however, the relative density does not account for the non-uniformity of void ratio throughout the sand column due to human error. The primary challenge to getting the consistent results from laboratory tests is to achieve a homogenous soil sample every time. Information about the spatial variability in the void ratio is required for accurate interpretation of the experimental data.

Different methodologies have been used to determine the distribution of local void ratio along the height of a soil specimen. Typically, void ratio is calculated by the using the specific gravity, the volume, and the weight of soil; however, this ignores the effect of human error and disturbance caused while preparing the different layers. Oda (1976) presented the first attempts to quantify the local void ratio (porosity) distribution of particulate materials from magnified 2D images of the grains. Later researchers have used digital image analysis for the study of cohesionless soil fabric (Bhatia and Soliman 1990), clay microstructure (Smart et al. 1992), and fluid permeability of porous material (Berryman and Blair 1986). Bhatia and Soliman (1990) used

Oda's method to measure local void ratio distribution from 2D plane sections with the aid of an image analyzer. The global void ratio of soil specimen used by Bhatia and Solomon (1990) was 1.02, but the mean value of local void ratios was determined to equal to 0.59. Kuo and Frost (1996) modified Oda's method and found that the mean local void ratio was 0.954 times the global void ratio with a standard deviation of 0.323. These techniques required high-level image processing. Magnetic resonance imaging (Amin et al.,1998; Hedberg et al., 1993) and x-ray tomography (Andersson et al., 1990; Peyton et al. 1992) have been used to identify small features such as small fissures and cracks. These techniques provide small scale resolution but are very expensive and not widely available. For undisturbed soils in the field, void ratio distribution is interpreted from dispersion wave measurements and resonant column tests (Grabe et al., 2010). These methods require specialized techniques and demand massive computational effort. Ayoubian and Robertson (1998) froze samples at different stages of triaxial extension tests to measure the void ratio distribution along the length of the specimens. The different samples were used to compare the change in the void ratio at the various stages; however, this ignores the effect of human error and variation in a void ratio that occurs every time a new sample is prepared. The electromagnetic (EM) wave propagation method (EM-wave based technique) is an economical alternative and has the advantage of being non-destructive (Cho et al., 2004). Dong and Wang (2005) also used the EM-wave propagation method for saturated sand and found a standard deviation of 0.356 for local void ratio distribution. However, this methodology requires specialized equipment and skilled labor.

2.4 Permeation grouting

Permeation grouting is the injection of fluid grout into granular, fissured or fractured ground to produce a solidified mass to carry more load or to fill pores and fissures to control water flow. For levees located near an urban area, one method to mitigate under seepage includes the treatment of the granular soil deposits with an engineered fluid delivered by permeation, which results in a less permeable deposit. Permeation grouting does not destruct the original soil structure in the process and creates minimal ground disturbance and can be used for in-situ remediation of existing structures. Since the permeation grouting is an in-place technique, disposal cost and labor work can be reduced. The performance of permeation grouting depends both on the formation to be grouted and the type of grout used. It is difficult to ensure continuity of grouting as well as predict the permeation radius and the flow of grout in heterogeneous soil because the grout tends to follow the path of least resistance.

There are two types of permeation grouting based on injection materials: particulate (bentonite and cement) and chemical grouting (resin or other polymers). Typically, Portland cement is most often used to prepare cement grout. In permeation grouting, the type of cement selected is based on the relation of the particle sizes of the cement to the sizes of openings being grouted. Therefore, cement grout composed of Portland cement has limited applications in permeation grouting because of the possibility of filtration and unsuccessful grouting due to the relatively large particle sizes of Portland cement. Recently, microfine cement have been used over Portland cement because of the smaller particle size. Although the cost of microfine cement is

typically three to four times higher than that of OPC, this higher cost is often more than offset by the advantages and overall superior performance of microfine cement grout. Additionally, the properties and groutability of grouts vary with water to cement ratio. Moreover, the blending of an additive, such as sodium silicate or bentonite, which is used primarily to reduce the settlement of cement particles in grout, is recommended. Cement grouts are commonly used to strengthen the existing structure, whereas, the bentonite grout is commonly used for waterproofing to stop water infiltration into existing structures.

Bentonite grout is a high-solid grout consisting of a blend of bentonite, water, and ionic additive minerals. It is specially formulated to stop water leaks. There are many benefits of using bentonite grout injection, but the main advantage is that it is environmentally friendly. Also, bentonite grout is a pliable material, which has the ability to self-seal if the structure continues to settle. Additives like sodium pyrophosphate are used to change the rheology of bentonite grout to make it more permeable.

Chemical grout can penetrate finer grained soils that are inaccessible to particulate grouts. Even with this unique advantage, there are certain limitations to the applications of chemical grouts. Because of the chemical make-up, proper safety precautions must be followed, particularly during the mixing phase of the solution. Additionally, the material is not desirable or suitable for potable water applications, the grout is subject to shrinkage and pre-mature polymerization if exposed to constant UV rays, and the material will degrade over time if exposed to continual freeze-thaw and wet-dry cycles.

Permeation grout is classified into two main categories based on the injection method: point injection and sleeve pipe injection (tube A Manchette). In the point injection method, the casing is installed to the full depth, and grout is injected as the casing is withdrawn (Rtuner et al. (1995). The Tube-A-Manchette method involves grouting a sleeve pipe in the grout hole and injecting grout through holes in the pipe (Figure 2-2). The holes are covered and placed at 1-foot intervals along the pipe, and the grout is injected under a constant pressure or flow rate into the soil. The determination of injection pressure or flow rate highly depends on the type of soil, depth of injection, confining stress and structural pressure. The advantage of Tube-A-Manchette method is that different grouts can be injected into different holes and grout can be re-injected if there is a problem (Perlaman, 1999)

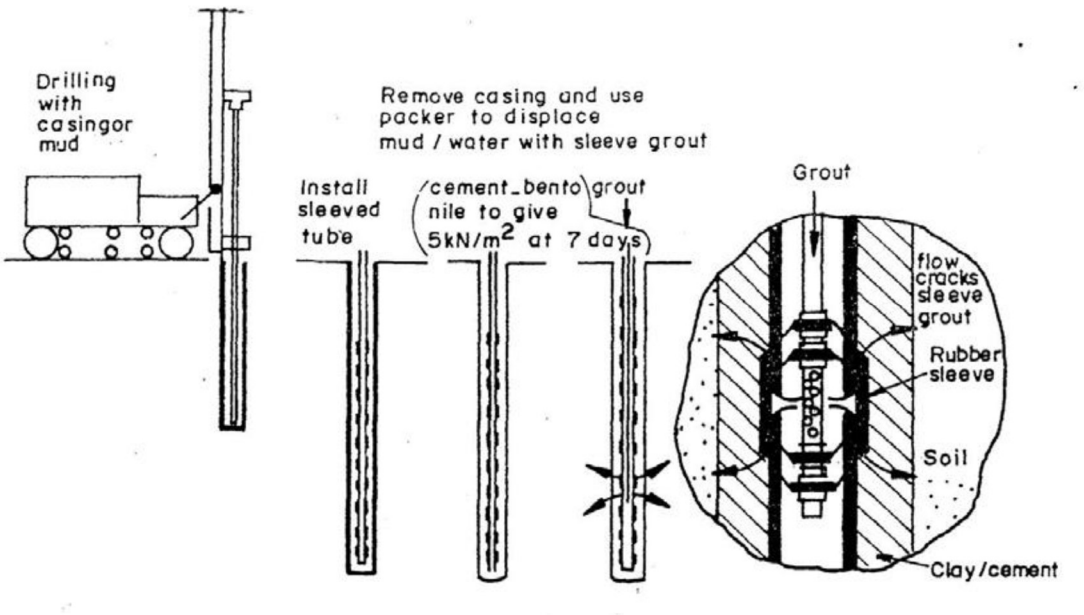

Figure 2-2: Schematic of permeation grouting procedure using Tube-A-Manchette (ref: http://www.ce.metu.edu.tr)

2.4.1 Application of permeation grouting

Permeation grouting is widely used in geotechnical engineering as a ground improvement technique that involves the injection of a suitable suspension and/or solution into soil and rock to either reduce the permeability or improve the mechanical properties. Permeation grouting has vast applications in tunneling, mining, levees, foundations and many other industries. Xanathakos et al. (1994) mentioned the applications of grouting in granular soils in tabulated form (Table 2-1) and the different types of grout (Table 2-2)

Table 2-1: Fields of application of grouts for granular soils (Xanthakos et al. 1994)

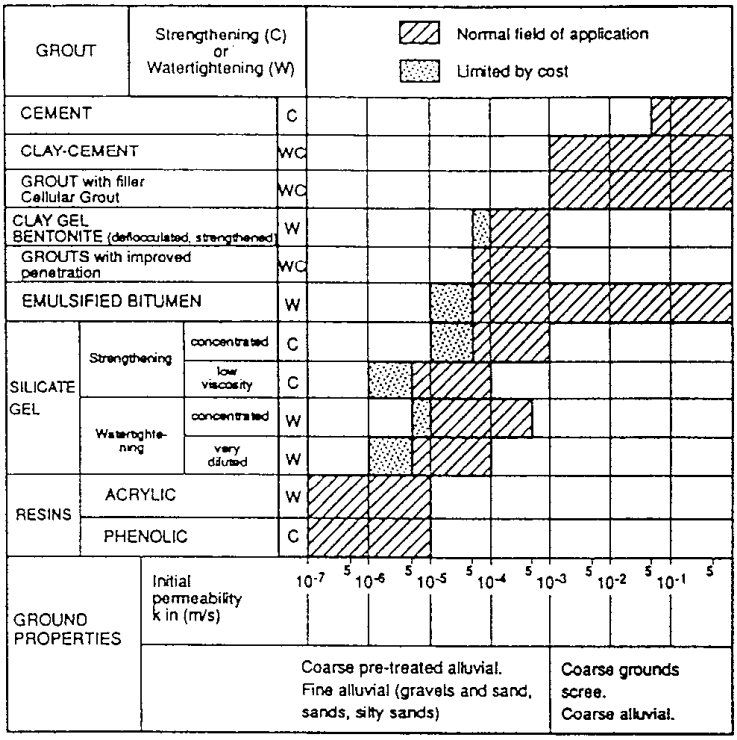

Source: From AFTES (1991).

Table 2-2: Types and application of grout

Type of Grout	Varieties	Applications
Cementitious	Neat cement, microfine cement, clay/bentonite cement, fillers, special applications, and enhanced permeability	Most commonly used and generally cheapest for waterproofing and ground strengthening
Silicate	Monoesters, diesters, triesters, and aldehydes	Used for waterproofing; too soft for ground strengthening
Resin	Acrylic, phenolic, aminoplastic, and polyurethane	Used for waterproofing and ground strengthening when cements and silicates are inadequate because they have lower viscosity, more rapid strength gain, adjustable setting times, good chemical resistance, psuedoplastic properties, and resistant to flow
Others	Bitumen, latex, polyesters, epoxies, furanic resins, silicones, and silacsols	Used for waterproofing and ground strengthening when high strength, resistance to corrosion, or flexibility is required

(a) Mining

In some situations, different grout types are combined as was the case at the Quirke II Mine in the Elliot Lake uranium mining area (Carter et al. 1992). During mining operations in this usually dry mine, a composite sub-vertical and splay fault structure filled with silt was encountered leading to piping out of the glacial silt infill and large water inflows of about 3, 785 lpm (1,000 gpm). Water reactive pre-polymer chemical grout was injected into the mine face to stem the massive inflow of water quickly. To facilitate further mining in this area, chemical grouting was followed up with cement grouting of the fractures in the rock mass. A water/cement grout mix of

1/1 was injected at pressures up to 552 kPa (80 psi) These measures took a period of about one week before mining operations could resume.

(b) Underground excavation/Tunneling

Another dramatic demonstration of how chemical permeation grouting can provide major improvements in the ground prior to underground excavation was the improvement of alluvial soils on the Los Angeles Metro project prior to tunneling underneath a major highway (Gularte et al. 1992). A sodium silicate grout was used to prevent run-ins and control settlements during the excavation of twin 6.4-meter-diameter (21 ft) tunnels under the Hollywood Freeway in Los Angeles, California. After a major fire in the tunnel had occurred during construction and subsequent fire-fighting activities, portions of the tunnel collapsed on either side of the grouted area, but the grouted area was undamaged by the disaster. The tunnel alignment and extent of grouting is shown in Figure 2-3. Finite element analyses and measurements in the field during construction had a high degree of agreement and proved the efficacy of the grouting program.

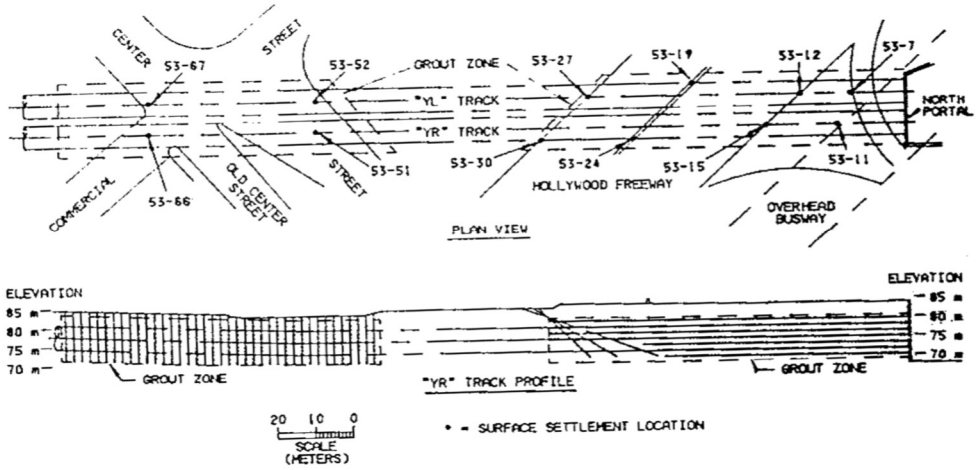

Figure 2-3: Tunnel alignment and extent of grouting (Gularte et al. 1992)

Chemical Grout was also used to treat the ground vicinity of San Francisco Bay Area Rapid Transit (BART) tunnels to permit construction of new Municipal Railroad tunnels within 5 ft (1.5 m) of the existing tunnels (Hashash et al. 1995).

The longest and deepest operational rail tunnel in the world is the Seikan tunnel in Japan. 34 fatalities and construction delays occurred due to four disastrous water inflows (Anderson and Roskrow, 2003). The excavation of the Vardo subsea tunnel in Norway was performed through some very unstable faults. At one of these faults, sliding took place and started to develop upwards towards the sea bed (Palmström, 1982). During construction of the Oslofjord subsea tunnel in Norway, an unexpected 15–20 m wide cleft filled with gravel material was detected, only 15 m in front of the tunnel cutting face. Tremendous efforts were made to deal with this unfavorable condition (Berggren, 2000). Zhang et al 2014 proposed a conceptual model of grouting to

introduce the five stages of a typical grouting process, i.e. backfill and permeation grouting, compaction grouting, primary fracture grouting, secondary compaction grouting, and secondary fracture grouting. Due to the effects of backfill grouting and permeation grouting, the ground permeability is reduced, and the ground is strengthened and stiffened.

(c) Hydraulic barrier in Levee construction

Soil-bentonite mixtures are commonly used in levee construction to create a hydraulic barrier and retard water flow. These mixtures are also efficient in waste water and waste confinement. However, disastrous consequences tend to occur when the soil-bentonite barriers fail. In the past century, levee failures and subsequent floods have caused life loss and massive property damages in the United States. During Hurricane Katrina in 2005, three major levee breaches inundated the city of New Orleans, Louisiana. Thousands of lives were lost, and damages worth over a 100 billion were generated. More recently, a levee failure in Moonachie, NJ during hurricane Sandy caused over a thousand people to evacuate the town, which was flooded to a water level up to 1.5 meters.

There are different mechanisms by which levees fail, one of which is under seepage. Under seepage occurs when the level of water increases on one side of the river and causes the water flow through the underlaying granular material to increase. A high hydraulic difference initiates the flow through the granular deposits under the dam or levee. Once the water pressure exceeds the submerged unit weight of the topsoil on the landslide, heaving and/or piping occurs. Figure 2-4 shows the different under seepage mechanism of levees. Heaving and piping are the most dominant failure mechanisms of under seepage. Heaving happens when the under-seepage forces push the

substrata upwards, while piping is the process of retrograde erosion in the sandy layers underneath levees. When the vertical seepage forces, caused by the upward flow on the landslide, surpass the weight of the topsoil, the water flow carries and deposits sand grains at the surface to create sand boils. Sand boils are usually created when a critical gradient of 0.85 for silty sands and sand, and 0.8 for silty clay and clay, is exceeded (Turnbull and Mansur, 1959).

Under seepage problems are mitigated by permeating the granular material with bentonite to create soil-bentonite mixtures. However, it is important to understand the behavior of these soil-bentonite mixtures by understanding the rheological properties of bentonite suspensions and the mechanisms involved in permeating sand with bentonite. Moreover, the stability of the soil-bentonite mixture is essential to avoid levee failure. Therefore, the stability of the bentonite suspensions in the permeated soil under increasing hydraulic gradients should be investigated. Once the critical hydraulic gradient is exceeded, bentonite suspensions will washout, which increases the hydraulic conductivity of the soil-bentonite mixture and ultimately leads to the failure of the levee.

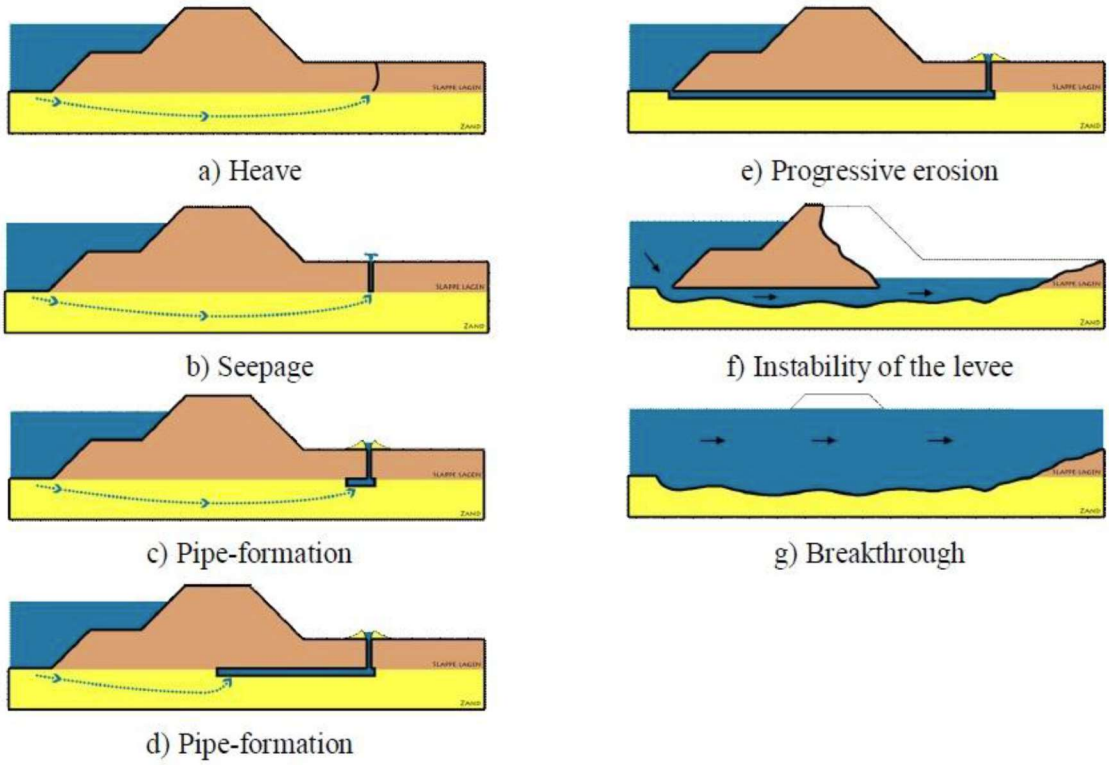

Figure 2-4: Under seepage mechanism (Adopted from Vries, Koelewjin, and Hopman)

(d) Resistance against liquefaction

The liquefaction and dynamic properties of grouted sand were investigated by Maher and Gucunski (1995). They found that grout decreased the liquefaction potential of sands (Fig 35-6) More specifically, they found that acrylate polymer and polyurethane grouts increased the damping capacity of soil under high strain loads, while sodium silicate grout mostly contributed to the dynamic shear modulus. This is substantiated by a case history reported by Mitchell et al. (1995) in which they list a bridge, the Riverside Avenue Bridge in Santa Cruz, California, that sustained no damage during the Lorna Prieta Earthquake. The Riverside Avenue Bridge is underlain by

submerged sands that were improved with sodium silicate and microfine cement grout. At this site, the 69-moment magnitude earthquake in October 1989 generated a maximum acceleration of 0.45g. No settlements or movements of the bridge piers were observed.

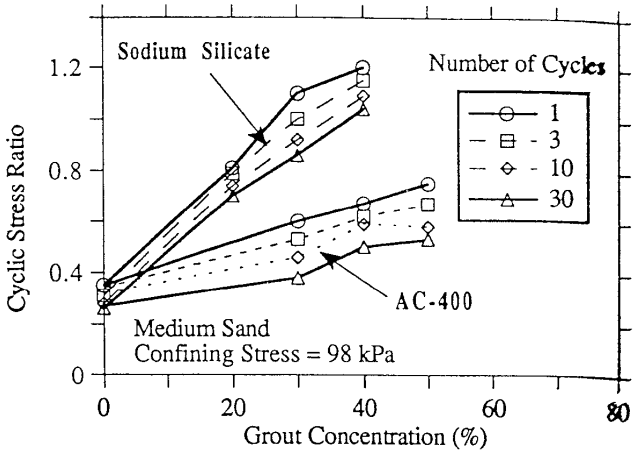

Figure 2-5: Stress ratio and number of cycles to initial liquefaction for loose sand grouted with sodium silicate (Maher and Gucunski 1995)

(e) Dams

Aswan Dam, Egypt case history: The 1,982-meter-long masonry Aswan dam in Egypt was built to regulate the Nile river in 1900. Originally 34 meters high, it was raised to 39 meters and later to 48 meters (Figure 2-6). It consists of granite blocks and flagstones set in cement mortar with low chemical resistance to the soft river water. Seepage through the structure increased progressively over the years, which lead to leaching of mortar and deposition of calcium carbonate on the downstream face. The remedial work consisted of an internal grout curtain, installed in

1960-61. The water cement ratio of the grout varied from 3:1 to 0.6:1 and the injection pressures ranged from 1.5 to 2.0 MPa in the rock. Grouting of each ascending 3m stage was conducted to leakage or a maximum take of 500kg/m. The effectiveness was demonstrated visually by the drying up of downstream seepage. Piezometer data confirmed that basal uplift pressure had been reduced substantially.

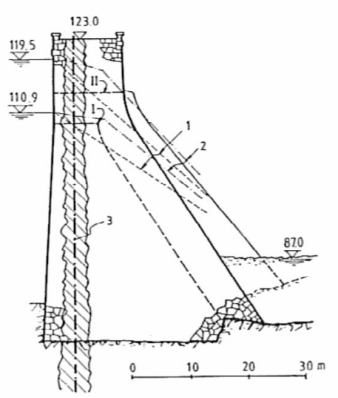

Figure 2-6: Typical cross section of Aswan Dam and the position of curtain grout: I and II dam construction phases, 1 linear distribution of uplift pressure in the foundation plane, 2 uplift pressures measured in piezometers, 3 center line of grout curtain.

Tarbela Dam Auxiliary spillway, Pakistan*:* One of the major concrete structures at the Tarbela Dam Complex is the Auxiliary spillway (Figure 2-7). It is found on a complex sequence of weathered dolomitic limestone, and limestone, interbedded with phyllite and beds of cohesionless marly silt. It is folded, faulted and fissured, and contains some small karstic features. Soft erodible material exists in some of the faults and karsts.

The spillway was originally protected by an upstream triple row grout curtain, a drainage system, and a connecting surface blanket. Over the years, some movement of fines into the drainage system was noted, and as a first step was rectified by replacing the original drain liners with special filtered liners at 3m centers along the line of the drainage curtain. Thereafter, the systematic grouting of "preferred paths" and voids in the rock mass upstream of these new drains was planned. To effectively seal these long water passageways of relatively small cross sections, the required grout had to be fluid, but stable during and after injection. Based on requirements of bleed, pump ability, stability and set strength (14MPa at 28 days) the mix of w/c = 1 by weight with bentonite of 1.5% by weight of cement was selected. During the injection, the mix design was kept constant, both to encourage flow and help site quality control.

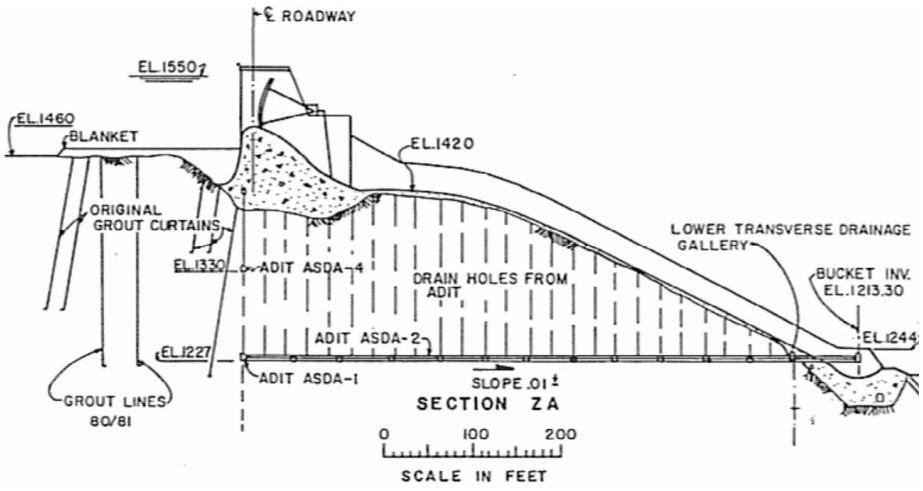

Figure 2-7: Auxiliary Spillway section, Tarbela Dam.

2.4.2 Placement of grout and verification of permeation grouting in field

2.4.2.1 Placement of grout in field

Grout is injected into the soil slowly to avoid excessive disturbance to the soil matrix. The permeation of grout is controlled by the size and fine content of soil, grain size distribution, grout type (e.g.,. solution or suspension), gel time, grout rheology and injection pressure. Figure 2-8 indicates a relationship between injection volume, soil porosity, and the radius of individual grout injection.

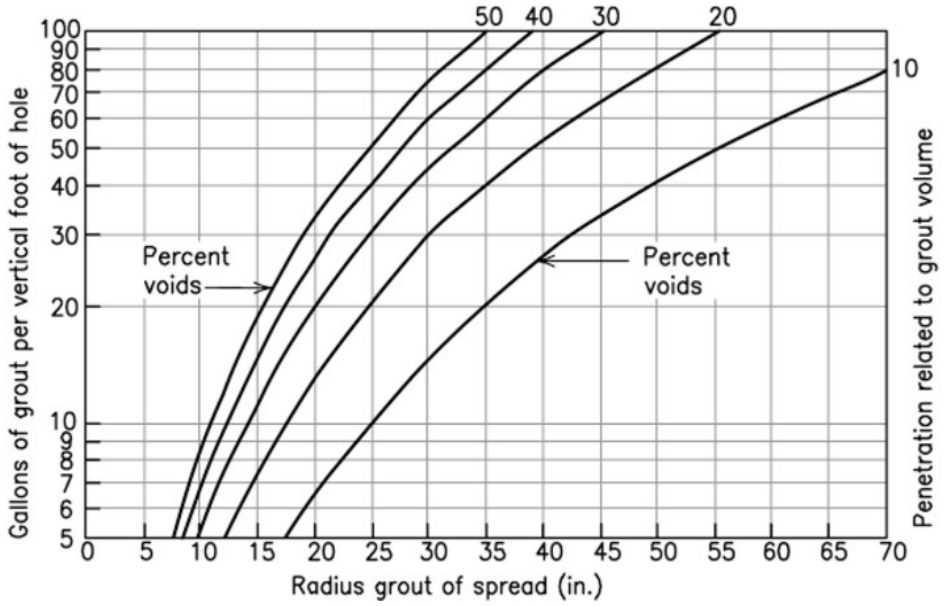

Figure 2-8: Penetration related to the grout volume

Once the geometry of grouted zone is determined, the volume of liquid grout can be calculated. The overpumpage factor is applied to account for irregularity in the grouted injection mass and loss of grout beyond the target grout zone. Higher overpumpage factor and tighter grout

pipe spacing are recommended for critical application. The overpumpage factor for water-tightening is generally between 15-30% for undisturbed, relatively homogenous soils. The grout pipes must be installed to create the intended grouted soil configuration. Multiple rows are typically required with a staggered spacing of pipe. Pipes can be spaced further apart in stratified and variable ground condition. Figure 2-9 shows the typical grout pipe patterns.

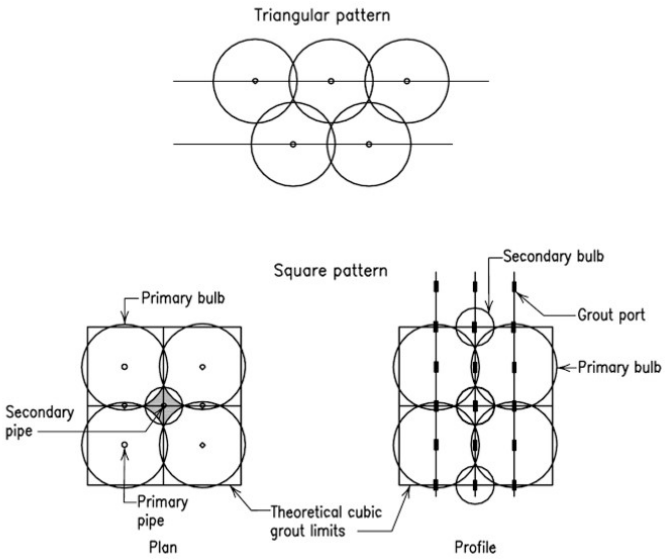

Figure 2-9: Typical grout pipe arrays

"Tube-a-manchette" TAM pipes permit the controlled placement of grout at specific locations and repeated injections at any location as well as the use of different grouts in same grout pipe. TAM pipes can be installed by vertically, inclined, or horizontally drilled boreholes. A double packer assembly is used to isolate the injection of grout to a distinct location. The grout pressure lifts the rubber sleeve off the TAM pipe and injects the grout into the ground.

Careful observations should be made while drilling to detect the presence of highly permeable zones, which may be a route on uncontrolled grout loss. The annular space between a TAM pipe and the borehole is filled with a sheathing grout to prevent grout travel along the drilled hole. The sheathing grout is brittle so that it can be fractured with injection. Therefore, high injection pressure (150+ psi) must be used to crack the hole. The production grouting process is performed at slightly lower pressure. The rule of thumb in North American practice, is to limit grout injection pressure to 1 psi per foot of depth, which is quite conservative. In European practice, allowable pressures are significantly higher. Injection flow rate is monitored rather than controlled. During production grouting, the injection pressure is determined by the injection pressure and resistance of the formation.

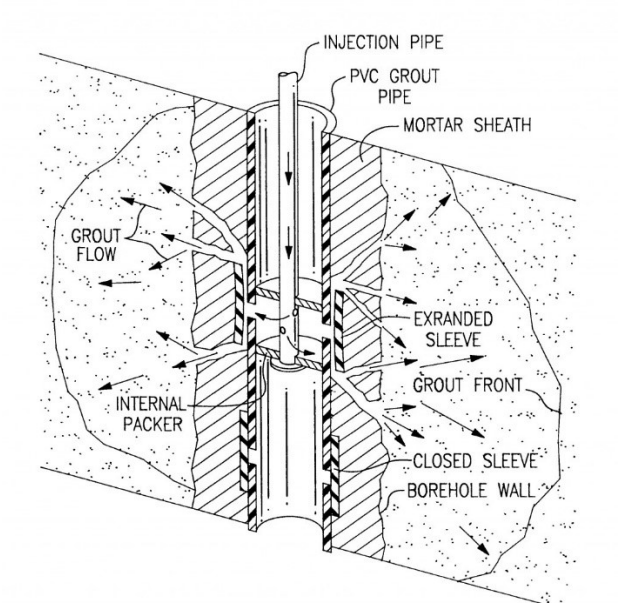

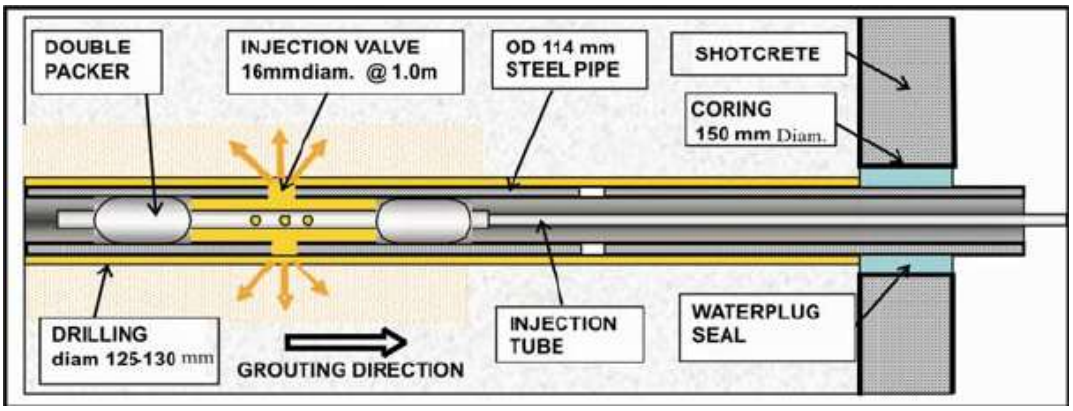

Figure 2-10: Tube a manchette (TAM) grout pipe

Real-time monitoring of pressure, flow, and cumulative grout intake is used to evaluate and determine the direction of the grouting program constantly. The implementation of real-time monitoring also conveniently results in the measurement of the completed work for the compilation of records and computation of useful data such as theoretical grout spread and determination of the hydrofracturing threshold. The holes should be grouted in primary, secondary

and tertiary sequence. Different grout materials can be combined to create most effective grout curtain. A less expensive, somewhat less permeable (ultrafine or sodium silicate grout) can be utilized for outer rows, with a more penetrable and costly, acrylate grout utilized for the middle row for final closure.

2.4.2.2 **Verification of permeation grouting**

Any grouting program should have a well-defined objective, a clear and measurable definition of success (i.e. how the ground condition should change due to grouting) and verification with the measurement of specific properties of the ground that is consistent with the objective. Typically, the objective is either increased the strength, reduced permeability, or both. A proper post-grouting verification program should always begin with the proper understanding of the pre-existing soil condition.

Verification of the performance of permeation grouting specifically for groundwater cutoff is best performed with the measurement of in situ ground hydraulic conductivities rather than proof holes with coring and testing of unconfined compressive strength, which is a parameter that is inconsistent with the objective of the work. Similarly, success or failure of a grouting program for strength improvement should not be gauged by grouted ground hydraulic conductivities. Cone penetrometer testing (CPT) and split spoon sampling are common, easily implemented indicator tests to evaluate the presence of grout in soil by measuring the increased resistance in the grouted soil.

2.4.3 Rheology of grout

The permeation of grout through a porous medium is significantly affected by both the rheological properties of the grout and the properties of the porous medium. Rheology is the study of deformation and flow of matter based on Hooke's law of elasticity and Newton's law for viscous fluids. For relatively small stresses, stresses and strains are related linearly through a constant. Beyond this range, the material tends to exhibit strain softening or hardening behavior. Equations (2-6) and (2-7) show Hooke's law for an elastic material.

$$\sigma = E\varepsilon \tag{2-6}$$

$$\tau = G\Upsilon \tag{2-7}$$

Where σ is the normal stress, E is Young's modulus, ε is the normal strain, τ is the shear stress, G is the shear modulus, and γ is the shear strain. The viscous behavior of materials is explained by Newton's law where shear strain is related to the applied shear rate through viscosity. Similar to the elastic modulus, the viscosity is a material property which is a measure of the resistance to shear flow.

$$\tau = \eta\dot{\Upsilon} \tag{2-8}$$

Table 2-3: Relation between Deborah number, type of material and Internal structure

Bentonite suspension used in this study have Deborah number greater than or equal to 1. Oscillatory tests were performed to characterize the linear and non-linear flow behavior of

bentonite and cement suspensions. The theory behind oscillatory tests relies on Equations (2-9) to (2-11).

$$\gamma=\gamma_o \sin(\omega t) \tag{2-9}$$

$$\tau=\tau_o \sin(\omega t + (\delta+\Phi)) = \tau_o' \sin(\omega t) + \tau_o'' \cos(\omega t) \tag{2-10}$$

$$\ddot{\upsilon}= \gamma_o \omega \cos(\omega t) = \ddot{\upsilon}_o \cos(\omega t) \tag{2-11}$$

Where γ_o is the strain amplitude, ω is the angular frequency, τ_o is the stress amplitude, τ_o' is the elastic stress amplitude. τ_o'' is the viscous stress amplitude, $\ddot{\upsilon}_o$ is the shear rate amplitude, t is time, and δ and Φ are the phase angles in phase with the strain and strain rate. Oscillatory shear tests subject the specimen to elastic-like behavior when the stress and strain occur in phase ($0^\circ<\Phi<45^\circ$), and to viscous like behavior when strain lags behind the stress by 90 degrees. ($45^\circ<\Phi<90^\circ$). When $\Phi=45^\circ$, the material is viscoelastic. Oscillatory tests measure the in-phase elastic modulus G', the out-of-phase viscous modulus G", and the phase angle Φ.'

Flow behavior becomes shear rate dependent when the Deborah number is less than 1, which indicates significant changes in the internal structure of the material. Figure 2-11 shows the different flow behavior of fluids dependent on shear rate.

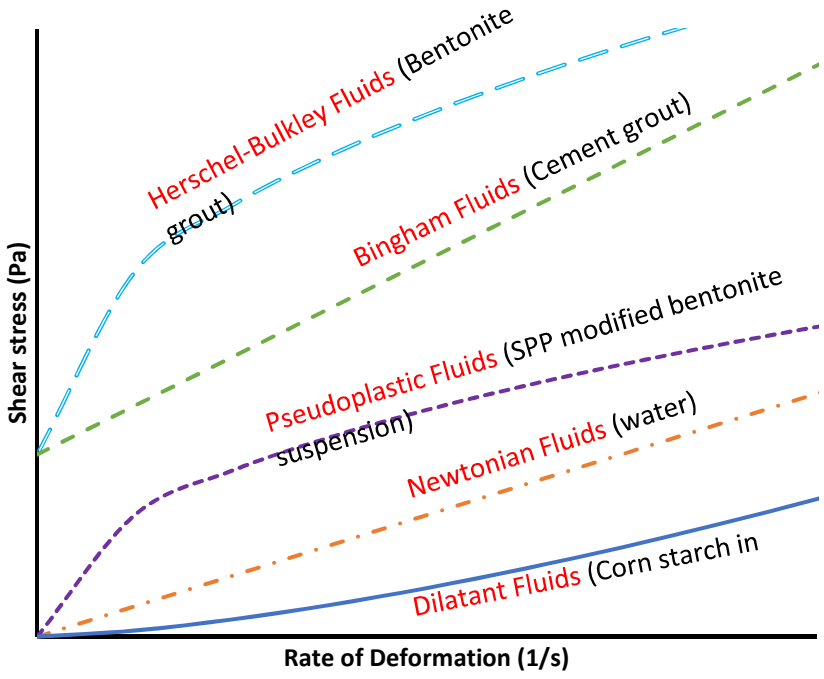

Figure 2-11: Flow behaviors of different fluids

The observed flow behaviors are described by constitutive models. The flow curve of Newtonian fluids is straight; hence the applied shear rate is directly proportional to the stress. Fluids which show dilatant and pseudo-plastic flow display shear thickening and shear thinning behavior respectively. Bentonite suspensions are generally described by the Herschel-Bulkley model which incorporates the yield stress. Shear thickening occurs due to the buildup of the internal structure with increased shearing; whereas, shear thinning is a phenomenon where the internal structure of the fluid breaks continuously due to increased shearing. Dilatant and pseudo-plastic behavior can be modeled using the power law equation ((2-12).

$$\tau = \eta \dot{\Upsilon}^n \qquad (2\text{-}12)$$

where η is the apparent viscosity and n is the flow behavior index. Shear thinning behavior has an n value less than 1 whereas a shear thickening fluid has an n value greater than 1. Some fluids show yield stress, which is the minimum stress to initiate flow. Below this stress, a material shows solid-like behavior with an infinite viscosity. Above yield stress, the fluid behaves like a liquid and viscosity changes with the applied shear rate. If power-law fluids have a yield stress, it is expressed by the Herschel-Bulkley model, which incorporates the yield stress term into the power law equation (1-12).

$$\tau = \tau_0 + \eta \dot{\Upsilon}^n \qquad (2\text{-}13)$$

Bentonite suspensions show flow behavior dependent on the bentonite fraction and testing conditions. A diluted suspension with bentonite concentration less than 1% exhibits a low viscosity, similar to that of water. Badenburg and Lagly (1988) reported that flow behavior of a bentonite suspension also depends on the particle shape of bentonite and that the flow of a bentonite suspension is Newtonian up to about 5% solid concentration below the shear rate of 200 s^{-1}. Above 5% solid concentration, the suspension behaves as non-Newtonian fluid with a yield stress and exhibits shear thinning behavior. Bentonite suspensions can be modeled by the Herschel-Bulkley model (Bekkour et al., 2005 and Kelessidis et al., 2007).

2.4.3.1 **Rheometry**

Rheometry is used to study the rheological behavior of suspensions. The most common geometries in apparatus to measure the rheometry of a suspension are parallel plates, cone and plate, cup and bob, and vane and cup. During this study, the vane and cup geometry was utilized to measure yield stress, viscosity, elastic modulus, viscous modulus, and phase angle. The vane geometry is widely used when testing thixotropic fluids such as bentonite suspensions (Mahaut et al., 2008). The vane is dropped into a cup of bentonite suspensions and rotated at different speeds determined by the applied torque. The shear stress and rate are calculated from the measured torque and rotational speed. The bentonite suspensions between the vane blades are assumed to be part of the vane that has the shape of a cylinder with a diameter equal to that of the vane. The bentonite is sheared at the boundaries of the cylinder.

The vane and cup geometry is less susceptible to sample disturbance and experimental errors. Sample disturbance is reduced by inserting thin blades into the cup (Barnes and Nguyen, 2001) rather than smearing a lump of bentonite over the area of the base of the plate in the plate-plate and cone-plate geometries. Yoon and El Mohtar (2013) showed that reducing sample disturbance by using the vane becomes essential when measuring yield stresses over time where using the cone and plate can be under-estimating the yield stress by as much as 60%. In addition to advantages due to the reduced disturbance, when using the vane the effects of large particles and wall slip can be neglected because the shearing plane is within the sample (Stokes and Telford, 2004). Nonetheless, the vane geometry is limited to fluids that are not highly affected by inertia

effects because secondary flow and end effects are neglected when using this method (Barnes and Carnali, 1990).

2.4.4 Structural kinetics of bentonite particles

Bentonite is clay mainly constituted of the mineral montmorillonite, which consists of an octahedral Alumina sheet sandwiched between two tetrahedral Silica sheets. The alumina sheet is composed of aluminum, iron, or magnesium atom equidistant from six hydroxyls of oxygen or hydroxyls. The atoms are tightly packed in an octahedral structure. Similarly, the Silica sheet includes a silicon or aluminum atom equidistant from four tightly packed oxygen atoms. The octahedral and tetrahedral sheets are symmetric and share the oxygen atoms to form a unit layer. The units line up on top of each other in a parallel manner to form a Hoffman structure. The bonds in the unit are covalent and hence stable; however, the crystal lattice formed between the units is unstable. Van der Waals forces connect the units together, and so they are easily separated by the adsorption of water and other polar molecules (van Olphen, 1977). The surface of the layers is negatively charged due to isomorphic substitutions; cation replacement of Si^{4+} by Al^{3+} in the octahedral layer, and replacement of Al^{3+} by Mg^{2+} in the tetrahedral layer. Figure 2-12 shows the atomic structure of montmorillonite.

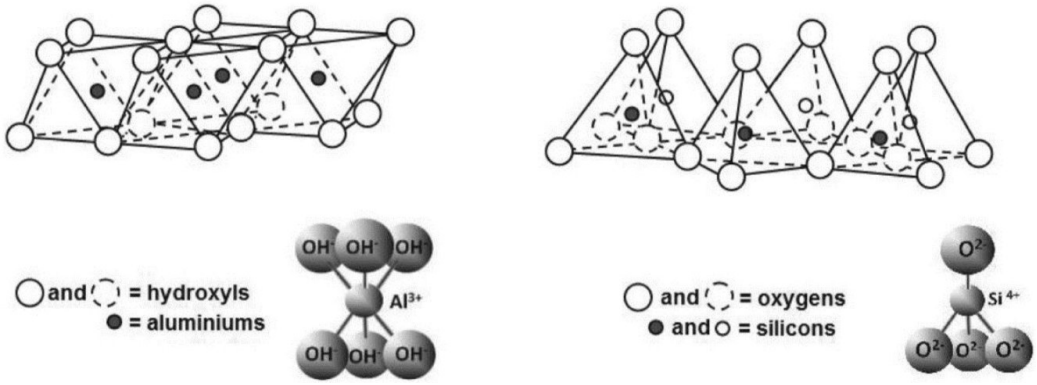

Figure 2-12: Atomic structure of Montmorillonite (Adopted from geoscienceworld.com)

It is crucial to determine the stability of the clay particles in an aqueous medium; therefore, the zeta potential is important. The zeta potential is the potential in the diffuse double layer between the fixed part and the mobile part. A high zeta potential implies that the colloids are stable; whereas, a low zeta potential implies high repulsion and flocculation. The zeta potential in sodium bentonite slurry is negative, almost insensitive to pH, and increases with increasing ionic strength (Callaghan and Ottweill, 1974). The stability of the clay particles is a function of the interparticle double layer repulsion energy and the Van der Waals attractive energy. Depending on the pH of the aqueous medium, the behavior of bentonite particles differs. The repulsion forces decrease, and the attraction forces increase when the concentration of cations in the aqueous solution increases. Contrarily, repulsion increases and attraction decreases with anions are abundant.

The orientation of the bentonite particles in the aqueous medium depends on the particle charges and hence on the pH. In an acidic environment at the isoelectric point, the particles edges and face are strongly attracted. This is due to the attraction between the negative face and the

positive charges created at the particle edges due to hydrogen adsorption. Also, the face-to-face repulsion is increased due to the presence of dissolved ions (Lagaly, 1989). A ‘card-house’ structure is hence created in the bentonite suspensions (van Olphen, 1977). As the pH decreases and more H^+ ions are present in the solution, the edge-to-face attraction increases and the particles form a cluster that moves independently under applied stress. However, as the pH increases, the attraction bonds are weakened, and unstable edge-to-edge contacts are formed (Lagaly, 1989).

In alkaline environments, the edges of the bentonite particles are negatively charged due to the adsorption of OH-. In dilute solutions, the bentonite particles are diffused because they are repelled from each other. In more concentrated solutions, the repulsion is reduced; however, the particle rotational and transitional motion is restricted. This causes the particles to be in a ‘band-like’ structure where the particles are placed in a parallel orientation (Fukushima, 1984). Nonetheless, if two particles approach each other, the Ca2+ ions create attractive electrostatic potential between the edges and the face. This produces voluminous networks with a greater yield stress and viscosity (Lagaly, 1989).

The concentration of bentonite and hence the concentration of Na+ affects the orientation of the bentonite particles in aqueous solution, but particle orientation is also dependent on pH conditions. In an acidic medium, as the concentration of Na+ increases, the stability of the card-house structure increases. However, if the medium becomes very acidic, face-to-face attractions are created, which decreases the stability of the structure. In an alkaline medium, the addition of Na+ increases the stability of the band-like structure, yet the addition of too much Na+ weakens the structure.

The addition of ionic additives such as sodium hydroxide, sodium silicate, and poly-phosphate reduces the viscosity and yield stress of bentonite suspensions and therefore, increases their mobility (Abend and Lagaly, 2000). The effect of ionic additives on bentonite suspensions varies depending on bentonite characteristics such as particle size, shape, surface charge, cation exchange capacity, and type of exchangeable cations (Goh et al., 2011). Sodium polyphosphate (SPP) decahydrate was used in this study because of its ability to effectively reduce yield stress and viscosity of bentonite suspensions. SPP modified suspensions produce a much lower yield stress right after mixing; however, the yield stress increases as the clay start to flocculate and the suspension will recover a large portion of its strength after 24 hours of mixing.

The yield stress of bentonite suspensions decreases upon the addition of polyphosphates because of increased negative charges and repulsion between particles (Penner and Largaly, 2001). The increased negative charge is due to the attachment or adsorption of polyphosphate ions at the particles' edges by OH- exchange. Although the phosphate ions disperse the bentonite suspensions, coagulation also occurs due to the presence of exchangeable cations and Brownian motion of particles. Critical coagulation concentration is achieved when the concentration of the additives is sufficient to initiate coagulation. The negatively charged faces are aligned in a parallel orientation due to repulsion (Mourchid et al., 1995). This causes coagulation to occur due to the attraction between the edges (Penner and Lagaly, 2001). The presence of SPP in bentonite suspensions increases the concentration of cations (Ca+ and Na+), which in return increases coagulation. The abundant cations reduce the thickness of the diffuse layer, which increases the attraction at the edges (Branderburg and Lagaly, 1988). Therefore, the bentonite network is built

up faster, and the bonds between particles are faster in modified suspensions as compared to pure bentonite suspensions. The effect of additives is greater in diluted suspensions.

2.4.5 Cement grout

Chemical grouts have been used in permeation grouting for improvement of mechanical properties and behavior of soils. Suspension grouts are less expensive and harmless to the environment, but cannot be injected into the soils with gradation finer than coarse sands. Chemical grouts can be injected in fine sands and silts, but are more expensive and not environmental friendly. Efforts have been made to extend the injectability range of suspension grouts by developing materials with very fine gradation, and as a result, a number of microfine and ultrafine cement have been developed and marketed in the past few decades. Ordinary Portland cement is pulverized by performing dry grinding in a mill to produce microfine cement with the maximum nominal size of 20 to 10 μm.

In the typical chemical composition of Portland cement, CaO and SiO_2 are the two most important oxides and constitute around 83% of the cement mass. The chemical composition influences hydration. The hydration of cement particle depends on the grains size and shape, which is most important for bleeding and penetrability. Bleeding and penetrability will not be based on the hydration of the specific oxides.

Table 2-4: Typical chemical composition of Portland cement (Betonghandbok 1994)

Oxides	Interval[%]	Typical analysis [%]
CaO	60-70	63
SiO_2	17-25	20
Al_2O_3	2-8	4
Fe_2O_3	0-6	2
MgO	0-4	3
SO_3	1-4	3
K_2O	0.2-1.5	1
Na_2O	0.2-1.5	0.3

2.4.5.1 **Morphology of the cement grains**

The shape of the cement grains is important for bleeding because of the settlement of the grains on the sediment surface. Sediments with a larger porosity result in a lower bleeding. The shape of the cement grains could also influence penetrability of the grout due to the stability of the grains in the pore space. A more irregular shape could give a lower contact surface between the grains, which decreases the stability of the arches. According to Lei and Struble (1997), the grains of hydrated cement have an irregular particle shape with sharp edges (Smaller grains flocculate with each other and produce larger agglomerates). After 60 minutes, smaller particles are more rounded than the larger particles due to greater hydration. Larger grains have a more even surface. After 36 minutes of hydration, the surface becomes uneven.

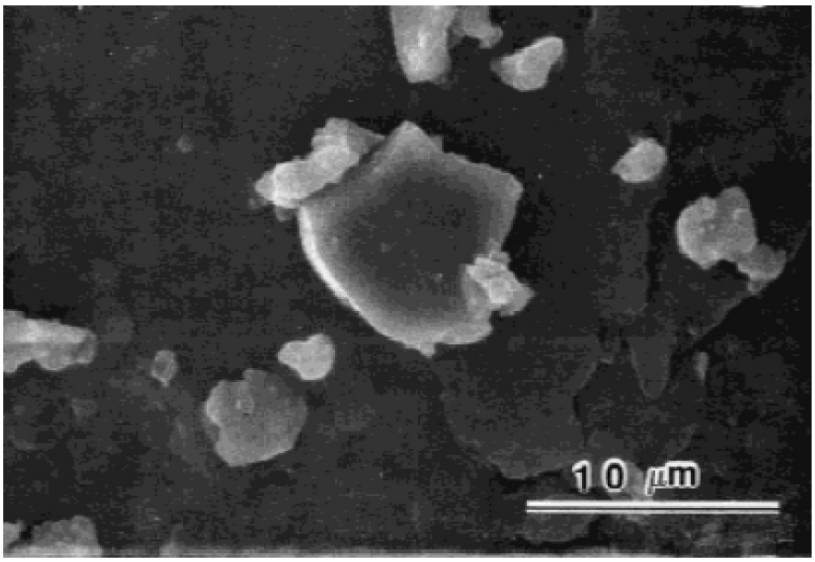

Figure 2-13: SEM (scanning Electron Microscopy) picture of unhydrated cement shows the shape of cement grains (Lei and Struble 1997)

2.4.5.2 **Hydration of cement particles**

The hydration process starts when water and cement are in contact and continues until the entire amount of cement has hydrated. The rate of hydration α is the ratio of the amount of hydrated cement Cn and the total amount of cement C in a given time t. According to Betonghandbok (1994), total hydration of 1 kg cement needs 0.25 kg water.

The hydration process in Betonghandbok (1994) is described as follows: Hydration of the cement is a reaction between cement and water. When cement is in contact with water, easily soluble synthesis, mainly alkali sulfate, are soluted in water which becomes saturated with K+-, Na+-, Ca2+-, SO42- - and OH- -ions. Crystals of Ca(OH)2 and ettringite fallout.

The surface of the cement grains is covered with reaction products. The compactness, thickness, and consistency of this surface layer, govern how fast water can penetrate through this

layer to the unreacted cement and continue to react. Reaction products fill the voids between cement grains and the cement paste hardens.

The gel particles at the grains' surfaces, developed by hydration, increase the size of the grains and thus their surfaces become rough. If the hydrated grains are in contact with each other, the gel particles develop bonds between them.

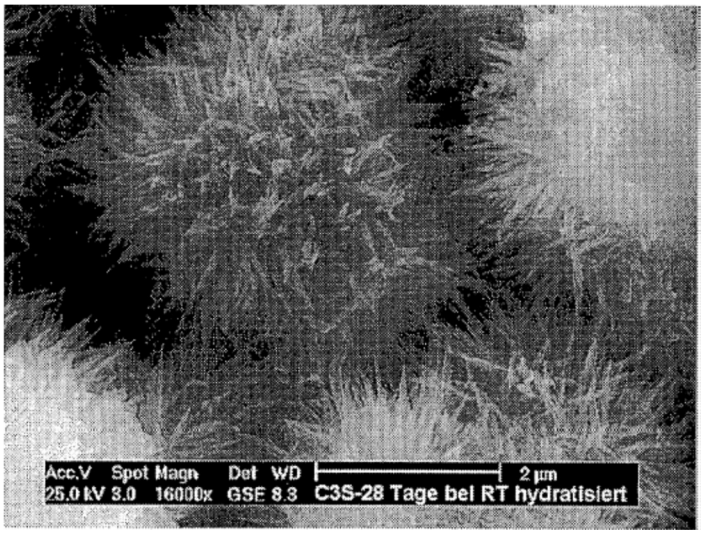

Figure 2-14: ESEM-FEG picture of hydrated three calcium silica (C3S) after 28 days at room temperature (Tritthart and Haubler (2003)

Figure 2-14 shows the how cement grains would look after a certain time of hydration. This changed surface influences the packing of the grains during sedimentation and consolidation. The sediment will be more porous for larger degrees of hydration, which decreases bleeding. The increased size of the grains will also decrease penetrability of grouts. Further, bonds between the grains could improve the stability of the eventual arches that could be developed during

penetration, which also contributes to lower penetrability. The rate of hydration (α) over the first half hour of hydration is an especially important aspect of bleeding and penetration due to the fact that the grout could stay in the agitator up to half hour before grouting. Due to the dormant period of the grout, almost the entire hydration that was developed during this first half hour happens at a time when the cement comes in contact with the water. A grout with fine cement will be more influenced by hydration than a grout with coarser cement due to a larger grain surface area.

Flocculation is also an important process which occurs in the grout. This process influences both bleeding and penetrability, especially in the grouts based on fine-grained cement. Juenger et al. (2005) show what a floc of hydrated cement grains looks like over time (Figure 1-15).

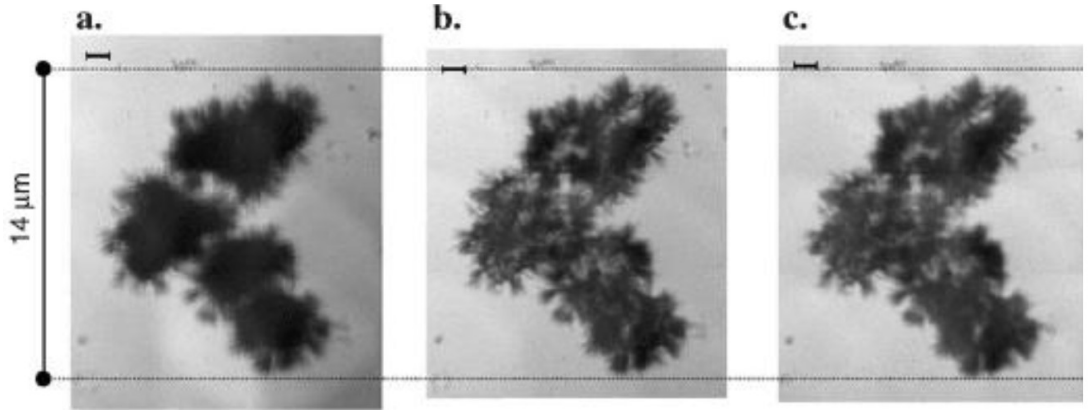

Figure 2-15: Flocculation of hydrated cement particles after (a) 30 (b) 60 and (c) 158 min (Juenger et al. 2005)

2.4.6 Filtration mechanism during permeation grouting

The understanding of suspensions flow through porous media with continuous particle deposition is important in the various engineering fields. When a suspension grout (like bentonite and cement grout) flows through porous media (sand), the particles encounter retention sites where they deposit or get carried away with the stream. This phenomenon is complex and has many contributing parameters. Injectivity of grout through a sand column declines because of reduction in permeability of the sand column due to sand matrix plugging by solid particles suspended in the injected fluid (Hjelmas et al. 1996; Sharma et al. 2000; Moghdasi et al. 2002). Particulate clogging in the porous media is an interesting subject in several disciplines in addition to geotechnical and environmental engineering.

The filtration mechanism is the mass transfer between grout particles and skeleton particles. Pang (1994) proposed that retention occurs mainly by four mechanisms: (a) surface deposition, (b) size exclusion, (c) bridging and (d) log-jam, as shown in Figure 2-16 . Size exclusion occurs when particle sizes within suspension are larger than pore throat size. Surface deposition occurs because of attraction surface forces between suspension particles and porous media grains. Bridging is a dynamic process where previously retained particles form a bridge. The fourth mechanism is log-jam, which occurs when more than one particle tries to flow through pore throat simultaneously. Retention mechanisms depend on various factors: (a) size, concentration, shape and surface properties of the grout particles (Eriksson et al., 2000, Abichou et al., 2002, Dupla et al., 2004) (b) grain and pore size distribution, shape and surface properties

of the formation (c) rheology of grout (Eriksson et al., 2000), and (d) interstitial velocity and physiochemical properties.

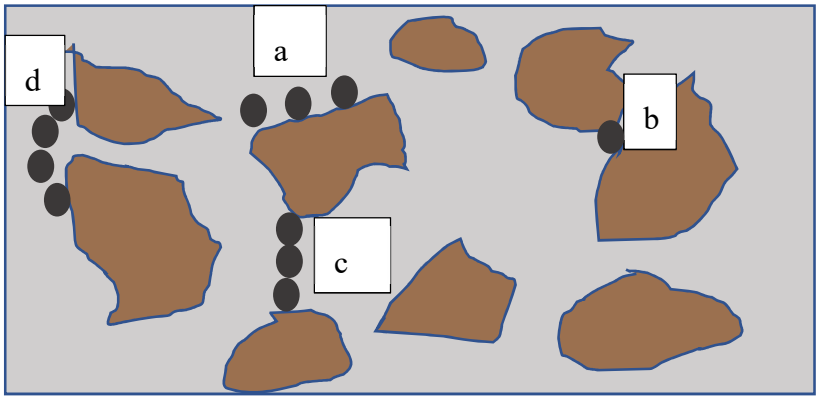

Figure 2-16: Different filtration mechanism

In order to better predict the success of grouting process, it is important to understand the filtration mechanism thoroughly. Many researchers (Maghous et al., 2007; Dupla et al., 2004) gave the mathematical solution to explain filtration mechanism of suspended particles flowing through porous media using mass balance equations. A general mass conservation equation for flowing particles can be written as

$$\nabla.(uC - D\nabla C) + \frac{\partial}{\partial t}(\varphi C + \sigma) = 0 \qquad (2\text{-}14)$$

here u is Darcy velocity, C is a concentration of suspended particles (volume of particles per unit fluid volume), D is dispersion coefficient, ϕ is the porosity and σ are the specific deposit (volume of deposited particles per unit bulk volume).

The mass balance equation was simplified in the literature by three approximations (a) particle diffusion is neglected, (b) change in porosity due to clogging is neglected (c) all moving particles are much less compared to the retained one, so moving particles are neglected (Herzig, 1970). In this study, two approximations are considered (a) dispersion is neglected as the diffusion of a particle is negligible for a size greater than 1μm (b) flow is considered to be incompressible hence, $\nabla u = 0$. The porosity of the media changes as deposition of particles occurs. Rheology of grout (viscosity, density) of grout changes with filtration (Eriksson et al., 2000). The density of grout increases close to injection point because of particle retention, and the grout that passes has filtered and reduced density as compared to initial density (

Figure 2-17).

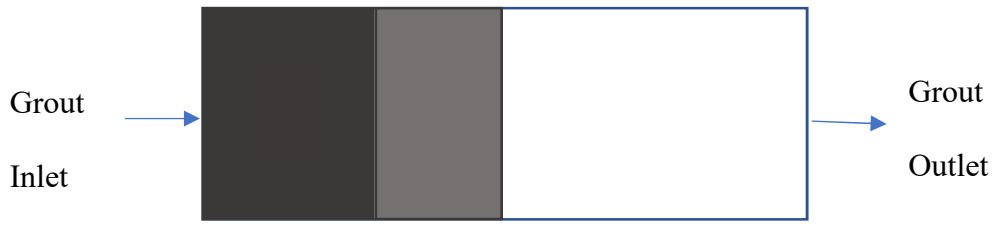

Figure 2-17 Increase in density of grout at injection point due to filtration (ρa > ρb>ρw)

Equation (2-1) define the rate of particle deposition which uses the empirical filtration function λ(σ).

$$\frac{\partial \sigma}{\partial t} = \lambda u C \tag{2-15}$$

Where σ is the volumetric concentration of deposited particles, λ is the filtration coefficient, u is the flow velocity, and C is the volumetric concentration of particles in suspension.

The filtration coefficient is a dynamic property that depends on previously deposited particles. In literature, the simplified models with constant filtration coefficient were mainly used (Pang and Sharma (1994), Wennberg and Sharma (1997) and Bedrikovetsky et al., 2000 and Bedrikovetsky et al., 2001). Considering λ as a constant is a limitation for simulating the filtration mechanism for bentonite grout permeated through sand. It may decrease or increase with time. It usually increases in the early stage of filtration because of molecular attraction between suspended particles and sand grains. This stage of filtration is called ripening. This can alter the flow (interstitial velocity) so that more suspended particles collide to sand grains or more particles carried away with the flow. Typically, surface forces are considered. Heertjes and Lerk (1967) considered only the Van der Waals forces, whereas Ives (1962, 1965) considered Van der Waals as well as electro-kinetic forces as retention forces. Sand grains are progressively coated with deposited particles, which leads to double layer repulsion. The filtration coefficient may decrease drastically when repulsive layer begins to form. If particles continue to deposit, they will finally start blocking the pore throat due to bridging and filter cake will start to form.

Researchers have developed empirical relations of the evolution of the filtration coefficient with the deposition of particles based on different theories (Iwasaki,1937; Stein, 1940; Ives, 1965; and Heertjes and Lerk, 1967). If the grout is injected through a sand specimen of length L and the

inlet (C_{in}) and effluent (C_{eff}) concentration was measured, then the filtration coefficient can be found experimentally using the equation (2-16)

$$\lambda = \frac{1}{L}\ln(\frac{C_{in}}{C_{eff}}) \tag{2-16}$$

Wennberg et al. (1997) experimentally determined the power law dependence of Darcy velocity (u), grain size of porous media (d_g), and injected particle size (d_p) as

$$\lambda \propto u^{-\alpha} {d_p}^{\beta} {d_g}^{-\gamma} \tag{2-17}$$

Where α, β and γ are positive constants. Researchers have done computer simulations to determine the filtration coefficient. Rajgopalan and Tein (1976) derived a semiempirical equation for the initial collector efficiency (η), which is the ratio of the trapped concentration to the initial concentration.

$$\eta = 0.72 A_s N_{Lo}^{1/8} N_R^{15/8} + 2.4\times10^{-3} A_s N_G^{1.2} N_R^{-0.4} + 4 {A_s}^{1/3} N_{Pe}^{-2/3} \tag{2-18}$$

Where A_s is Happel's geometric factor and N_{Lo} (London group parameter), N_G (gravity number), and N_{Pe} (Peclet number) are dimensionless parameters.

Happel's cell developed a relation between λ and η as:

$$\lambda_o = \frac{3(1-\varphi)^{1/3}}{2d_g}\eta \tag{2-19}$$

The filtration coefficient (λ) is a dynamic property that changes with the specific deposit. λ increases with time during the initial stage of filtration, a process that is called filter ripening. Iwasaki described the ripening period with an equation:

$$\lambda = \lambda_o(1 + b\sigma) \tag{2-20}$$

Deposited particles increase the surface area, and hence themselves act as collectors for subsequent retention of flowing particles. During the later stage of filtration, λ starts decreasing with time for several reasons. The continuous deposition of particles finally initiates the bridging of the pore throats, and filter cake starts forming. Sometimes, the accumulation of deposited particles increases the interstitial velocity as well as the hydrodynamics forces. These forces cause the breakaway of retained particles. However, voltage and decolletage occur simultaneously. Ives (1967) proposed that the interstitial velocity increases while the tortuosity and specific surface area decreases and derived λ as:

$$\lambda = \lambda_o\left(1 + \frac{b\sigma}{\varphi_o}\right)^{a_1}\left(1 - \frac{\sigma}{\varphi_o}\right)^{a_2}\left(1 - \frac{\sigma}{\sigma_M}\right)^{a_3} \tag{2-21}$$

Where b_1, b_2, a_1, and a_2 are constants and σ_M is the maximum value of σ. Macrle et al. (1965) considered all phases of filtration (ripening, constant removal and breakthrough) and defined the filtration coefficient as:

$$\lambda = \lambda_o \left(1 + 7.5\frac{b\sigma}{\varphi_o}\right)(1 - \frac{b\sigma}{\varphi_o})^2 \qquad (2\text{-}22)$$

Most theoretical and numerical work (Saada et al., 2005; Maghous et al., 2007, Bouchelaghem, 2009; Eklund and Stille, 2008) related to suspension transport in the past has been devoted to water filtration treatment and cement grout. A phenomenological linearized filtration law was formulated through mass exchange between cement and skeleton particles. The rate of cement mass filtered by the solid skeleton increases as the cement volume fraction increases (i.e. the concentration of cement grout) and as the porosity decreases as deposition occurs (Saada et al., 2005; Bouchelaghem, 2009). Some researchers (Bouchelaghem, 2009) have found the filtration rate to be proportional to the cement accumulation rate. The filtration law developed for cement grout cannot be used for bentonite grout because of the difference in rheological properties, particle size, and shape of the two materials.

There is a gap in the literature regarding the understanding of the filtration mechanism of bentonite suspensions at a constant flux. Bentonite suspensions are complex, non-Newtonian fluids. The flow behavior of a bentonite grout depends on the filtration mechanism and its

rheology. In this study, a permeation experiment is simulated, and various filtration models are investigated to define the filtration mechanism of bentonite grout best.

Considering the flow behavior of grout, it is known that its rheology is different from that of a Newtonian fluid. Bentonite is a Bingham fluid, which behaves as a rigid solid at low stresses and a viscous fluid at high stresses. Bentonite grouts require minimum shear stress (yield stress) to flow and have properties that are time dependent. Eriksson et al., 2000 defined a blockage mechanism of Bingham fluid flow through porous media in terms of a plug term (Z); when the plug term reaches 0.5, flow stops. The plug term is defined for the rectangular channel of width b:

$$Z = \min\left(\frac{\boldsymbol{\tau_o}\,(\mathbf{t})}{b.\,\boldsymbol{\rho_w}.\,g\,\frac{h_o - h_l}{L}}\,,\frac{1}{2}\right) \tag{2-23}$$

Where $\boldsymbol{\tau_o}\,(\mathbf{t})$ is the yield stress of the grout, $\boldsymbol{\rho_w}.\,g\,\frac{h_o - h_l}{L}$ = P is the pressure gradient.

The viscosity and shear stress of a bentonite grout depend on the applied shear rate. The suspension behaves as rigid material at low shear rates and a viscous fluid at higher shear rates. Bentonite grout flows only when sufficiently large stress is imposed, but thereafter it flows with constant velocity. The convection of yield-stress fluids through porous media is complicated because of the presence of unyielded portions in the channels. In this study, the yield stress and apparent viscosity of each bentonite grout have been determined using a rheometer.

Bentonite suspensions behave as Bingham fluids whose properties and can be defined as:

$$\tau = \tau_0 + \mu\dot{\gamma} \tag{2-24}$$

Where τ is shear stress, τ_0 is yield stress, μ is apparent viscosity and $\dot{\gamma}$ is the shear rate. Bentonite suspensions require the shear stress to be more than the yield stress in order to flow.

Pascal (1981) defined the threshold gradient model for the flow of Bingham fluids through porous media. The one-dimensional form of threshold gradient model is:

$$u = \begin{cases} -\frac{K}{\mu}\left[1 - \left(\frac{G}{|p_x|}\right)\right] p_x & if\ |p_x| > G \\ 0 & otherwise \end{cases} \tag{2-25}$$

Where G is threshold gradient and p_x is the pressure gradient.

Consider the motion of a Bingham fluid in a uniform channel of width b and under a pressure gradient (P). Channel boundaries are at y = $\pm\frac{b}{2}$.

$$\tau = Py \tag{2-26}$$

Hence, $\frac{Pb}{2} \geq \tau \geq -\frac{Pb}{2}$ in the channel. If Pb/2 < τ then there is no flow in the channel. If there is flow, then the yield surface lies at $= \pm\tau_0/P$. Let $y = \pm\varepsilon b/2$ represent the portion of channel which is unyielded. Where $\varepsilon = \frac{2\tau_0}{Pb}$.

The total volumetric flux Q in one channel is given by:

$$\mu Q = \int_{-b/2}^{b/2} u dy = \frac{b^3 P}{12}[1 - \frac{3\varepsilon}{2} + \frac{\varepsilon^3}{2}] \quad (2\text{-}27)$$

$$Q = \frac{b^3 P}{12\mu}[1 - \frac{3\varepsilon}{2} + \frac{\varepsilon^3}{2}] \quad (2\text{-}28)$$

The Buckingham-Reiner model considers the void space of porous media as a bundle of circular tubes. The overall permeability of sand column is K = N*b^3/12 or φ*b^2/12, where N is a total number of circular tubes and φ is the porosity of the sand column. Hence, the total volumetric flux through the sand column is:

$$Q_t = \frac{K}{\mu} P[1 - \frac{3\varepsilon}{2} + \frac{\varepsilon^3}{2}] \quad (2\text{-}29)$$

The Buckingham-Reiner model is used in this study to determine the pressure at the injection point for a constant flux of grout flow through porous media. In the present study, Sodium pyrophosphate (additive) is used to lower the viscosity of the bentonite suspension and lower the yield stress of the bentonite suspension very close to zero at the time of injection. Hence, the threshold gradient is close to zero, which means the term ε can be neglected in equation(2-29).

$$Q_t = \frac{K}{\mu} P \quad (2\text{-}30)$$

Prediction of grout spread requires the consideration of the hardening of grout with time. For this study, the hardening of grout with time is not considered in the modeling because of the very small injection time. Fingering or dilution of grout is not considered because the viscosity of grout is greater than that of water (Gustafsson and Stille, 1996). The pressure gradient obtained from equation (2-30)from a known, constant flux is used in inverse modeling to determine the filtration parameter.

Particle entrapment occurs due to a variety of physical mechanisms like interception, sorption, sedimentation, bridging and attraction by molecular forces (Payatakes et al., 1974 and Roque et al., 1995). Rouqe et al. (1995) proposed four different particle retention phases: deposition, bridging, internal accumulation and external accumulation. Whereas, Chauveteau et al. (1998) explained the effect of each retention mechanism on the permeability reduction. Permeability reduction was extensively studied for (a) oil recovery operations (Barkman and Davidson 1972; Abrams 1977; Davidson 1979; Eylander 1988; Vetter et al.1987; Sharma and Yortsos 1987; Todd et al. 1990; van Oort et al. 1993; Roque et al. 1995; Veerapen et al. 2001; Moghdasi et al. 2004;Al-Abduwani et al. 2003; Al-Abduwani et al. 2005) and (b) waste-water filtration (McDowell-Boyer et al. 1986; Amirtharajah 1988; Tobiason and O'Melia 1988; Reddi et al. 2000). In petroleum engineering, practitioners require this knowledge to determine the formation damage while injecting drilling fluid through wellbores. This study is critical for permeation grouting as well to determine the grout spread post-stability.

Mathematical models combined with laboratory studies can provide insight into the spatial and temporal development of bentonite grout permeation into porous media. The mathematical

model for deep bed filtration was explained by Herzig at al. (1970), which contains two empirical parameters: the filtration coefficient and the formation damage coefficient. Knowledge of these two parameters is essential for simulating the suspension grout through porous media mathematically. Pang and Sharma (1994) and Wennberg and Sharma (1997) showed that these parameters could be determined from core flood tests, from the combined measurement of core pressure drop and from the suspended particle concentration in core outlet water. Pang and Sharma, 1994, Van Oort et al., 1993, Wennberg and Sharma, 1997, Bedrikovetsky et al., 2001 and Bedrikovetsky et al., 2003 performed laboratory core flood tests on rock core to determine the constants. These tests are meant to be performed on rock samples. There is a gap in the literature for describing the filtration coefficient and formation damage coefficient data for sand permeated with bentonite grout. The motivation of this paper is to determine the filtration coefficient, and permeability reduction function for bentonite grout injected through sand.

The porosity of porous media is reduced as particles get trapped within the pore throats. This causes the permeability to decline, which in turn leads to restricted grout injectivity. Permeability reduction due to particle deposition is due to the combined effect of a change in tortuosity, surface area, and hydraulic radius. The Kozney-Carman equation is often used to present the relationship of permeability versus porosity, grain size, and tortuosity.

$$k = \frac{n^3}{K(1-n)^2 S_v^2} \tag{2-31}$$

Where k is permeability, n is porosity, Sv is the specific surface and K is the Kozney constant which includes a factor relating to the tortuous flow to the channel length. Permeability

can be predicted consistently using the Kozney-Carman equation by changing the radii of conduits and their number and type. However, it requires additional assumptions, especially regarding the tortuosity evolution due to porosity reduction. Particle deposition within the pore space has a considerable effect on the tortuosity and direction of flow. Several relationships have suggested relating the decline in permeability with the concentration of deposited particles (Herzig et al. 1970 and Dullien,1982). Sharma et al. 2000 defined the reduction of permeability for water injection wells considering three factors (a) reduced porosity, (b) increased surface area and (c) increased tortuosity.

$$\frac{k}{k_0} = k_{dn} k_{ds} k_{dt} \tag{2-32}$$

Where the permeability reduction due to the reduced porosity of block i at time t = j is:

$$k_{dn}(i,j) = \frac{{n_{i,j}}^3 (1-n_0)^2}{{n_0}^3 (1-n_{i,j})^2} \tag{2-33}$$

The retained bentonite particles and sand grains are considered as spheres with their entire surface exposed to flow for the calculation of the reduction in permeability due to increase in surface area.

$$k_{ds}(i,j) = \left[\frac{1 + \frac{\sum_{i,0}^{i,j} \sigma_{i,j}}{(1-n_0)}}{1 + \frac{d_g}{d_p} \frac{\sum_{i,0}^{i,j} \sigma_{i,j}}{(1-n_0)}} \right]^2 \tag{2-34}$$

Where d_g is the size of the sand grain, d_p is the size of bentonite particle, and σ is the specific deposit.

The reduction in permeability due to tortuosity is:

$$k_{dt}(i,j) = \frac{1}{1 + \beta \sum_{i,0}^{i,j} \sigma_{i,j}} \tag{2-35}$$

Where β is damage factor, which depends on pore structure.

Most of the above-mentioned filtration coefficient and permeability reduction relationships are for cement suspension grouts or for water injection in an oil reservoir. There is very limited literature available for the filtration and permeability reduction function for bentonite suspension grouts.

CHAPTER 3 DETERMINATION OF UNSATURATED HYDRAULIC CONDUCTIVITY OF GRANULAR SOIL USING INVERSE MODELING TECHNIQUE

3.1 Abstract

Soil water characteristics curve (SWCC) is an important soil function describing the moisture stress condition of unsaturated soil. Various methods are described in the literature to determine the unsaturated hydraulic properties of soil by direct and indirect methods. Most of these techniques are costly, time consuming, require specialized equipment and are limited when testing sandy soils due to the low capillary pressures. This paper proposes a simple, inexpensive and quick method, the Sangroya-El Mohtar (SEM) method, to characterize the unsaturated hydraulic properties of sandy soils. The SEM method combines a multistage constant flux water flushing experimentation with inverse modeling using Hydrus 1D to obtain the unsaturated hydraulic properties of a soil. The multistage flushing includes multiple stoppage and resumption of flow to capture the moisture redistribution from the saturated zone to the unsaturated one (right after flow has stopped). The unsaturated hydraulic parameters of Richard's equation for SWCC are then determined by inverse modeling of the experimental setup in Hydrus 1-D software using local (Levenberg- Marquardt algorithm) and global (Shuffled Complex Evaluation algorithm) optimization schemes. The objective function for the parameter estimation analysis is the root means square error (RMSE) of the pressure heads obtained experimentally (recorded by pressure transducer) and numerically (Hydrus 1D modeling) at the base of the sand column. The paper presents the results from testing three different sands with varying grain size distribution using the

SEM method as well as the hanging column test method. The results showed that the multistage flow testing combined with the modelling allows for accurate capturing of the special and temporal changes in water content within the sand specimen using only one pressure transducer at the base. The van Genuchten parameters obtained from the Levenberg-Marquardt (local) optimization scheme were within 2 percent of results from Shuffled Complex Evaluation algorithm implying that the simpler local optimization might be sufficient to obtain the desired properties. The unsaturated hydraulic properties obtained from the SEM method were comparable to those obtained using conventional hanging column test for sands B and C. Sand A properties were only obtained using the SEM method because its large particle sizes made it challenge to run the test using the hanging column test.

3.2 Introduction

There are various geotechnical and geo environmental engineering problems where unsaturated soils are encountered. SWCC is a relationship between suction and volumetric moisture content (or gravimetric moisture content or degree of saturation) in the active pore space of a material. It defines soil's ability to store and release water. In the last few decades, many researchers have developed various direct and indirect suction measurement techniques to determine the unsaturated hydraulic properties of soil in the laboratory. Direct measurement techniques include: axis-transition technique (Tempe pressure cell), tensiometer and suction probes; whereas indirect suction measurement techniques include: time domain reflectometry (TDR), in-contact filter paper, thermal conductivity sensor (TCS), and thermocouple psychrometer

techniques. All these experimental techniques vary widely in terms of cost, complexity and measuring ranges.

For decades, researchers have tried to find a simplified method to determine unsaturated hydraulic properties. Suction measurements are still considered challenging for researchers and engineers compared to saturated soil properties. There is no single device that covers the entire range of total suction that can be encountered by the different soils. Measurement of SWCC for sandy soils can be particularly challenging due to the low total suction values. For obtaining low suction values, hanging water column technique was used (Haines 1930). A hanging column setup consist of three parts: a specimen chamber, an outflow measurement tube and a suction supply. Specimen chamber consists of glass funnel referred as 'Buchner funnel' containing porous plate and the specimen being tested. Suction is applied across the specimen by adjusting the elevation of two reservoirs. The magnitude of applied suction is measured with a manometer. Water expelled from a specimen during the test is measured using a capillary tube connected to the outflow end of funnel.

Various researchers used flow experiments accompanied with inverse modeling technique to determine SWCC for sandy soils, either through a one-step flow (Gardner, 1958) or multistep flow (Eching et al., 1993; van Dam et al., 1994) testing. Parameter identification by inverse modeling has evolved in last few decades. Measured flow data, water content or suction during testing, was used to determine the unsaturated hydraulic properties by inverse simulation (Ahmed et al., 2014; Zardav at al., 2011). The first usage of inverse method in the field of unsaturated water flow was reported in the early 80's by Zackmann et al. (1982) and Dane and Hruska (1982). Yeh

et al. (1996) and Zhang and Yeh (1997) developed an iterative geostatistical inverse method in which a successive linear estimator (SLE) was used to include the nonlinear relationship between the hydraulic parameters and the hydraulic heads. This technique was validated both in the laboratory, using sandbox experiments (Liu et al., 2002, 2007), and in the field (Straface et al., 2007; Cardiff et al., 2009). Durner et al., (1999) reported that the inflow/outflow experiments provide sufficient information to uniquely identify the parameters of the retention function and the unsaturated conductivity function by inverse modeling.

Most of the techniques for measuring suction mentioned earlier are expensive and time consuming and require skilled labor. This paper introduces the Sangroya-El Mohtar (SEM) method as a simpler, cost effective and quick alternative method for determining the SWCC for sandy soils. The new method consists of running multistage transient flow experiments on sand columns while measuring the total head at its the base. The same testing protocol is modeled numerically using Hydrus 1D. An optimization logarithm is then used to obtain the unsaturated properties of the soil by matching the pressures at the base of the column from the experimental and numerical modeling. The paper presents the results from experimental tests and inverse modeling for three different sandy soil to determine the effectiveness of this method (in comparison with the hanging column testing method).

3.3 Materials Used and Experimental Set up

Sand columns have been reconstituted to perform various geotechnical laboratory testing in the past (ASTM D4320, Yoon and El Mohtar, 2013). The new proposed method in this study

utilizes sand columns to characterize unsaturated hydraulic properties of cohesionless soils. Three different coarse material with different average particle sizes and particle size distribution were used in this study.

3.3.1 Materials

Three different coarse materials (Sand A, Sand B and Sand C) were used in this study. Table 3-1 summarizes the index properties of tested soils based on ASTM standards (ASTM D422, D854, D4253 and D4254) and Figure 3-1 shows their grain size distribution. Sand A consists of 2.4 mm uniform spherical beads while Sand B and Sand C are natural sands with different average grain sizes but similar finer gradation. Filter material was used between the water inlet and the bottom of the specimen to obtain a uniform waterfront through the whole cross-sectional area of the specimen. Gravel (with particle sizes between 4.75mm and 10mm) and blast sand (with particle sizes between 1.2mm and 1.7mm) were used for the two-layer filter material at the top and bottom of the sand. De-aired distilled water was used in this study to reduce the inclusion of air while flushing with water.

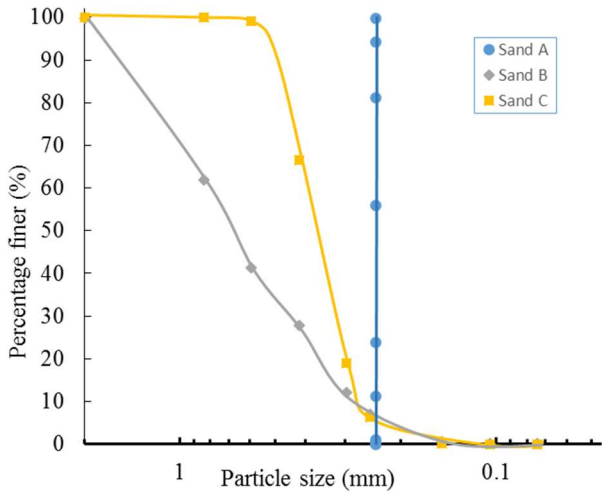

Figure 3-1: Grain size distribution of the tested sands

Table 3-1: Index Property of the tested sands

Soil	G	D_{10}(mm)	D_{30}(mm)	D_{50}(mm)	D_{60}(mm)
Sand A	2.65	2.4	2.4	2.4	2.4
Sand B	2.70	0.25	0.8	0.7	0.425
Sand C	2.65	0.25	0.38	0.37	0.3

3.3.2 Experimental Setup

The sand column setup used in this study consisted of a transparent permeation cell with a height of 178mm height and a 64mm internal diameter. The cell has one central water inlet and one central outlet. A sand specimen of 128mm height is prepared inside the cell with 25mm of filter material at top and bottom of the sand (Figure 3-2). The filter material consisted of 12.5mm of fine gravel and 12.5mm of blast sand. The large particle size of the gravel ensured horizontal

flow of water as it entered the cell from one central inlet and the blast sand serves as a transitional material between the gravel and the sand specimen due to the large difference between the grain size of the gravel and tested sands. The dry sand is pluviated on top of the filter material using a long funnel with zero drop height in increments. The weight of pluviated sand and its corresponding height are recorded for each increment to determine the relative density along the height of the sand specimen. A similar filter material is then placed on top of sand specimen to prevent the washing out of sand particles through the outlet.

After assembling the top platen and clamping the column assembly, the specimen is flushed with CO_2 to replace the air in the voids. This step is intended to reduce the chances of having entrapped air bubbles in the specimen during water flushing because CO_2 is more dissolvable in water than air and has a lower surface tension. De-aired water is then flushed through sand column from the bottom to the top at one of three constant fluxes (25, 50 and 100ml/min) using a GeoTac pump. The GeoTac pump was chosen over a peristaltic pump because it generates a constant continuous flux rather than a pulsating one. A pressure transducer is connected to the inflow line to measure the pressure head buildup required to maintain the constant flux. The pressure transducer used in this study has a pressure range of $\pm$70kPa (7m of water pressure).

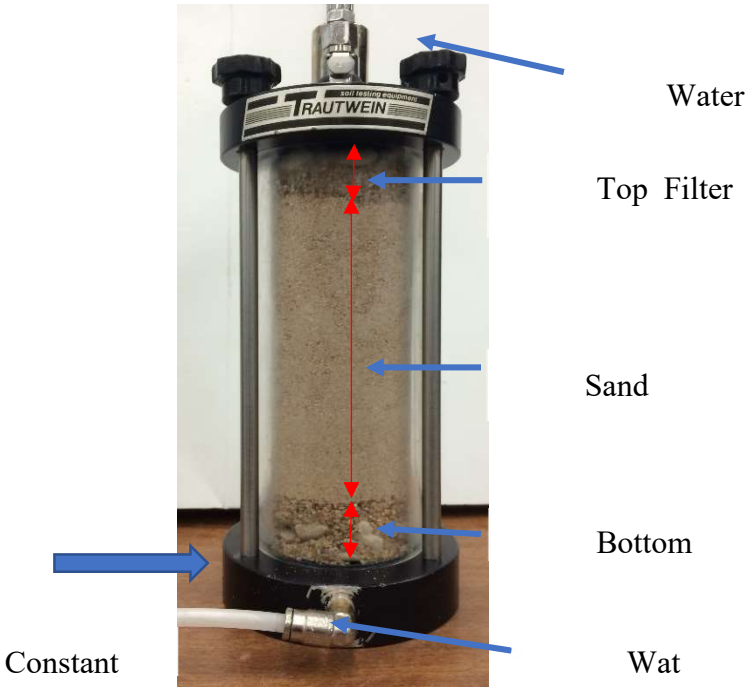

Figure 3-2: Assembled Sand Column

One of the advantages of the newly proposed method is its simplicity, which allows for performing the experimental testing using within many existing laboratory sand testing setups (such as rigid wall permeameter, flexible wall permeameter, triaxial testing). For example, if using a triaxial testing setup, two porous stones replace the top and bottom filter material and the specimen would be prepared using a traditional split mold procedure. To measure the unsaturated hydraulic properties of a triaxial specimen using the SEM method, a constant flow pump and a digital pressure transducer are the only additional equipment needed (both are commonly available in most Geotechnical laboratories). In comparison, most proposed similar methods in the literature require the use of more specialized sensors such as tensiometer (Yeah and Harvey, 1990) or TDR sensors (Scheffler and Plagge, 2011) and have them installed at different locations within the

specimen to determine the spatial variation of water content at different times. The simplicity of the setup and equipment limits the ability of measuring the spatial and temporal variation of water content. However, as part of the inverse modeling described later, the distribution of water content can be obtained from the numerical modeling using Hydrus 1D.

3.4 The SEM Method

The newly proposed SEM method consists of two stages: 1) Experimental testing and 2) inverse modeling. In the experimental testing phase, the pressure buildup is continuously recorded during the multistage constant flux permeation. The inverse modeling is performed to back-calculate the unsaturated hydraulic properties of the sand (particularly, the van Genuchten parameters) by matching the recorded pressures from the experiments with those obtained from Hydrus 1D simulation of the same experiments. Results from forward modeling are presented to evaluate the sensitivity of the model to changes in the unsaturated hydraulic properties of the sand.

3.4.1 Experimental Testing

After completion of the specimen preparation described earlier, the column is flushed with water at a constant flux while recording the pressure buildup at the bottom of the permeation cell. The propagation of the waterfront depends on the flow rate, pore size distribution of the specimen and its unsaturated hydraulic properties. Waterfront is the interface between the saturated and unsaturated regions. If the specimen is uniform, then the height of capillary fringe (unsaturated zone) will remain the same as the waterfront propagates through the specimen (at least until the capillary zone reaches the top filter material). As part of the new proposed method, the flow is

stopped at multiple stages as the waterfront propagates from the bottom of the specimen to the top filter material. With each stoppage in flow, the change in pressure values are recorded over time and used to determine the redistribution of water in the vadose zone. When flow stops, water redistributes itself near the waterfront to reach an equilibrium between the saturated zone and the capillary fringe. The timing of flow stoppage is carefully selected to capture the redistribution of water in the specimen without being biased by the bottom or top filter material.

Figure 3-3 shows the pressure data recorded during the water flushing of Sand C column at a rate of 50 ml/min. The water movement through the different components of the setup, including the specimen, can be distinguished by the change in slope of pressure buildup over time.

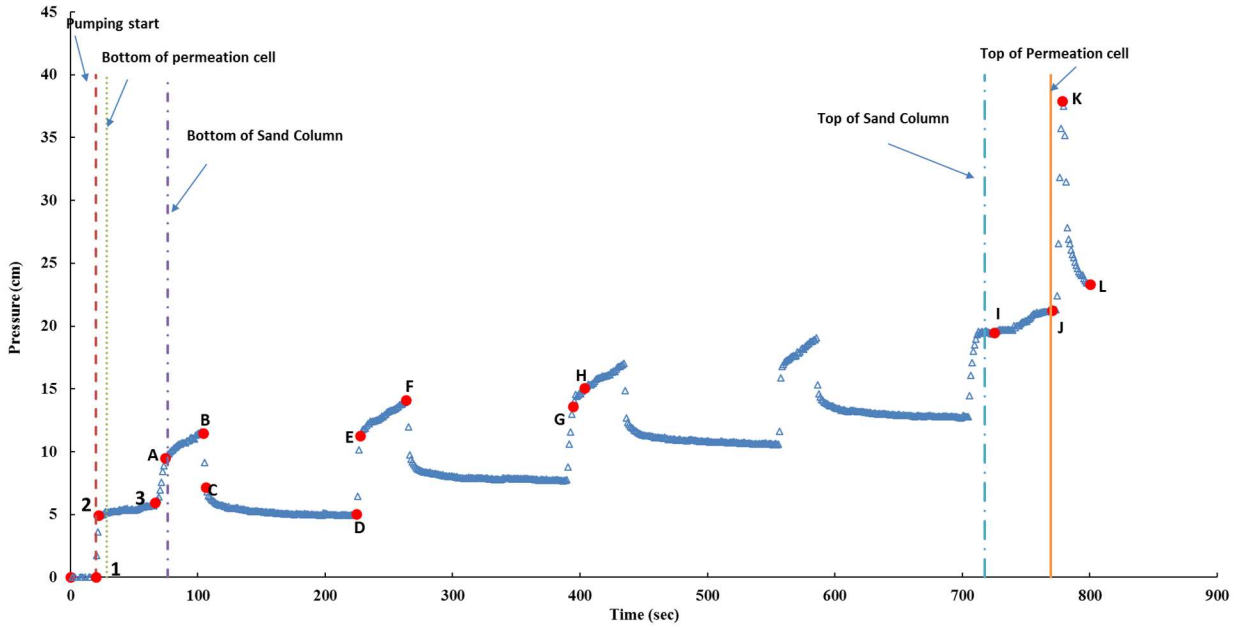

Figure 3-3: Pressure Data from Pressure transducer

The pump was turned on at the 20 seconds' mark and the following is a description of the pressure timeline as it relates to the different stages of the testing:

0 ➔ 1: The flat part of the curve is prior to start of flow. At this time, the water has filled the line up to the inlet point of the permeation cell;

1 ➔ 2: Water flow starts and it is propagating vertically in the tubing all the way up to the bottom of the filter material. Due to the small cross-sectional area of the tubing and inlet, the water level is increasing rapidly at the constant flow rate and resulting in a high rate of increase in pressure despite low resistance to flow;

2 ➔ 3: This flat part of the curve is when the waterfront is propagating through the filter material. The very high porosity of the filter material generates very slow rate of pressure buildup due to its low resistance to flow and needing more time to fill up the pore space to generate additional head pressure;

3 ➔A: The steep increase in pressure is due to the waterfront reaching the sand specimen which has a much higher resistance to flow and results in high buildup of pressure to maintain the constant flow;

A ➔ B: The waterfront reach the sand specimen at point A and continues propagating through the sand. The rate of pressure change depends on the porosity and unsaturated properties of the sand as well as flow rate;

B ➔ C: The Pump is turned off at the point B resulting in a sudden drop in pressure from point B to point C due to the loss of the pressure head that was built up to maintain the applied flow. This loss is instantaneous as soon as the pump is turned off;

C ➔ D: The water is redistributing from the saturated zone to the unsaturated zone. As the height of capillary fringe increases towards equilibrium, it is pulling water out from the saturated zone below. This water migration results in lowering the location of the waterfront which is reflected in a decrease of total pressure recorded by the pressure transducer (The magnitude of the drop along with its time rate are dependent on the unsaturated hydraulic properties of the tested sand).

D ➔ E: pump is turned back on at point D and the pressure increases instantaneously to point E. The total pressure at E is the head required to maintain the same constant flux at that time.

E ➔ F: The waterfront is progressing again through the sand specimen. There is a small curved portion right after E where the pressure is increasing at a higher rate than the remaining part of the E ➔ F segment. This higher rate of pressure buildup is due to the higher degree of saturation in the voids right above the waterfront due to water redistribution during flow stoppage (as compared to the degree of saturation above the waterfront during initial permeation). At a constant flow, voids with higher initial degree of saturation reaches full saturation faster resulting in faster increase in head pressure. The rate of pressure buildup then levels out at a similar slope to that from A➔B. The curved portion of the curve can be seen in the other times the pump was restarted after a stop, similar to between points G and H.

The water flow is stopped three additional times to obtain multiple records of pressure drop during water redistribution. The timing of flow stoppage is selected such that at the end of the last flow stoppage, the waterfront is short enough of the top filter to allow for a complete capillary rise without any interference from the top filter material.

I ➔ J: After reestablishing the flow following the final stoppage, the water front reaches the top of the sand specimen at point I and then propagates through the top filter at a slower rate, similar to that in the bottom filter from 2 to 3.

J ➔ K: water is filling up the outlet and associated vertical tube until the pump is shut off at K.

K ➔ L: After the sand column is completely flushed with water and the pump is stopped, the recorded instantaneous head loss is then used to determine the hydraulic conductivity of sand.

3.4.2 Inverse Modeling using Hydrus 1D

Inverse modeling is utilized to estimate the unsaturated hydraulic properties of material by fitting the hydraulic heads measured experimentally and simulated head data. In this study, an interactive software program called HYDRUS 1D was used to develop the one-dimensional finite element model for simulating the laboratory experiments. Hydrus1D use the Levenberg-Marquardt nonlinear minimization method for inverse modeling. Levenberg-Marquardt scheme use local gradient optimization algorithm (Marquardt, 1963) which is computational efficient compared to global optimization algorithms such as simulated annealing, stochastic approximation methods,

evolution algorithms, and genetic algorithms (Šimůnek et al., 2012). A comparison of using the Levenberg-Marquardt versus Global optimization algorithms is provided later in this paper in Section 4.2.

For the inverse modeling stage of the SEM method, a one-dimensional finite element model is developed using Hydrus 1D to simulate the sand column from the experimental testing stage and the same testing protocol is programmed. The governing flow and transport equations in Hydrus 1D are solved numerically using Galerkin type linear finite element schemes. Water movement in partially rigid saturated sand is described by a modified form of the Richard's equation (3-1) using the assumption that the air phase plays an insignificant role in the liquid flow process.

$$\frac{\partial \theta}{\partial t} = \frac{\partial}{\partial x}\left[K\left(\frac{\partial h}{\partial x} + cos\alpha\right)\right] - S \tag{3-1}$$

where h is the water pressure head [L], θ it the volumetric water content [L^3L^{-3}], t is time [T], x is the spatial coordinate [L] (positive upwards). S is the sink term [$L^3L^{-3}T^1$], α is the angle between the flow direction and the vertical axis and K is the unsaturated hydraulic conductivity function [LT^{-1}].

The soil hydraulic function proposed by Van Genuchten (1980) was used because its inversions are better for the sand than other functions (Schapp et al., 2003). Van Genuchten (1980) used the pore size distribution model of Mualem (1976) to obtain a predictive equation for the

unsaturated hydraulic conductivity function in terms of soil water retention parameters. The expressions of Van Genuchten (1980) are given by:

$$S_e = \frac{\theta - \theta_r}{\theta_s - \theta_r} \tag{3-2}$$

$$\theta(h) = \begin{cases} \theta_r + \dfrac{\theta_s - \theta_r}{[1 + |\alpha h|^n]^m} & h < 0 \\ \theta_s & h \geq 0 \end{cases} \tag{3-3}$$

$$K(h) = K_s S_e{}^l [1 - \left(1 - S_e{}^{\frac{1}{m}}\right)^m]^2 \tag{3-4}$$

$$m = 1 - 1/n \tag{3-5}$$

The above equations contain five independent parameters: θ_r and θ_s: the residual and saturated volumetric water contents, respectively; α is a scaling parameter inversely proportional to the pore diameter; n is a shape parameter of the soil water characteristic curve which is directly proportional to pore size distribution; and K_s is the saturated hydraulic conductivity. The pore connectivity parameter *l* in the hydraulic conductivity function (Equation (3-4)) is set to a value of 0.5 (Mualem, 1976).

These five parameters for the tested soil are determined through the inverse solution by minimizing the objective function. The objective function for this study is defined as the difference between the measured and modeled pressure generated at the bottom of sand column for the whole

testing protocol (during flow and when flow is stopped). Since Hydrus 1D uses the local optimization gradient method for parameter identification, an initial estimate of the unknown parameters is required. It should be noted that this minimization is sensitive to the initial values of the parameters and the final objective function may not be the global minimum but rather a local one if the initial values were off. Therefore, it is important to begin inverse parameter estimation with reasonable range of initial van Genuchten parameters (θ_s, θ_r, α, n and K_s) to determine global minimum instead of local minimum.

3.4.3 Forward Modeling for Initial Validation

A soil column of 18.143 cm was modeled in Hydrus1D with two materials: the tested sand and a filter material at the bottom and at the top of soil specimen. Predetermined θ_s, θ_r and K_s parameters from laboratory measurement were used for the model validation simulation. A range of values for parameters α and n were chosen based on the grain-size distribution of the sand and filter material (Ghanbarian-Alavijeh et al., 2010). Multiple realizations of the random parameters (α and n) were generated based on these ranges. The flow problem for each realization was solved using forward modeling in Hydrus 1D. Uncertainties of the objective function (difference in measured and simulated potential head) were evaluated by calculating the root mean square value. Figure 3-4 shows that the objective function is sensitive to both parameters, α and n. RMSE value reached a minimum for a range of α and n from 0.35 to 0.45 and 2 to 2.75, respectively. Based on these results, an initial estimate of the van Genuchten parameters can be determined for forward modeling (Table 3-2).

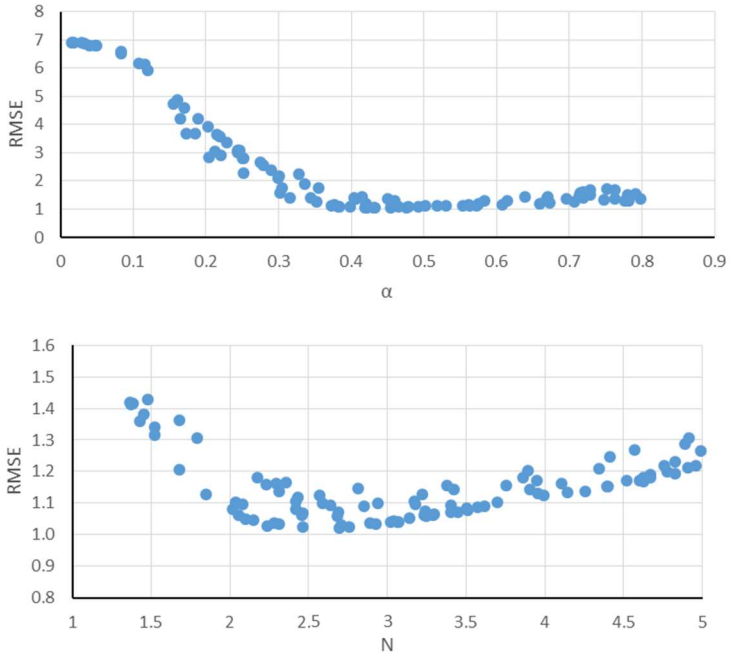

Figure 3-4: multiple realization of parameter alpha and n for Test 1

Table 3-2: Initial guess if Van Genuchten parameter of material's hydraulic function

Layers	Thickness (cm)	Material type	θr	θs	Alpha (1/cm)	n	Ks (cm/sec)	l
1	3.269	Bottom Filter	0.016	0.438	1.00	3.00	0.024	0.5
2	12.962	Sand A	0.001	0.416	0.40	2.25	0.395	0.5
3	1.912	Top Filter	0.010	0.650	1.00	3.00	0.038	0.5

The simulation was initiated with a relatively dry soil column at an initial volumetric moisture content of 0.07. The multistage flushing experimental protocol was simulated in Hydrus 1D by applying a variable flux boundary condition at the bottom of soil column. The top boundary surface of soil column is set at constant pressure equal to the atmospheric pressure with surface run off. Figure 3-5 shows a good general agreement between the results obtained from Hydrus1D simulation and the experimental data. The pressure recorded at the bottom of the soil column is equal to the sum of hydrostatic pressure (positive, equal to the elevation of the waterfront) and head loss due to flow (positive, and zero when pump was off). It should be notes that these results were obtained based on the estimated values of α and n along with the measured porosity (same as saturated volumetric water content) and saturated hydraulic conductivity of the sand without performing any inverse modeling analysis. These initial values can be used as the starting point for inverse modeling to ensure that optimization is providing accurate outcome and not a random local minimum.

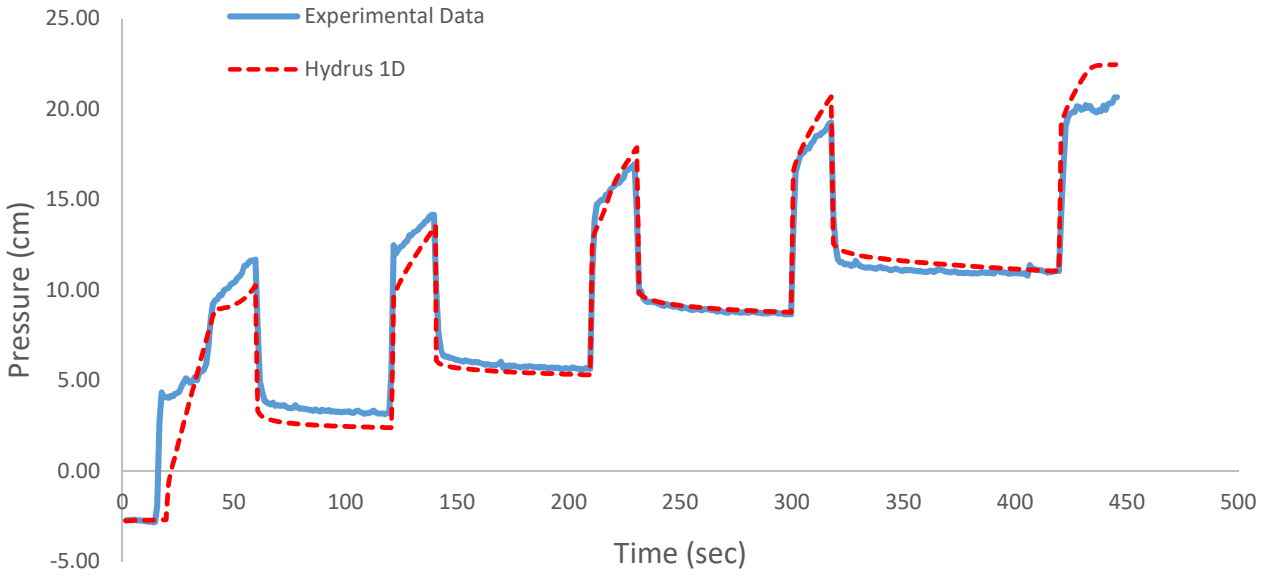

Figure 3-5: Pressure versus Time data by Hydrus 1D and laboratory results

3.5 Results

The van Genuchten parameters (α, n, θ_r, θ_s and K_s) for the three different soils were determined using the SEM method. The results were obtained from multiple tests on each sand at different flow rates. These results were then used to determine the SWCC for each of the materials. The SWCC for Sand b and Sand C was determined from the hanging column test as well.

3.5.1 Inverse modeling Results

Unsaturated hydraulic properties of materials were determined using the inverse modeling for experimental tests listed in Table 3-3 were repeated thrice and the reported porosity and hydraulic conductivity are the average values of these repetitions. The average porosity is

calculated from the weight and height measurement recorded while preparing each column. The hydraulic conductivity is calculated using the measured head difference required to maintain constant flux after the sample was completely flushed with water. The saturated hydraulic conductivity of the used materials was determined independently using the falling head hydraulic conductivity test and are included for reference.

Table 3-3: List of experiment tests performed

Test Name	Sand column material	Flow rate (ml/min)	Average Porosity*	Hydraulic Conductivity (cm/s)*	Saturated Hydraulic Conductivity (cm/s)
Test 1	Sand A	100	0.414	0.122	
Test 2	Sand A	50	0.416	0.106	0.395
Test 3	Sand A	25	0.413	0.153	
Test 4	Sand B	100	0.345	0.057	
Test 5	Sand B	50	0.346	0.064	0.058
Test 6	Sand B	25	0.364	0.063	
Test 7	Sand C	100	0.362	0.060	
Test 8	Sand C	50	0.366	0.065	0.086
Test 9	Sand C	25	0.377	0.065	

* the reported values are the average of at least three tests under same conditions.

The inverse solution is obtained using the pressure data obtained from one pressure transducer attached to the bottom of sand column in laboratory test. Initial and boundary conditions for laboratory tests were well defined which were simulated using Hydrus 1D. Initial values of van Genuchten parameters were determined from model calibration to obtain pressure values at the bottom of sand column close to experimental data. Then these parameters were used as initial guess for inverse modeling to determine the van Genuchten parameter of material by best fitting

numerical results to predicted data. Because of the nonlinear nature of Richard's equation, an iterative process is used to obtain solution for global matrix equation at each new time step. For every iteration, system of linearized algebraic equations is derived and solved. After inversion, the parameters are re-evaluated using the first solutions and new equations are again solved. This iterative process continues until a satisfactory convergence is obtained with the change in pressure head at all nodes between two successive iterations becomes less than the imposed pressure head tolerance value of 0.5cm. Water content tolerance value of 0.001 was used in this study. The maximum number of iterations allowed was capped at 50 for this study to minimize the calculation time. However, none of the simulations required all 50 iterations for convergence to occur.

The results obtained from the inverse modeling fitted the experimental data for the three sands with an average R^2 value greater than 0.95. The parameters were accepted as best fit only if the standard error for each coefficient was acceptable and within 95% confidence upper and lower limit, regardless of a good RMSE value. The mass balance error for all simulations were less than 0.001% which indicates the accuracy of model. Parameter estimations using SCE method are within 5% of those obtained from Levenberg-Marquardt method for all materials.

Table 3-4 shows the averaged van Genuchten parameters for Sand A, Sand B and Sand C obtained from inverse modeling for flow rate of 100ml/min, 50 ml/min and 25 ml/min. The tests permeated at100mL/min were analyzed using the LM and SCE optimization methods. The parameters obtained from each of the three repetitions were within 2.5% of the average value.

The results obtained from the inverse modeling fitted the experimental data for the three sands with an average R^2 value greater than 0.95. The parameters were accepted as best fit only if the standard error for each coefficient was acceptable and within 95% confidence upper and lower limit, regardless of a good RMSE value. The mass balance error for all simulations were less than 0.001% which indicates the accuracy of model. Parameter estimations using SCE method are within 5% of those obtained from Levenberg-Marquardt method for all materials.

Table 3-4: Van Genuchten Parameters estimated from Inverse solution

Test Name	Material	Optimization Method	Flow Rate (ml/min)	θ_r	θ_s	α (1/cm)	n	K_s (cm/s)	R^2*
Test 1	Sand A	SCE	100	0.031	0.428	0.381	2.55	0.450	0.98
Test 1		LM	100	0.033	0.425	0.378	2.62	0.448	0.97
Test 2		LM	50	0.032	0.432	0.373	2.08	0.500	0.98
Test 3		LM	25	0.032	0.432	0.377	2.34	0.450	0.98
Test 4	Sand B	SCE	100	0.060	0.310	0.085	2.61	0.050	0.98
Test 4		LM	100	0.060	0.300	0.077	2.71	0.055	0.97
Test 5		LM	50	0.060	0.301	0.088	2.56	0.056	0.94
Test 6		LM	25	0.058	0.309	0.110	2.35	0.057	0.96
Test 7	Sand C	SCE	100	0.052	0.356	0.041	3.95	0.085	0.94
Test 7		LM	100	0.051	0.340	0.039	4.00	0.090	0.94
Test 8		LM	50	0.053	0.370	0.044	4.29	0.088	0.91
Test 9		LM	25	0.053	0.390	0.041	4.29	0.087	0.91

* R^2 is a statistical measure of how experimental data close to the computed values.

3.5.2 Hanging Column Test Results

The hanging column test is the most commonly used method for determining the SWCC curve for sands with expected suction less than 70 kPa. Therefore, hanging column tests were performed on the three sands to obtain their unsaturated properties following current procedures for reference. Figure 3-6 shows the van Genuchten fit to the hanging column head and water content data for Sand B and Sand C tested at the same saturated volumetric moisture content as predicted from the inverse modeling. It was difficult to perform hanging column test on Sand A because of its larger grain size.

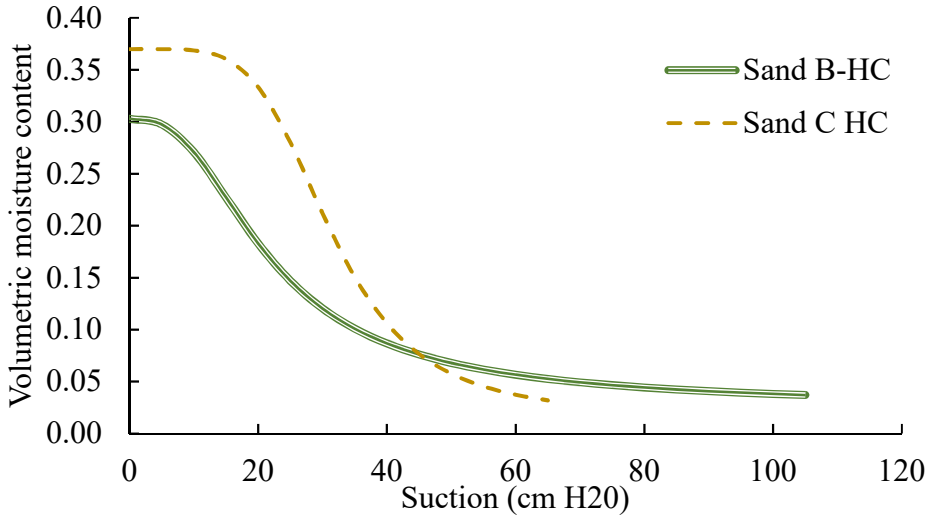

Figure 3-6: Hanging Column results of Sand B and Sand C

3.6 Analysis

3.6.1 Optimization of the Inverse Modeling

As mentioned earlier, Hydrus1D use the Levenberg-Marquardt nonlinear minimization method for inverse modeling. This minimization scheme use local gradient optimization algorithm (Marquardt, 1963) which is computationally efficient compared to global optimization algorithms. However, this method requires inputting an initial estimate of the unknown parameters and the minimization outcome is sensitive to these values (might provide a local rather than a global minimum). On the other hand, the global optimization algorithms provide more consistent global minimum value but on the expense of additional computational requirements. The results from the Levenberg-Maquardt (LM) and the Shuffle Complex Evolution (SCE) are compared in this section to determine if using the higher complexity analysis would improve on the results.

Hydrus 1D can optimize up to 15 parameters. However, the problem becomes non unique as the number of optimized parameters increase, particularly when using the LM optimization method. In this paper, the proposed optimization method was performed in two steps to minimize the number of unknown parameters per optimization. The first optimization was performed to determine the residual moisture content (θ_r) along with α and n parameters for each material (for a total of 6 optimized parameters). For this stage, the value of the saturated volumetric moisture content (θ_s) and saturated conductivity (K_s) are input as known properties based on available experimental data. For the second stage, θ_s, α and K_s are optimized to obtain minimum root mean square error (RMSE).

The results obtained from the inverse modeling fitted the experimental data for the three sands with an average R^2 value greater than 0.95. The parameters were accepted as best fit only if the standard error for each coefficient was acceptable and within 95% confidence upper and lower limit, regardless of a good RMSE value. The mass balance error for all simulations were less than 0.001% which indicates the accuracy of model. Parameter estimations using SCE method are within 5% of those obtained from Levenberg-Marquardt method for all materials.

Table 3-4 showed the van Genuchten parameters for Tests 1, 4 and 7 obtained from Levenberg-Marquardt (LM) optimization scheme and the SCE optimization scheme. The local optimization method gave a solution very similar to that obtained by the SCE method. The results from both optimizations for Test 1, along with the experimental data, are shown in Figure 3-7 for comparison.

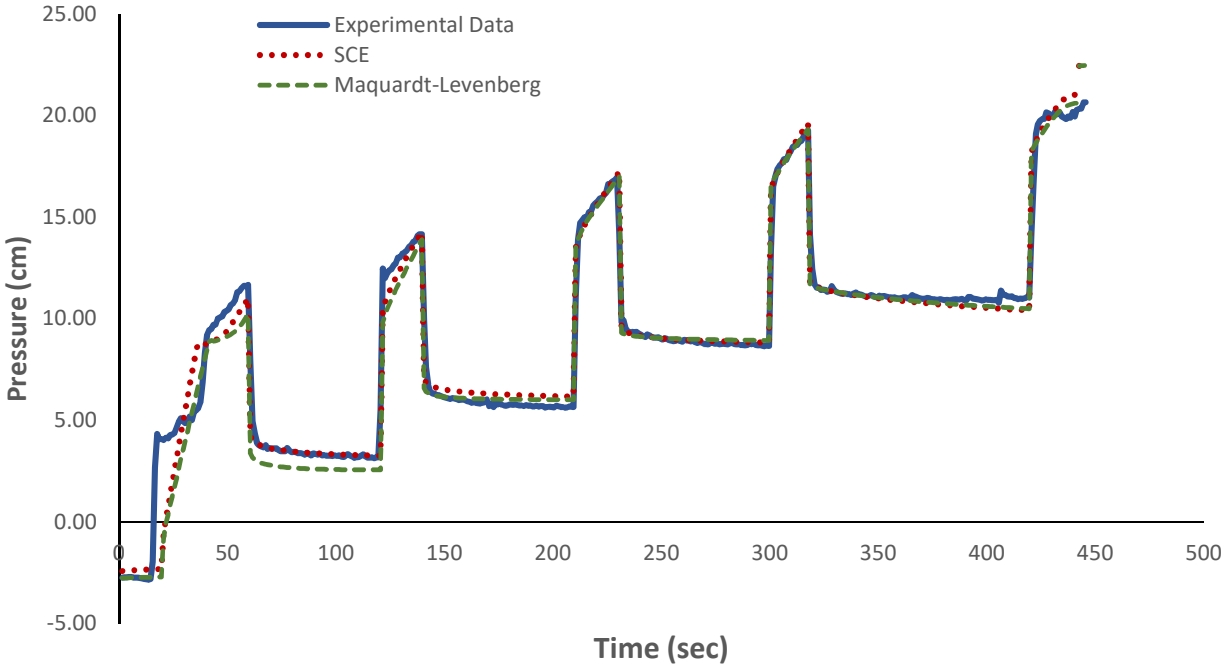

Figure 3-7: Comparison of pressure-time data obtained experimentally, by Levenberg-Marquardt technique and by SCE technique

Global optimization algorithms play powerful role for field-scale problem where multiple soil horizon or uncertain initial and boundary conditions are involved and if fitting parameters are large (Bäck, 1996; Zhang et al., 2010). However, the experiments in this study have well defined boundary conditions as well as uniform layers of soil with some known parameters (θs, θr and Ks). If we combine this information with reasonable initial estimates of the three van Genuchten parameters, results obtained from Levenberg-Marquardt method can be as reliable as those obtained from the SCE method.

3.6.2 Comparison between SEM and hanging column results

Table 3-5 shows that predicted unsaturated hydraulic parameters using the SEM method are comparable to those obtained from hanging column test. The value for each parameter from inverse modeling results is calculated as the average value of that parameter for all three different flow rates. Figure 3-8 shows the soil water retention curves for Sand B and Sand C as determined from the SEM method and the hanging column test along with that for Sand A as obtained from the SEM method only. The curves agree for the most part with the hanging column predicting suction values as the volumetric water content decreases. It was difficult to perform hanging column test on material Sand A because of very low value of suction (due to lack of fines). However, Sand A was tested using the SEM method without the need to modify the testing protocol. The ability to test Sand A highlights the extended range of sands that can be tested using this new technique compared to the hanging column test.

Table 3-5: Comparison of van Genuchten parameters from SEM and hanging column methods

Sand		θ_r	θ_s	α	n
Sand C	Predicted	0.052	0.370	0.041	4.19
	Hanging Column	0.017	0.370	0.03	4.97
Sand B	Predicted	0.059	0.303	0.091	2.54
	Hanging Column	0.024	0.303	0.060	2.75

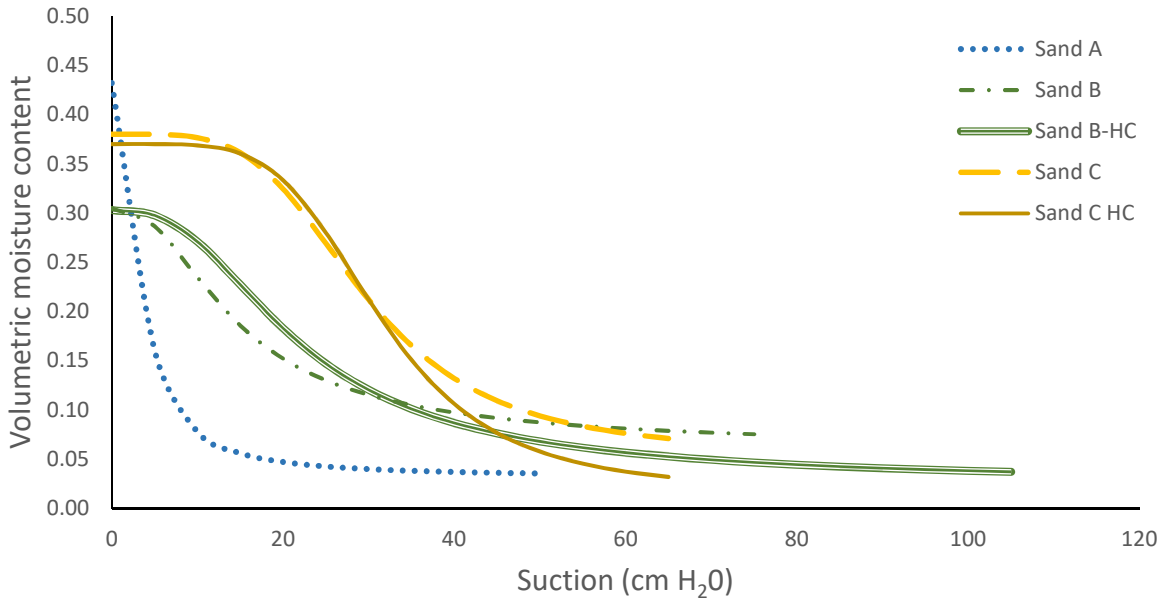

Figure 3-8: SWRC curve of Sands from inverse modeling and hanging column test

3.6.3 Water Redistribution during No-Flow

The simplified experimental setup proposed in this method does not require the installation of any sensors other than the pressure sensor at the inflow line. This implies that the spatial and temporal variation of water content cannot be captured using direct measurements. However, such information can be obtained from the Hydrus 1D modeling and can be validated using the pressures recorded during flow as well as after stoppage of flow. An example of such data is shown in Figure 3-9 from modeling Test 1. Figure 3-9(a) shows the water front and unsaturated fringe propagation with time during flow. The water front at any given time can be determined as the point of deviation from the constant volumetric water content (equal to the saturated one). Figure 3-9(b) shows the redistribution of water from the saturated zone to the unsaturated zone resulting in a drop in the water front level and an increase in the water content in the soil above it. Figure 3-9(c)

shows the change in water content profile as the flow starts again. It is worth noting that the increase in water front in the first 3 seconds in Figure 3-9(c) is larger than that in Figure 3-9(a) due to the higher degree of saturation in the soil above the water front when flow is resumed compared to before flow stopped. This confirms the observation made in Figure 3-3 between points G and H.

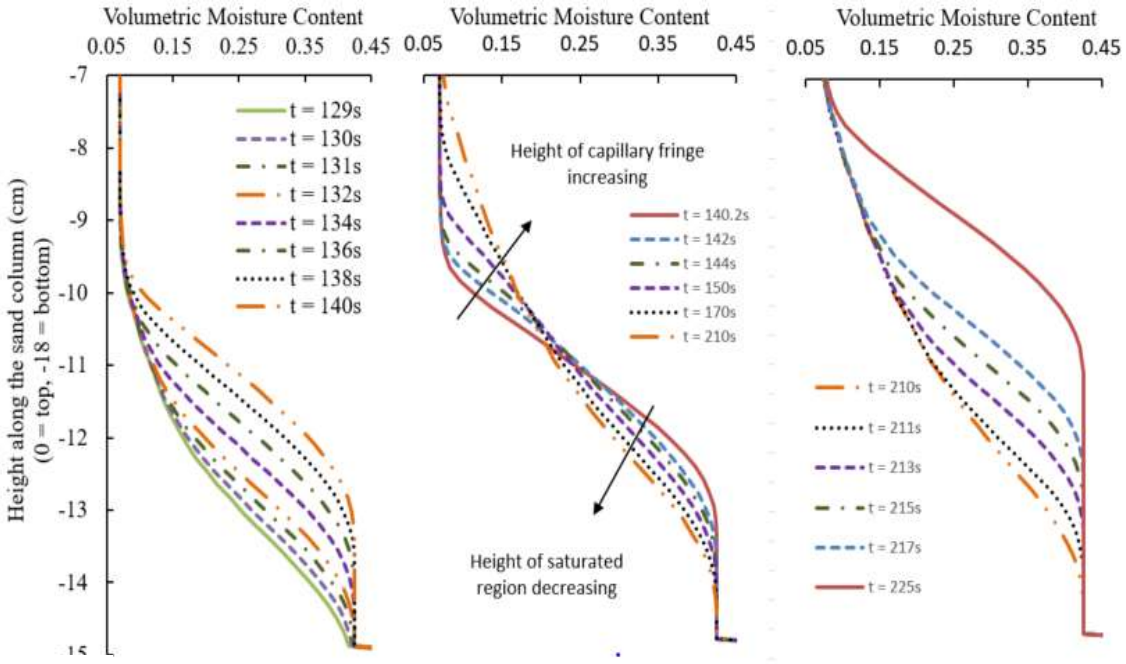

Figure 3-9: Movement of water when (a) pump is on before any stoppage of flow(b) pump is turned off at t = 140.2s (c) pump is turned back on at 210.5s

Figure 3-9 shows the drop-in elevation of the saturated region (water front location) over time after the flow has stopped as obtained from the Hydrus 1-D modeling. The drop in total head recorded experimentally after the flow ceases is also included on the same plot. This drop excludes the instantaneous total head loss due to flow stoppage (B➔C in Figure 3-3). The results show that

the time-dependent pressure drop recorded experimentally matches with the decrease in elevation of the saturated front. These results validate the previous analysis of the pressure changes observed in Figure 3-3 as well as the ability of Hydrus 1D inverse modeling to capture the water special and temporal distribution along the height of the column.

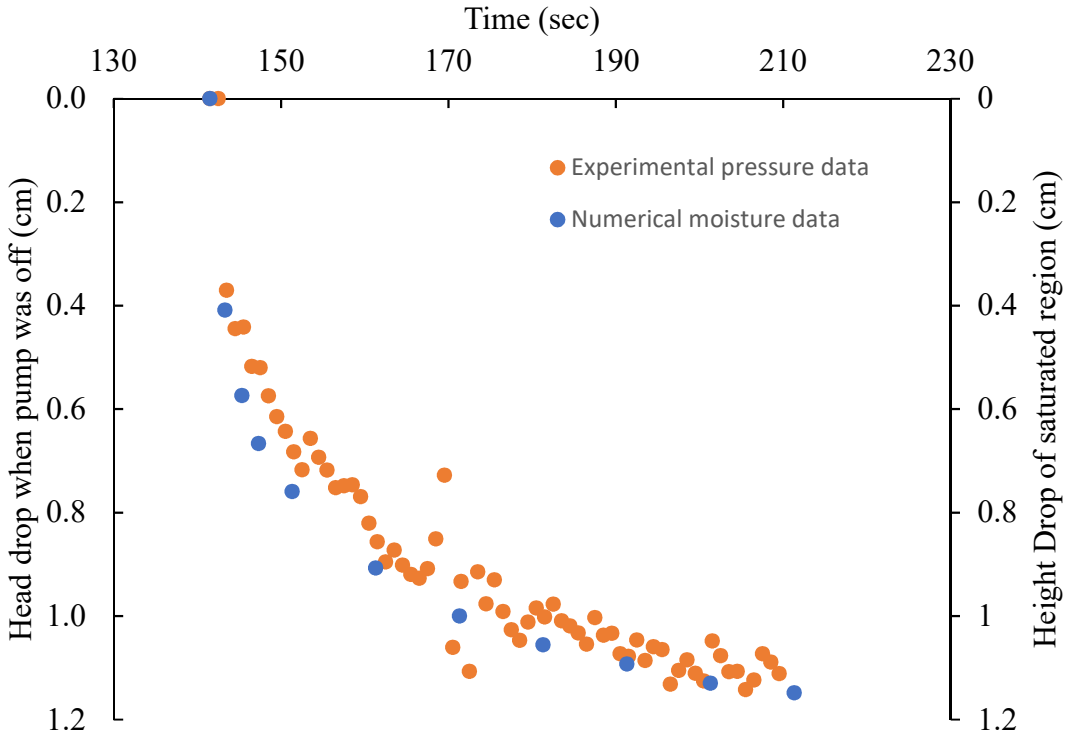

Figure 3-10: Decrease in total head and height of saturated region when flow stops

3.7 Conclusions

In this paper, simple method is proposed to determine the unsaturated hydraulic properties of sandy soil using a combination of experimental testing and inverse numerical modeling. An unsaturated sandy soil specimen is subjected to a multistage constant flux flushing while recording pressure buildup at the base of the specimen. The multistage flushing includes consecutive stages of flow and no flow to allow for capturing the water redistribution between the saturated and unsaturated zone. The experimental protocol is then simulated using Hydrus 1D and the unsaturated hydraulic parameters were estimated using two optimization techniques (Levenberg-Marquardt and Shuffled complex evolution).

The experimental testing required for the proposed method can be performed using rigid wall/flexible wall permeameter as well as on triaxial specimens with minor modifications to existing setups. This makes it feasible for most geotechnical lab to perform this testing without having to invest in major new equipment.

The Levenberg-Marquardt optimization method provided reasonable results and is recommended for inverse modeling of these laboratory test, where boundary conditions and initial values of θ_r, θ_s and Ks were known from laboratory measurement. A reasonable estimation of the initial values of the van Genuchten parameters make the optimization converge in reasonable number of iterations, which reduces the computational time needed.

Simulated pressure head values from optimized van Genuchten parameter fitted very well with predicted one. Predicted van Genuchten parameters are in reasonable range of parameters obtained using the conventional hanging column test. The spatial and temporal changes in volumetric moisture contents were obtained by combining the Hydrus 1D modeling with pressure measurements at the base of the sand column, without the need to install additional sensors along the height of the specimen.

It was difficult to obtain van Genuchten parameters and SWCC for Sand A using the hanging column test because of very low suction values due to lack of fines. However, with the SEM method, the unsaturated hydraulic properties of Sand A were obtained without the altering the testing procedure. Therefore, despite the simplicity of the experimental testing procedure for the SEM method, it allows for testing properties of materials with very low suction, which wouldn't have been possible with the hanging column test method.

CHAPTER 4 RAPID CHECK TO DETERMINE THE HOMOGENEITY OF A SPECIMEN IN LABORATORY

4.1 Abstract

When reconstituting sand specimens for laboratory testing, researchers try to achieve the same void ratio as expected in the field. Generally, the void ratio is reported as a single value for the whole specimen. However, the distribution of local void ratio rather than a single average value is more pertinent to the mechanical behavior of sand, particularly if the specimen was not uniform. Inconsistency in experimental results for specimens of same relative density can be caused by local heterogeneity, which is not commonly measured. Ideally, the local distribution of void ratio along the height of a specimen would be determined for each test; however, this is not practically feasible with the existing methods for measuring local variability in void ratio. Most of the existing methods to determine the pore structure of a soil specimen do not allow to further use the specimen in any experimental testing, and therefore, these methods evaluate a specimen preparation procedure rather than providing individual variability in void ratio of a particular specimen being tested (and thus, any potential for operator errors on a given specimen). This study introduces a simple method to determine the spatial variability of pore space within a sand specimen as an intermediate step that can be incorporated into existing experimental testing procedures. The only limitation on this approach is that it can't be performed on water sedimented specimens that are already saturated. The proposed testing method consists of flushing water through a specimen from the bottom to the top under constant flux while recording the pressure at the injection point using a low range pressure transducer (a transducer with a ±2psi range was used in this study). When flushing under a constant flow rate, the increase in pressure over a period of time (corresponds to

the increase in water front elevation) can be converted to a change in void ratio with the knowledge of the specimen diameter. The measurement of the distribution of pore space obtained from this method reflects the arrangement of soil particles after reconstitution is completed, which may differ from incremental measurements during specimen preparation due to rearrangement of particles in lower layers while reconstituting the upper layers within a specimen. For the uniform specimens tested in this study, the local porosity varied within 10 percent to the average porosity of the whole specimen. The effectiveness of the new proposed method to capture void ratio changes under ideal conditions was verified using Hydrus 1Dnumerical modeling. The newly proposed rate of pressure increase (RPI) method is a quick and easy method to check the homogeneity of every specimen prepared in the laboratory as an intermediate step in specimen preparation that can provide insightful information on the uniformity of each tested specimen.

4.2 Introduction

The void ratio is a critical factor to various engineering properties of sandy material. In most cases, a unique value of void ratio is determined for the whole specimen. However, the specimen response can be controlled by the local void ratio distribution rather than the average value, particularly when the specimen is not uniform. For instance, the drained or undrained behavior of cohesionless soil is dominated by the loosest or the densest portion of void distribution (Frost and Jang 2000); same soil with identical void ratio demonstrates different liquefaction potential (Lee et al., 1999). The distribution of local void ratio is an important parameter that affects the geotechnical properties (shear strength, hydraulic conductivity, etc.) of granular material. Many researchers rely on preparing the reconstituted specimen of the cohesionless soil for laboratory testing. Various methods like dry pluviation, wet pluviation, slurry deposition,

vibration or moist tamping have been developed to obtain homogenous reconstituted specimens in the laboratory. Ibrahim and Kagawa (1991) examined the effect of the specimen preparation on the void ratio of sand and found that the dry pluviation tended to produce a larger deviation of local void ratio than wet tamping for samples prepared at same relative density. A major challenge to getting consistent results from the laboratory tests is to achieve a homogenous soil sample every time. Therefore, information about the spatial variability in the void ratio are required for the accurate experimental data interpretation.

Different methodologies have been used to determine the distribution of local void ratio along the height of soil specimen. Typically, void ratio is calculated from the specific gravity of the soil, the volume of the specimen and the weight of soil (water content is required as well if the soil is wet). These measurements can be done per section of the specimen or as an average number for the whole specimen. However, the sectional calculations usually count on measurements performed during specimen construction, which ignores the disturbance caused to these sections while preparing adding the layers on top. Oda (1976) presented the first attempt to quantify the local void ratio (porosity) distribution of particulate materials from magnified 2D images of the grains. Later researchers have used digital image analysis in the study of cohesionless soil fabric (Bhatia and Soliman 1990); clay microstructure (Smart et al. 1992); and fluid permeability of porous material (Berryman and Blair 1986). Bhatia and Soliman (1990) used Oda's method to measure local void ratio distribution from the 2D plane sections with the aid of an image analyzer. The global void ratio of soil specimen used by Bhatia and Solomon (1990) was 1.02, but the mean value of local void ratio was determined to equal to 0.59. Kuo and Frost (1996) modified Oda's method and found mean local void ratio equals to 0.954 close to global void ratio with a standard deviation of 0.323. These techniques required high-level image processing and can only provide

local void ratios during specimen construction (need access of the sand surface to image) rather than after completion of specimen preparation. Magnetic resonance imaging (Amin et al.,1998; Hedberg et al., 1993) and x-ray tomography (Andersson et al., 1990; Peyton et al. 1992) have been used to identify small features such as small fissures and cracks. These techniques provide small scale resolution but are very expensive and not widely available and require transferability of the specimen to the imaging facility, which can be challenging for sandy specimens. Ayoubian and Robertson (1998) froze the samples at different stages of triaxial extension tests to measure the void ratio distribution along the length of the specimens. Different samples were used to compare the change in the void ratio at the various stages, a procedure that ignores the variation in void ratio from one specimen to another. The electromagnetic (EM) wave propagation method (EM-wave based technique) is an economical alternative and has the advantage of being non-destructive (Cho et al., 2004). Dong and Wang (2005) also used (EM) wave propagation method for saturated sand and found the standard deviation of 0.356 for local void ratio distribution. However, this methodology requires specialized equipment and skilled labor.

This chapter presents a simplified test procedure, the rate of pressure increase (RPI) method, to determine the spatial variation of void ratio along a specimen height. The preliminary results obtained from experimental and numerical modeling shows that the RPI method is reliable while still being economical and fast. It is a non-destructive method to check the homogeneity of the unsaturated soil by determining the variation of void ratio throughout the specimen before performing any laboratory tests. The method consists of flushing a soil column with water using a constant flux pump while recording the pressure buildup at the inlet. The rate of change in pressure at the inlet is a function of the void ratio, particularly at slow flow rates where the change in head to maintain flow over a short time increment is minimal. The chapter describes the experimental

setup and proposed procedure for the RPR method and provides the conceptual framework to determine the homogeneity of soil specimen by analyzing the change in the rate of pressure increase pressure. The method is verified by simulating the similar experimental setup numerically using Hydrus 1D.

4.3 Material and Experimental setup

4.3.1 Materials

Fiver different coarse materials (Sand A, Sand B, Sand C, Sand D and Sand E) were used in this study. Table 4-1 summarizes the index properties of tested soils based on ASTM standards (ASTM D422, D854, D4253 and D4254) and Figure 1 shows their grain size distribution. Filter material was used between the water inlet and the bottom of the specimen to obtain a uniform waterfront through the whole cross-sectional area of the specimen. Gravel (with particle sizes between 4.75mm and 10mm) and blast sand (with particle sizes between 1.2mm and 1.7mm) were used for the two-layer filter material at the top and bottom of the sand. De-aired distilled water was used in this study to reduce the inclusion of air while flushing with water.

Table 4-1: Index Property of tested sands

Material	Gs	D_{10}(mm)	D_{30}(mm)	D_{50}(mm)	D_{60}(mm)	Cu	Cc
Sand A	2.70	2.40	2.40	2.40	2.40	1.00	1.00
Sand B	2.65	1.10	1.50	1.80	1.90	1.73	1.08
Sand C	2.65	0.35	0.39	0.41	0.50	1.43	0.87
Sand D	2.65	0.25	0.37	0.40	0.45	1.80	1.22
Sand E	2.60	0.20	0.25	0.30	0.38	1.90	0.82

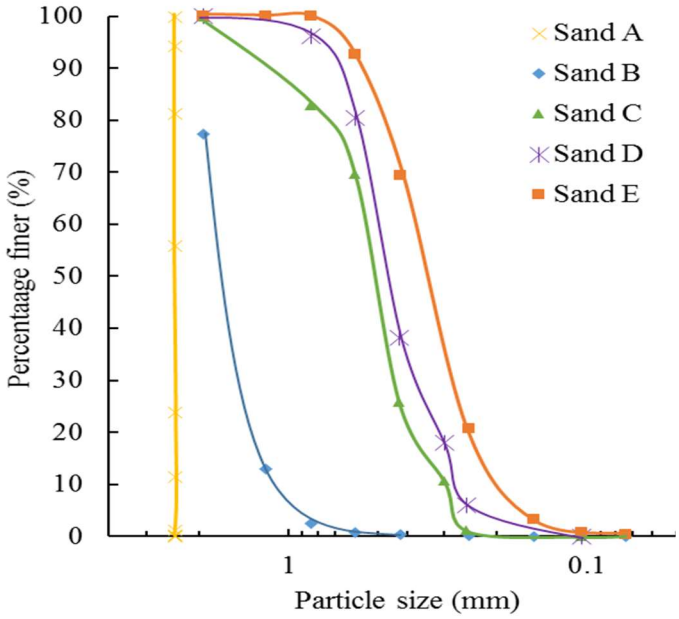

Figure 4-1: Grain size distribution of materials used for this study

4.3.2 Experimental Setup

The new proposed method can be performed as an intermediate step in the specimen preparation process for most of existing geotechnical testing setups (such as triaxial tests, resonant column test, flexible and rigid wall hydraulic conductivity tests,). It requires the addition of a

digital pressure sensor at the inflow line connected to the base of the specimen and a constant flux pump to flush out the specimen. Multiple methods have been used in the literature to reconstitute sand specimens for geotechnical laboratory testing. The dry funnel deposition method was used for this study to generate the dry specimens. The proposed method cannot be used on specimens prepared using water pluviation deposition method or any modification of it that would result in a nearly saturated specimen at the end of reconstitution. However, it can be used with methods generating partially saturated specimens (such as moist tamping) as long as good record of moisture content versus depth is recorded. The results presented in this chapter were obtained from tests performed on a 61 cm (2-foot) long cylindrical rigid wall permeameter shown in

Figure 4-2 (a setup typically used for testing groutability of soils). The rigid wall permeameter was chosen for these proof-of-concept tests because of the simplicity of specimen preparation compared to flexible wall permeameters or triaxial specimens. Peristaltic adjustable pump manufactured by Stenner pump company (model 85MPH40) and Validyne differential pressure transducer (range $\pm 2psi$)was used in this study.

The transparent cell of the permeameter consists of four 15.24 cm height cylinders stacked on the top of each other with a 3.81 cm cylinder at the top and another at the bottom. The bottom and top 3.81 cm cylinders are filled with filter material to provide uniform supply and drainage of water. Because of the length of the permeameter cell, the soil column was prepared in sections of 15.24 cm to have better control on the uniformity of the prepared specimen. This was possible because of the unique configuration of the clamping system which allows each of the 15.24 cm cylinders to be clamped down individually and filled with sand before the one on top of it is added. Multiple measurements of weight and volume of soil poured in each section was recorded to

determine the void ratio distribution using the traditional weight-volume calculations. The prepared soil column was then flushed with CO_2 to replace the air present in the pore space.

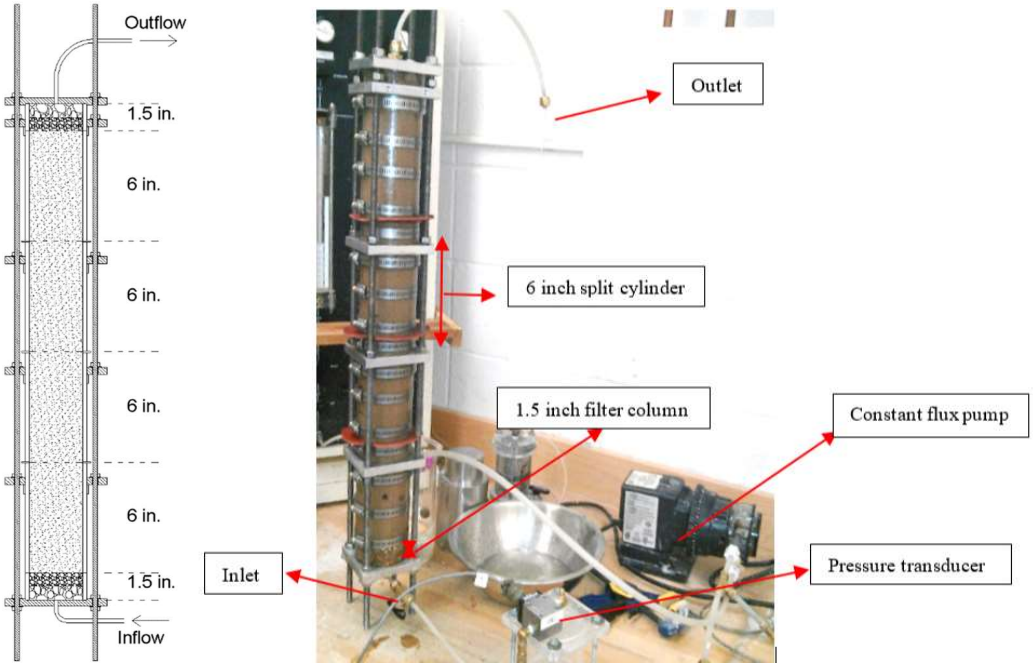

Figure 4-2: Constant flux water infiltration experimental setup

4.4 The RPI Method

The newly proposed RPI method consists of two stages: 1) Experimental testing and 2) Analysis. In the experimental testing phase, a specimen is flushed with water at a constant low flow rate and the pressure buildup is recorded over time. The recorded pressure values are then analyzed to determine the change in the rate of pressure increase and use that to back-calculate the void ratio values along the height of the specimen.

4.4.1 Experimental Procedure

After completion of the specimen preparation described earlier, the column is flushed with water at a constant flux while recording the pressure buildup at the bottom of the permeation cell. For shorter specimens or slower data acquisition systems, a slower flow rate can increase the resolution of the void ratio distribution. Under low flow rates, the head difference required to maintain the flow is small, particularly, over a short period of time. Therefore, the change in pressure is a good representation of the change in the water front level in the specimen. Waterfront is the interface between the saturated and unsaturated regions. If the specimen is relatively uniform, then the height of capillary fringe (unsaturated zone) will remain the same as the waterfront propagates through the specimen (at least until the capillary zone reaches the top filter material). The rate of propagation of the waterfront depends on the pore size distribution of soil column and total cross-sectional area for dry sands (in case of moist specimens, the existing water content should be accounted for as well). Hence, the rate of pressure build-up depends on the void ratio of the specimen, considering that the area is constant in a rigid wall setup. The homogeneity of a soil column can be determined by analyzing the consistency of the rate of pressure buildup with time as the waterfront propagates along the specimen height.

A column is prepared with four different sands (Sand B, Sand C, Sand E and Sand A, respectively from bottom to top) to demonstrate the impact of change in void ratio of a specimen on the rate of pressure buildup. The top of Sand A didn't reach the top of the permeameter, leaving a vertical section of empty tube that will be tested as well. Three measurements of the specimen diameter and the section height were made with the use of vernier calipers. The void ratio of each section was determined by the following formula:

$$e = \frac{V_v}{V_s} \tag{4-1}$$

where e is the void ratio, V_v is the volume of voids and V_s is the volume of solids. The total volume of the section was calculated by taking the average diameter and height of the specimen. The volume of solids was found by multiplying the weight of the sample by the density of the soil, and the volume of voids was found by subtracting the volume of solids from the total volume. Packing of soil particles depends on the drop height for dry pluviation method. Each experiment was performed at a drop height of 1 cm to maintain the uniform relative density. Table 4-2 shows the result of porosity along the soil column of multiple sand layers determined by the conventional method. The relative standard deviation is a standardized measure of the difference in the porosity obtained while reconstituting the sample through dry pluviation. Deviation in porosity was found to be small, within 2.5 percent for all soil types.

Table 4-2: Porosity along the soil column of Test 1 determined using the conventional method

Materials	Height of center of soil layers from injection point (cm)	Weight of soil poured (g)	Height of specimen poured (cm)	Volume of voids (cm^3)	Porosity	Average Global Porosity	Relative Standard Deviation
Sand B	2.15	288.18	4.31	70.55	0.398	0.410	2.01%
	5.26	316.29	4.85	82.36	0.413		
	10.40	411.68	6.32	107.38	0.413		
	16.01	175.03	2.73	47.36	0.422		
Sand E	18.73	172.69	2.70	44.65	0.402	0.418	1.40%
	21.63	227.85	3.71	65.09	0.426		
	25.57	301.47	4.83	82.64	0.416		
	30.02	169.67	2.95	56.19	0.427		
Sand C	33.13	239.59	3.72	62.70	0.409	0.399	2.53%
	36.77	222.33	3.30	51.83	0.382		
	40.21	259.50	4.01	66.89	0.406		
	44.28	283.99	4.32	70.74	0.398		
Sand A	48.78	331.33	5.25	90.73	0.421	0.420	0.79%
	53.98	318.61	5.00	85.40	0.415		
	59.31	421.48	6.71	116.93	0.424		

Figure 4-3 shows a schematic of the sand column as well as the readings of the pressure transducer as water flushed through the whole setup and flushed out of the top water outlet.

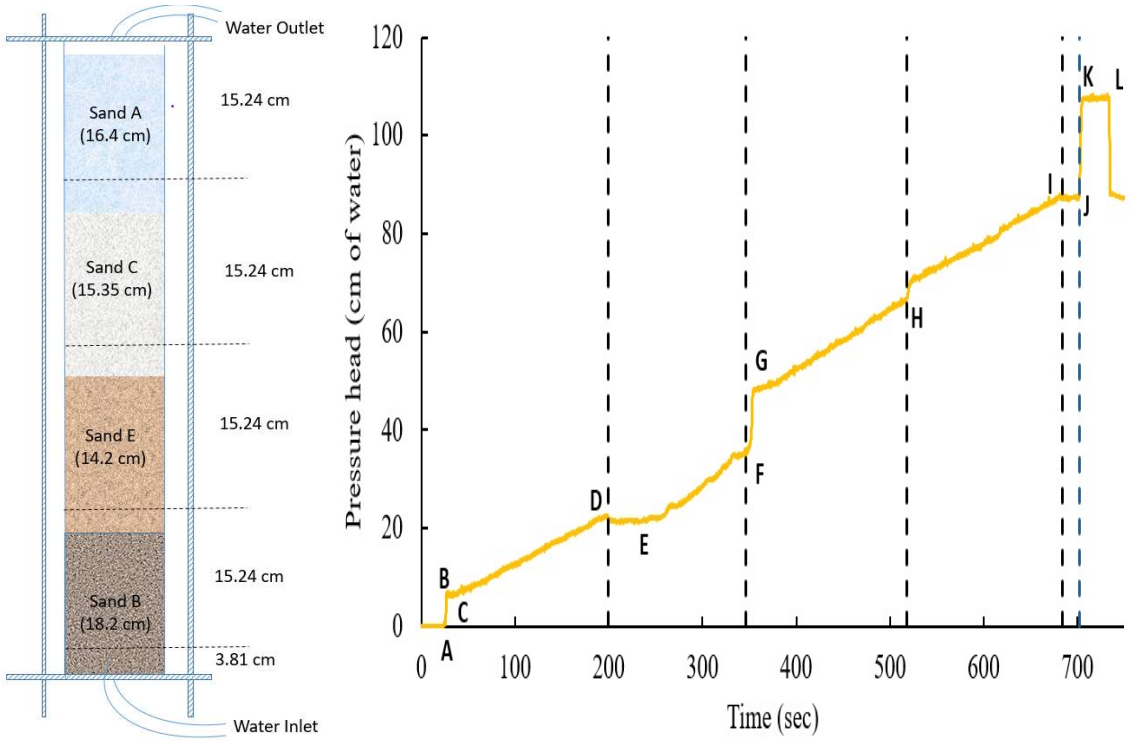

Figure 4-3: Pressure-time curve recorded while flushing through soil column of four different sand layers

Pressure data was recorded every 100 milliseconds and the slope of pressure increase over time was calculated over 5-seconds windows (50 data points per calculated slope). Pressure-time curve show the transition of the waterfront moving from one sand layer to another. The pump was turned on at 20 sec. Below is a detailed description of the pressure curve:

1) 0 ➔ A: The flat part of the curve is because of no flow of water before the pump was turned on.

2) A ➔ B: The waterfront has reached the vertical tubing and is propagating upwards through the tubing and inlet to the permeation cell, all the way up to the bottom of the filter material. Due to the smaller cross-sectional area of the tube and inlet, the waterfront is rising rapidly at the constant flow rate resulting in an increase in high RPI value.

3) B ➔ C: The waterfront just reached the bottom of the Sand A. The water is being pulled by the capillary suction of the dry sand to create the capillary fringe and therefore, the waterfront is not progressing. Hence the pressure reading is almost constant.

4) C ➔ D: The waterfront is propagating through the pores of sand A. The rate of increase of the waterfront (and pressure) is dependent on the distribution of local void ratio.

5) D ➔ E: Waterfront reaches the top of Sand A layer at point D. Sand E has small pore size because of the presence of smaller particles and therefore, has a higher capillary suction. From D to E, the water is being pulled up to satisfy the higher capillary suction of Sand E and therefore, the saturated waterfront is not increasing significantly.

6) E ➔ F: The saturated waterfront is rising in Sand E layer. Hence, the slope of pressure increase from E to F is the function of the local void ratio of Sand E.

7) F ➔ G: The steep increase in pressure is due to waterfront reaching bottom of Sand C layer which has a lower capillary pressure (larger particle gradation). As the capillary front from Sand E reaches Sand C, it will start accumulating at the base of it due to the lower capillary rise in Sand B. Therefore, as the waterfront reaches bottom of sand C, it will increase very rapidly to the top of the already almost saturated zone in the lower portion of Sand C (void space already filled up by water that was in the capillary fringe of Sand E).

8) G ➔ H: Water is moving through Sand C layer, and pressure buildup is the function of the distribution of the local void ratio of Sand C. Waterfront reaches to the top of Sand C layer at point H.

9) H ➔ I: Sand A has lower capillary suction than Sand C and the response is similar to that between points F and G.

10) I ➔ J: Waterfront is propagating through Sand A layer.

11) J ➔ K: Water reached to the top of Sand A layer at point K. There was an empty portion of the cylinder at the top of Sand E layer. Due to the large cross-sectional area to be filled at the same constant flux, the rate of pressure build-up is very low.

12) K ➔ L: water is filling up the outlet and associated vertical tube (low cross-sectional area leading to high rate of pressure increase)

13) L ➔ M: Water is flowing out of the outlet tube no additional pressure increase is recorded until the pump is shut off at M.

It should be noted that the analysis of typical specimens made of one material will be much simpler since there wont be radical changes in the properties over a predefined interface. Particularly, the changes in the capillary suction of a given sand are minimal with minor changes in void ratio, eliminating these sudden changes in RPI values over short period of time.

4.4.2 Analysis

Recorded pressure data depends on the moisture transport in the soil column. Water movement in the partially rigid saturated sand is described by a modified form of Richard's equation (4-2) using the assumption that the air phase plays an insignificant role in the liquid flow process.

$$\frac{\partial \theta}{\partial t} = \frac{\partial}{\partial x}\left[K\left(\frac{\partial P}{\partial x} + \cos\alpha\right)\right] - S \tag{4-2}$$

where P is the water pressure head [L], θ it the volumetric water content [L^3L^{-3}]; t is time [T]; x is the spatial coordinate [L] (positive upwards). S is the sink term [$L^3L^{-3}T^1$]; α is the angle between the flow direction and the vertical axis and K is the unsaturated hydraulic conductivity function [LT^{-1}]. Pressure transducer at the injection point records the total head that is the summation of the hydrostatic head and the pressure head required to maintain the constant flux for water movement. Pressure (P_1) at any time T_1 equals to

$$P_1 = H_1 + \frac{V * H_1}{K_s} \tag{4-3}$$

where H_1 is the height of saturated waterfront from injection point in soil column, K_s is the equivalent saturated hydraulic conductivity of soil column from the injection point to the waterfront (H_1), and V is the constant flow velocity. The rate of increase in pressure ($\frac{\Delta P}{\Delta t}$) is the function of the constant flow velocity (V), saturated hydraulic conductivity of that region and rate of saturated front rise ($\frac{\Delta H}{\Delta t}$) as shown in equation (4-4)

$$\frac{\Delta P}{\Delta t} = \left(\frac{\Delta H}{\Delta t}\right) * (1 + \frac{V}{K_s}) \quad (4\text{-}4)$$

The rate of the waterfront increase is a function of pore space (φ) and flow velocity for the constant flux permeation.

$$\left(\frac{\Delta H}{\Delta t}\right) = \frac{V}{\varphi} \quad (4\text{-}5)$$

The saturated hydraulic conductivity (K_s) of the specimen can be estimated based on the equation provided Kozney Carman (add reference):

$$K_s = \frac{\delta g}{\mu} \times C \times (D_{10})^2 \times (\frac{\varphi^3}{(1-\varphi)^2}) \quad (4\text{-}6)$$

where δ is the density of the permeant fluid (water for this study) in g/cc, g is the acceleration due to gravity (981 cm^2/s), D_{10} is the particle size of material used at which 10% of soil mass is finer, and C is the Kozney-Carman constant depends on the tortuosity and is considered as 8E-3 $cm^{-1}s^{-1}$ in this study.

The heterogeneity of a soil column is determined by observing the consistency of the slope of pressure increase while water is flowing through the different regions of the soil column. The porosity profile along the soil column is quantified by combining equations (4-3) to (4-6). The porosity of a region (ϕ), defined between two points (H_1 and H_2) along the height of the specimen at time T_1, and T_2 (*Figure 4-4),* can be determined from the following equation:

$$D\varphi^4 - (1 + D\varphi_i)\varphi^3 - E\varphi^2 + 2E\varphi - E = 0 \quad (4\text{-}7)$$

where, $D = \frac{\frac{\Delta P}{\Delta t}}{V}$; $E = \frac{V}{(8\times10^{-3})D_{10}{}^2}$; and ϕ_i = initial water content of specimen;

After measuring the porosity of that region, the saturated water conductivity (K_s) and height of saturated waterfront were calculated using equations (4-6)and (4-3) respectively.

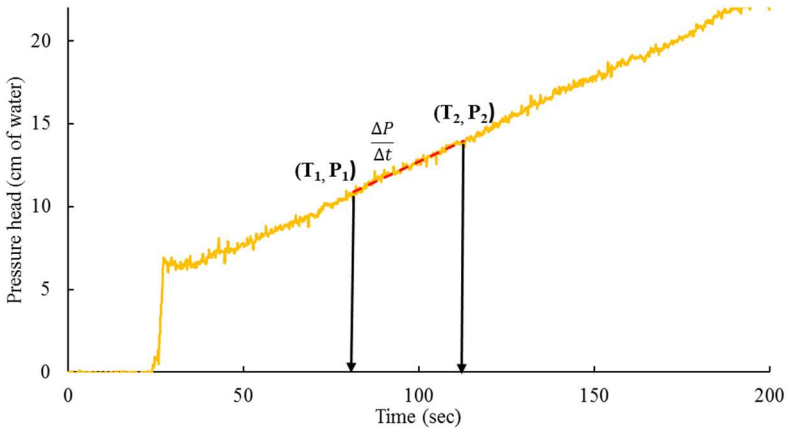

Figure 4-4: Determination of porosity profile from RPR method

Table 4-3 shows the porosity along the specimen height of Sand B layer of Test 1 using the RPI method, which gives the average local porosity of 0.405 with a relative standard deviation of 12.3%. The calculated average local porosity is less than the average global porosity of 0.410. The difference in the average porosity can be a result of densification of the lower layer due to disturbance caused while preparing the top layers.

Table 4-3: Porosity along specimen height of Sand A layer of Test 1 using RPR method

Material	Time(T_1) (sec)	Time(T_2) (sec)	Pressure(P_1) (cm)	Pressure(P_2) (cm)	Rate of pressure rise (dP/dt)	Porosity	Saturated Hydraulic conductivity(Ks) (cm/s)	Average height of saturated water front (cm)	Average Local Porosity	Relative standard deviation
Sand B	5	15	0.894	1.535	0.058	0.454	3.099	1.199	0.405	12.34%
	15	25	1.535	2.495	0.098	0.419	2.140	1.986		
	25	35	2.495	3.289	0.079	0.416	2.087	2.847		
	35	45	3.289	4.520	0.114	0.367	1.220	3.832		
	45	55	4.520	5.749	0.130	0.328	0.769	5.012		
	55	65	5.749	6.583	0.079	0.514	5.653	6.010		
	65	75	6.583	7.525	0.100	0.411	1.963	6.885		
	75	85	7.525	8.723	0.090	0.453	3.069	7.938		
	85	95	8.723	9.790	0.109	0.382	1.443	9.048		
	95	105	9.790	10.822	0.112	0.373	1.302	10.068		
	105	115	10.822	11.806	0.085	0.480	4.010	11.055		
	115	125	11.806	12.644	0.110	0.379	1.394	11.949		
	125	135	12.644	13.541	0.079	0.413	2.018	12.797		
	135	145	13.541	14.787	0.107	0.386	1.500	13.843		
	145	155	14.787	15.628	0.122	0.345	0.940	14.853		

Relative standard deviation of 12.34% shows the variation in pore space due to packing arrangement of soil grains. Similarly, the heterogeneity of other layers of soil column for Test 1 was determined using the RPI method, and the results are presented as the relative standard deviation to measure the variability. Three trials of the RPI method were made for each soil column by considering the slopes of pressure rise for different time spans to evaluate the impact of the data analysis on the final results. The results from the conventional method along with the three RPI trials are presented in Figure 5 and the summary of the results is presented in Table 5.

Table 4-4: Variation of porosity along height using the conventional method and RPI method

Material	Conventional		Local (1st trial)		Local (2nd trial)		Local (3rd trial)	
	Average	Relative SD	Average	Relative SD	Average	Relative SD	Average	Relative SD
Sand A	0.420	1%	0.418	7%	0.412	9%	0.416	8%
Sand B	0.411	2%	0.398	10%	0.401	12%	0.405	12%
Sand C	0.399	3%	0.395	1%	0.397	4%	0.395	5%
Sand E	0.418	1%	0.400	2%	0.402	8%	0.408	9%

The average local porosity determined using the RPI method is smaller than the average porosity calculated using the conventional method. The maximum variability of porosity within the specimen is 12% using RPI method whereas the conventional method underestimated the variability of porosity.

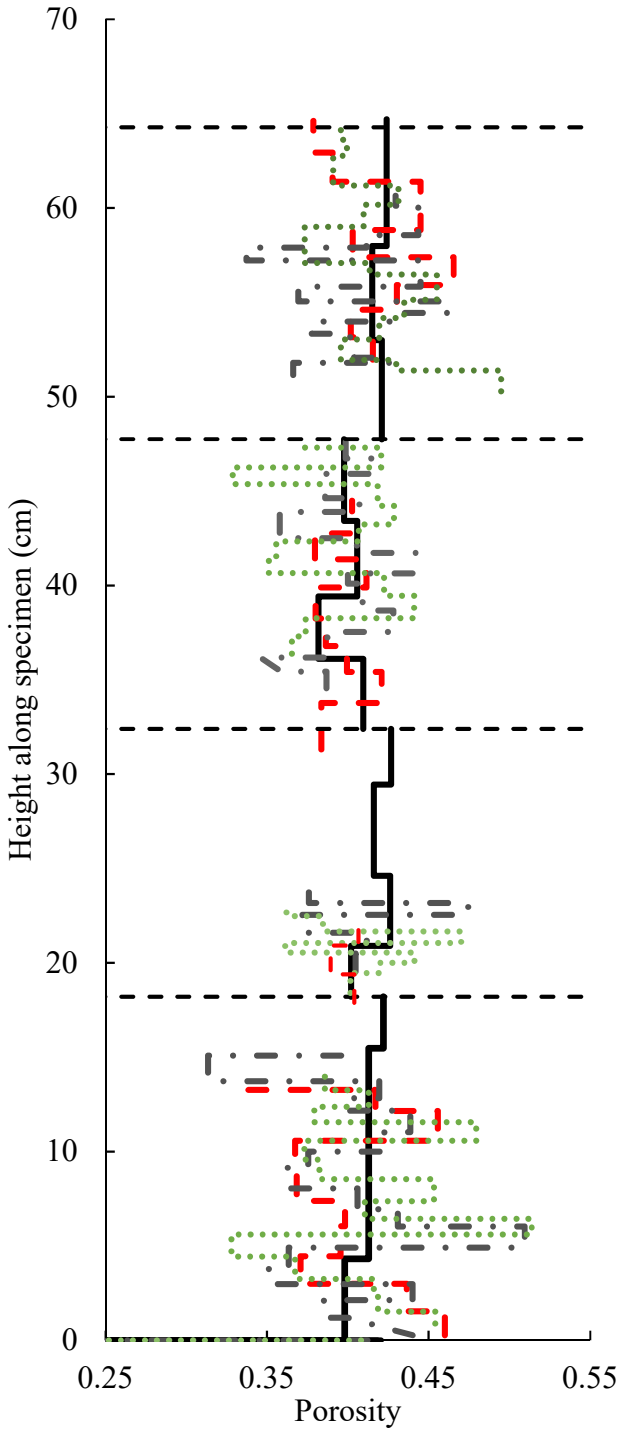

Figure 4-5: Porosity profile of soil column of Test 1 representing the variation in local porosity

4.4.3 Results

Six total sand column tests were evaluated using the RPI method and the experimental details of each test are summarizing in Table 4-5. Except for Test 1 described earlier, each of the five columns was prepared using one type of sand following the previously highlighted procedure. The only modification from the previous procedure is using different specimen heights for the different tests. Figure 4-6shows the pressure curves for the five tests. The curves show more subtle changes in the RPI values compared to the pressure curve obtained for Test 1 with the four different sands. The only major changes in RPI values occur during the transition from the filter material to the sand near the base and vice versa near the top. The calculated porosity using the RPI method along the height of each specimen is presented in Figure 4-6 along with the calculated values using the conventional weight-volume method.

Table 4-5: List of soil columns studied for this paper

Test No.	**Materials**	**Height of soil layer (cm)**	**Total height of soil column (cm)**	**Flow rate (cm/s)**
1	Sand B	18.20	64.70	0.0403
	Sand E	14.20		
	Sand C	15.35		
	Sand A	16.95		
2	Sand A	14.80	14.80	0.0503
3	Sand B	37.34	37.34	0.0440
4	Sand C	38.34	38.34	0.0440
5	Sand D	51.92	51.92	0.0405
6	Sand E	56.21	56.21	0.0440

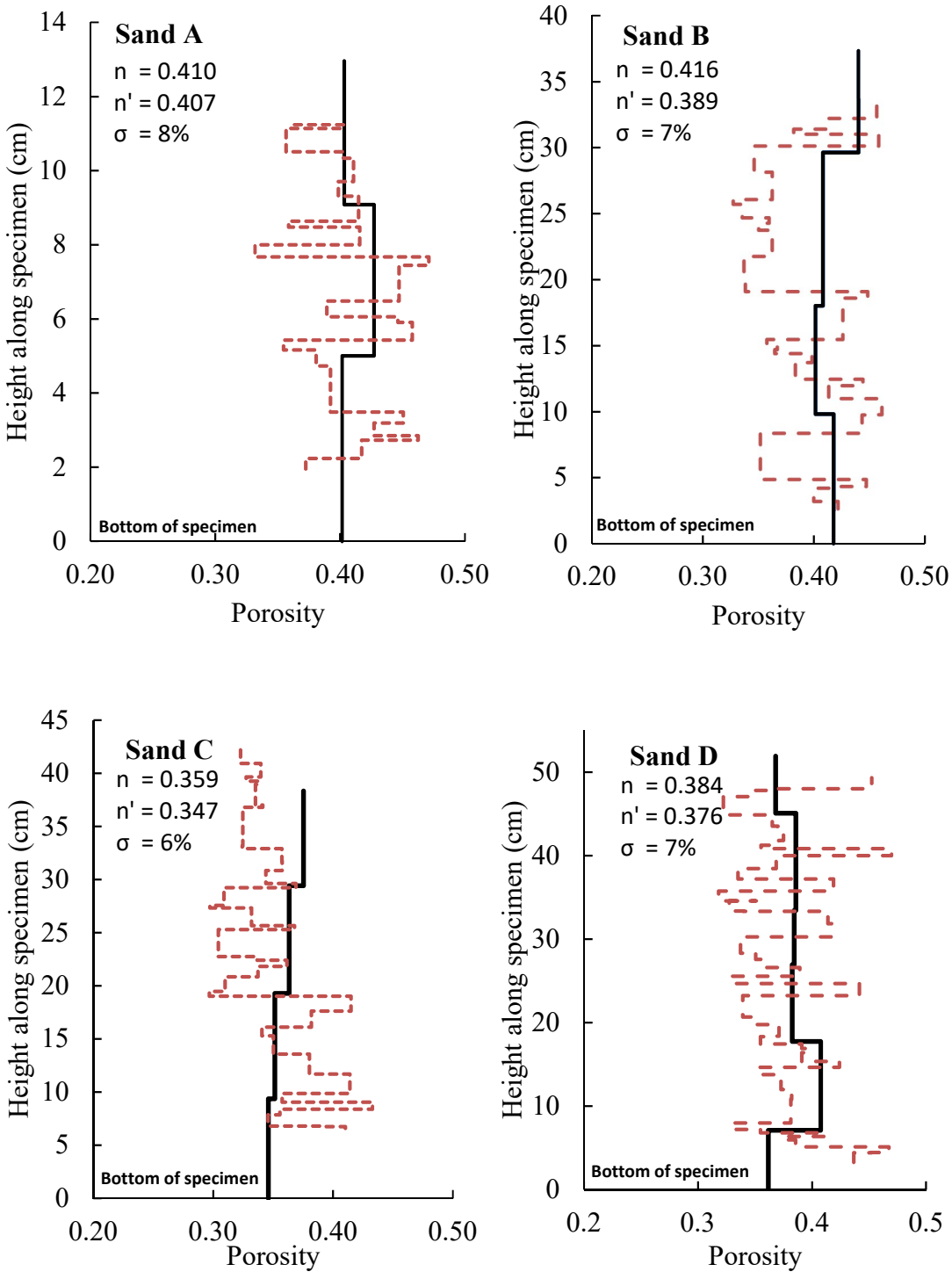
Sand A
n = 0.410
n' = 0.407
σ = 8%
Bottom of specimen
Height along specimen (cm)
Porosity
Sand B
n = 0.416
n' = 0.389
σ = 7%
Bottom of specimen
Height along specimen (cm)
Porosity
Sand C
n = 0.359
n' = 0.347
σ = 6%
Bottom of specimen
Height along specimen (cm)
Porosity
Sand D
n = 0.384
n' = 0.376
σ = 7%
Bottom of specimen
Height along specimen (cm)
Porosity

Figure 4-6

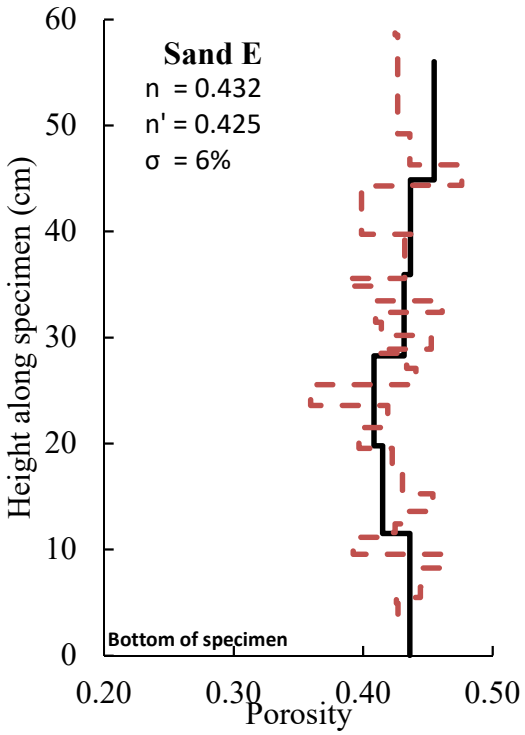

Figure 4-6: Porosity profile determined by RPI method (dashed lines) compared with conventional global porosity (solid black line); where n = average global porosity; n' = average local porosity; and σ = relative standard deviation

Table 4-6 shows the average porosity determined using the conventional weight-volume (W-V) method and RPI method. The values obtained from the RPI method reflect the spatial variation of local pore space within the specimen after the whole assemblage of soil column whereas those obtained from the conventional method represent the porosity of each section at the end of its reconstitution, before completion of the whole soil column. Relative standard deviation for each method is included as well to evaluate the spatial variation of porosity within the specimen. The lower relative standard deviation from the conventional method is expected due to the limited number of averaged values compared the RPI method. The deviation in the RPI porosity within the soil columns were found to be approximately 6-8% for all materials.

The difference between the average conventional and RPI porosity can be a result of the densification of the lower portion of the specimens while preparing the subsequent layers. Sand A consists of one size spherical beads and is prone to least disturbance during the preparation. This is reflected in the lowest difference between W-V and RPI results at only 0.61%. On the other hand, Sand B is a gap graded soil, with a range of particle sizes from 0.7 to 2mm, leading to a less stable structure that densified the most (the difference in the average porosity is 7%).

Table 4-6: Difference in average porosity determined by RPI method and W-V method

Materials	Average Porosity (Conventional W-V method)		Average Porosity (RPI method)		Difference between average W-V and RPI porosity (%)
	Average	Relative Standard deviation	Average	Relative Standard deviation	
Sand A	0.410	3%	0.407	8%	0.73%
Sand B	0.416	3%	0.389	7%	6.49%
Sand C	0.359	2%	0.347	6%	3.34%
Sand D	0.384	4%	0.376	7%	2.08%
Sand E	0.432	4%	0.425	6%	1.62%

4.4.4 Verification of the RPI method

The RPI method uses an analytical solution to determine the distribution of the local porosity based on Darcy's law and Kozney-Carman equation. In this section, the conceptual

framework of the RPI method is evaluated numerically as well as experimentally. Numerically, a hypothetical soil column of known porosity was modeled using the Hydrus 1D software to generate the pressure curve at the base of the specimen. This pressure curve is then analyzed following the RPI procedure to determine the local porosity for verification. Experimentally, a soil column of glass beads of known diameters was prepared carefully with a known particle arrangement (known porosity) and tested using the PRI method and the results are compared to the actual distribution.

a) Numerical Verification

A hypothetical heterogeneous sand column was simulated numerically using Hydrus 1D to verify the RPI method. Layered soil column was modeled with known porosity and saturated hydraulic conductivity as shown in Figure 4-7. A constant flow rate of 0.0425 cm/s was applied at the bottom of soil column and an atmospheric pressure with surface runoff was applied at the top boundary (Figure 4-7-a).

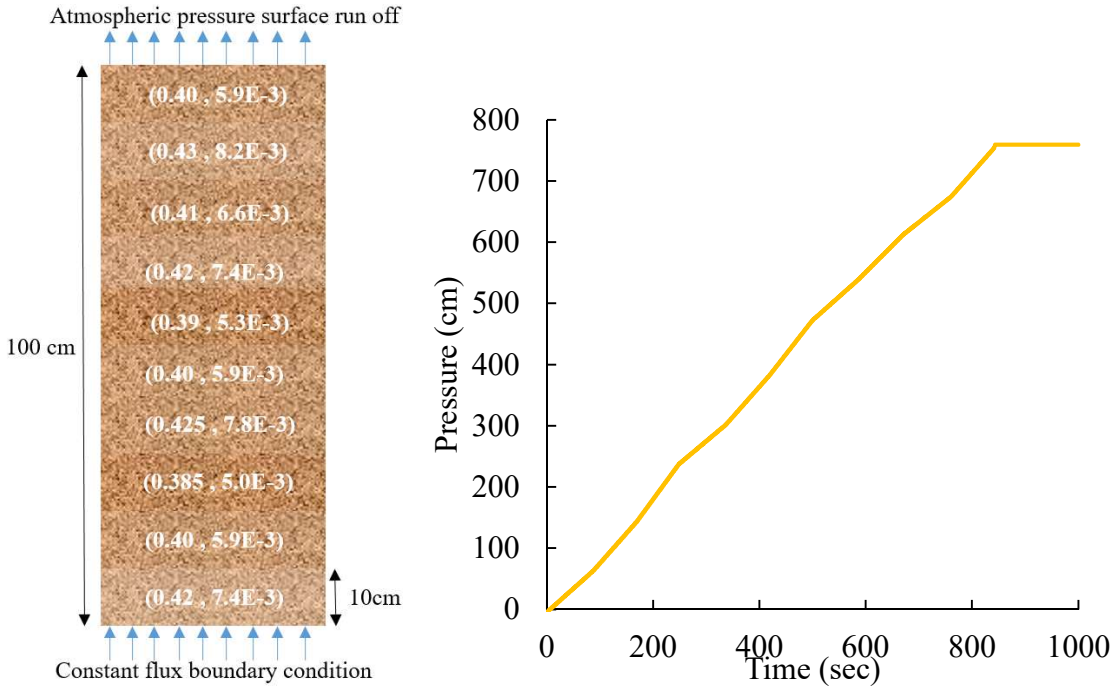

Figure 4-7: (a) Modeled layered soil column by Hydrus1D (b) Measured pressure at the bottom node while applying the constant flux boundary condition at the bottom boundary

The pressure buildup over time at the inlet was obtained numerically (Figure 4-7: b) from the Hydrus 1D analysis. The porosity profile was determined by analyzing the curving following the RPI procedure (Equation (4-6)). Equation 6 is independent of any known information about the soil properties in the column and is solely based only on the pressure data. The calculated local porosity from the RPI method is presented along with the known porosity profile in Figure 4-8. The results show that the RPI method can predict local variability in a soil column.

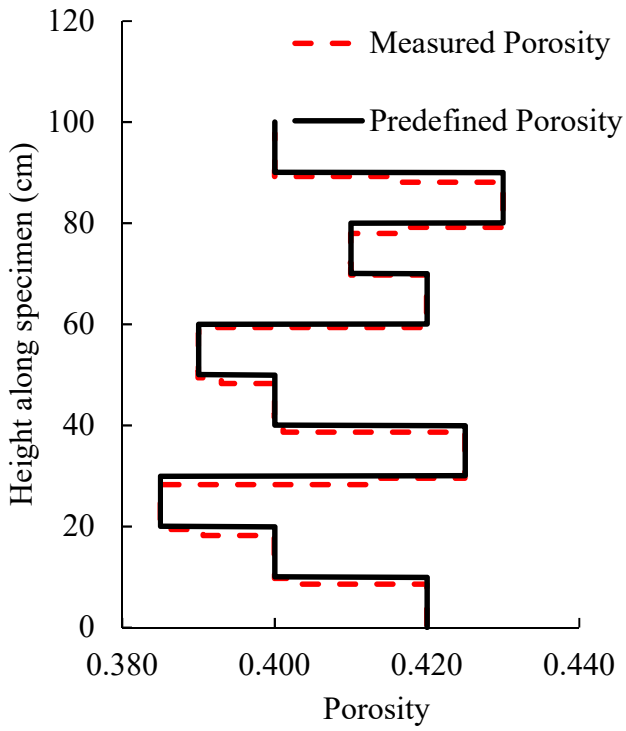

Figure 4-8: Comparison of measured pressure using RPR method with predefined porosity verifies the proposed method

b) Experimental Verification

For this verification method, a soil column of glass beads with known diameter (1.58cm) was prepared. The actual average porosity of the soil column can be measured by knowing the number of glass beads used to prepare the column. 135 glass beads were used to prepare the soil column of 6.35cm diameter and 16.69cm height resulting in an average porosity of 0.465 (Figure 4-9). After the soil column preparation, water was flushed from bottom to top at constant flow rate of 0.0391 cm/s and the pressure was recorded at the injection point. Larger diameter glass beads were chosen for this experimental verification for three reasons: (a) to neglect the capillary rise; (b) for clear visibility of waterfront; and (c) glass beads are not prone to any disturbance while preparing the subsequent layers.

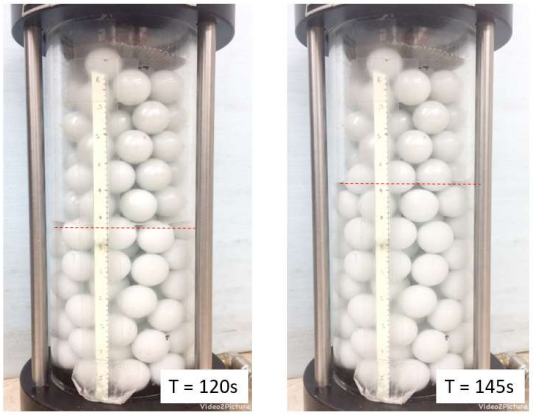

Figure 4-9: Clear visibility of waterfront at different times

The height of the waterfront was recorded with time during the constant flux water flow. The local porosity distribution was measured by knowing the volume of water filling the height of the soil column and are shown in Figure 4-9. Figure 4-9 shows the clear vision of waterfront at 8.38 and 10.795 cm at time 120 and 145s, respectively.

Table 4-7: Porosity measurement from the inflow volume of water at constant flow rate

Time (sec)	Height of Waterfront from injection point (cm)	Volume of voids (cm^3)	Total Volume of section (cm^3)	Porosity
35	1.524	-	-	-
45	2.286	12.28	23.93	0.513
55	3.175	12.28	27.91	0.440
65	3.937	12.28	23.93	0.513
75	4.826	12.28	27.91	0.440
85	5.715	12.28	27.91	0.440
95	6.477	12.28	23.93	0.513
105	7.366	12.28	27.91	0.440
115	8.255	12.28	27.91	0.440
125	9.017	12.28	23.93	0.513
135	9.906	12.28	27.91	0.440
145	10.795	12.28	27.91	0.440
155	11.557	12.28	23.93	0.513
165	12.446	12.28	27.91	0.440
175	13.335	12.28	27.91	0.440
185	14.097	12.28	23.93	0.513
195	14.986	12.28	27.91	0.440

The local porosity distribution was determined using the RPI method as well using strictly the pressure measurements at the inlet. Figure 4-8 shows the comparison of the local porosity distribution from the RPI method and those measured by the volume of inflow water. The arrangement of glass beads in the cell, and their large diameter compared to that of the permeameter (ratio of 1:4), created a sinusoidal trend of porosity along the specimen height as reflected in Figure 4-10. The local porosity distribution measured by RPI methods is in good

agreement with the expected results from the volume of inflow water despite the high changes in porosity.

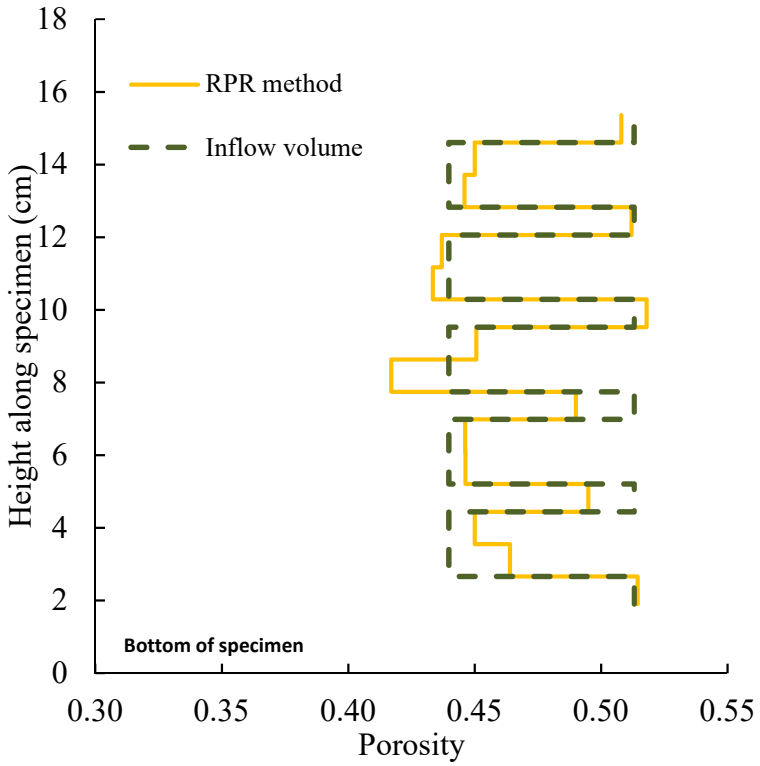

Figure 4-10: local porosity distribution measured by RPR method and the volume of inflow water

The average local porosity was determined by three different methods: (a) the known volume of glass beads and total volume of the permeameter; (b) the volume of water flushed through to fill the pores and the total volume of the permeameter; and (c) the RPI method. Average porosities calculated from all three methods were identical (0.465), which further verifies the validity of RPI method. The variation of pore space within the specimen by RPI method also matches with that for the volume of water inflow calculations Table 4-8).

Table 4-8: Verification of RPR method experimentally

Methods	1st Trial		2nd Trial	
	Average Porosity	Relative SD	Average Porosity	Relative SD
Volume of water inflow	0.465	5%	0.465	5%
RPR method	0.465	5%	0.465	5%
Volume of glass beads	0.465	-	-	-

4.5 Conclusion

This paper proposed a non-invasive, simple and quick method (the RPI method) to determine the local porosity distribution of laboratory prepared sandy specimens. Dry pluviated sand columns were flushed with water from bottom to top at a constant flux while recording the pressure buildup at the injection point. The concept behind this method is that the rate of pressure increase and seepage velocity are a function of the pore space through which water is flowing. The RPI method is based on Darcy's law and Kozney Carman equation. The spatial variation of local porosity is calculated from the rate of change in the pressure data. The results obtained from the RPI method were validated numerically as well as experimentally under controlled conditions. The relative standard deviation was used to define the deviation of pore space within the specimen from the average value and found to be approximately 6-8% for the five specimens tested. The average porosity of the assembled specimen obtained using the RPI method was between 1 and 7% lower than the mean porosity determined by the conventional W-V method. These results are

not unexpected as the specimen could undergo some densification during placement of upper layers and final assembling of the sand column.

While the RPI method is not applicable to specimens prepared using water sedimentation or any other technique resulting in high degree of saturation, its simplicity and minimal impact on the specimen makes it a viable candidate to be incorporated into many existing geotechnical specimen preparation procedures to obtain void ratio distribution for each individual specimen being tested.

CHAPTER 5 EMPIRICAL PREDICTION OF PERFORMANCE OF CONSTANT FLUX PERMEATION GROUTING OF BENTONITE SUSPENSION GROUT

5.1. Abstract

Permeation grouting using bentonite suspension grout is an effective method to improve the soil characteristics regarding reducing permeability and enhancing the mechanical characteristics. Penetration capability of fresh grout depends on the structure of porous media, rheology and filtration tendency of grout. During the design process of grouting work, the consultant or the site engineer have to rely on empirical correlations to evaluate the performance of grout permeation. Most correlations available are based on the particle size (of grout and soil). There is scarce of literature on the effect of the grout rheology and flow rate on penetration depth for constant flux permeation of bentonite grout. In this study, constant flux permeation tests were performed on 68.6 cm soil column at various experimental conditions to determine the effect of each experimental parameters on the penetration depth. The pressure at the injection point was recorded with time, and the pressure-time plot was used to understand the grouting performance and filtration of bentonite grout passing through granular soils. During the constant flux permeation, the pressure at the injection point increases at a slower rate firstly but later the pressure builds up rapidly because of filtration or rheological blockage. The experimental results show that penetration length of bentonite grout increases with a decrease in its apparent viscosity, bentonite concentration, and flow rate. Moreover, the addition of an ionic additive, sodium pyrophosphate (SPP), stabilizes the suspension grout and reduces its apparent viscosity. Hence penetration depth

increases with the addition of SPP. An empirical correlation is proposed to determine the pressure-time curve for known grouting material and porous media. The fitting coefficients are functions of bentonite concentration, percentage of additives, rheology of grout, grain size distribution of porous media and bentonite particles, and flow rate. This empirical correlation can be used by consultants to evaluate the performance of permeation grouting before practicing on a large scale.

5.2.Introduction

Permeation grouting using bentonite suspension grout is an effective method to improve the soil characteristics regarding reducing permeability and enhancing the mechanical characteristics. Bentonite grout consists mainly of sodium montmorillonite; therefore, it has high plasticity and swelling potential. Bentonite grout is commonly used in hydraulic barriers for nuclear waste repositories, cut off walls, landfill liners (Liu and Neretiniks 2006; Houg and Wong 1992; Chapuis 1990). Recently, researchers (Rugg et al. 2011; El Mohtar et al. 2013; Yoon and El Mohtar 2013c) have found a possible application of bentonite grout for liquefaction mitigation. For these applications, an accurate prediction of the penetration depth of bentonite grout is required to determine the performance of permeation grouting. Researchers have studied the penetrability of cement-based grout experimentally as well as numerically considering the filtration phenomena, but their results are not applicable to bentonite grout. There is scarce of literature on bentonite suspension grouting. Penetration of bentonite suspensions through granular soil is a very complex phenomenon owing to the diversity of the mechanisms involved. Penetration capability of fresh grout depends on the structure of porous media, rheology and filtration tendency of grout.

Bentonite grout possesses yield stress because of card or band-like structure formation of bentonite particles (depending on pH) in aqueous media. The addition of ionic additives such as sodium hydroxide, sodium silicate, and polyphosphate reduces the viscosity and yield stress of bentonite suspensions, and therefore increases its mobility (Abend and Lagaly, 2000). The effect of ionic additives on bentonite suspensions varies depending on bentonite characteristics such as particle size, shape, surface charge, cation exchange capacity, and type of exchangeable cations (Goh et al., 2011). Ions are attached to the edges by adsorption due to exchanging structural OH-, which increases the repulsion and disperses the bentonite particles. Sodium polyphosphate (SPP) was used in this study because of its ability to disperse the bentonite particles and effectively reduce yield stress and viscosity of bentonite suspensions for better penetrability of grout in soils. However in a modified concentrated suspension with same rheological properties as a diluted suspension, the significant amount of bentonite particles still limits the penetration depth due to filtration.

It is hypothesized that grout spread in granular soils does not only depend on the rheology of grout but also is affected by the filtration of bentonite particles. Suspension grouts have a tendency to leave grout particles on the surface of the solid skeleton and lead to plugging of cavities which affects the suspension flow. Liquid-solid separation of bentonite particles by filtration can be accomplished either by solid accumulation in front of a porous medium or by retention inside a porous bed. In the first case, a filter cake is built-up, and it stops the suspended particles from entering the porous medium. In the second case, the suspension flows through the porous medium in which the particles are retained. The penetration capability of grout depends on two parts, one

on rheological properties and the other on the filtration tendency (plug formation), and both must be optimized to attain adequate penetration of the grout (Rostami Barani et al. 2014). It is important to determine the parameters of grout material and porous media influencing the injectivity of grout.

During the design process of grouting work, the consultant or the site engineer have to rely on empirical correlations to evaluate the performance of grout permeation. In literature, most correlations are based only on two parameters; the larger particle size of the suspension grout and the pore size of sand (related to smaller particle size of sand). Burwell (1958) suggested that the groutability parameter N be the ratio of d_{10} of grouted soil to d_{95} of the grout:

$$N = \frac{D_{10}}{d_{95}} \tag{5-1}$$

N is the permeability number, d_{10} is the diameter at 10% of the cumulative particle size distribution of the grouted soil, and d_{95} is the diameter at 95% of the cumulative particle size distribution of the grout solids. The soil is considered to be easily groutable if N is greater than 11, and not groutable if N is less than 5. In this model, the effects of rheological properties of grout, flow rate, and filtration tendency were ignored. Therefore, there is need of a new empirical correlation to evaluate the performance of constant flux permeation grouting of bentonite suspensions.

In this paper, the new empirical correlation was developed to define the flow behavior of bentonite grout through porous media for constant flux permeation. First, constant flux permeation tests were performed on 68.6 cm soil column under various experimental conditions to determine the effect of each experimental parameter on bentonite permeation. Rheological properties of bentonite grout (yield stress and equilibrium apparent viscosity) were determined using the Anton Paar rheometer. Pressure transducer at the injection point recorded pressure build up with time while grout was permeating the soil column from bottom to top. The pressure-time curves echoe the flow behavior and therefore are used to determine the factors influencing permeation. Experimental results were analyzed using the bentonite content profile. Second, an empirical correlation is proposed to determine the pressure-time curve for known grouting material and porous media. The fitting coefficients are functions of bentonite concentration, percentage of additives, rheology of grout, grain size distribution of porous media and bentonite particles, and flow rate.

5.3.Rheological properties of grout

The key component of bentonite is montmorillonite, which has a plate-like structure with layers consisting of a central octahedral sheet between two tetrahedral sheets. They have colloidal properties, swelling properties, and high plasticity when mixed with water due to the formation of a 3-D network structure. The gel formation of montmorillonite can have two possible mechanisms: (a) face-to-face or edge-to-edge interaction through electrostatic double layer repulsion, and (b) electrostatic attraction between negatively and positively charged edges. Yield stress is used to characterize a viscoplastic network of suspended bentonite particles in aqueous media. Yield stess

is the magnitude of stress required to initiate flow. The viscosity of bentonite suspension is controlled by its colloidal and hydrodynamic factors which depend on flow rate. Suspension reaches an equilibrium state at a very high shear rate, and that is called the equilibrium apparent viscosity. In this paper, bentonite suspensions are characterized by two rheological properties: (a) yield stress, and (b) equilibrium apparent viscosity. Sodium bentonite is used in this study, and the raw bentonite was screened through sieve number 200 to avoid large sized impurities.

In the rheometer setup, the vane has six blades with a thickness of 0.1 cm and a length of 1.6 cm. The vane radius is 1.1 cm leaving a gap of 0.346 cm between the sides of the cup and the vane (Figure 5-1). Sample volume was maintained at 37ml which allows the vane to penetrate approximately twice its depth. With this configuration, the end effects were small enough to ignore. The rheometer has a built-in Peltier temperature control system, and the tempreature was maintained at 22^{o}C for all the tests for consistency. Fresh grout was used for permeation experiments hence thixotropic properties of bentonite grout was ignored.

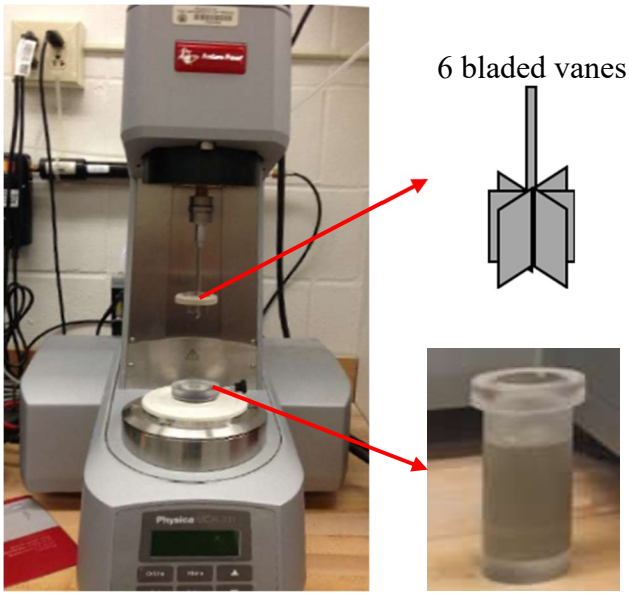

Figure 5-1: Anton Paar MCR 301 rheometer with cup and vane measuring system

The stress ramp method is used to measure the static yield stress and viscosity of bentonite suspension. Yield stress and equilibrium apparent viscosity of grout measured by the rheometer are determined as shown in Figure 5-2. The minimum stress required to break the cohesion between particles is known as yield stress which is determined graphically from shear stress (τ)-shear strain (γ) plots using log(τ)-log(γ) plot (Clarke, 2008). The apparent viscosity of bentonite grout depends on the applied shear rate. At a very high shear rate, bentonite grout reaches steady state (equilibrium state). The equilibrium apparent viscosity is chosen for the analysis because the mixture was prepared in a high-speed mixer and instantaneously placed as a slurry. It's hard to inject high bentonite concentration grout in granular soil to obtain the desirable results. Hence sodium pyrophosphate (SPP) is added to grout to lower down the viscosity of grout. Rheological properties for different bentonite grout concentrations used in experimental tests are listed in Table 5-1

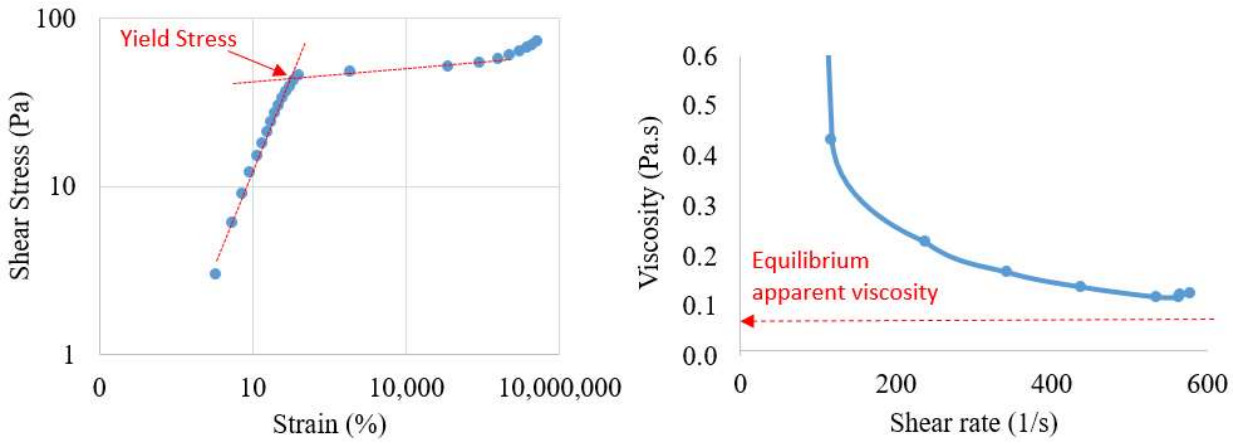

Figure 5-2: Determination of (a) Yield stress and (b) equilibrium apparent viscosity (Pa.s)

5.4.Constant flux permeation test

Permeation tests were performed using a transparent cell of 68.6 cm height and 7.24 cm diameter. The 68.6 cm long permeation cell was prepared in sections to obtain uniform sample. The permeation cell consisted of four cylinders, each of 15.24 cm height placed in between two 3.81 cm cylinders. The 15.24 cm cylinders were split cylinders, which could be assembled and dissembled independently to take out the grouted sample. All the cylinders were connected to each other by latex membranes and hose clamps to make one unit. 2.54 cm of filter materail was placed at the bottom and then dry pluviation was used to pour the sand using a funnel. Height and weight of the soil filled in each section were noted to determine the relative density. After filling all four 15.24 cm cylinders, a 3.81 cm cylinder was connected and filled with filter material. Figure 5-1shows the diagram of permeation test.

The prepared soil column was flushed with CO_2 to replace the air present in the pores. CO_2 dissolves easily in water hence gives better saturation when flushed with water. After CO_2 flushing, the soil column was connected to the pressure transducer and an adjustable flow rate

pump. The soil column was then flushed with at least two pore volumes of water from bottom to top, with the pressure transducer recording pressure at the bottom inlet.

The soil column was then flushed with grout. Similar to water flushing, pressure was recorded by transducer while grout is pumped at constant flow rate. Flow is terminated when grout reaches to the top of the soil column or when pressure buildup reaches 120psi, whichever occurs first. Table 5-1 shows the list of laboratory tests performed at various experimental conditions. Each test was replicated thrice to control the testing errors.

Table 5-1: List of experiments performed for this study

Test No.	Bentonite concentration (%)	SPP (%)	Viscosity of grout (mPa.s)	Flow rate (cm/s)	Sand Type	Porosity
1	5	0	59.51	1.66	Sand A	0.351
2	7	0	82.84	1.66	Sand A	0.351
3	8	0	95.34	1.66	Sand A	0.352
4	7	1	71.92	1.66	Sand A	0.355
5	8	1	77.35	1.66	Sand A	0.356
6	8	2	76.56	1.66	Sand A	0.355
7	12	5	164.21	1.66	Sand A	0.356
8	12	7	156.21	1.66	Sand A	0.358
9	12	9	117.77	1.66	Sand A	0.356
10	11	4	119.40	1.66	Sand A	0.359
11	10	2	115.90	1.66	Sand A	0.359
12	9	2	90.00	1.66	Sand A	0.360
13	9	2	90.00	1.25	Sand A	0.359
14	9	2	90.00	0.83	Sand A	0.358
15	10	3	107.93	1.66	Sand A	0.358
16	10	3	107.93	1.66	Sand B	0.398
17	10	3	107.93	1.66	Sand C	0.410
18	8	2	76.56	1.66	Sand B	0.400
19	8	2	76.56	1.66	Sand C	0.415

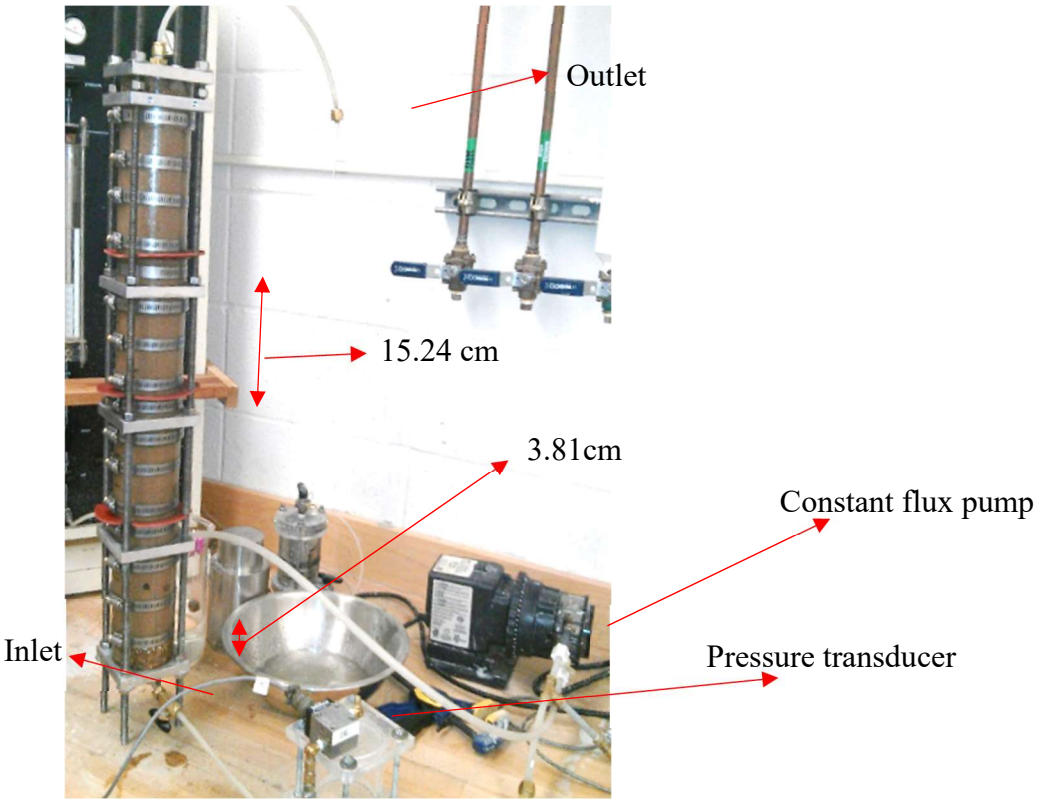

Figure 5-3: 1D permeation cell setup

5.5.Factors affecting Permeation depth

The pressure was recorded at the injection point while permeating the bentonite grout. Pressure buildup at the injection point is equal to the increased resistance of grouted region to the applied constant flux. Increase in pressure at injection point should be linear with time if there is no change in properties of grout and pore space of soil in the process. However, the increase in pressure was not linear for the performed tests: it increased nonlinearly at a slow rate in the beginning and then increases exponentially. As grout penetration occurs, some bentonite particles

get retained on the skeleton and decrease the pore space, hence increase the resistance to flow. The reduction in pore space eventually causes complete sealing, and no grout can pass further. The mechanism of solid particle separation from grout and its retention on the skeleton is known as filtration.

Filtration mechanism limits grout spread and permeation depth. In this study, pressure build-up at injection point for different combinations of experimental conditions is compared to understand the factors affecting filtration. Bentonite content profiles were determined after permeation to evaluate the distribution of bentonite particle with depth. The obtained bentonite content profiles indicated higher filtration with higher bentonite percentage and closer to the injection point. In this study, permeation depth is considered to be the depth of at least 80% of expected bentonite content. Expected bentonite content is the ratio of the weight of bentonite present in pore space to the weight of soil if there is no filtration. In Table 5-1 all the experiments performed to determine the factors affecting the grout spread and permeation depth are listed.

5.5.1. Effect of viscosity of bentonite grout on permeation depth

The viscosity of grout increases with increase in the bentonite concentration because of formation of the 3D network. Concentrated bentonite grout has more interparticle forces among bentonite particles than diluted suspensions, and the coagulated bentonite particles settle faster and increase the filtration rate. Permeation test results with bentonite grout having 5%, 7% and 8% bentonite with no additives are compared in Figure 5-4.

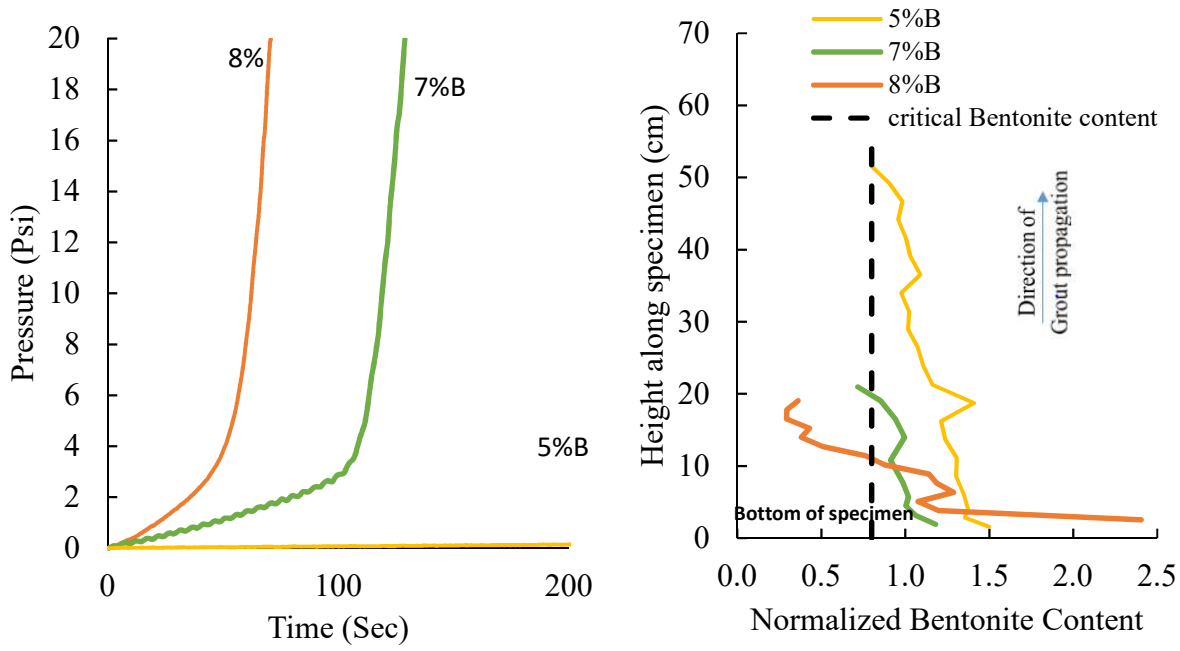

Figure 5-4: Pressure versus time plot and bentonite content profile for 5%, 7% and 5% bentonite grout with no additive

Pressure-time curve reflects the flow behavior of grout through porous media. The slope, in the beginning, is steeper for 8% bentonite grout because of its higher viscosity compared to 7% and 5% bentonite grout. Bentonite particles are retained on the sand grains as the grout passes through the pore space. The first stage of filtration is the coating of bentonite particles around the sand particles, which reduces the pore space. The slope of the pressure-time curve is not linear in the beginning because of a consistent decrease in pore space as permeation progress. The second stage is bridging, and it ioccurs when pore size decreases to less than the bentonite particle size. At this point, internal cake filter begins to form, leading to rapid increase in pressure. Rapid increase in pressure may be either because of rheological blockage or because of filtration. The second stage of filtration limits further spread of grout. The third stage is the formation of the

external filter cake. Pore space decreases to the critical porosity, and the grout cannot permeate through the porous medium anymore, and filter cake starts to form at the injection surface. Permeation depth is smaller for grouts with the earlier beginning of bridging. After grouting, the sand columns were dissected in small samples to determine the distribution of bentonite along their depth. The injection point is at 0 cm depth. Figure 5-4 shows a decrease in bentonite content with depth because of filtration. Measured bentonite content is normalized to the expected bentonite content. If the permeation depth is equal to the depth of sand column with at least 80% of expected bentonite content, then it is 50.8 cm, 20.32 cm and 11.43 cm for 5%, 7%, and 8% bentonite grout respectively.

A normalized bentonite content greater than one indicates the retention of bentonite particles on sand grains. Bentonite content decreases along the height of specimen, because of the reduction in grout concentration along specimen height due to filtration. The region of the soil column with normalized bentonite content less than one has a limited amount of grout flow because of initialization of internal cake formation.

5.5.2. Effect of addition of SPP

Sodium pyrophosphate (SPP) controls the rheological behavior of bentonite grout. It acts as a dispersing agent, which lowers the yield stress and viscosity of bentonite grout and allows the time-dependent recovery of rheological properties by the formation of the 3D network. Figure 5-5 shows that the addition of SPP breaks the 3D network and increases the mobility of bentonite grout during the injection and improves the permeation depth.

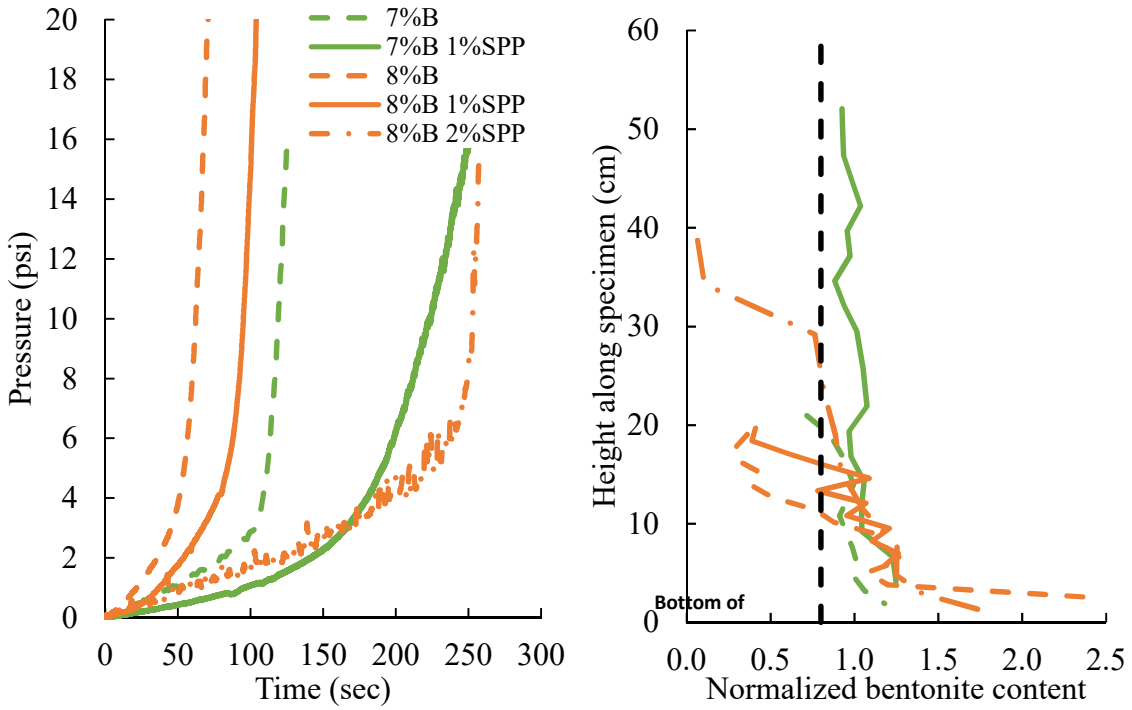

Figure 5-5: Effect of addition of SPP on pressure at injection point

Permeation depth for 7% bentonite grout doubles with the addition of 1% of SPP, whereas a similar amount of SPP to 8% bentonite grout made a minor difference in permeation depth. Figure 5-6 shows the effect of SPP on 12% bentonite grout. Time to start building internal cake almost doubles for 7% SPP compared to 5% SPP, but the effect of increasing SPP amount from 7 to 9% is not significant (Figure 5-6). Figure 5-5 shows similar results for the addition of SPP to 8% bentonite grout. Modified bentonite grout with 1% SPP has an almost same initial slope, which indicates that 1% of SPP didn't change the rheology of grout significantly. The addition of 2% of SPP almost doubles the penetration depth. Permeation depth for unmodified 8% bentonite grout is about 12.7 cm, whereas it increases to 17.02 and 24.13 cm for 1% and 2%SPP modified bentonite

grout (Figure 5-5). There is minimum and maximum limits of SPP amount to be added for bentonite grout to obtain significant results.

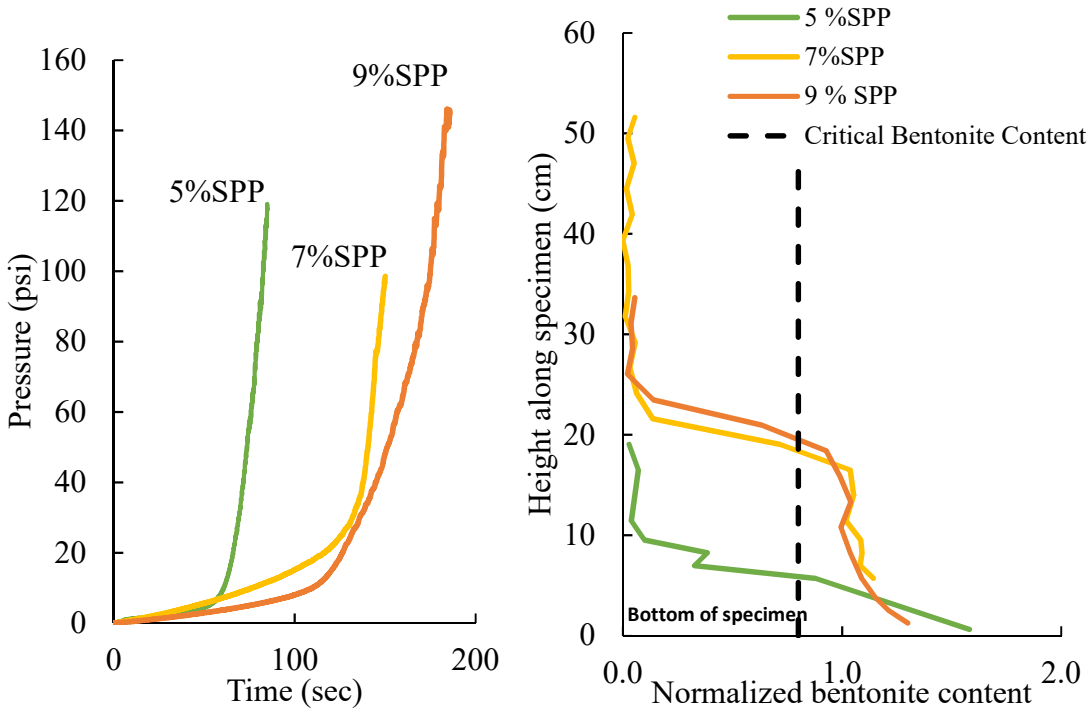

Figure 5-6: Effect of addition of SPP to 12% bentonite grout on pressure-time curve

5.5.3. Effect of bentonite concentration in grout on permeation depth

Figure 5-7 shows the effect of the amount of bentonite particles present in the grout of same apparent viscosity. The equilibrium apparent viscosity of 12% bentonite grout with 9% SPP, 11% bentonite grout with 4% SPP and 10% bentonite grout with 2% SPP is approximately 118 mPa.s. Bentonite grouts having same rheology show more filtration for a higher percentage of bentonite concentration. The rheology of grout defines the ease of flow of grout but doesn't solely control grout spread. Filtration mechanism also depends on the percentage of solid particles

present in the grout. Filtration rate is maximum for 12% bentonite grout because of a higher proportion of solid particles present (Figure 5-7). Similar results are replicated in bentonite content profile.

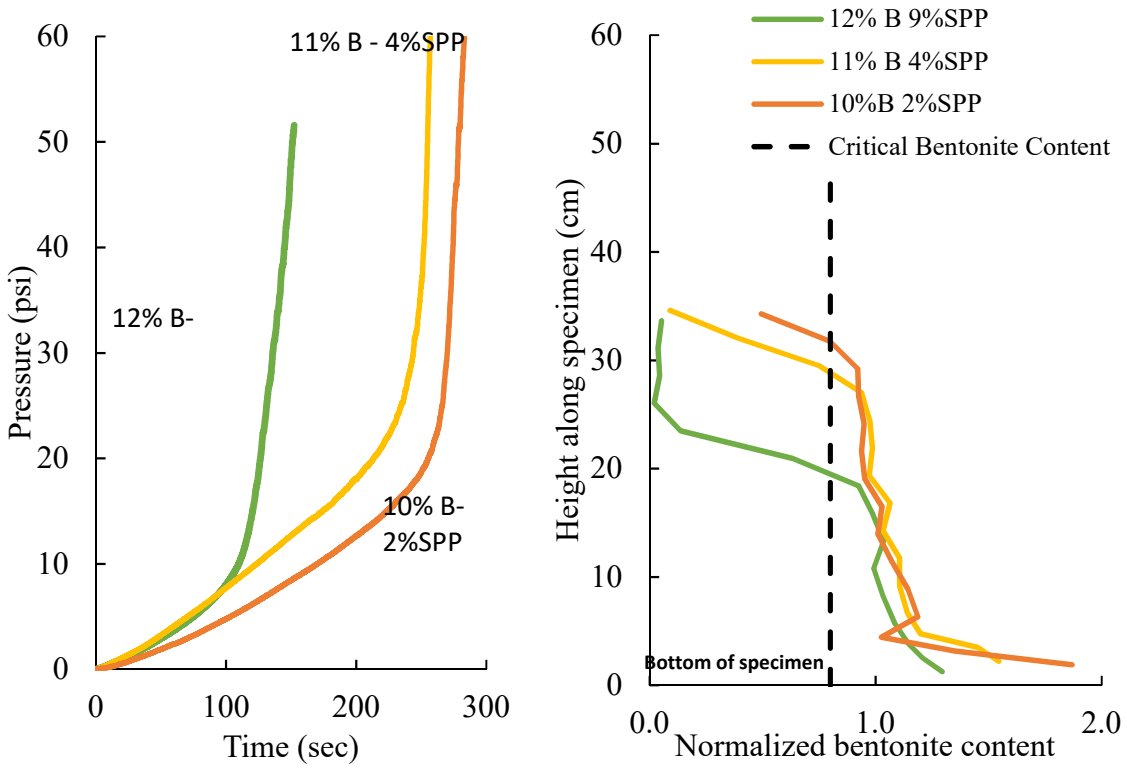

Figure 5-7: Effect of percentage of bentonite amount in grout on pressure-time plot

5.5.4. Effect of flow rate on permeation depth

If grout particles follow the laminar streamline in pore space, only those which are adjacent to sand grains get retained on the surface. There are three forces which control the transport phenomena of grout particles in pore space (Ives, 1987). First, the gravity force on particles is due to density difference and is represented as a ratio of Stokes velocity to the advective velocity of suspension flow. The gravity effect is given by

$$G = \frac{v_s}{v} = \frac{g(\rho_s - \rho_w)d^2A}{18\mu Q} \quad (5\text{-}2)$$

for suspension of 10% B and 3%SPP

g	= acceleration due to gravity	[9.81 m/s^2]
ρ_s	= density of particles	[1070 kg/m^3]
ρ_w	= density of water	[1000 kg/m^3]
d	= diameter of bentonite particle	[2.4 x 10^{-6} m]
Q	= flow rate	[1.66 x 10^{-6} m^3/s]
A	= Area of flow	[0.0039 m^2]
μ	= dynamic viscosity	[0.176 Kg/m/s]

$$G = \frac{v_s}{\mathrm{v}} = \frac{9.81 * (1070 - 1000) * (2.4\,x\,10^{-6})^2 * 0.0039}{18 * 0.176 * (1.66\,x\,10^{-6})} = 2.93\,x\,10^{-6} \quad (5\text{-}3)$$

The gravity effect of all suspensions used in experiments is in the range of 1.84 x 10^{-5} to 3 x 10^{-6} which is small to consider as a dominating factor for filtration.

Second, Brownian motion is the random thermal motion of water molecules which increases the probability of filtration of clay particles in water. The Brownian mechanism referred to as diffusion and is represented by Peclet number, a ratio of advective velocity to Brownian velocity.

$$\frac{1}{P} = \frac{D}{dv} = \frac{kT}{\pi\mu dv\beta} \quad (5\text{-}4)$$

k	= Boltzmann's constant	[1.38 x 10^{-23} J/K]
T	= Absolute temperature	[22K]

v	= advective velocity	[m/s]
d	= diameter of bentonite particle	[2.4 x 10^{-6} m]
β	= diameter of grain particle	[3.1 x 10^{-4}m]
μ	= dynamic viscosity	[Kg/m/s]

Efficient filtration range of Peclet number is 10^{-8} to 0.5 x 10^{-5}. The Peclet number for bentonite suspensions with different flow rates is in the range of 1.5 x 10^{-14} to 3.8 x 10^{-15}, which is small compared to the filtration range. Hence filtration because of Brownian motion in pore space is neglected.

Third, hydrodynamic forces are significant for plate-like clay particles. Laminar flow velocity is not uniform through pore openings, resulting in a gradient causing clay particles to rotate as they move through water. For particles floating through water with rotation, turn and twist motions intersect grain boundaries and increase the opportunity of clay particles collection. It is complicated to analyze the trajectory of the particle to determine filtration. Figure 5-8 depicts the effect of flow velocity on permeation of bentonite suspension. Velocity gradient across pore opening increases with increase in flow rate which causes rotation, turn and twist motions of clay particles add more probability to accumulate on the grain surface. Clay particles accumulate at a faster rate when passing through pore space at higher flow rate. Hence the volume of grout permeated is less for higher flow velocity because of the earlier formation of the external filter cake.

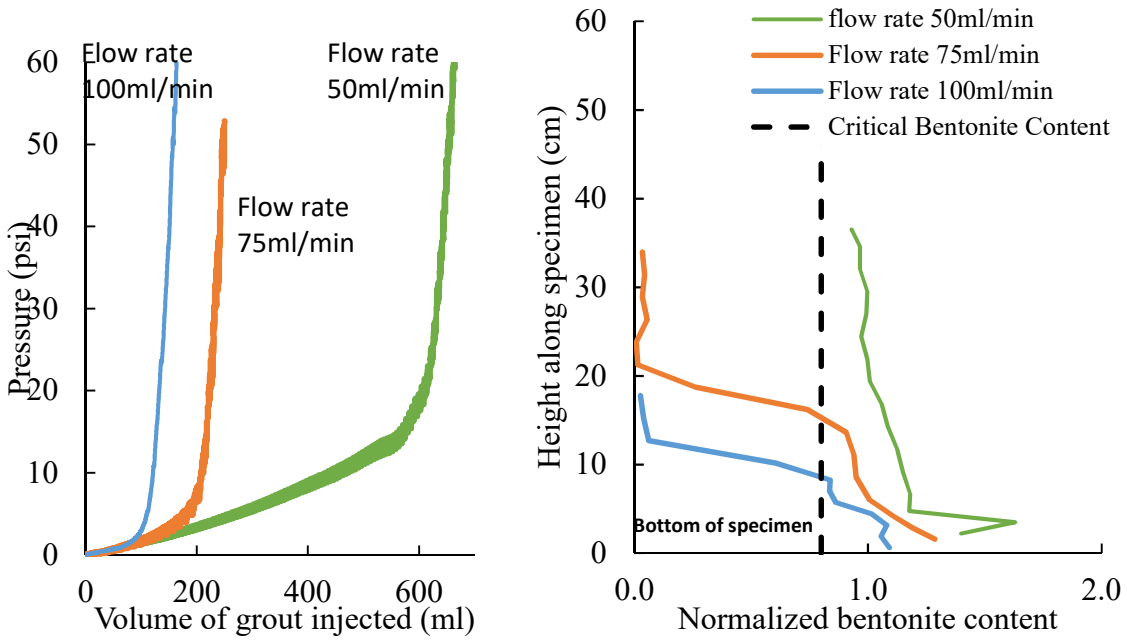

Figure 5-8: Result of permeation experiment of 9%B 2%SPP bentonite suspension at different flow rate

Permeation depth at a flow rate of 50ml/min is higher because of slow filtration rate compared to permeation at higher flow rates of 75 ml/min or 100 ml/min. The grout injected at slow flow rate resulted in the uniform bentonite content profile.

5.5.5. Effect of grain size distribution of soil

Filtration due to size exclusion depends on the grain size distribution of suspension and porous media. Penetration length is affected by the finer pore space of soil and coarser particle size of suspension. D_{95} of bentonite particles is 25µm for all grouts. Figure 5-9 shows the grain size distribution of three sands used for penetration tests: Sand A (D_{10} = 0.07mm), Sand B (D_{10} = 0.2) and Sand C (D_{10} = 0.3mm). The grain size (D_{10}) of porous media was normalized by the grain size (d_{95}) of bentonite and termed as a normalized effective grain size ($N = D_{10}/d_{95}$).

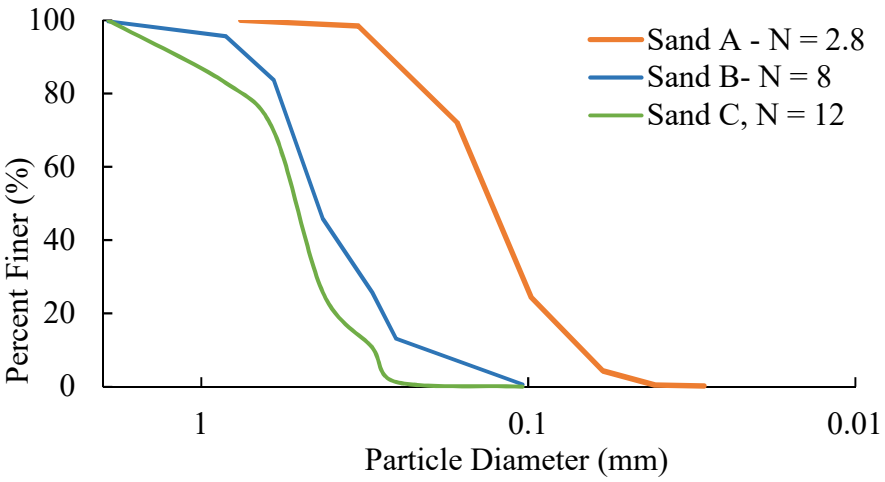

Figure 5-9: Grain size distribution of soils used in this study

The grain size of sand and suspension particles influences the permeation of bentonite grout (Figure 5-11 and Figure 5-11). Pressure starts building exponentially faster for the grout passing through the finer soil (Sand A) than that passing through soils with larger normalized effective grain size (Sand B and C) because of filtration due to size exclusion.

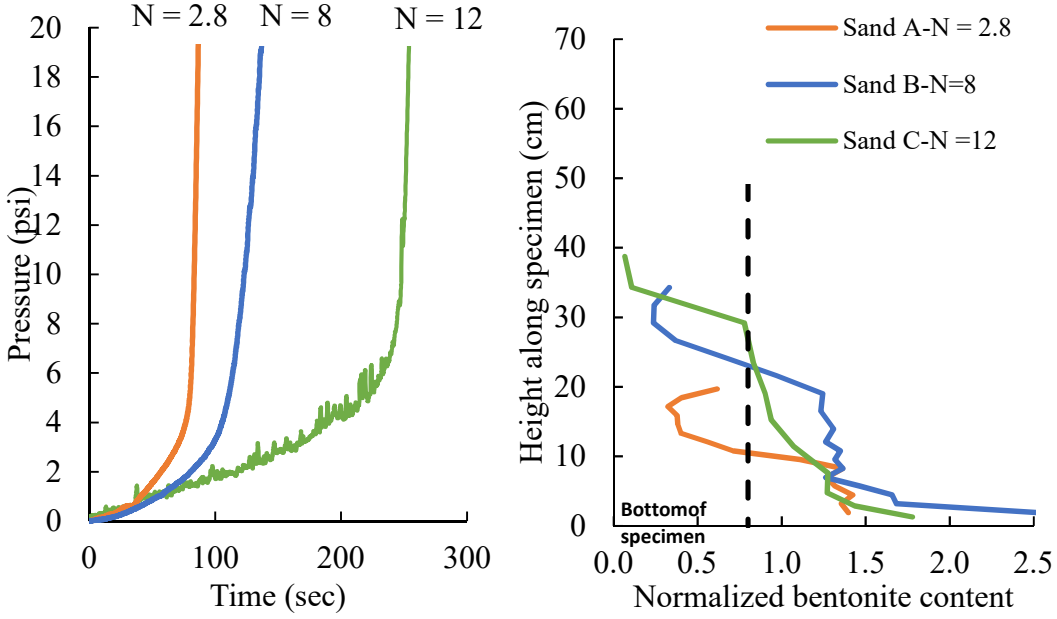

Figure 5-10: Permeation result of 8%B 2%SPP grout passing through three different type of soil

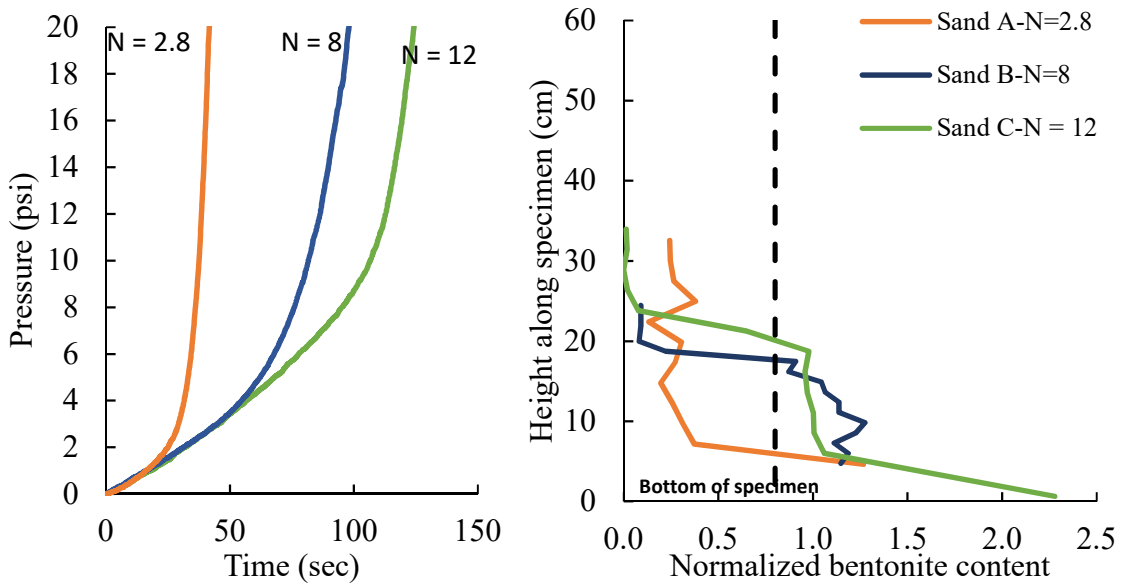

Figure 5-11: Permeation result of 10%B 3%SPP grout passing through three different type of soil

The possibility of bentonite particles filtering in pore space decreases with increase in D_{10} particle size of porous media. Permeation depth increases with increase in pore size of porous media; it is 6.35 cm for grout passing through Sand A (N = 2.8), 17.78 cm for Sand B (N = 8) and 20.32 cm for Sand C for 10%B 3%SPP suspension grout (Figure 5-11).

5.6.Empirical solution

Consultants are required to predict, relying on empirical relationships, the result of permeation grouting before performing on a large scale. Until now, empirical groutability ratio, $Nc = D_{10}/d_{95}$ was used to assess the penetrability of suspension grout (Mitchell, 1981) where D_{10} is the diameter at 10% of the cumulative particle size distribution of the porous media and d_{95} is the diameter at 95% of the cumulative particle size distribution of the grout solids. The

experimental results revealed that the performance of permeation grouting not only depends on grain size distribution of porous media and grout particles but also on the rheology of grout, the injection rate of grout, grout concentration, and filtration tendency. The pressure-time curves were found to be a good indicator of the groutability of suspension grouts and penetration depth.

Empirical relationships were developed to assess the performance of constant flux permeation grouting by determining the injection pressure. Various factors were determined which influence the shape of the pressure-time curve. Pressure-time curve is approximately linear at the beginning of injection and then eventually starts increasing at a faster rate because of rheological blockage or path blockage due to filtration. An equation which captures the linear as well as the exponential trend of the pressure-time curve is suggested. The temporal increase of pressure at the injection point is defined as follows:

$$P = (A \times t)^{exp(B \times t)^C} \tag{5-5}$$

where, t is time, A, B, and C are fitting coefficients based on laboratory data and grout material properties. Fitting coefficient A defines the rate of pressure build-up at the beginning of permeation process which is function of the grout viscosity, injection flux rate and pore space of porous media. The rate of pressure increase changes drastically after a while because of rheological or path blockage. Fitting coefficients B and C control the latter part of the pressure-time curve where pressure build-up trend changes drastically and they are functions of bentonite concentration, percentage of SPP additives, normalized size ratio, and injection flux rate. Figure 5-12 shows that the equation fits well experimentally obtained pressure-time curves.

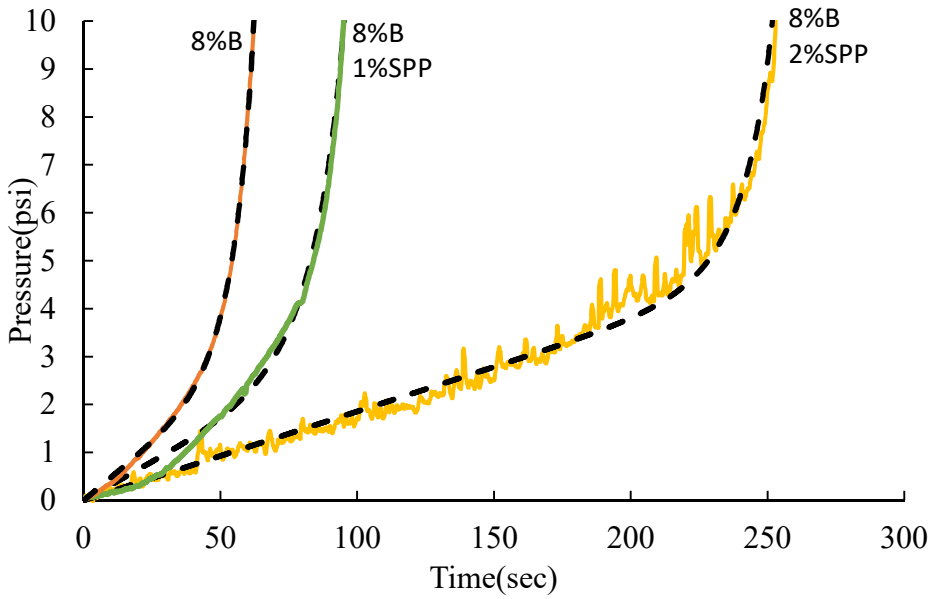

Figure 5-12: Curve fitting of the equation to the pressure-time curve of laboratory tests

Table 5-2 shows the fitting coefficients A, B, and C of the pressure-time curves obtained in the laboratory using the SOLVER tool in MS excel.

Table 5-2: Fitting Coefficient of the equation of pressure-time curve of laboratory tests

Bentonite concentration (%)	SPP (%)	Apparent viscosity (mPa.s)	Flow rate (cm/s)	Normalized effective grain size ($N = D_{10}/d_{95}$)	A	B	C
5	0	58.00	1.67	12	0.001	0.000	12.000
7	0	82.84	1.67	12	0.028	0.008	7.125
8	0	95.34	1.67	12	0.049	0.014	2.590
9	2	90.00	1.67	12	0.035	0.017	4.409
9	2	90.00	1.25	12	0.021	0.005	4.231
9	2	90.00	0.83	12	0.017	0.001	10.120
8	2	76.56	1.67	12	0.019	0.006	7.365
8	2	76.56	1.67	8	0.022	0.009	8.500
8	2	76.56	1.67	2.8	0.029	0.012	5.470
8	0	95.34	1.67	12	0.049	0.014	2.590
8	1	77.35	1.67	12	0.022	0.009	5.000
8	2	76.56	1.67	12	0.019	0.006	7.365

The correlations of fitting coefficients with bentonite concentration, percentage of SPP, injection flux rate, rheology of grout and normalized grain size ratio were developed using multivariate regression. Following are the correlations of the fitting coefficients

$$A = (1.15 \times 10^{-3} * V) + (2.63 \times 10^{-2} * F) - (7.77 \times 10^{-4} * S) - 0.102; \quad (5\text{-}6)$$

$$B = (0.546 * B) - (0.429 * SPP) + (2.11 \times 10^{-4} * F) - (6.40 \times 10^{-4} * S) - 0.0427; \quad (5\text{-}7)$$

If B <0 then B = 0;

$$C = -(355.02 * B) + (183.74 * SPP) + (9.54 \times 10^{-2} * F) + (1.75 \times 10^{-1} * S) + 39.89 \quad (5\text{-}8)$$

Fitting coefficient A is linearly dependent on the viscosity of grout and flow rate, and inversely proportional to normalized grain size ratio. The exponential increase of injection pressure starts earlier for a grout with higher bentonite concentration and for higher injection rate, whereas it starts later with an increase in pore space and with the addition of SPP which stabilize the suspension grout and lowers its viscosity. Hence the coefficient B increases with increase in bentonite concentration and flow rate and decreases with the addition of SPP and increase in pore space.

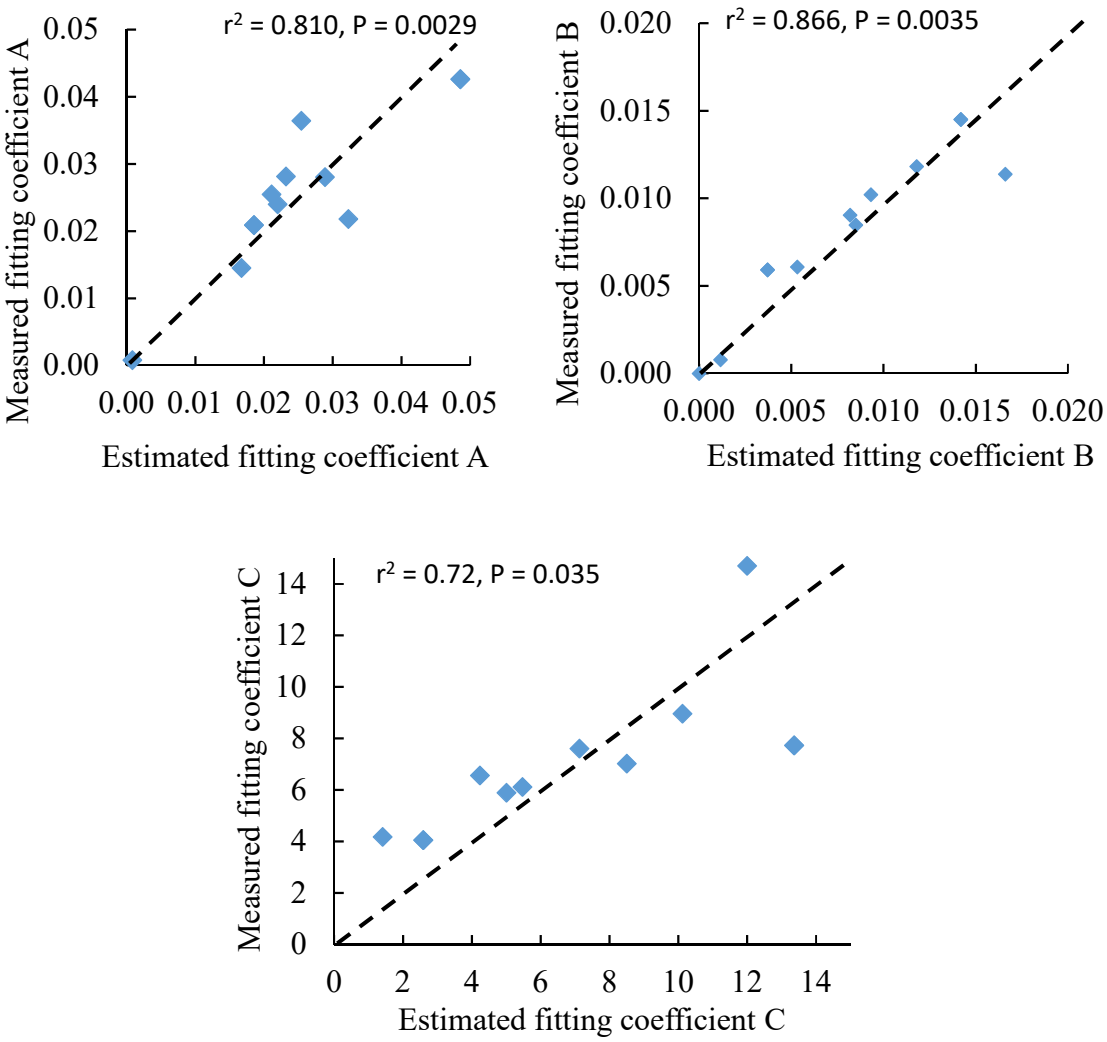

Figure 5-13: Plots of estimated and measured fitting coefficient determined by multivariate regression

The empirical equations of fitting coefficients (Equations (1) to (4)) were used to assess the injection pressure for constant flux permeation grouting. Figure 5-14 shows that estimated pressure time curves using empirical equations fit very closely the experimentally measured pressure-time curves.

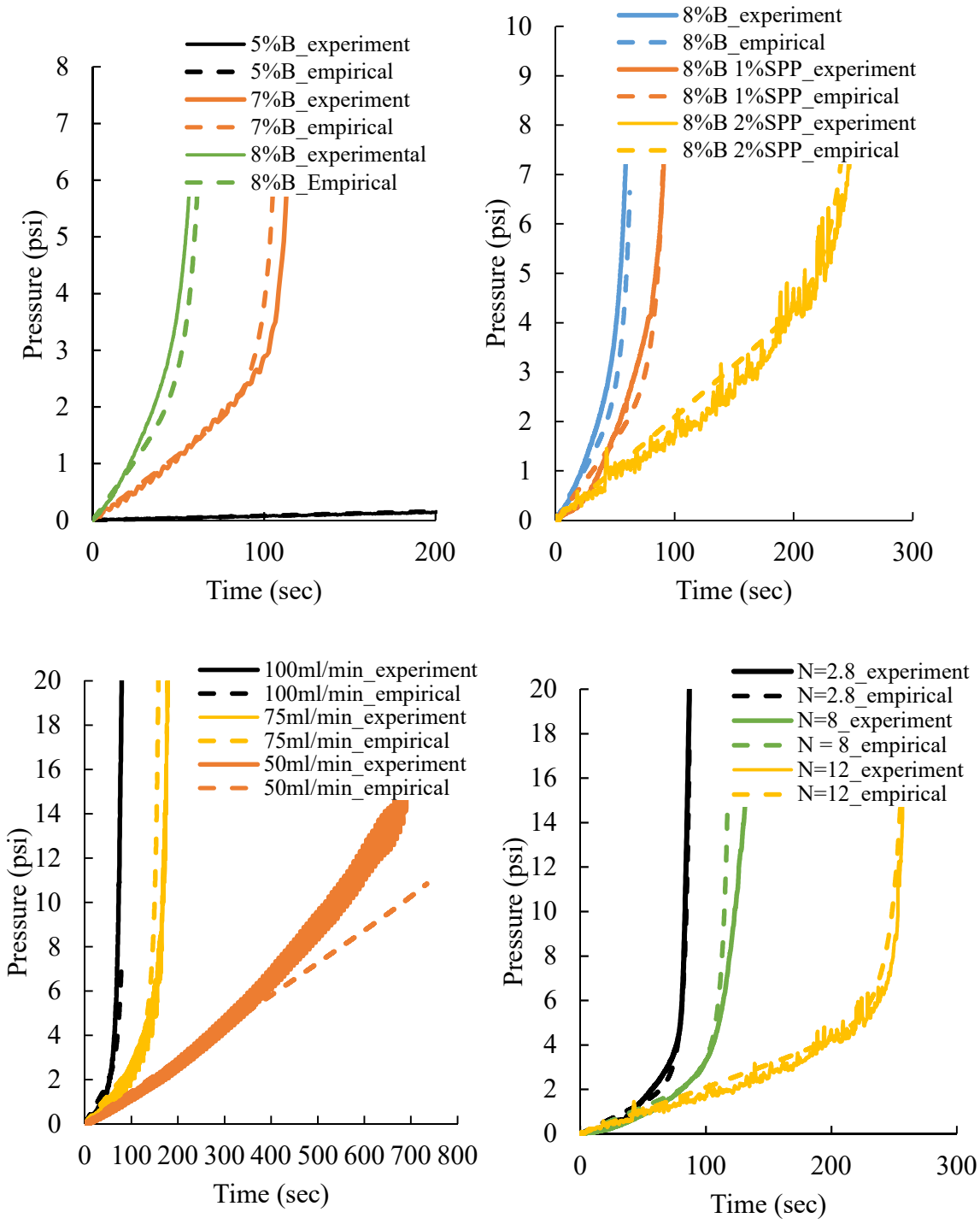

Figure 5-14: Comparison of estimated pressure-time curve using empirical equations and measured pressure-time curve in the laboratory.

5.7.Conclusion

In this chapter, an attempt to predict the performance of permeation grouting was made by developing an empirical solution. First, the laboratory tests were performed to determine the controlling factors in constant flux permeation grouting. The performance of permeation grouting was evaluated through the pressure-time curves and bentonite content profiles. It is found that rheology of grout, bentonite concentration, percentage of additives, injection flux rate and grain size distribution of porous media and grout are controlling factors for permeation grouting. An equation was developed to define the characteristics of the pressure-time curves, where the fitting coefficients are function of the controlling factors. Hence the injection pressure can be determined for a known grout material and given porous media information under constant flux permeation grouting. Empirically estimated injection pressures were found to closely match the measured injection pressures. The results of this study are particularly useful for consultants to predict the behavior of suspension grout in the ground before aplying it in the field.

CHAPTER 6 PERFORMANCE OF MICROFINE CEMENT GROUTS IN PERMEATION GROUTING: A COMPARISON OF TWO CEMENT TYPES AND TWO STABILIZATION ADDITIVES

6.1 Abstract

In some cases, permeation grouting might be a very cost effective soil improvement technique. It is commonly used for underground flow control or strengthening a body of soil. In soil strengthening applications, cement grouts are widely used for sands with relatively high permeability. Extensive studies were performed to understand cement grouting over the past years. However, due to the complexity of the behavior of cement grouts, and the large number of variables involved (related to the grout as well as soil properties) more studies need to be done to accomplish a better understanding of this problem. Recently, the use of fine grained cement (microfine) in addition to chemical additives improved the performance of cement grouts and widened the range of soils it can penetrate. However, different types of microfine cements result in completely different performances in grouting operations. Also, different additives are used to improve grouts' performance by changing different grout properties. An experimental study is conducted to evaluate and compare the performance of two microfine cement types and the effect of two commonly used additives with cement grouts. Rheology and stability tests are performed on 1.5 in. sand column with different grout mixes. Then, constant flow permeation tests are done using a two feet long rigid wall permeameter, followed by measurements of the unconfined compressive strength of the grouted sand as function of the distance from injection point. These results are used to evaluate the performance of different grout mixes and the quality of the end product in each case.

6.2 Introduction

Over the past decade, the use of Microfine cement in grouting has grown substantially, and is expected to continue expanding worldwide in the future (Henn 2010). Microfine cement grouts provide better performance than Portland cement grouts. For instance, they have superior flow characteristics and bleed resistance, and they can penetrate finer sand (Henn 2010, Mollamahmutolu and Avci, 2014, Markou et al. 2014). Although the cost of Microfine cement is considerably high compared to Portland cement, this cost is offset by its superior performance (Henn 2010).

Neat cement grouts tend to be unstable, and have generally filtration problem. Due to the many problems associated with its use, an unstable grout is very undesirable in cement grouting operations (Rosquoët et al. 2003, Naudts et al. 2004, Tan et al. 2004, Bremen 1997). Different additives are used to stabilize cement grouts and improve their performance, among them are superplasticizers and bentonite. The addition of superplasticizer disperses the grout and reduces its apparent viscosity and yield point (Hakansson et al. 1992, Bremen 1997), and leads to higher success in grouting operations (Mollamahmutolu and Avci, 2014). Bentonite is also used for the stabilization of cement grouts (Tan et al. 2004, Hakansson et al. 1992). However, the bentonite increases the yield strength and viscosity of the suspension and therefore is not recommended if high penetrability is targeted (Bremen 1997).

In this chapter, the performance of two types of Microfine cements in addition to two additives used for grout stabilization are investigated experimentally. The experimental program consists of rheological measurements, stability evaluation, permeation tests, and unconfined compression tests for the different grout mixes. First, neat cement grouts with different water to

cement ratios were used to compare the performance of two types of Microfine cements, M1 and M2. Then, the cement type with better performance is used to investigate two popular stabilization additives: Superplasticizer (SP), and Bentonite (B).

6.3 Experimental Program

The viscosity of the different grout mixes used in this study is measured using a Rheometer. The suspension's viscosity controls the pumping pressure required to move the grout through the soil's voids. For constant flow grouting, higher viscosity results in higher pressure buildup at the injection point. Therefore, a low viscosity grout is desirable from injectability point of view.

The stability of grouts is a key factor affecting the uniformity of grout propagation and filtration. Suspensions consisting of only cement and water, neat cement grouts, tend to be unstable. Therefore, they are usually stabilized using different additives. To assess the stability of cement grouts, the water to cement ratio of grout samples is measured at different heights of a grout column, for different sedimentation periods.

The performance of the different cement grouts is determined by permeating them through a two feet long sand column. During the permeation stage, pressure vs. time curves are generated, in addition to measurements of cement particles front's height vs. time. Also, cement particles filtration through a 1.5 in. sand column is evaluated by measuring the cement content at the permeameter outlet with time. This information is used to analyze the effectiveness of the different grout mixes. Finally, the strength of the grouted sand is measured at different distances from the injection point. These measurements reflect the uniformity of cement content within the grouted

sand. Table 6-1 summarizes the different grout mixes used for this experimental work, in addition to general samples' properties.

Table 6-1: Grout Mixes used for experimental work

Cement type	w:c ratio	Stabilizing additive	Sand's void ratio	Test Type
M1	10:1	-	0.76	Permeation, UC*
M1	7:1	-	0.71	Filtration
M1	5:1	-	0.72	Permeation, Filtration, UC
M1	3:1	-	0.73	Permeation, Filtration, UC
M1	1.5:1	-	0.75	Permeation, UC
M2	10:1	-	0.72	Permeation, UC
M2	5:1	-	0.73	Permeation, UC
M2	3:1	-	0.74	Permeation, UC
M1	10:1	2.5% SP	0.73	Permeation, UC
M1	1.5:1	2.5% SP	0.74	Permeation, UC
M1	7:1	2.5% SP		Filtration
M1	5:1	2.5% SP		Filtration
M1	3:1	2.5% SP		Filtration
M1	10:1	1% B	0.74	Permeation

6.3.1 Rheology measurements

Rheology is one of the most important properties that control the flow of grout within the pores of the soil. It controls the pressure required to move grout of pressure buildup for an applied flow rate. This is important in low confinement and for viscous blocking phenomenon. Therefore, the rheology of the different suspensions is measured using a rheometer, shown in Figure 6-1.

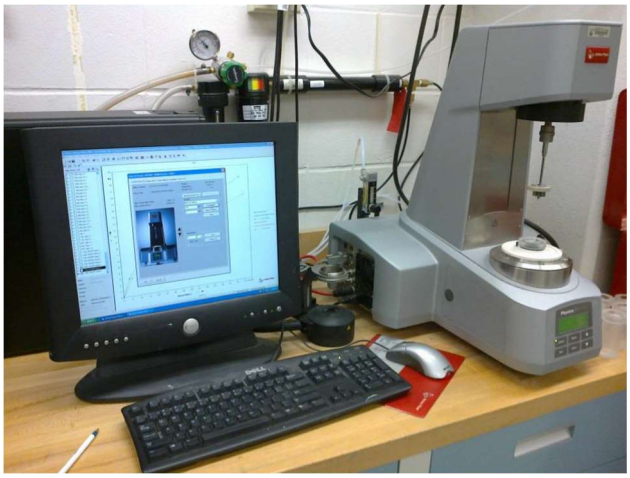

Figure 6-1: Rheometer with data acquisition

6.3.2 Sedimentation Tests

When water comes in contact of cement particles the hydration begins and then the water is part of free water and part of chemically bonded particle. Physical phenomena occurring during the hydration of cement pastes are linked to sedimentation. A simple gravitational sedimentation test was performed to determine the stability of each grout used in this study. The cement pastes were filled in 50ml transparent measuring cylinder and after the beginning of sedimentation, the upper part of column had more water than the lower part. Stoke's law governs the sedimentation of particles, the finer they are, the slower the process is. The level of cloudy water was noticed visually with time to determine the sedimentation rate. The gravitational sedimentation has limited practical value due to (a) visual interpretation of the level of cloudy water (b) being performed in no condition. But this test could give a rough estimate of the stability of cement based grout. Figure 6-2 shows the measuring cylinder used for the sedimentation tests and volume of clear water is recorded with time.

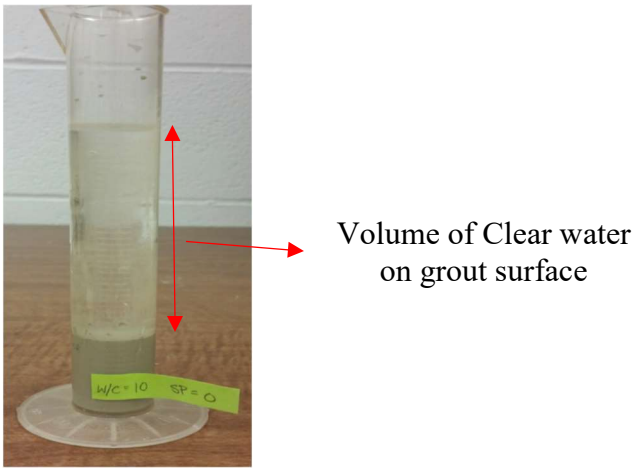

Figure 6-2: Gravitational sedimentation test setup of cement based grout

6.3.3 Stability tests

The stability of different grout mixes is evaluated by measuring the settlement of cement particles in a grout column with time. At time zero, a freshly mixed suspension is placed in four 100 ml cylinders with the same height. At a given time, the content of one of the cylinders is removed in sections based on the grout height, and each section is placed in a can for cement content measurement (Figure 6-3). Four cylinders are used to measure the cement content distribution with height after 5, 10, 30, and 60 min. A total of four suspensions having a water to solids ratio of 3:1 are tested, with the following compositions: water+M1, water+M2, water+M1+2.5% SP, water+M1+1% B. The additives' content is by weight of cement.

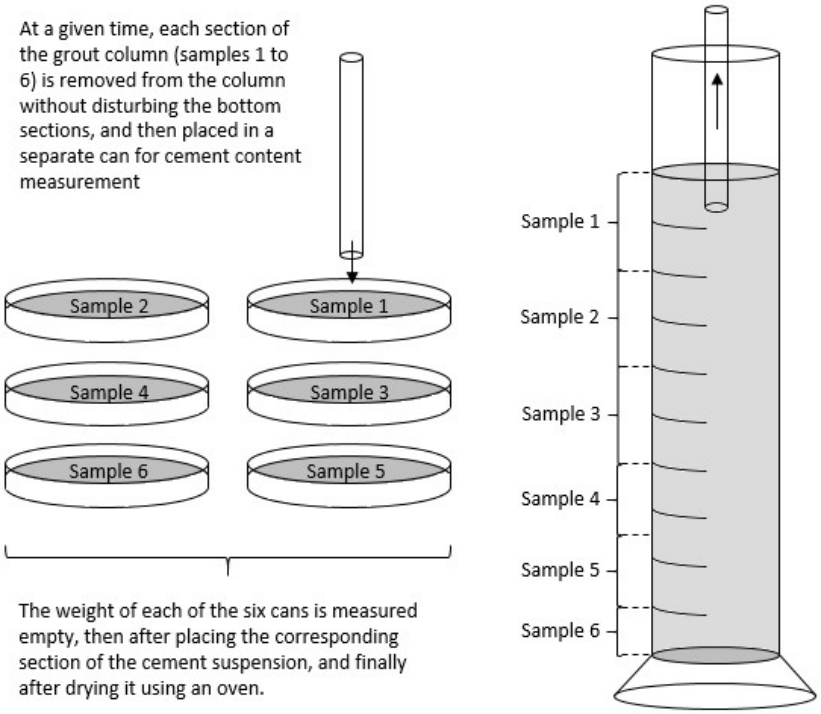

Figure 6-3: Schematic of Stability test

6.3.4 Hydrometer test of cement grout

Hydrometer test was performed on suspension to determine the size of hydrated cement particles in grout. 100ml of grout was prepared with and without additives. The grout was placed in 1000ml hydrometer jar and distilled water was added. Jar was sealed by stopper and the content was shake until all the material is moving freely, then continued mixing by inverting 25 times allowing the air bubbles movement to control the cycle interval. Then, cylinder is placed on a firm, level, vibration free position in constant temperature environment. Immediately timer was started and sedimentation reading was taken by placing the hydrometer in the hydrometer cylinder.

6.3.5 Permeation tests

The permeation setup shown in Figure 6-4 contains a 2 ft. long, 2.8 in. diameter sand column. The 2-ft. column consists of four 6 in. long split tubes that can be fixed independently in place before placing the rest of the top tubes and the top cap. The sand is pluviated into the 6 in.

tubes individually, allowing for a more uniform sample preparation. Two 1.5 in. long tubes filled with filter material, gravel and coarse sand, are added to the top and bottom of the 6 in. tubes stack. The filter materials guarantee a uniform grout flow into and out of the sand column.

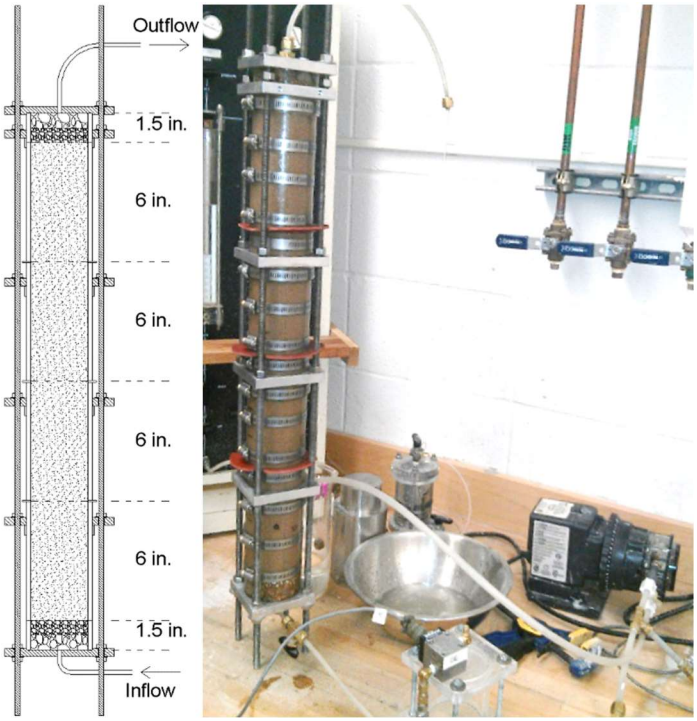

Figure 6-4: Permeation test set up

After the sand column is constructed, it is flushed with CO_2. This step is done before water flushing to achieve a higher water saturation later. Then, the sand column is flushed with water for at least two pore volumes. Finally, the sand column is flushed with cement grout while pressure at the injection point and grout front's height are recorded with time. A constant flow pump with a flow rate of 100 ml/min is used for water and cement flushing. Three days after grouting, the grouted sand specimens are tested under unconfined compression. Each column produces four 6 in. high, 2.8 in. diameter cemented sand specimen to be tested.

6.3.6 Unconfined compression tests

The unconfined compressive strength of each of the 6 in. samples is measured after a setting time of three days (Figure 6-5). A displacement rate of 1% per minute is applied for all samples. This test gives a direct evaluation for a grout's performance. The variation of strength as function of the distance from the injection point reveals the quality of the grouting operation's outcome. A non-uniform strength profile indicates a low-quality end product, and is due to filtration of cement particles.

Figure 6-5: Unconfined compressive strength test on 6in sample

6.4 Results

In this section, results of the previously described tests are presented and discussed. First, the rheological tests provide the apparent viscosity of cement grout mixes at different shear rates. Second, stability tests comparing M1 to M2 and SP to B are presented. The stability tests results in water to solids ratio (inversely proportional to cement content) profiles with height for different sedimentation times. Third, permeation tests' results including pressure at the injection point and cement particles' front height are plotted against time. Finally, the unconfined compressive

strength profiles of the grouted sand columns are presented. The strength profiles provide a direct measurement of the uniformity of cement propagation and the quality of grouted soil.

6.4.1 Rheology results

The rheology of cement grout mixes is measured using a rheometer. Figure 6-6 compares the apparent viscosity of M1 to M2 at two different shear rates: 100 and 1000/sec. M2 cement grouts have slightly higher apparent viscosity than M1 cement grouts at 100/sec shear rate, this difference is more significant for the grout with 1.5 to 1 water to solids ratio. The results also show that these cement grouts are shear thinning since their apparent viscosity decreases as the shear rate increases.

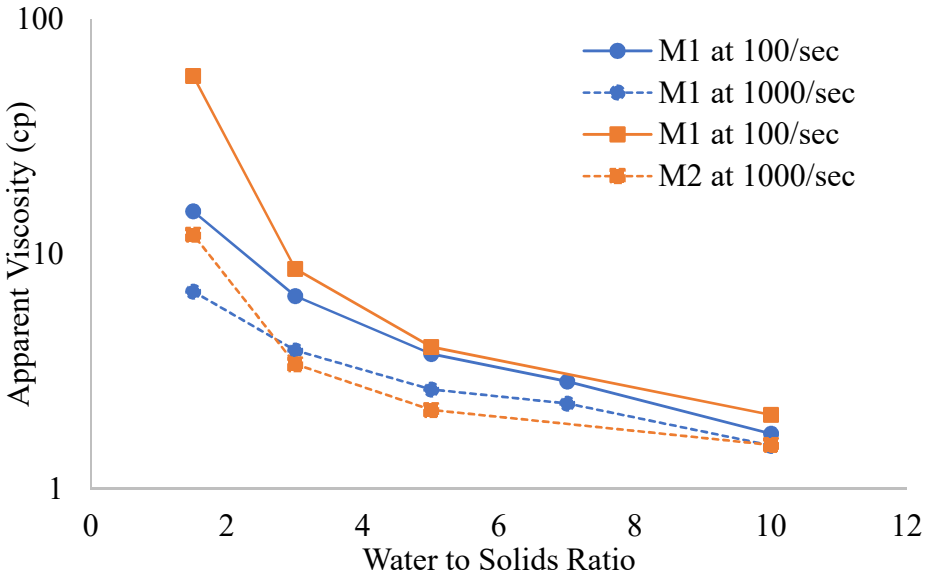

Figure 6-6: Rheology of M1 and M2 cement grout without additives at shear rate of 100 1/s and 1000 1/s

The effects of additives on the grout rheology are presented in Figure 6-7. Adding superplasticizer reduces significantly the apparent viscosity of the grout for both 100 and 1000/sec shear rates. Adding bentonite to the cement grout increases its apparent viscosity at 100/sec shear

rate. However, as the shear rate increases to 1000/sec, the effect of bentonite addition on the grout's rheology decreases. Note that the grout experiences relatively low shear rates during permeation, and therefore the viscosity measurements at 100/sec are more relevant for comparing the expected grout performances.

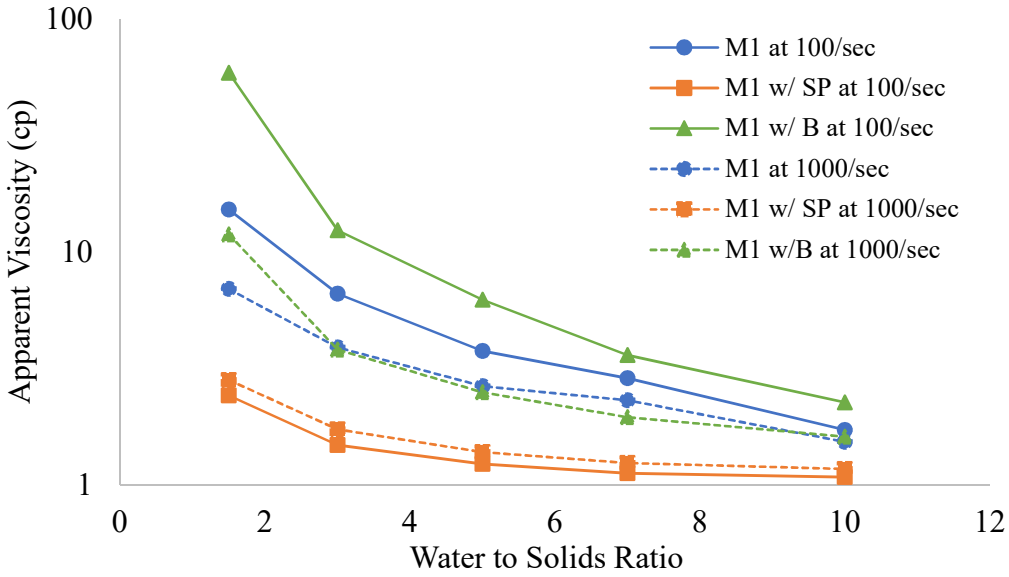

Figure 6-7: Rheology of M1 cement with and without additives at shear rates of 100 1/s and 1000 1/s

The characteristics and microstructure of grout change constantly due to level of hydration. The change in the rheology of grout with and without additives is observed with time. Thixotropic property is commonly encountered when using low water/cement ratio. Thixotropic behavior of cement grout of water/cement ratio of 1.5 and 3 are showed in Figure 6-8.

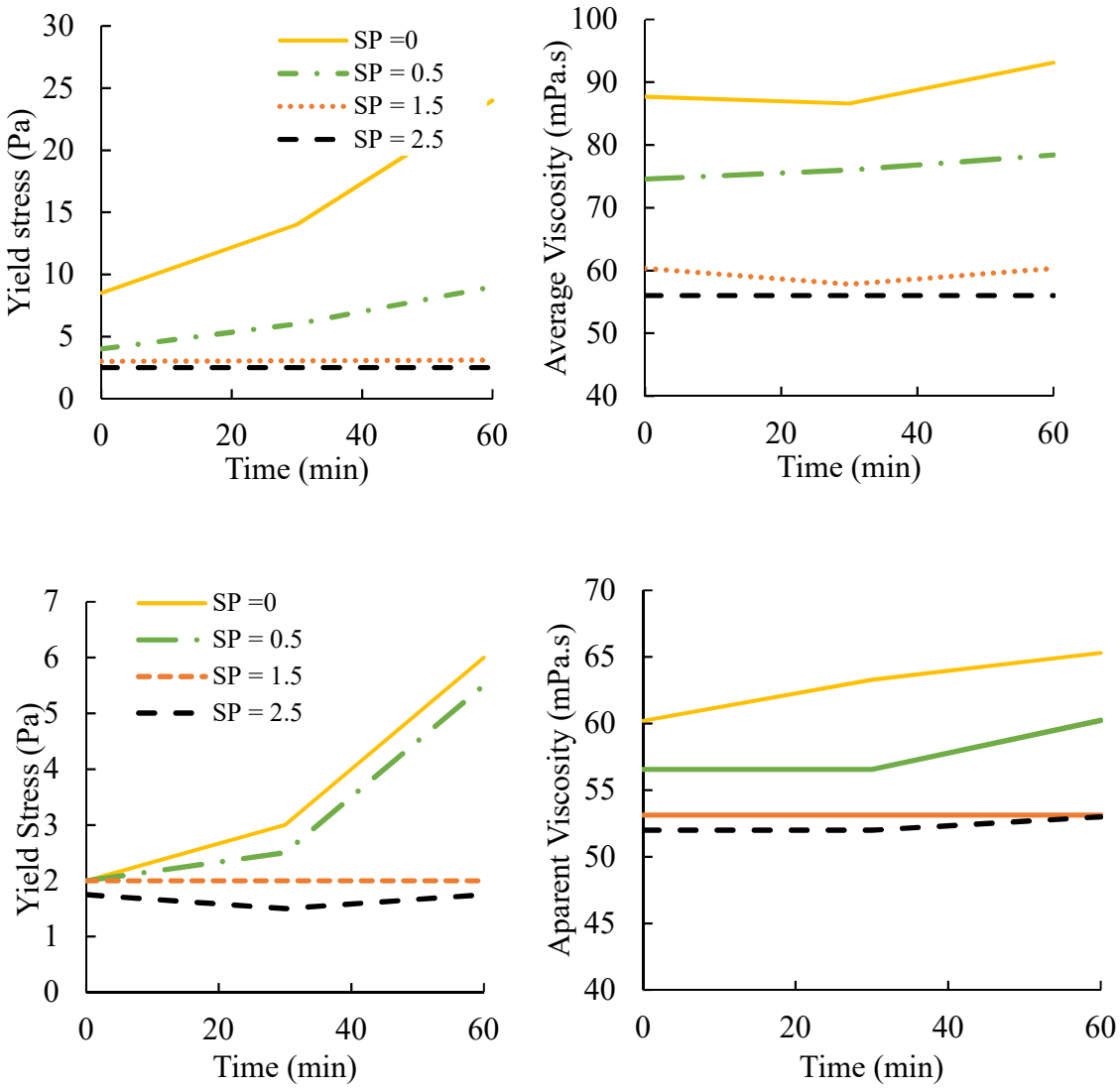

Figure 6-8: Thixotropic rheological property of cement grout of W/C of 1.5 and 3

It is observed that addition of superplasticizer affects the thixotropic property of grout. Cement grout with additives doesn't build bondage and get thicker with time. All the grouts were kept in high speed mixer before the injection to negate the effect of thixotropy.

6.4.2 Sedimentation test results

Figure 6-9 shows the result of the sedimentation test of cement grout of W/C raio of 10 after two hours.

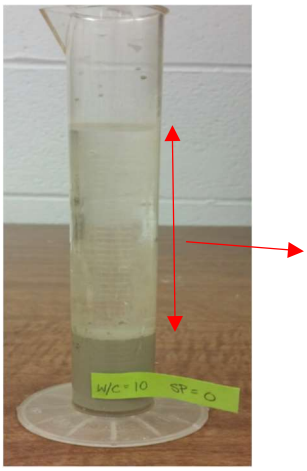

Volume of Clear water on grout surface

Figure 6-9: Gravitational sedimentation test of cement based grout of W/C 10:1 without SP

Figure 6-9 shows the bleeding caused by the sedimentation of cement particle of 70% in two hours. The height of clear water is recorded with time and plotted to evaluated the sedimentation rate and stability of grout used in this study.

Figure 6-10 shows the sedimentation results of grout of concentration of W/C of 3,5,7 and 10 without additives. Low concentrated grout is less stable and has faster sedimentation rate than concentrated grout. In the low concentrated grout, there is large amount of free water and cement particles are not well bonded and settled easily.

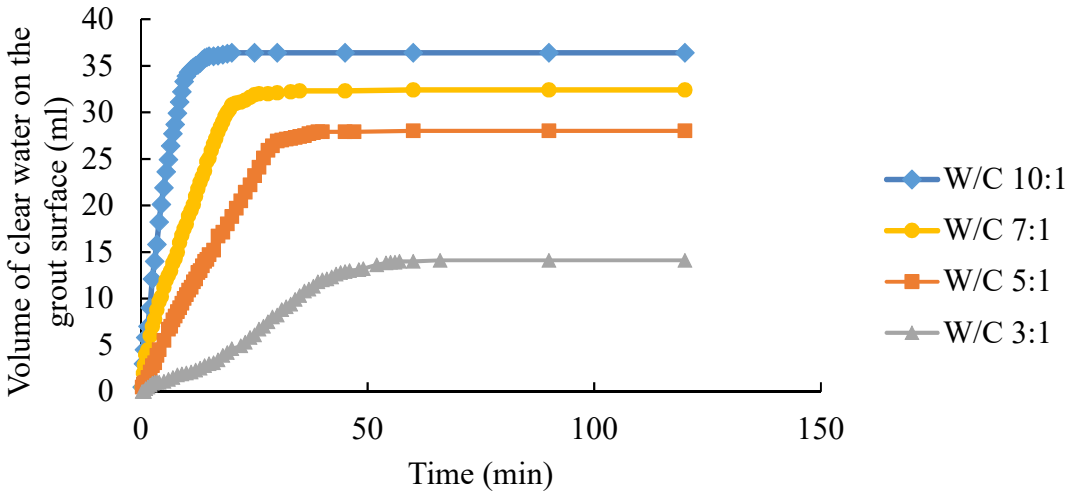

Figure 6-10: Height of suspended cement particle in the measuring cylinder for sedimentation test (a) without additives (b) with additives

Bleeding process is very complex and is governed by different physical and chemical processes like sedimentation, consolidation, flocculation and hydration. Almir Dragonovic (2009) showed that consolidation has a small influence on bleeding in fractures. In grout, other processes such as hydration, attraction and repulsion between particles influencing sedimentation take place. It could also be important to know if particles in grout settle as single particles or in flocks. If they settle as single particles it should result in a particle size gradient in the sample. Larger particles should be more concentrated at the bottom and finer particles should be more concentrated in the upper part of the sample since, according to Stock's law, sedimentation velocity is proportional to the square of a particle's diameter. If there is no particle size gradient in the grout, it could mean that particles have been flocculated. Flocculation is a process in which single particles build clumps of particles. This happens when attractive forces between particles are larger than repulsive forces. Herzig et al. (1970) showed that behavior of colloid particles is more controlled by surface effects than by gravitation. This will have an impact on flocculation.

Sedimentation due to flocculation can be resolved by adding the super plasticizers to the grout. Super plasticizer stabilizes the grout by dispersing the cement particles i.e. particles that have joined together to form agglomerates are separated. A radical increase in the specific surface available for water will take place, leading to increased activity in the hydration process. Also, the particles will be negatively charged by adsorption, which means that they will repel each other and not come close enough to form agglomerates. Figure 6-11 shows that addition of superplasticizer significantly reduces the bleeding of free water. The bleeding reduced to 4.4% from 70% for the cement grout of W/C of 10:1 with and without superplasticizer.

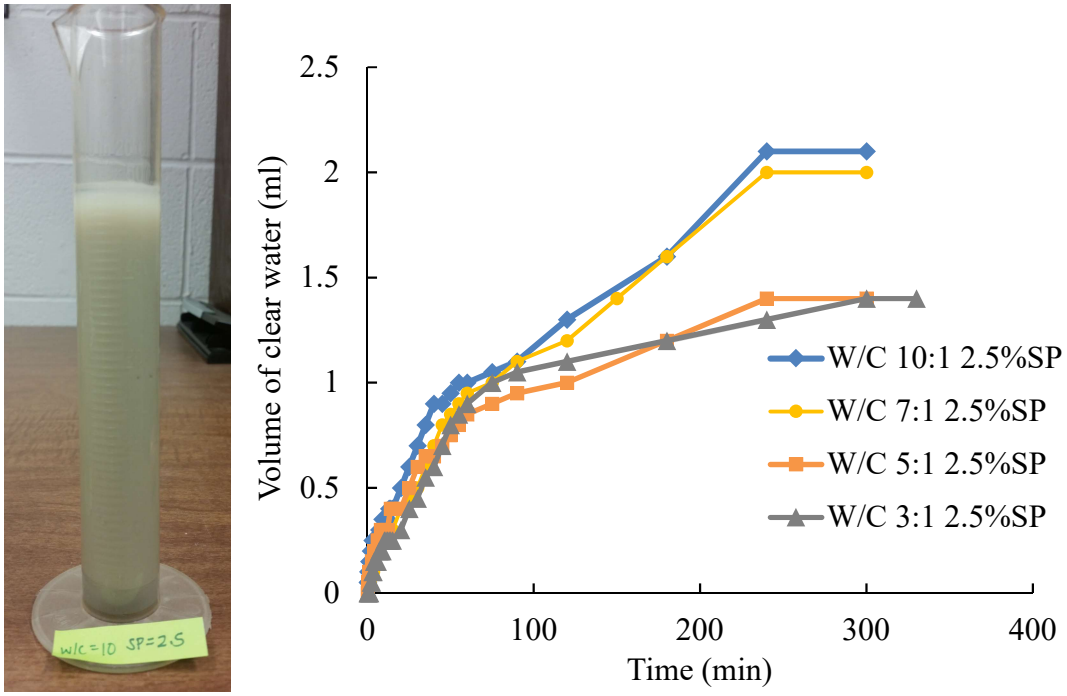

Figure 6-11: Sedimentation tests results for cement grout with the addition of 2.5% of superplasticizer

6.4.3 Stability test results

The stability of cement grouts is evaluated using sedimentation tests. A limitation of this test is being performed under no flow conditions. In fact, the flow of cement grouts through sand

highly affects the sedimentation of cement particles. Therefore, this test is used as a qualitative test and is limited to rough comparison of different grouts. In fact, the results of this test present a direct reflection of the inter-particles forces of the grouts' solids, which could be used in the analysis of the permeation tests' results.

The results of two tests comparing neat M1 to M2 suspensions with a water to cement ratio of 3:1 are presented in Figure 6-12.

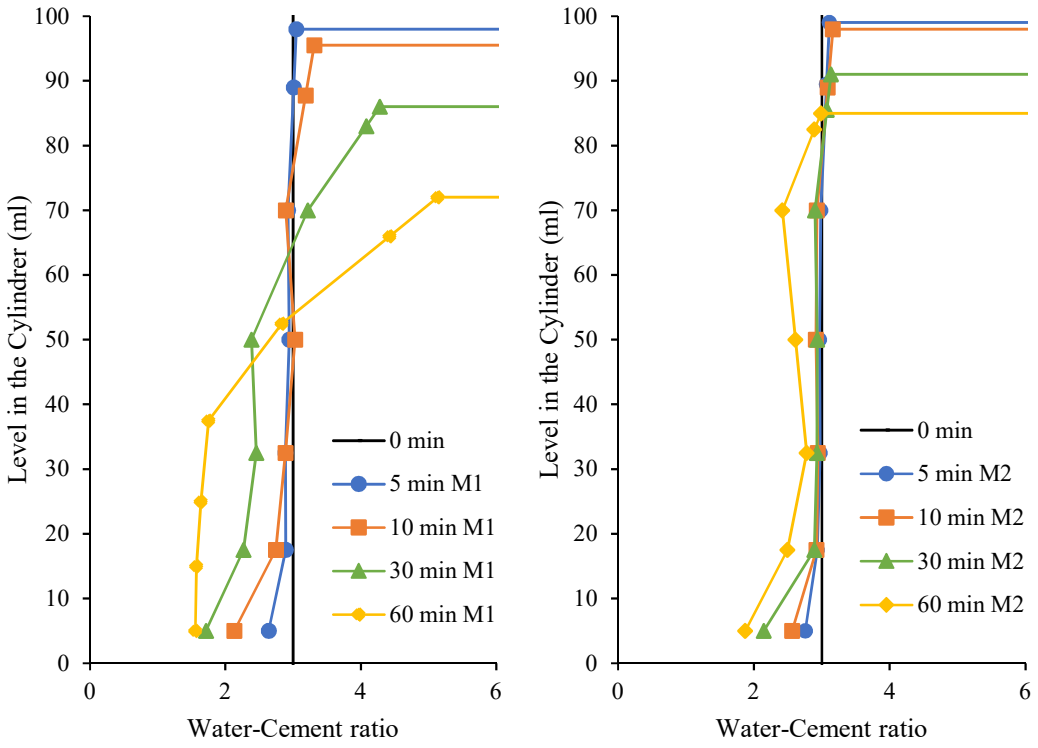

Figure 6-12: Result of sedimentation test of M1 and M2 cement grout

The results show that the M2 cement suspension experiences less sedimentation than M1 cement. This could be due to larger inter-particle forces which are reflected by the higher apparent viscosity measured for M2 cement suspensions.

The effect of additives, superplasticizer and bentonite, on the stability of M1 cement grout is shown in Figure 6-13. The addition of superplasticizer eliminated the appearance of a clear water layer at the top of the grout. This is usually interpreted as reduction of cement particles' sedimentation and increase in grout stability. However, the water to solids ratio profiles presented in Figure 6-13 (b) shows that the cement experiences significant sedimentation with time. It is also interesting to see that the water to solids ratio at the bottom of the cylinder reaches very low values compared to the no additives case shown in Figure 6-13(a). This test shows that although some of the dispersed cement particles require more time to sediment, higher sedimentation and water loss are expected after sufficient time is allowed. This finding is later confirmed by observations, discussed later, after the end of permeation. Adding 1% bentonite, by weight of cement, reduces the sedimentation and results in more uniform water-cement ratio profile throughout the cylinder. The addition of bentonite increases the yield strength of the cement grout, and therefore hinders cement particles' settlement and keeps them in suspension. This effect is reflected by the increase in apparent viscosity.

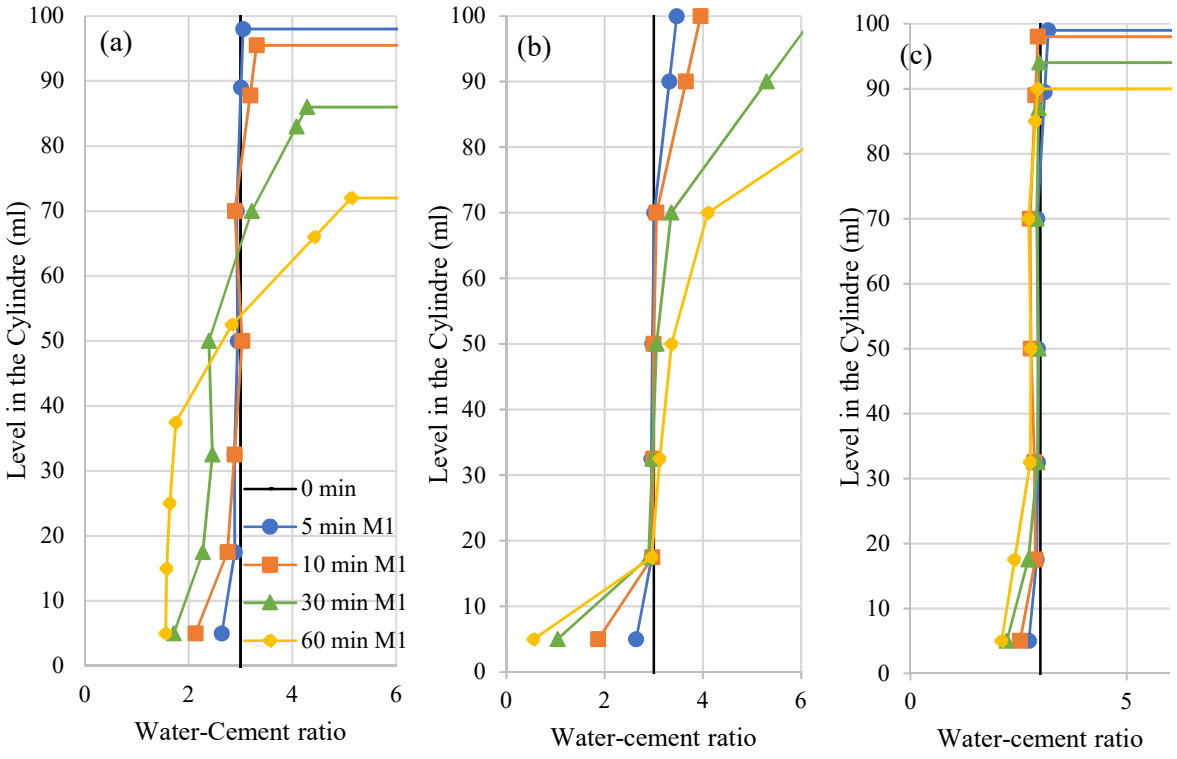

Figure 6-13: Stability test results of M1 cement grout (a) without additives (b) with 2.5% SP (c) with 1% B

6.4.4 Hydrometer tests results

The same cement is used for the hydrometer test on the grout with and without superplasticizer (SP). Hence, the particle size of cement before mixing with water is same for both tests. Figure 6-14 shows that cement particles of the grout without SP has larger grain size particles. Cement particles hydrated after encountering water and joined together to form agglomerates. Addition of superplasticizer dispersed the cement particles. Therefore, the grout with SP has large number of smaller size particles. D50 of grout with SP is 0.004mm, 80% smaller than the D50 (0.02mm) of grout with no SP

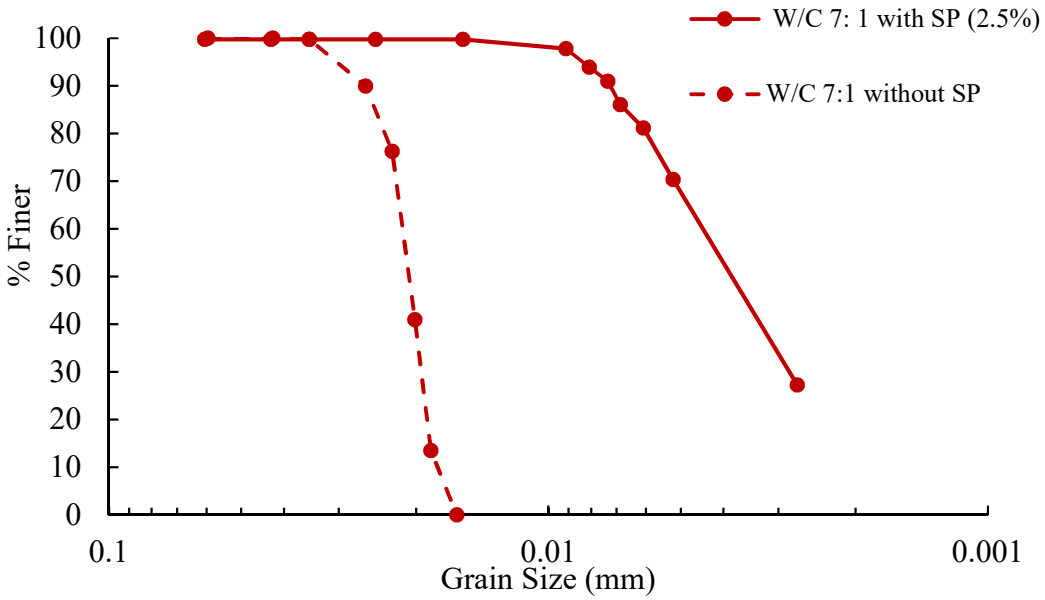

Figure 6-14: hydrometer results of cement grout of W/C ratio of 7:1 with and without superplasticizer

The tests mentioned above are for the stability analysis of grout with no flow. These tests are preliminary tests to determine the basic characteristic of grout and the effect of additives. The mechanism of particle retention of cement grout flowing through small fractures or pore space is different. Therefore, tests are required to determine the particle retention of cement grout due to pore clogging, or accumulated friction or particle separation due to differential pressure.

6.4.5 Permeation test results

The pressure at the injection point is recorded using a pressure sensor connected to a data acquisition system. The pressure data are used to construct pressure-time curves, which are widely used for quality control during grouting operations. The pressure time curves comparing the performance of M1 to M2 cement, for different water to solids ratio, are presented in Figure 6-15

and Figure 6-16. For both cement types, a lower water to solids ratio results in higher pressure buildup at the injection point due to faster filtration and pore space blockage. The pressure-time curves show that M1 cement's performance is superior to that of M2 cement. The use of M2 results in earlier pressure buildup, indicating earlier blockage of the pores, and higher pressure at the injection point than M1 cement grouts. Also, the pressure curves for M2 shows decrease in slope or small drops in pressure at a certain time after pressure buildup starts. This could be caused by mobilization of the previously filtered cement particles. This problem was not encountered with M1 cement as shown in Figure 6-15. Finally, for both micro fine cement types and the different water to solids ratios, the pressure-time curves indicate clearly the occurrence of filtration.

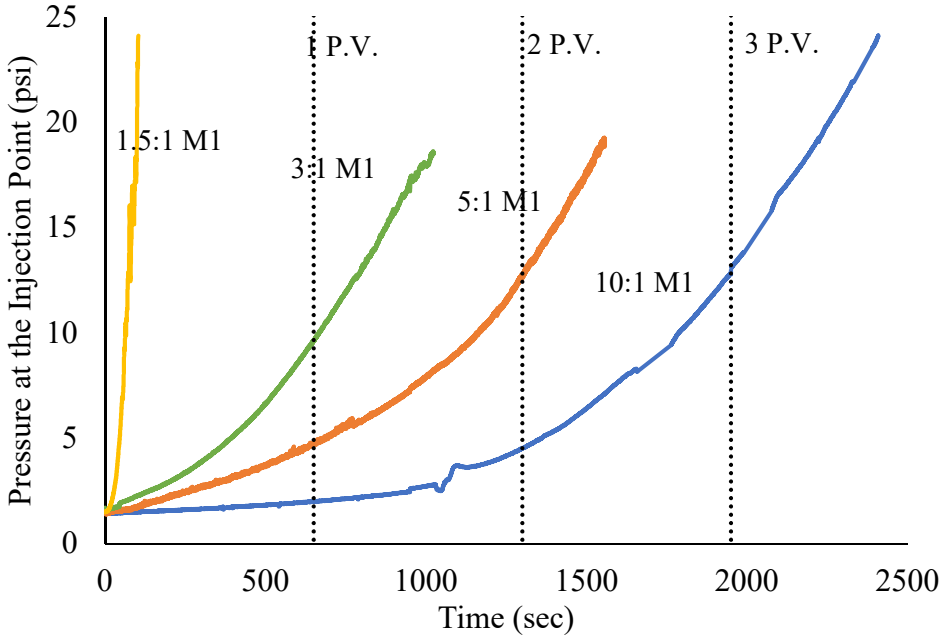

Figure 6-15: Pressure buildup for injecting M1 cement grout at constant flux

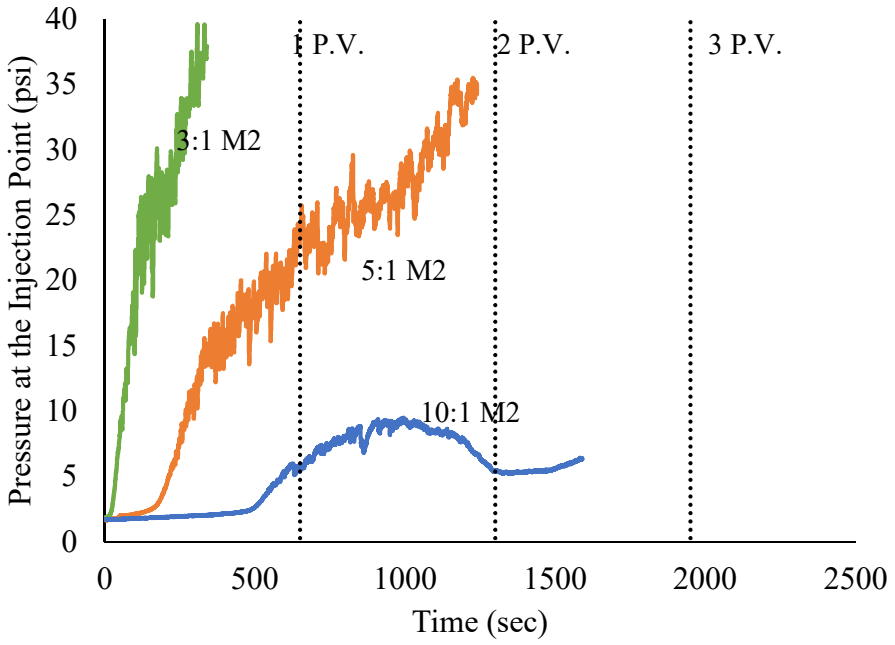

Figure 6-16: Pressure buildup for injecting M2 cement grout at constant flux

The propagation of cement particles through the sand column is monitored manually with time. The front of cement particles could be visually detected since transparent plastic tubes are used. The plot of height of cement front with time reflects sedimentation and filtration of cement particles during filtration. The height vs. time plots are presented in Figure 6-17. Ideally, the front of the cement should reach the top of the sand column (25 in. height) at the end of the first pore volume (1 P.V.) injection as indicated on the figure. However, excessive filtration might delay that front. It is important to note that the solids' front plots do not account for variations in the cement concentration below the solids' front. It is true that a delay in the solids' front indicates filtration, however, a no-delay in that front does not certainly indicate no filtration. Therefore, for some cases, the solids' front movement at the same speed as the grout should not be interpreted as uniform grout propagation with no filtration. Rather, this information could be more accurately detected in the pressure time curves, and could be directly quantified using the unconfined compressive strength measurements.

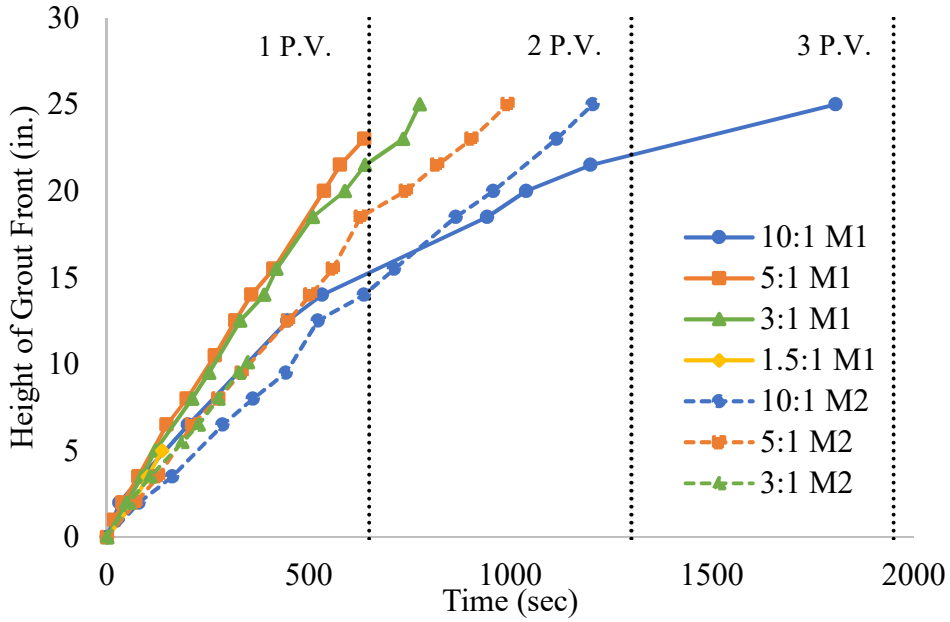

Figure 6-17: Permeation depth with time for M1 and M2 cement grout

For M1 cement, the solids' front starts moving at the same speed of the grout. However, the slope of the height vs. time curve for the most diluted suspension, with a w/c ratio of 10:1, deviates from ideal. In fact, around three pore volumes were injected into the sample in order to have the cement particles front reach the top of the sand column. Regarding the M2 cement suspensions the three suspensions presented experience delay in the rise of cement front from the beginning of the test. This agrees with the early pressure buildup at the injection point shown in the pressure vs. time curves previously. Similar analysis was done for M1 cement grout with superplasticizer and bentonite additives. Viscosity of cement grout decreases with the usage of superplasticizer hence reduces the pressure build up during permeation as shown in Figure 6-18. Whereas with the addition of 1% bentonite, pressure build up increases (Figure 6-18), and penetration depth decreases (Figure 6-19) due to increase in viscosity of cement grout.

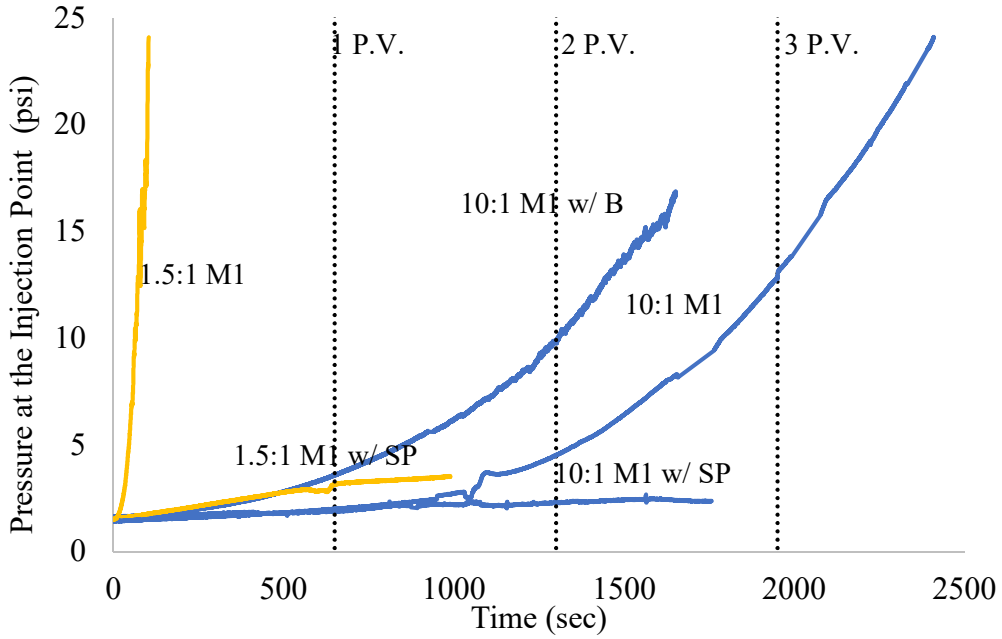

Figure 6-18: Effect of additives on pressure build up at injection point for M1 cement grout

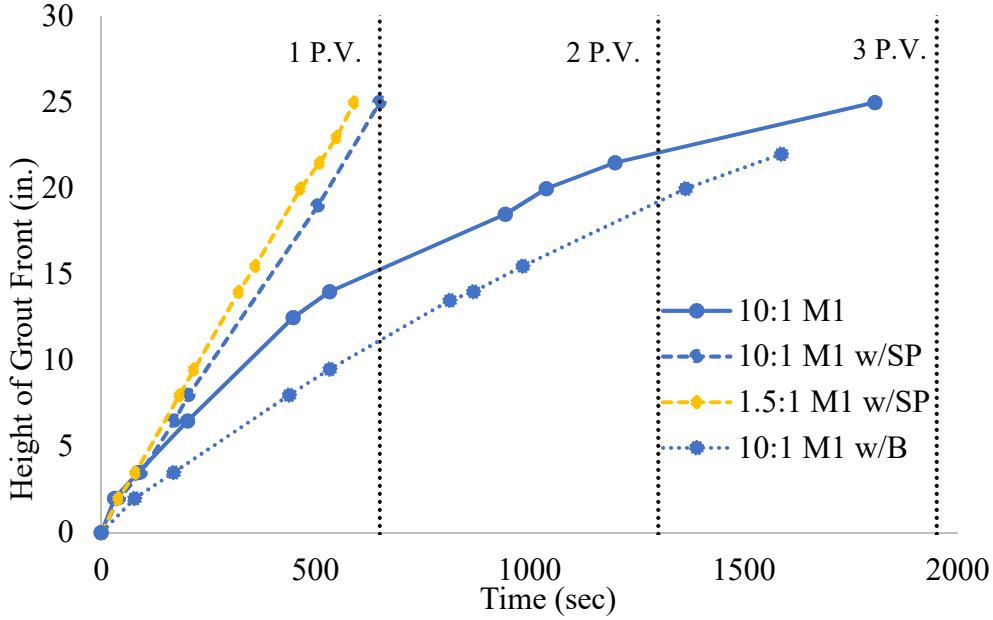

Figure 6-19: Effect of additives on permeation depth for M1 cement grout

6.4.6 Unconfined compression test results

After three days of setting time, the grouted samples are tested under unconfined compression. In Figure 6-20, the results are plotted with the strength values on the x-axis and the height of the samples' centers relative to the bottom of the sand column on the y-axis. The strength results show that the cement did not permeate through the sand uniformly. The samples closer to the injection point have higher strength than those further from it due to filtration. Also, the samples grouted with M1 cement have higher strength than those grouted with M2 cement.

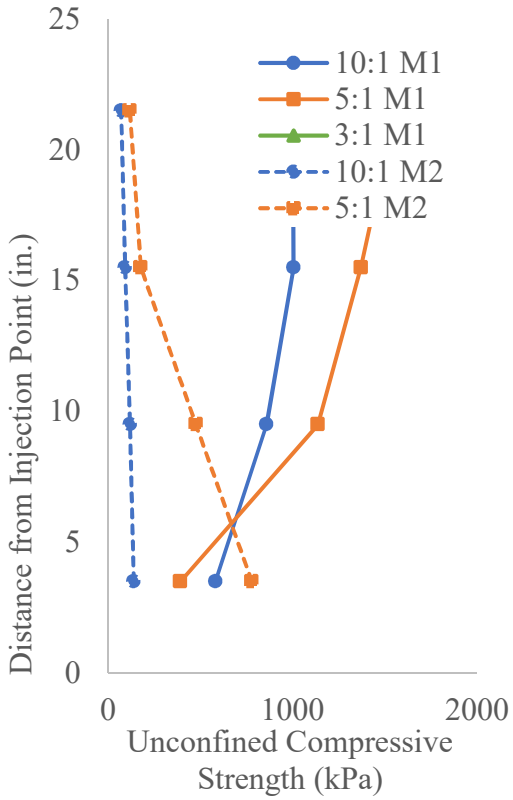

Figure 6-20: Unconfined compression strength of M1 and M2 cement grout

Cement grout with superplasticizer gives uniform unconfined compression test throughout the soil column indicating no filtration. Whereas with 1%bentonite and without additives, compressive strength is decreasing as going away from injection point due to filtration (Figure

6-21). It is found that addition of 1% bentonite to cement grout has reduced filtration, but because of the resulting increase in viscosity, pressure build up at the injection point increased and permeation depth decreased.

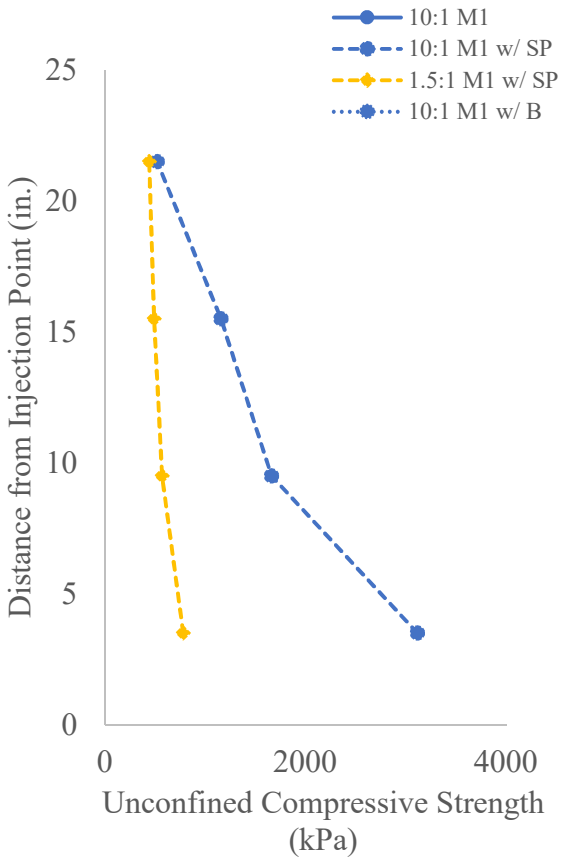

Figure 6-21: Effect of additives on unconfined compression strength of M1 and M2 cement grout

6.5 Conclusions

In this chapter, performance of cement grout in permeation grouting has been investigated experimentally. Rheology, stability and permeation tests were performed to understand the filtration mechanism. Unconfined compression test was done on grouted samples to evaluate the quality of end product of permeation grouting.

Cement grout was found to be a shear thinning material because of decrease in viscosity with increase in shear rate. Viscosity of cement grout decreases with increase in water-cement ratio and with addition of superplasticizer. Stability of grout was determined using the sedimentation tests. Addition of superplasticizer and 1% bentonite by weight reduces the cement particle sedimentation and hence increases the stability of grout.

Pressure at injection point is recorded during the permeation test to evaluate the performance of cement grout of two cement types M1 and M2. The results of sedimentation test show that M2 cement grout is more stable than M1 cement grout, hence M2 cement grout should have better permeation. But permeation depth for M2 cement grout is less than M1 because of pore blockage due to large hydrated cement particle. Addition of superplasticizer dispersed the cement particles and therefore reduced the apparent viscosity of grout and increased the permeation depth. Whereas cement-bentonite grout built up high pressure because of increase in viscosity of grout. The permeation test results conclude that there are various factors like size of hydrated cement particles, rheology of grout and stability of grout affecting the permeation grouting simultaneously.

Strength of grouted samples is determined by the unconfined compression test after three days of setting. The 2-ft. grouted sand column was divided into four sections. The strength data shows the non-uniform permeation of grout. Strength of sections closer to injection point is higher than those further due to filtration. Cement grout with superplasticizer gives uniform unconfined compression strength throughout the sand column indicating no filtration. Whereas strength of sections permeated with cement–bentonite grout decreases as going away from the injection point.

It is found that addition of 1%bentonite to cement grout has reduced the filtration but because of increase in viscosity, there was increase in pressure build up and decrease in permeation depth.

CHAPTER 7 FILTRATION MODEL FOR CONSTANT FLUX PERMEATION OF BENTONITE GROUT THROUGH GRANULAR SOIL

7.1 Abstract

The flow of suspensions through porous media is a complex phenomenon owing to the diversity of the mechanisms involved. It is important to determine the filtration behavior to understand the decline in injectivity of suspension as flow progress and for that, knowledge of the rate of particle retention is crucial. In this paper, a numerical model has been developed for the permeation of bentonite suspension grout through granular soil. The filtration model defines the rate of retention of solid particles which depends on the rheology and concentration of grout, particle size and shape of suspended particle, grain size distribution of porous media, and physio-chemical interaction of grout with the porous medium through which it is flowing. The novelty of the newly proposed numerical model is that it accounts for the change in rheology of grout and the porosity and permeability of the porous medium as a function of the retention of particles, none of which has been considered in the past. In this paper, six filtration models were used with different filtration coefficients and solid retention empirical relationships. It was found that using a filtration coefficient that increases linearly with cumulative solid retention was best suited to model the filtration mechanism of bentonite suspension grout permeation in granular soil. Bentonite content profile along the height of the sand column determined numerically using the proposed filtration model was similar to that obtained from the experimental results from post-permeation analysis.

7.2 Introduction

Filtration mechanism is mass transfer between grout particles and skeleton particles. Pang proposed that retention occurs mainly by four mechanism: (a) surface deposition, (b) size exclusion, (c) bridging and (d) log-jam as shown in Figure 7-1 . Size exclusion occurs when particle size of suspension is larger than pore throat size. Surface deposition occurs because of attraction surface forces between suspension particles and porous media grains. Bridging is dynamic process when previously retained particles forms bridge. Fourth mechanism is log-jam occurs when more than one particle tries to flow through pore throat simultaneously. Retention mechanism depends on various factors (a) size, concentration, shape and surface properties of grout particles (Eriksson et al., 2000, Abichou et al., 2002, Dupla et al., 2004) (b) Grain and pore size distribution, shape and surface properties of formation (c) rheology of grout (Eriksson et al., 2000) , interstitial velocity and physiochemical properties.

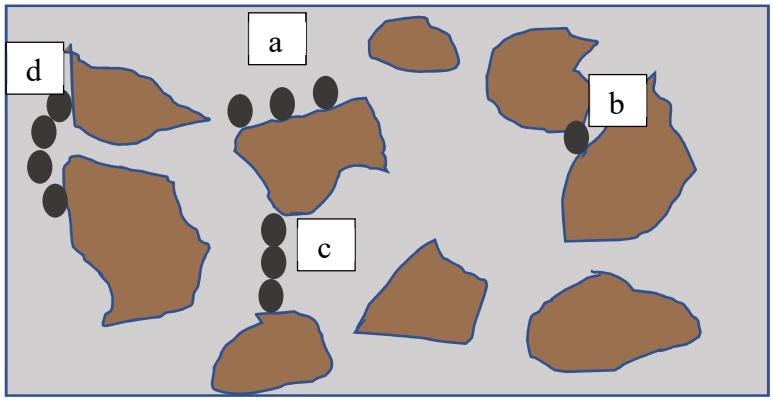

Figure 7-1: Different filtration mechanism

To better predict the success of grouting process, it is important to understand the filtration mechanism thoroughly. Many researchers (Maghous et al, 2007; Dupla et al., 2004) gave the mathematical solution to explain filtration mechanism of suspended particles flowing through

porous media using mass balance equations. A general mass conservation equation for flowing particles can be written as

$$\nabla.(uC - D\nabla C) + \frac{\partial}{\partial t}(\varphi C + \sigma) = 0 \qquad (7\text{-}1)$$

where, u is Darcy velocity, C is concentration of suspended particles (volume of particles per unit fluid volume), D is dispersion coefficient, ϕ is the porosity and σ is the specific deposit (volume of deposited particle per unit bulk volume).

Mass balance equation were simplified in literature by three approximations (a) particle diffusion has been neglected, (b) change in porosity due to clogging is neglected (c) all moving particles are very less compared to the retained one, so moving particles are neglected (Herzig, 1970). In this study, two approximations are considered (a) dispersion is neglected as diffusion of particle is negligible for size greater than 1μm (b) flow is incompressible hence, $\nabla u = 0$. Porosity of media changes as retention of particles occur. Rheology of grout (viscosity, density) of grout changes with filtration (Eriksson et al., 2000). Density of grout increases close to injection point because of particle retention, and the grout which passes has filtered and reduced density compared to initial density (Figure 7-2).

Figure 7-2: Increase in density of grout at injection point due to filtration (ρa > ρb>ρw)

Rate of retention $(\frac{\partial}{\partial t}\ \sigma)$ is proportional to Darcy velocity and particle concentration (Iwasaki, 1937)

$$\frac{\partial}{\partial t}\,\sigma = \lambda u C \tag{7-2}$$

where, λ is filtration coefficient.

Wennberg et al. (1997) experimentally determined the power law dependence of darcy velocity (u), grain size of porous media (d_g), injected particle size (d_p) as

$$\lambda \propto u^{-\alpha}\, {d_p}^{\beta}\, {d_g}^{-\gamma} \tag{7-3}$$

Where α, β and γ are positive constants. Researchers have done computer simulations to deteremine filtration coefficient. Rajgopalan and Tein (1976) derived semiempirical equation for initial collector efficiency (η), which is the ratio of trapped concentration to initial concentration.

$$\eta = 0.72 A_s N_{Lo}^{1/8} N_R^{15/8} + 2.4{\times}10^{-3} A_s N_G^{1.2} N_R^{-0.4} + 4{A_s}^{1/3} N_{Pe}^{-2/3} \tag{7-4}$$

Where As is Happel's geometric factor, NLo (London group parameter), NG (Gravity number) NPe (Peclet number are dimensionless parameters.

Happel's cell developed a relation between λ and η as

$$\lambda_o = \frac{3(1-\varphi)^{1/3}}{2d_g}\eta \tag{7-5}$$

Filtration coefficient (λ) is dynamic property which changes with the specific deposit. λ increases with time during the initial stage of filtration; a process is called filter ripening. Iwasaki described the ripening period with an equation

$$\lambda = \lambda_o(1 + b\sigma) \tag{7-6}$$

Deposited particles increase the surface area, and hence themselves act as a collector for subsequent retention of flowing particle. During the later stage of filtration, λ start decreasing with time because of several reasons. The continuous retention of particles finally begins the bridging of pore throat, a filter cake start forming. Sometime accumulation of retained particles increases the interstitial velocity as well as hydrodynamics forces. These forces cause breakaway of retained particles. However, colmatage and decolmatage occur simultaneously. Ives (1967) proposed that the interstitial velocity increases and the tortuosity as well as specific surface area decreases and derived λ as

$$\lambda = \lambda_o \left(1 + \frac{b\sigma}{\varphi_o}\right)^{a_1} \left(1 - \frac{\sigma}{\varphi_o}\right)^{a_2} \left(1 - \frac{\sigma}{\sigma_M}\right)^{a_3} \tag{7-7}$$

Where b_1, b_2, a_1, and a_2 are constants and σ_M is the maximum value of σ. Macrle et al. (1965) considered all phases of filtration (ripening, constant removal and breakthrough) and defined filtration coefficient as

$$\lambda = \lambda_o \left(1 + 7.5\frac{b\sigma}{\varphi_o}\right)(1 - \frac{b\sigma}{\varphi_o})^2 \tag{7-8}$$

Most theoretical and numerical work (Saada et al., 2005; Maghous et al., 2007, Bouchelaghem, 2009; Eklund and Stille, 2008) related to suspension transport has been devoted in the past to water filtration treatment and cement grout. A phenomenological linearized filtration law was formulated through mass exchange between cement and skeleton particles. The rate of cement mass filtered by solid skeleton increase with the increase of cement volume fraction (i.e. the concentration of cement grout) and decrease with a decrease in porosity as retention occurs (Saada et al., 2005; Bouchelaghem, 2009). Some researchers (Bouchelaghem, 2009) have found the filtration rate proportional to cement accumulation rate. Filtration law developed for cement grout cannot be used for bentonite grout because of difference in their rheological properties, particle size, and shape.

There is a gap in the literature regarding the understanding of filtration mechanism of bentonite suspension at constant flux. Bentonite suspension is complex, non-Newtonian fluid. Flow behavior of bentonite grout depends on the filtration mechanism and its rheology. In this study, permeation experiment is simulated, and various filtration model is investigated to best define the filtration mechanism of bentonite grout.

Considering the flow behavior of grout, it is known that its rheology is different from the Newtonian fluid. Bentonite is Bingham fluid which behaves as a rigid solid at low stresses and viscous fluid at high stresses. Grout requires minimum shear stress (yield stress) to flow, and properties are also time dependent. Eriksson et al., 2000 defined a blockage mechanism of Bingham fluid flow through porous media in terms of plug term (Z) when plug term reaches 0.5, flow stops. Plug term is defined for the rectangular channel of width b,

$$Z = \min\left(\frac{\boldsymbol{\tau_o}\,(\mathbf{t})}{b.\,\boldsymbol{\rho_w}.\,g\,\frac{h_o - h_l}{L}}\,,\frac{1}{2}\right) \tag{7-9}$$

where $\boldsymbol{\tau_o}\,(\mathbf{t})$ is the yield stress of grout, $\boldsymbol{\rho_w}.\,g\,\frac{h_o-h_l}{L}$ = P is the pressure gradient.

Viscosity and shear stress of bentonite grout depends on the applied shear rate. Suspension behaves as rigid material at low shear rate and viscous fluid at the higher shear rate. Bentonite grout flows only when sufficiently large stress is imposed, but thereafter it flows with constant velocity. Convection of yield-stress fluids through porous media is complicated because of the presence of unyielded portion in channels. Yield stress and apparent viscosity of each bentonite grout have been determined using the rheometer.

Bentonite suspension behave as Bingham fluid properties and can be defined as

$$\tau = \tau_0 + \mu\dot{\gamma} \tag{7-10}$$

where τ is shear stress, τ_0 is yield stress, μ is apparent viscosity and $\dot{\gamma}$ is the shear rate. Bentonite suspension requires shear stress to be more than yield stress to flow.

Pascal (1981) defined the threshold gradient model for the flow of Bingham fluid through porous media. One dimensional form of threshold gradient model is

$$u = \begin{cases} -\frac{K}{\mu}\left[1 - \left(\frac{G}{|p_x|}\right)\right]p_x & if\ |p_x|>G \\ 0 & otherwise \end{cases} \tag{7-11}$$

where G is threshold gradient and p_x is the pressure gradient.

Consider the motion of a Bingham fluid in uniform channel of width b under the pressure gradient (P). Channel boundaries are at y = $\pm\frac{b}{2}$.

$$\tau = Py \tag{7-12}$$

Hence, $\frac{Pb}{2} \geq \tau \geq -\frac{Pb}{2}$ in the channel. If Pb/2 < τ then there is no flow in channel. If there is flow then yield surface lies at $= \pm\tau_0/P$. Let $y = \pm \varepsilon b/2$ is the portion of channel which is unyielded. $\varepsilon = \frac{2\tau_0}{Pb}$

The total volumetric flux Q in one channel is given by

$$\mu Q = \int_{-b/2}^{b/2} u dy = \frac{b^3 P}{12}[1 - \frac{3\varepsilon}{2} + \frac{\varepsilon^3}{2}] \tag{7-13}$$

$$Q = \frac{b^3 P}{12\mu}[1 - \frac{3\varepsilon}{2} + \frac{\varepsilon^3}{2}] \tag{7-14}$$

Buckingham-Reiner model considered the void space of porous media as a bundle of circular tubes. The overall permeability of sand column is K = N*b^3/12 or φ*b^2/12, where N is a total number of circular tubes and φ is the porosity of sand column. Hence, total volumetric flux through sand column is

$$Q_t = \frac{K}{\mu} P[1 - \frac{3\varepsilon}{2} + \frac{\varepsilon^3}{2}] \tag{7-15}$$

Buckingham-Reiner model is used for this study to determine the pressure at injection point for a constant flux of grout flow through porous media. In the present study, Sodium pyrophosphate (additive) is used to lower the viscosity of bentonite suspension and yield stress of bentonite suspension very close to zero at the time of injection. Hence, threshold gradient is close to zero which means term ε can be neglected in equation (7-15)

$$Q_t = \frac{K}{\mu} P \tag{7-16}$$

Prediction of grout spread requires the consideration of hardening of grout with time. For this study, hardening of grout with time is not considered in modeling because of very small injection time. Fingering or dilution of grout is not seen because the viscosity of grout is greater than water (Gustafsson and Stille, 1996). Pressure gradient obtained from equation ***(7-16)*** from known constant flux are used in inverse modeling to determine the filtration parameter.

In this study, a numerical model is proposed that considers the changes in rheology and concentration of the grout and porosity and permeability of porous medium as a function of the retention of particles; none of these factors have been considered in the past. The porosity of medium and rheology of grout (viscosity, density) changes with filtration, and these changes should be accounted for as the grout progress through a porous medium (Eriksson et al., 2000). Six different filtration models were investigated to determine the best model to describe the filtration mechanism of bentonite grouts. Model 1 through Model 5 considers a linear increase in the filtration coefficient with solid retention. Filtration Model 6 considers the colmatage and decolmatage of solid particles simultaneously. Experimental tests were performed to study the mono-directional grout injection process in which pressure buildup at the injection point was recorded during constant flux permeation test. This pressure data was used to determine the filtration parameters numerically using inverse modeling technique. The sensitivity of the filtration model parameters was determined using the uniform random search (URS) method. The optimal filtration parameters were obtained using the inverse process through global optimization method, shuffle complex evolution (SCE). The objective function for URS and SCE was defined as the difference between the pressures generated at the injection point numerically and experimentally. Last, the bentonite content profile was determined numerically from the optimal filtration model

and compared to that measured experimentally along the height of sand column for the validation of the model.

7.3 Constant flux permeation cell test

Permeation tests were performed using a transparent cell 24 inches in height and 2.8 inches in diameter. Because of the length of the permeation cell, the sand specimen was prepared in 6-inch sections to have better control over the uniformity of the specimen and reduce disturbance during the preparation process. The permeation cell consists of four cylinders; each is 6 inch in height stacked on top of each other with a 1.5-inch cylinder at the bottom and another at the top to be filled with filter material. The 6-inch cylinders are split along their long axis and can be assembled and dissembled independently (in sequence) to take out the grouted sample.

The permeation cell was filled with Ottawa sand by dry pluviation with a coarser filter material placed at the bottom and top of the sand specimen. The prepared sand column was then flushed with CO_2 to replace the air present in the pores. After CO_2 flushing, a pressure transducer and a constant flux pump were attached to the bottom of the permeation cell (*Figure 7-3*) and the whole column was then flushed with at least two pore volume of water to increase the degree of saturation. The specimens were then permeated with grouts having different bentonite concentrations, and the pressure buildup at the base of the cell was recorded. The rate of increase in the recorded pressure can be used as an indicator of the occurrence of filtration during the permeation. The pressure record was used to determine the filtration parameters numerically using the inverse modeling technique.

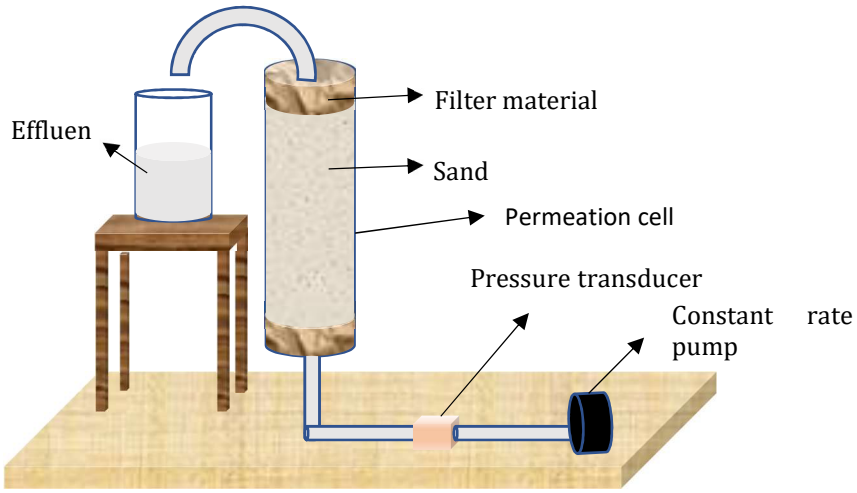

Figure 7-3: Schematic diagram of bentonite grout permeation test

Figure 7-4 shows the pressure data with time for 7% and 8% bentonite suspension. For these two cases, the increase in pressure with time is linear for the initial phase, but the rate starts increasing exponentially, albeit at different times, for the 7% and 8% suspensions. In the initial phase of permeation, the slope of the pressure-time plot is larger for the 8% bentonite grout than that of the 7% suspensions due to its higher viscosity. The difference between the exponential increase in pressure build up for the 7% and 8% bentonite is due to the difference in the filtration rate for the two grouts.

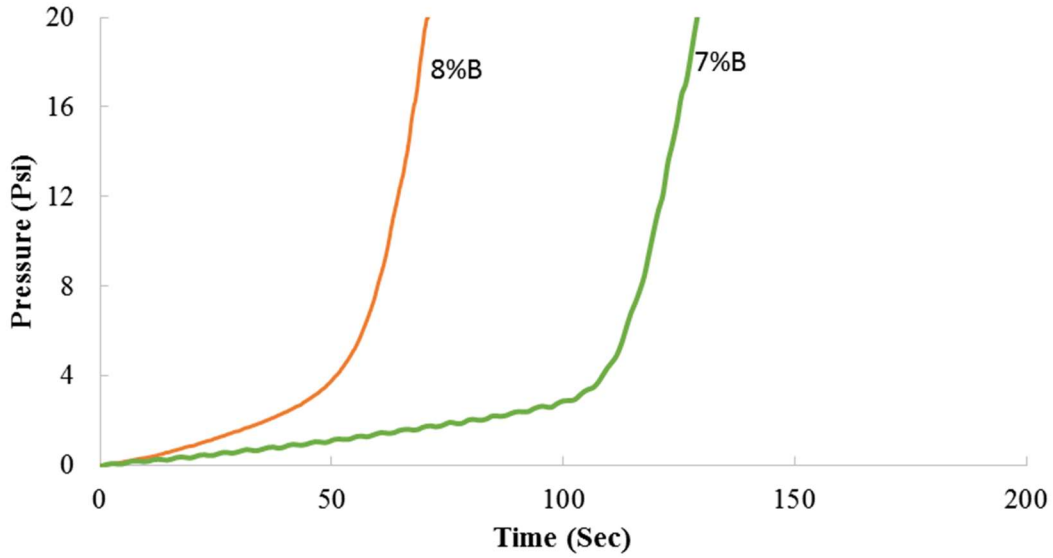

Figure 7-4: Pressure -time curve from experimental permeation tests

7.4 Mathematical modeling of bentonite grout flow through sand

A numerical model is developed to simulate the experimental test of 1-D bentonite grout permeation through a sand column at a constant flux. Iwasaki (1937) and Ives (1965) basic filtration models were used as the basis for the new proposed models and were expanded to incorporates the change in porosity of the porous medium as well as changes in the rheology and concentration of the grout as permeation and filtration progress. The parameters of the filtration model were determined by inverse modeling using pressure values at the injection point obtained both, numerically and experimentally. The objective of developing this model is to understand the filtration mechanism by estimating the filtration parameters which can then be used to determine the permeation depth, bentonite content and grout concentration profiles with depth, filter cake thickness, and effective permeability; none of which can be easily determined from experimental permeation tests.

The filtration of bentonite grout flowing through the porous medium can be accounted for as a mass exchange between the bentonite grout and the porous medium. The mass balance equation (7-17) can be simplified by assuming two approximations: (a) dispersion is assumed to be minimal and therefore can be ignored since diffusion of particle larger than 1μm is negligible; and (b) flow is considered to be incompressible hence, $\nabla u = 0$. The simplified mass balance equation can then be written as:

$$u\nabla C + \left(\varphi \frac{\partial}{\partial t} C + C \frac{\partial}{\partial t} \varphi + \frac{\partial}{\partial t} \sigma\right) = 0 \qquad (7\text{-}17)$$

The numerical solution of the model was implemented in stepwise (*Figure 7-5*). The concentration of the bentonite grout changes with distance from injection point and time and can be determined as:

$$C_{i+1,j} = C_{i,j} exp(-\lambda_{i,j}.dx) \qquad if \quad t \geq \frac{\phi x}{u} \qquad (7\text{-}18)$$

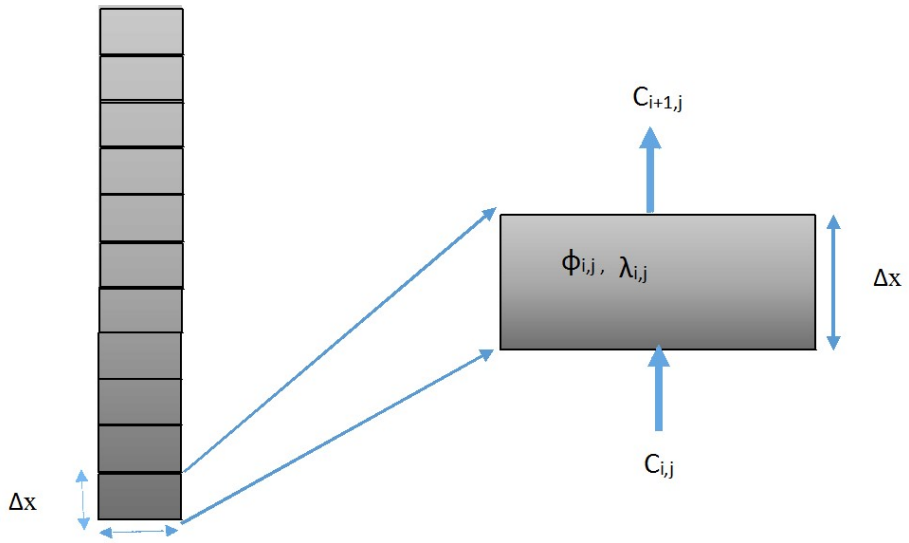

Figure 7-5: Schematic diagram of model, i is spatial node of thickness Δx and j is time step

The filtration coefficient determines the rate of particle entrapment, and it changes as particle retention proceeds. The rate of retention of solid particles is defined by equation (7-19)

$$\frac{\partial \sigma}{\partial t} = \lambda u c \tag{7-19}$$

Six filtration models were tested to determine which one describes the filtration mechanism of bentonite suspension (Table 7-1)

Filtration Model 1, 2, 3, 4 and 5 are modified from Iwasaki (1937) filtration model which considered only the ripening stage of filtration where the filtration coefficient increases with particle retention. The surface area of the porous medium increases with retention of bentonite grout on sand grains, hence increase the attraction forces. Filtration Model 1, 2 and 3 evaluate the solid retention with the assumption that the filtration coefficient is constant for a small-time step of dt whereas for Filtration Model 4, 5 and 6 assume that the filtration coefficient changes as the retention proceeds. Filtration Model 6 is modified Ives (1965) model which considered both: ripening stage and later stage when interstitial velocity increases due to the decrease in porosity which can cause breakaway of previously retained particles. For Model 1, the change in filtration coefficient is directly proportional to the amount and rate of solid retained previously whereas, for Model 2, 4 and 6, it is only proportional to the amount of retained particles in the previous step. For Model 3 and Model 5, the filtration coefficient is dependent on the cumulative solid retention.

Table 7-1: List of the different filtration models used in the numerical modeling

Model Name	Filtration Model equation	Parameters to be estimated
Model 1	$\sigma(i,j)= \lambda(i,j)*V*C(i,j)*dt$ $\lambda(i,j+1)= \lambda(i,j)[1+b*\sigma(i,j)]$	b, λ_0 and k_t
Model 2	$\sigma(i,j)= \lambda(i,j)*V*C(i,j)*dt$ $\lambda(i,j+1)= \lambda_0[1+b*\sigma(i,j)]$	b, λ_0 and k_t
Model 3	$\sigma(i,j)= \lambda(i,j)*V*C(i,j)*dt$ $\lambda(i,j+1)= \lambda_0[1+b*sum(\sigma(i,1:j))]$	b, λ_0 and k_t
Model 4	$\sigma(i,j)= (exp(\lambda_0*b*V*C(i,j)*dt)-1)/b$ $\lambda(i,j+1)= \lambda_0[1+b*(\sigma(i,j))]$	b, λ_0 and k_t
Model 5	$\sigma(i,j)= (exp(\lambda_0*b*V*C(i,j)*dt)-1)/b$ $\lambda(i,j+1)= \lambda_0[1+b*sum(\sigma(i,1:j))]$	b, λ_0 and k_t
Model 6	$\sigma(i,j)= (exp(\lambda_0*(b+c)*V*C(i,j)*dt)-1)/(b+c*$ $exp(\lambda_0*(b+c)*V*C(i,j)*dt))$ $\lambda(i,j+1)= \lambda_0[1+b*(\sigma(i,j))]\ [1-c*(\sigma(i,j))]$	b, c, λ_0 and k_t

where, λ is the filtration coefficient, dt is the time step; V is the injection velocity; C(i,j) is the concentration of the grout; σ is the solid retention (ratio of the volume of retained particles to the bulk volume); b, c and λ_0 are the filtration coefficient parameters and k_t is the formation damage factor.

7.4.1 Determination of Pressure at injection point

The theoretical model simulated the experimental permeation test (a reference to experimental set up). Sand column was completely saturated with water before permeation of grout. At time t = 0 (before permeation of grout begins), the pressure at injection point is hydrostatic pressure of water height of sand column (60 cm). As permeation begins, there is an increase in pressure at injection point because of three reasons (a) flow resistance in grouted region

(b) flow resistance in ungrouted region (c) increase in static pressure because of the weight of grout. As grout injected in the sand column, bentonite particles retained on sand grains which decrease the porosity of media, increase the specific surface area and tortuosity with time. Assuming entire initial pore space is filled with bentonite particles, the resulting porosity would be the product of initial porosity and porosity of filter cake. A reasonable estimate of critical porosity is

$$\phi_c = \phi_0 \times \phi_{cake} \tag{7-20}$$

Once the porosity reaches to critical porosity, external filter cake start to build, which greatly influence the injectivity decline. The increase in pressure after the formation of external cake is (a) flow resistance due to ungrouted region (b) flow resistance due to grouted region (c) flow resistance due to external cake (d) increase in static pressure due to the weight of external and internal filter cake. Pressure at injection point for constant flux (Q) permeation at given time equals to

$$P_t = \left[i_{c(t)} \times H_{c(t)}\right] + \left[i_{d(t)} \times x_{c(t)}\right] + \left[i_{u(t)} \times (L - H_{c(t)} - x_{c(t)}\right] + \left[Q \times t \times (\delta_g - \delta_w)\right] \tag{7-21}$$

where

$i_{c(t)}$ = pressure gradient across external filter cake

$H_{c(t)}$ = thickness of filter cake at given time t

$i_{d(t)}$ = pressure gradient across damaged (grouted) region

$x_{c(t)}$ = thickness of grouted region at given time t

$i_{u(t)}$ = pressure gradient across ungrouted region

δ_g = density of grout

δ_w = density of water

(a) Pressure gradient across external filter cake $i_{c(t)}$

$$Q = K_c * i_{c(t)} * A \tag{7-22}$$

where A is the area of the sand column, Q is constant flux rate, and K_c is hydraulic conductivity

$$K_c = \frac{k_c * \rho_g}{\mu_g} \tag{7-23}$$

$$i_{c(t)} = \frac{Q * \mu_g}{k_c * A * \rho_g} \tag{7-24}$$

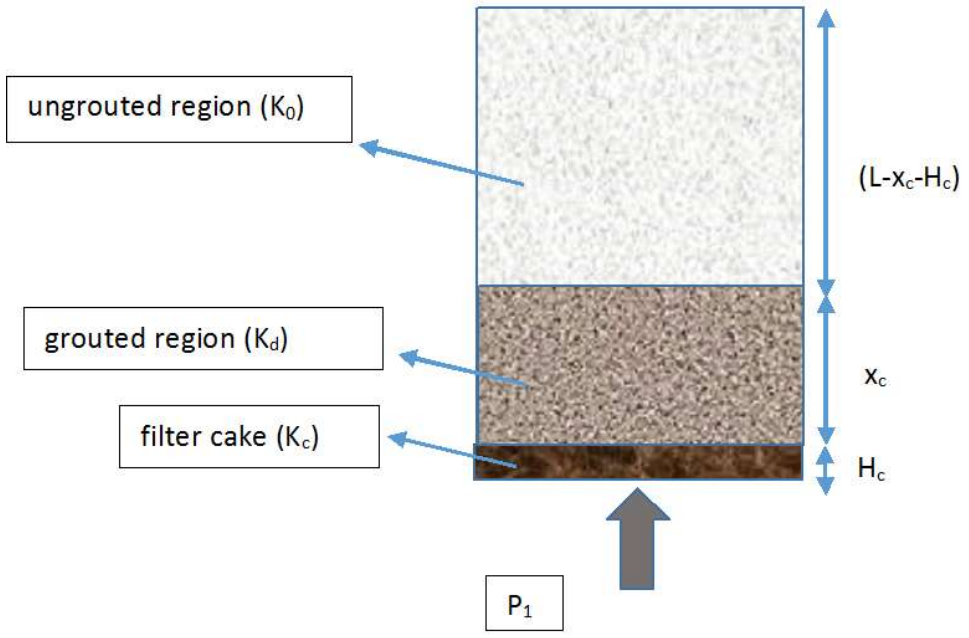

Figure 7-6 Effective permeability due to formation of various zone during grout injection

(b) Pressure gradient across damaged (grouted) region $i_{d(t)}$

In one-dimensional vertical grouting, flux is constant for vertical sections, and pressure gradient across each small section of thickness dx sums up to give the total pressure gradient across damaged region.

$$Q = K_{i,j} * i_{d(i,j)} * A = K_{i+1,j} * i_{d(i+1,j)} * A = so\ on \tag{7-25}$$

$$i_{d(i,j)} = \frac{K_{i,j} * A}{Q} = \frac{k_{d(i,j)} * \rho_{g(i,j)} * A}{\mu_{g(i,j)} * Q} \tag{7-26}$$

$K_{d(i,j)}$ is the reduced permeability of grouted region. As particles retained on skeleton, permeability change due to a decrease in porosity, increase in surface area and increase in tortuosity. $\rho_{g(i,j)}$and $\mu_{g(i,j)}$ are the density and viscosity of grout entering in block i of thickness dx at time t respectively. Concentration of grout decreases as filtration progress (Equation (7-17)) which also change the density, viscosity and yield stress of grout with space and time (Figure 7-7)

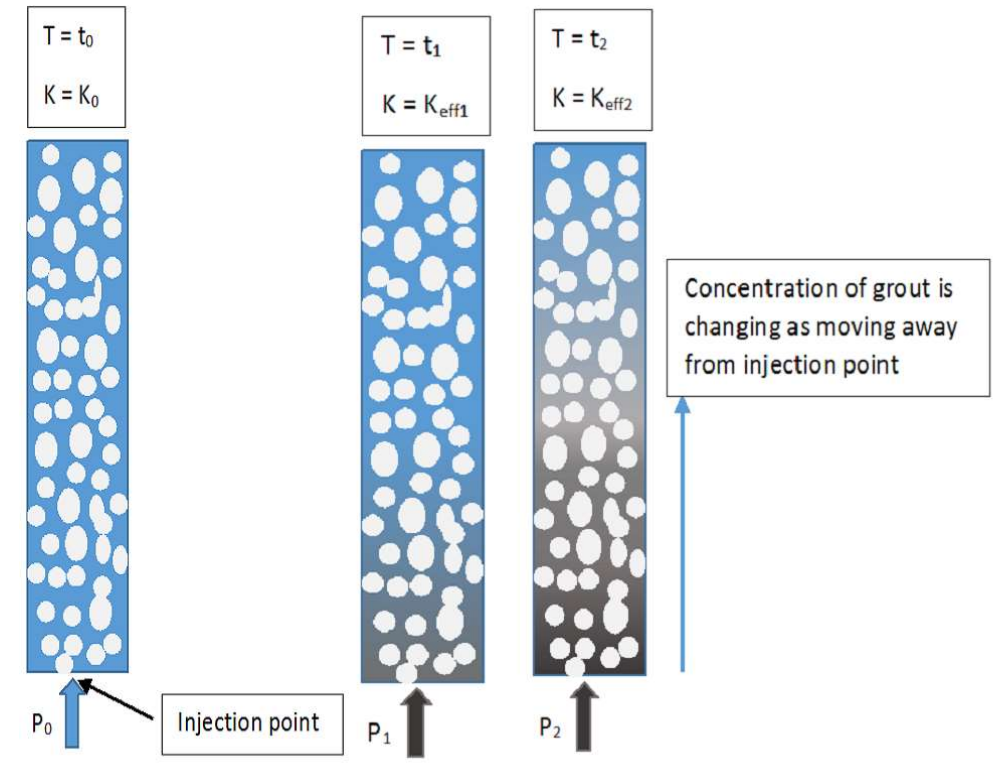

Figure 7-7 Schematic of change in concentration, effective permeability and pressure at injection point as permeation and filtration progress

$$B_{i,j} = \rho_b * C_{i,j}(1 + \frac{1}{1 - C_{i,j}}) \tag{7-27}$$

$B_{i,j}$ is the percentage of bentonite in the grout. ρ_b is the bentonite density.

$$\rho_{g(i,j)} = \frac{\rho_b}{B_{i,j}} + \left(1 - B_{i,j}\right) * \rho_b \tag{7-28}$$

$$\mu_{g(i,j)} = \mu_w \left[1 + (\frac{\mu_{eq}}{\mu_w} - 1)\frac{C_{i,j}}{C_{in}}\right] \tag{7-29}$$

where μ_w is the viscosity of water, C_{in} is the concentration of grout at the inlet, μ_{eq} is the apparent viscosity of grout at the inlet, which depends on the amount of bentonite and sodium pyrophosphate (SPP). Empirical equation is derived from experimental results to define the apparent viscosity of bentonite grout (Mortar & Yoon, 2012)

$$\mu_{eq}(Pa.s) = 0.01461 * exp(27.8 * B - 21.4 * SPP) \quad (7\text{-}30)$$

B and SPP are a percentage of bentonite and SPP respectively.

As particles retained in pore throat, the porosity and permeability declines which in turn reduce the injectivity. There are several relationships available in the literature which relates to the decrease of permeability with retention of particles and change in concentration of grout. Permeability reduction model used for this study is proposed by Pang. Kozeny-Carman defined permeability of porous media as

$$k = \frac{\phi^{1/3}}{K_k(1-\phi)^2 S^2 \tau} \quad (7\text{-}31)$$

where k is permeability, S is the specific surface area, τ is tortuosity and K_k is the Kozeny constant. Pang proposed that reduction in permeability could be broken down into permeability reduction due to three factors (i) reduced porosity ($k_{d\varphi}$) (ii) increased surface area (k_{ds}), and (iii) increased tortuosity (k_{dt})

$$\frac{k}{k_0} = k_{d\phi} k_{ds} k_{dt} \quad (7\text{-}32)$$

where permeability reduction due to the reduced porosity of block i at time t = j is

$$k_{d\phi}(i,j) = \frac{{\phi_{i,j}}^3 (1-\phi_0)^2}{{\phi_0}^3 (1-\phi_{i,j})^2} \quad (7\text{-}33)$$

The retained bentonite particles and sand grains are considered as sphere with their entire surface exposed to flow for calculation of reduction in permeability due to increase in surface area

$$k_{ds}(i,j) = \left[\frac{1 + \frac{\sum_{i,0}^{i,j} \sigma_{i,j}}{(1-\phi_0)}}{1 + \frac{d_g}{d_p}\frac{\sum_{i,0}^{i,j} \sigma_{i,j}}{(1-\phi_0)}}\right]^2 \quad (7\text{-}34)$$

where d_g is the size of the sand grain, d_p is the size of bentonite particle, and σ is the specific deposit.

The reduction in permeability due to tortuosity is

$$k_{dt}(i,j) = \frac{1}{1 + \beta \sum_{i,0}^{i,j} \sigma_{i,j}} \quad (7\text{-}35)$$

Where β is damage factor, depends on pore structure.

(c) Pressure gradient across ungrouted region

Grout replaces the water in pores while injecting through the saturated sand column. Hence, grout will oppose the pressure from the water. The pressure gradient across the ungrouted region is because of water at a constant flux of Q.

$$i_{u(i,j)} = \frac{K_0 * A}{Q} = \frac{k_0 * \rho_w * A}{\mu_w * Q} \quad (7\text{-}36)$$

7.4.2 Stoppage criteria

Filtration has a big influence on grout spread and sealing effects. Filtration of the grout can be due to mechanical reasons or chemical, as shown by Schwarz (1997). When bentonite grout is injected into the sand column, bentonite particles invade the formation and form internal filter cake in a porous medium. As the injection continues, particles are trapped and decrease the pore space; a point is reached where very few particles can invade the formation and formation of an external cake start to form. At this point, grout spread stops in the formation and there is a sudden increase in pressure at injection point because of formation of the external filter cake. No grout can pass once the porosity of formation reaches to critical porosity because of particle retention. Assuming that the entire initial pore space is filled with particles, the resulting porosity would be the product of initial porosity of sand column (φ_0) and the porosity of internal filter cake ($\varphi_{cake} = 0.2$). Hence a reasonable estimate of the critical porosity is

$$\phi_c = \phi_0 * \phi_{cake} \tag{7-37}$$

Another reason for no grout pass can be the rheology of grout. Bentonite grout is Bingham fluid which requires the minimum pressure gradient to flow. If the pressure gradient across any region in the sand column is less than the yield stress of grout, then there will be no grout flow. Bentonite grout gains yield stress with time and behave likes solid under low shear rate. This criterion is necessary to be considered if total injection time is huge. In the present study, grout was under high shear mixing during the whole injection process to prevent the buildup of yield stress. Injection process was also for very less time. Bentonite grout with high yield stress is treated by adding sodium pyrophosphate (SPP) which reduce the viscosity and yield stress of grout and

make it be easily permeable. Hence, no grout flow because of yield stress is not considered in this study.

7.4.3 Filtration parameter Estimation by Inverse modeling

Filtration of the grout can be due to mechanical reasons or chemical, as shown by Schwarz (1997). In the present study, filtration is considered as a mechanical phenomenon, but the underlying mechanism can be mechanical as well as physiochemical. Filtration model defines the rate of retention of particles, which depends on the grout properties, physical properties of porous media and physiochemical interaction between grout and porous media. Quantifying each filtration mechanism is difficult. In the present study, two filtration model will be discussed, (a) Iwasaki filtration model, which only considered the ripening stage (b) Ives filtration model, which examined the occurrence of colmatage and decolmatage simultaneously. Filtration coefficient in both filtration model has a relationship with the amount of particles retained and porosity of porous media, but filtration also depends on the interaction between grout particles passing through porous media. Filtration model parameters quantify the physiochemical interaction of grout particles flowing through porous media, which change with flow rate, the initial porosity of porous media, size, and shape of grout and skeleton particles, the initial concentration of grout and rheology of grout.

Filtration models have one variable which is the amount of retained particles and constants. The value of constants is unknown. Constants of filtration model are known as filtration parameters in this paper. It is important to understand the influence of filtration parameters and its sensitivity in predicting accurate filtration mechanism. There is inadequate knowledge of filtration parameters and permeability reduction parameter which are used in numerical modeling. Thus guesses are

made. Sensitivity analysis is the process of determining which of guesses really matter and to determine if slight different guess makes a significant difference in the behavior of the model.

Monte Carlo simulation is used for parameter sensitivity analysis to determine the effect of unknown filtration parameter and permeability reduction parameter. The behavior of the model is examined by calculating the root mean square error (RMSE) of the pressure at injection point obtained numerically and experimentally. Parameters are randomly generated with uniform probability distribution in the range of specified maximum and minimum values. All parameters are changed together, and a numerical model is solved by forward modeling, and RMSE is evaluated for each realization. The sensitivity of each parameter is analyzed by investigating its effect on RMSE value. This technique is called uniform random search method (URS). It helped to determine the range of parameters which could closely simulate the experiment results. This is a multivariate optimization problem. Hence there is the possibility of a different set of parameters which can provide the local minimum values of RMSE. The random search method is unable to obtain a good estimate of the global optimum of the model but could provide parameter values which are good starting point. Global search optimization methods are required to determine the optimal set of parameters. Shuffled complex evolution method is used to locate the global optimum and determine the best optimal set of filtration and permeability reduction parameters. SEC is based on a synthesis of four global optimization strategies (a) combination of probabilistic and deterministic approaches; (b) clustering; (c) systematic evolution of a complex of points spanning the space, in the direction of global improvement; and (d) competitive evolution. Incorporating these four global optimization strategies have proved SCE as a successful tool for global optimization. SCE method gives the best set of parameters and RMSE value for each filtration model.

7.5 Results and analysis

Permeation cell tests were modeled numerically using the six filtration models discussed in the previous section. The experimental results were used to determine the most appropriate filtration model to define the filtration mechanism of bentonite grout passing through the granular soil.

The parameters for each model were estimated by fitting the pressure-time curve obtained numerically to the experimental results using inverse modeling technique (SCE). The objective function for the inverse modeling is defined as the root mean square error (RMSE) between the pressure generated numerically and experimentally. The parameters' values vary for the different filtration models, and the filtration model which gave the best fit was chosen. The results from inverse modeling using the experimental data for the 8% suspension are summarized in Table 7-2, and the results from models are plotted in

Figure 7-8 with the experimental data. Filtration Model 5 gave the best fit with the lowest RMSE value of 1.74 with Model 2, 5 and 6 showing promise as well.

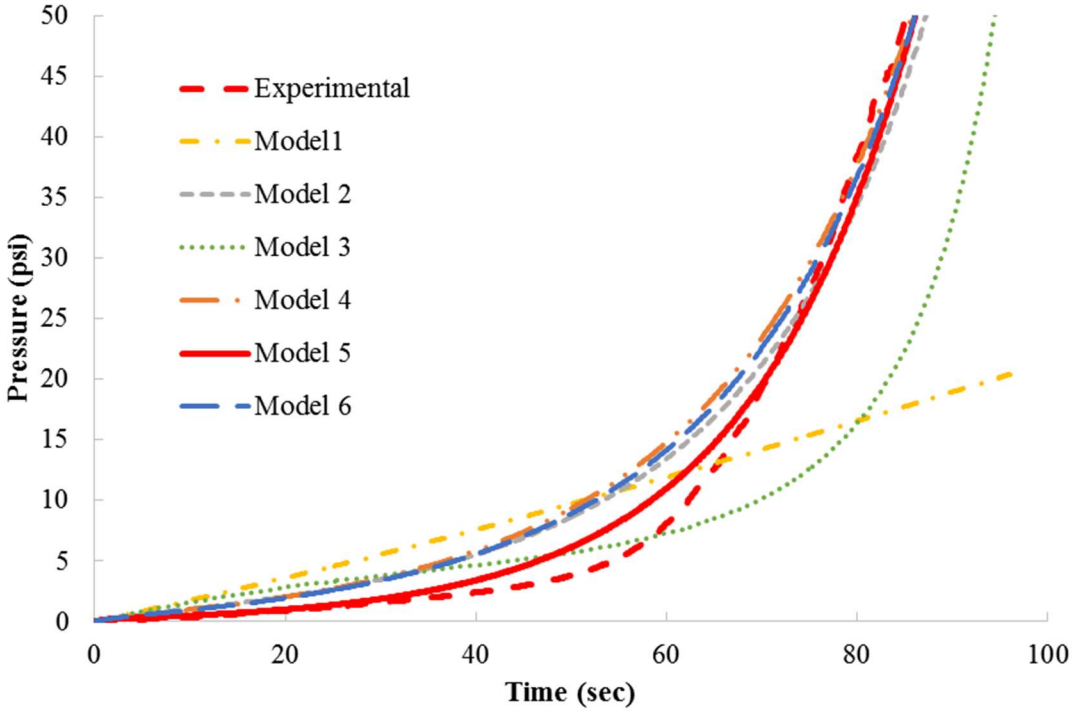

Figure 7-8 Pressure-time curves obtained numerically using different filtration model compared to experimental result for 8% bentonite suspension

Table 7-2 RMSE value, filtration coefficients and formation damage factor for 8% suspension

Model Name	RMSE (pressure-time curve fit)	b	c	λ_0	k_t
Model 1	18.40	244	-	0.02	355.40
Model 2	3.56	1000	-	0.87	1.00
Model 3	12.85	221	-	0.13	46.60
Model 4	3.50	38	-	1.85	1.00
Model 5	1.74	1000	-	1.46	101.41
Model 6	3.21	1000	5.06	1.71	1.00

The selected filtration models were then used to obtain the bentonite content (ratio of bentonite to sand by mass) profile numerically across the height of the sand specimen. The actual bentonite content in the permeated sand column was determined by disassembling the column, divide it into vertical slices and run wet sieve analysis on each slice. The numerically calculated bentonite content was then compared to the experimental data for verification of the model performance (Figure 7-9). The results show that the bentonite content profile obtained numerically using the filtration Model 5 are the closest fit to the experimental data. While Filtration Model 2, 5 and 6 showed promise in matching the pressure buildup curve, the bentonite content profile obtained from these models were not accurate. It should be noted that the experimental profile of the bentonite content was not used in determining the filtration model parameters and therefore, can be considered as an independent validation of the efficiency of any given model. Hence it is

verified that Filtration Model 5 can capture the filtration mechanism of bentonite suspension grout permeation through the granular soil.

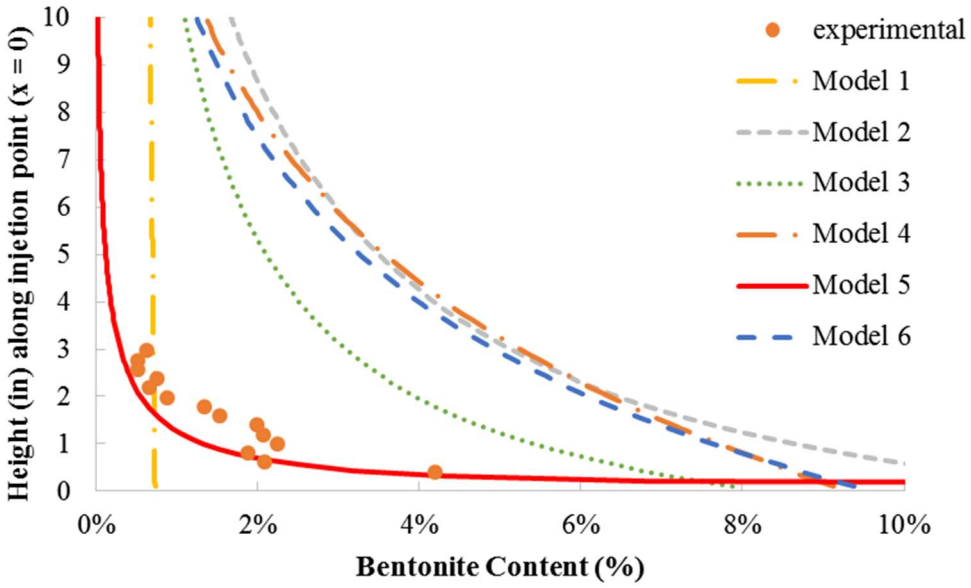

Figure 7-9 Verification of filtration model using bentonite-content profile for 8% bentonite suspension

Similarly, Model 5 was found to be the best fit for the permeation of the 7% bentonite suspension grout. The pressure-time curve obtained numerically fitted well with experimental data with a RMSE value of 2.015 (Figure 6(a)). The filtration coefficients and formation damage parameter for 7% bentonite suspension grout are b = 1000, λ_0 = 1.0 and k_t = 43.18. Figure 6(b) verified Model 5 for 7% bentonite suspension also. The results for the 8% suspension are included in Figure 6 as well for comparison.

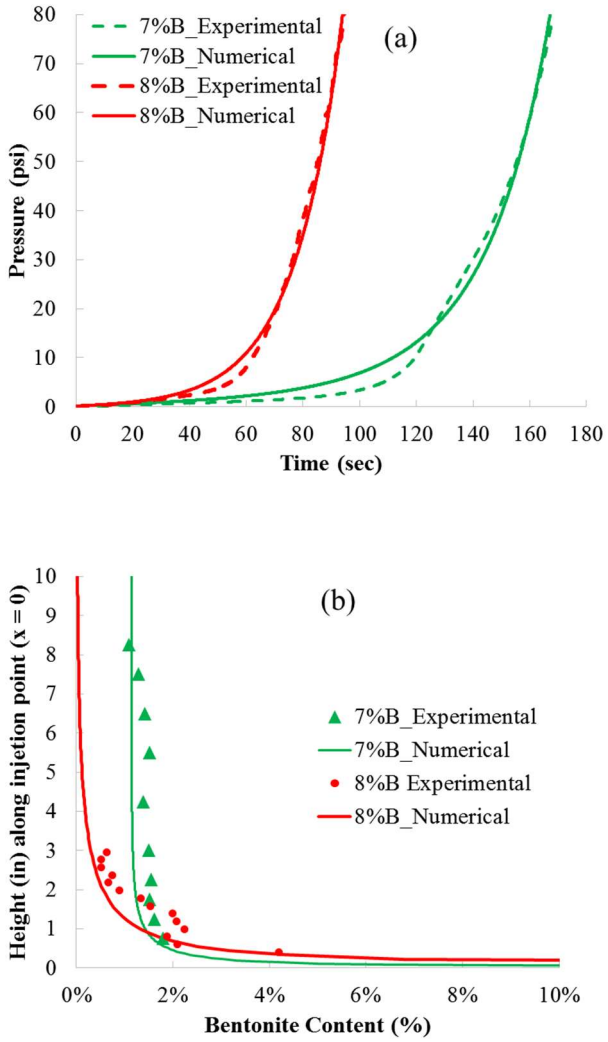

Figure 7-10 (a) Pressure-time curve and (b) bentonite content profile obtained experimentally and numerically (Model 5) for 7% and 8% bentonite suspension

7.6 Conclusion

Injectivity of a suspension grout through granular soil can be severely jeopardized because of filtration. The filtration mechanism for bentonite suspension grouts through sand was determined in this chapter. The dependence of the filtration coefficient on changes in rheology and concentration of grout and porosity of the sand were considered as permeation progressed. The filtration coefficient parameters and formation damage parameter were determined using the

experimental results obtained from a permeation cell by inverse modeling technique (SCE method). Six filtration models were used from literature to predict which model closely simulate the flow of bentonite suspension through porous media. It was found that Filtration Model 5 with filtration coefficient linearly increasing with cumulative solid retention could capture the filtration mechanism for 7% and 8% bentonite suspensions. Permeability reduction model used in the mathematical model for Model 1 to Model 6 is Sharma et al. (2000) model.

The limitation of using this mathematical filtration model is the usage of filtration and permeability reduction function which are the modified version of the Iwasaki (1937) filtration function. It was found that Model 5 can capture the bentonite flow and closely predict the bentonite content distribution but to get the better prediction, it is required to determine the elementary filtration parameters for the suspension grout. In next chapter, the experimental procedure is proposed to determine the elementary filtration and permeability reduction function for bentonite and cement suspension grout.

CHAPTER 8 FILTRATION AND PERMEABILITY REDUCTION FUNCTION OF GRANULAR SOIL DUE TO PERMEATION OF BENTONITE GROUT

8.1 Abstract

Grouting is widely used for strengthening and sealing the rock and soft soil. The flow of suspension grout through soil is a complex mechanism owing to the change in permeability because of particulate clogging. Permeability reduction caused by the retention of suspended particles within the porous media is a major problem affecting the performance of grouting. The knowledge of suspension grout injection through porous media with subsequent particle retention and permeability declination is very critical for many engineering applications. The probability of particle retention on sand grains is referred as filtration coefficient, which depends on the concentration of previously retained particles. Whereas, in literature, researchers have considered the unrealistic assumption of constant filtration coefficient throughout the permeation process. This paper represents the experimental investigation of (a) the filtration function i.e the relationship of filtration coefficient with the concentration of previously retained particles and (b) the permeability reduction i.e the relationship of reduced permeability with changed porosity and volume of retained particles. The large volume of bentonite grout was injected into the sand column of approximately 6.5 cm long, and 7.3 cm diameter from bottom to top at constant flux and then effluent was collected. Filtration function was determined by evaluating the temporal variation of effluent concentration. The differential pressure across the specimen was used to determine the absolute permeability using the Darcy' law and developed an empirical relationship

between the reduced permeability, porosity, and volume of retained particles. The determined filtration and permeability reduction function is used in mathematical filtration model (developed in chapter 7) and found that these functions predict the performance of permeation grouting more accurately.

8.2 Introduction

The understanding of the suspensions flow through porous media with continuous particle retention is important in the various engineering fields. When suspension grout (like bentonite and cement grout) flowing through porous media (sand), the particles comes into contact with retention sites; they deposit or get carried away with the stream. This phenomenon is complex and many parameters play a role. Injectivity of grout through sand column declines because of reduction in permeability due to sand matrix plugging by solid particles suspended in injected fluid (Hjelmas et al. 1996; Sharma et al. 2000; Moghdasi et al. 2002). Permeability reduction was extensively studied for (a) the oil recovery operations (Barkman and Davidson 1972; Abrams 1977; Davidson 1979; Eylander 1988; Vetter et al.1987; Sharma and Yortsos 1987; Todd et al. 1990; van Oort et al. 1993; Roque et al. 1995; Veerapen et al. 2001; Moghdasi et al. 2004;Al-Abduwani et al. 2003; Al-Abduwani et al. 2005) (b) waste-water filtration (McDowell-Boyer et al. 1986; Amirtharajah 1988; Tobiason and O'Melia 1988; Reddi et al. 2000). In petroleum engineering, practitioners require this knowledge to determine the formation damage while injecting drilling fluid through wellbores. This study is critical for permeation grouting as well to determine the grout spread its

post stability. Grout spread depends on the rate of retention of particles on the sand matrix and is referred as filtration coefficient.

The prediction of the groutability of a suspension grout into a soil and the efficiency of a permeation grouting is an important issue that may be addressed, based on a better understanding of the grouting process and the mechanisms controlling this process. This understanding may help to develop appropriate flow models, allowing simulation of the transport of a cement suspension through soil with application to the evaluation of the extension of the treated zone.). Mathematical models combined with laboratory studies can provide the insight into the spatial and temporal development of bentonite grout permeation into porous media. Different types of models have already been developed and published in the literature, ranging from macroscopic models to models based on discrete approaches, considering individual grains within the suspension (Bortal-Nafaa 2002. The mathematical model for deep bed filtration was explained by Herzig at al. (1970) which contains two empirical parameters; filtration coefficient and formation damage coefficient. Knowledge of these two parameters is essential for simulating the suspension grout through porous media mathematically. Models of the macroscopic type, as developed by Bouchelaghem and Vulliet (2001), Saada (2003), and Saada et al. (2005), need the identification of macroscopic parameters (e.g., the elementary rate of filtration per volume unit, which appears in the mass conservation equations) to be used. It appears that most experimental work carried out to date on cement grout injection has dealt with testing of long or intermediate length columns, which do not allow elementary filtration (or clogging) parameters to be obtained. Therefore, the objective of this study is to evaluate the elementary filtration properties of sands to determine filtration parameters

that are required in macroscopic grout injection models describing the flow of a suspension grout through sand.

Pang and Sharma (1994) and Wennberg and Sharma (1997) showed that these parameters can be determined from core flood tests from the combined measurement of core pressure drop and of suspended particle concentration in core outlet water. Pang and Sharma, 1994, Van oort et al., 1993, Wennberg and Sharma, 1997, Bedrikovetsky et al., 2001 and Bedrikovetsky et al., 2003 had performed laboratory coreflood tests on rock core to determine the constants. These tests are meant to be performed on rock sample. There is a gap of literature for filtration coefficient and formation damage coefficient data for sand permeated with bentonite grout. The motivation of this paper is to determine the filtration coefficient and permeability reduction function for bentonite grout injecting through the sand.

Particle entrapment occurs due to a variety of physical mechanism like interception, sorption, sedimentation, bridging and attraction by molecular forces (Payatakes et al., 1974 and Roque et al., 1995). Rouqe et al. (1995) proposed four different particle retentions phases: retention, bridging, internal accumulation and external accumulation. Whereas, Chauveteau et al. (1998) explained the effect of each retention mechanism on the permeability reduction. Equation (8-1) define the capturing process due to all different mechanism, which uses the empirical filtration function $\lambda(\sigma)$.

$$\frac{\partial \sigma}{\partial t} = \lambda u C \qquad (8\text{-}1)$$

Where, σ is the volumetric concentration of retained particles, λ is the filtration coefficient, u is the flow velocity, and C is the volumetric concentration of particles in suspension. Filtration coefficient is dynamic property which depends on previously retained particles. But mostly in literature, the simplified models with constant filtration coefficient were used (Pang and Sharma (1994), Wennberg and Sharma (1997) and Bedrikovetsky et al., 2000 and Bedrikovetsky et al., 2001). Considering λ as a constant is a limitation for simulating the filtration mechanism for bentonite grout permeated through sand. It may decrease or increase with time. It usually increases in the early stage of filtration because of molecular attraction between suspended particles and sand grains. This stage of filtration is called ripening. This can alter the flow (interstitial velocity) so that more suspended particles collide to sand grains or more particles carried away with the flow. Typically, surface force are considered. Heertjes and Lerk (1967) considered only the Van der Waals forces whereas Ives (1962, 1965) considered Van der Waals as well as electro-kinetic forces as retention forces. Sand grains progressively coated with retained particles which lead to double layer repulsion. Filtration coefficient may decrease drastically when repulsive layer begins to form. If particles continue to deposit, they will finally start blocking the pore throat due to bridging and filter cake will start to form.

Researchers have developed empirical relations of evolution of filtration coefficient with retention of particles based on different theories (Iwasaki,1937; Stein, 1940; Ives, 1965; and

Heertjes and Lerk, 1967). If the grout is injected through the sand specimen of length L and the inlet (C_{in}) and effluent (C_{eff}) concentration was measured, then the filtration coefficient can be found experimentally using the equation (8-2)

$$\lambda = \frac{1}{L}\ln(\frac{C_{in}}{C_{eff}}) \tag{8-2}$$

The porosity of porous media are reduced as particles get trapped within the pore throats, and the permeability declines which in turn leads to restricted grout injectivity. Permeability reduction due to particle retention is the combined effect of a change in tortuosity, surface area, and hydraulic radius. The Kozney-Carman equation is often used to present the permeability versus porosity, grain size, and tortuosity relationship. However, it requires additional assumptions, especially, regarding the tortuosity evolution due to porosity reduction. Particles retention within the pore space has a considerable effect on the tortuosity and direction of flow. Several relationships have suggested relating the decline in permeability with the concentration of retained particles (Herzig et al. 1970 and Dullien,1982). Sharma et al. 2000 defined the reduction of permeability for water injection wells considering three factors (a) reduced porosity, (b) increased surface area and (c) increased tortuosity.

Most theoretical and numerical work related to suspensions transport has been devoted in the past to the problem of water filtration and treatment, characterized by very diluted suspensions, with concentrations in solid matter lower than 0.5 g/l (Herzig et al., 1970 ; and Rege and Fogler, 1988). These researches refer to the phenomenon of deep bed filtration, for which four families of

models essentially may be distinguished as the phenomological model (Herzig et al., 1970); Trajectory analysis model (Rege and Fogler, 1988; and Mackie, 1989); Stochastic model (Tarafdar et al., 1992) and finally network model (Lee and Koplik, 2001; Payatakes et al., 1973; Eriksson et al., 2000)

Most of above mentioned filtration coefficient and permeability reduction relationships are for diluted suspension grout or for water injection in oil reservoir. There is very limited literature available for the filtration and permeability reduction function for the concentrated suspension grout (bentonite or cement)

The objective of this paper is to develop a specific setup allowing injection of suspension grout (bentonite and cement grout) into thin samples of soil to obtaining elementary filtration properties. Large volume of suspension grout was permeated through a 6.5 cm sand column at constant flux from bottom to top. The filtration coefficient was determined by measuring the change in effluent concentration as numbers of pore volume permeated and empirical equation was developed to establish a relationship between filtration coefficient and concentration of retained particle. The differential pressure was recorded across the specimen to analyze the change in permeability of porous media due to particle retention and its effect on grout spread. Reduced permeability function was developed and dependent on two variables, porosity and volume of retained particles. The determined filtration and reduced permeability function is used to model the flow of cement grout through sand mathematically. This allows to analyse the grout flow patterns on large scale application.

8.3 Experimental methods and materials

Figure 8-1 shows the schematic of experimental setup. The filtration test setup consists of three transparent columns each of 3.8 cm height which coupled together to form a permeameter. The diameter of each cylinder was 7 cm. Cylinder were aligned on top of each other using two aluminum hose clamps, placed tightly at the joints. Rubber liner was used between two cylinders to ensure the leak proof joint throughout the testing process. All three assembled cylinders were put on the bottom plate. Injection point was through the bottom plate. Bottom cylinder were filled with filter material to ensure the uniform front of flow through sand column. Sand was air pluviated on the top of filter material in the middle cylinder maintaining the uniform void ratio. Top cylinder is again filled with filter material to prevent the washing out of sand at high pressure. The size of sand column (6.2 cm approximately) was kept short enough to minimize the spatial dependence of particle clogging problem and large enough for representative sample.

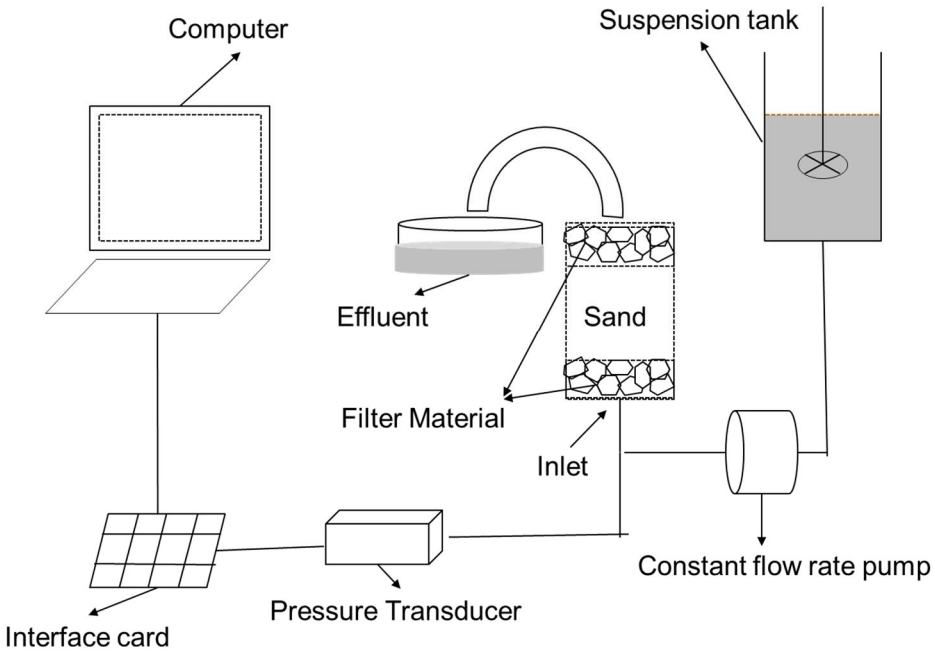

Figure 8-1: Schematic diagram of filtration test

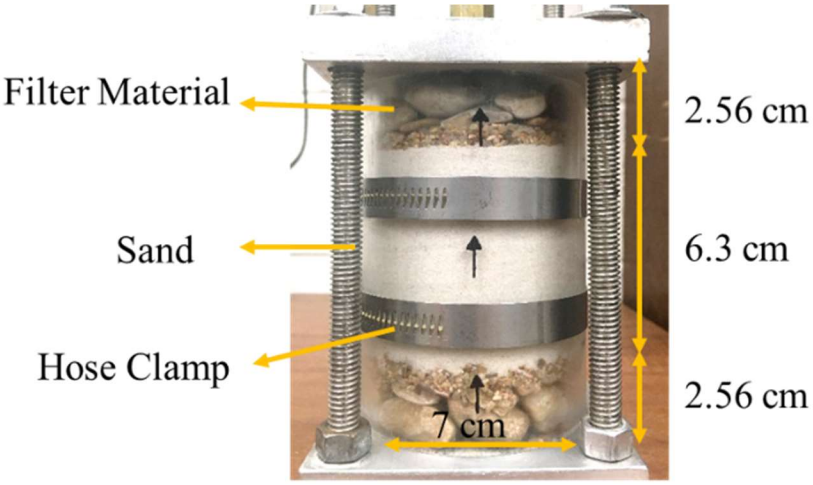

Figure 8-2: Detailed picture of soil column

Permeation cell was first flushed with CO_2 and then with at least two pore volume of de-aired water from bottom to top to completely saturate the sand column and to obtain the initial permeability. After the water flushing, bottom plate of permeation cell was attached to pressure transducer and constant flux water pump. The influent was prepared in high speed mixer at desired concentration and to keep the suspension stable, the electrical stirrer is used throughout the duration of experiment. Grout was injected at constant flux rate from bottom to top. The pressure increase across the sample caused by gradual particle retention was recorded using the pressure transducer, which is sensitive in the range of 1 to 140cm of water head. The absolute permeability evolution was calculated using the Darcy's law, with the recorded pressure difference and the flow rate of pump. The initial permeability of the soil with respect to pure water was found to be in range of 1E-3 cm/s. Effluent was collected in small cups to determine its concentration and amount of the retained particles.

Material: Two type of sand (Ottawa sand and Mortar sand) was used to study the effect of grain size distribution on particle retention. Properties of sand used in this paper are mentioned in Table 8-1. Gravels and blast sand were used as filter material in permeation cell.

Table 8-1: Index Property of sand used in this paper

Soil	Gs	D_{10}(mm)	D_{30}(mm)	D_{60}(mm)	Cu	Cc
Mortar Sand	2.70	0.07	0.425	0.8	3.2	0.90
Ottawa Sand	2.65	0.25	0.30	0.38	1.52	0.95

Two types of suspension grout were used in this study (a) bentonite suspension grout and (b) cement suspension grout. Wyoming bentonite was used to prepare bentonite grout. The particles have plate like structure and usually less than 1or 2 μm in size. Sodium Pyrophosphate (SPP) were used as additives with thicker bentonite suspension to reduce the apparent viscosity for smooth injection. Deionized water was used to prepare the bentonite grout because clays are very sensitives to ions. Microfine cement was selected instead of ordinary Portland cement for successful permeation of cement grout through small pore space of sand. Different concentration of cement grout of W/C ratio of 1.5,3, 5 and 7 were used. Super plasticizer stabilizes the grout by dispersing the cement particles i.e. particles that have joined together to form agglomerates are separated.

Preparation of bentonite grout: Bentonite grout were prepared in high speed mixer. Percentage of bentonite mentioned in this paper are measured by weight of bentonite powder to the total weight of grout. SPP were added as percentage of bentonite weight. Mixture of SPP, bentonite powder and water are mixed in high speed mixer in three steps of 5-minute mixing each total of 15 minute for consistency. After every 5 minute of mixing, bentonite powder was scraped from side and base of cup to remove the flocks of bentonite and reintroducing into the mixing cup. Bentonite grout were used right after the mixing to prevent the effect of any thixotropic before filtration test. Rheology of bentonite grout (equilibrium apparent viscosity and yield stress) were determined using the rheometer. Effect of bentonite concentration, additives (SPP), flow rate and grain size of sand on the filtration and permeability reduction were studied in this paper.

Table 8-2 shows the list of combinations of variables considered in experimental study.

Preparation of cement grout: Cement grout was prepared in high speed mixer. Water/cement ration used in this study is as per weight. Weight of cement and water is calculated for required concentration of cement grout. Super plasticizer was added as percentage of cement weight. Super plasticizer was first added to the water in measuring cup and mixed in high speed mixer for 5 minutes. Cement was added slowly to the water and superplasticizer mixture while the mixture is in motion in high speed mixer. After all the cement amount added in mixture, the grout was prepared in three steps of 5-minute mixing each total of 15 minute for consistency. After every 5 minute of mixing, cement powder was scraped from side and base of cup to remove the flocks of bentonite and reintroducing into the mixing cup. Cement grout were used right after the mixing to prevent the effect of any thixotropic before filtration test. Rheology of cement grout (equilibrium apparent viscosity and yield stress) were determined using the rheometer and discussed in Chapter 6.

Table 8-2: List of experiments of bentonite suspension discussed in this chapter

Test No.	Bentonite concentration (%)	Addition of SPP (%)	Yield stress (Pa)	Equilibrium apparent viscosity (mPa.s)	Flow rate (cm/s)	Media material
T1	5	0	3.00	62.80	1.66	Mortar
T2	5	0	3.00	61.00	1.66	Ottawa
T3	5	0	3.00	63.20	1.25	Ottawa
T4	5	0	3.00	62.50	0.83	Ottawa
T5	6	0	3.00	66.70	1.66	Ottawa
T6	7	0	10.80	82.84	1.66	Ottawa
T7	8	0	24.00	96.43	1.66	Ottawa
T8	8	1	3.50	78.80	1.66	Ottawa
T9	8	2	3.00	78.30	1.66	Ottawa
T10	8	2	3.00	78.00	1.66	Mortar
T11	10	3	6.00	120.00	1.66	Ottawa
T12	10	3	6.00	117.00	1.25	Ottawa
T13	10	3	6.00	121.00	0.83	Ottawa

Table 8-3: List of experiments of bentonite suspension discussed in this chapter

Test No.	Water/cement ratio	Addition of SPP (%)	Yield stress (Pa)	Equilibrium apparent viscosity (mPa.s)	Flow rate (cm/s)	Media material
T14	3	0	2.0	66.2	1.66	Mortar
T15	5	0	1.5	37.6	1.66	Mortar
T16	7	0	1.0	28.7	1.66	Mortar
T17	3	2.5	1.75	17.3	1.66	Mortar
T18	5	2.5	1.0	13.8	1.66	Mortar

8.4 Results and Discussion for bentonite grout

The performance of permeation grout can be predicted with the knowledge of two functions (a) the filtration function i.e. the change of filtration coefficient with particle retention (b) permeability reduction function i.e the relationship between reduced permeability and changed porosity and concentration of retained particles. In this section, first the variation of effluent concentration against the mass of bentonite particles injected is discussed to explain filtration mechanism. Second, a filtration function is derived which comprises of two relationships (a) a dependency of filtration coefficient on the concentration of previously retained particles (b) a relationship between particle retention rate and filtration coefficient. Third, the declination of permeability due to continuously particle retention is determined. The reduction of the

permeability is not only due to decrease in porosity but also affected by a change in tortuosity and surface area due to particle retention. Hence, the permeability reduction equation as function of porosity and volume of retained particles is developed. Suspension concentration, flow rate, percentage of additives in the grout, and grain size of porous media were varied to study the overall behavior of filtration. The overall behavior such as effluent concentration and pressure differential across the entire specimen were monitored to develop the filtration and permeability reduction model as function of concentration of retained particles.

8.4.1 Observed Effluent concentration

Figure 8-3 shows the variation of the normalized effluent concentration against the mass of injected particles for different flux rate. Normalized effluent concentration is the ratio of effluent concentration (C_{eff}) to the injected influent concentration (C_{in}). The mass of injected bentonite particles through the specimen was chosen as the x-axis instead of time, so results of different flow rate or different concentration can be compared on one plot. C_{eff}/C_{in} ratio less than one shows the particle retention within the specimen at that instant. Lesser the value of normalized effluent concentration indicates the large amount of particle retention. The particle retention rate was higher in the beginning of permeation process. The effluent concentration increases gradually with increasing injected volume of grout and fines and then the C_{eff}/C_{in} ratio tend to reach the asymptote. The constant value of C_{eff}/C_{in} ratio means the steady retention of particle on the sand grains.

8.4.1.1 Effect of flow rate on filtration

Figure 8-3 (a) shows the C_{eff}/C_{in} plot for 5% bentonite grout at different flow rate. Normalized effluent concentration levels off at a constant value of 0.95 after the injection of approx. 19.811, 25.11, 43.31g of bentonite particles at the flow velocity of 50, 75 and 100 ml/min respectively. In experiment T2 and T4, the injection was stopped earlier once the Ceff/Cin reached to asymptotic value.

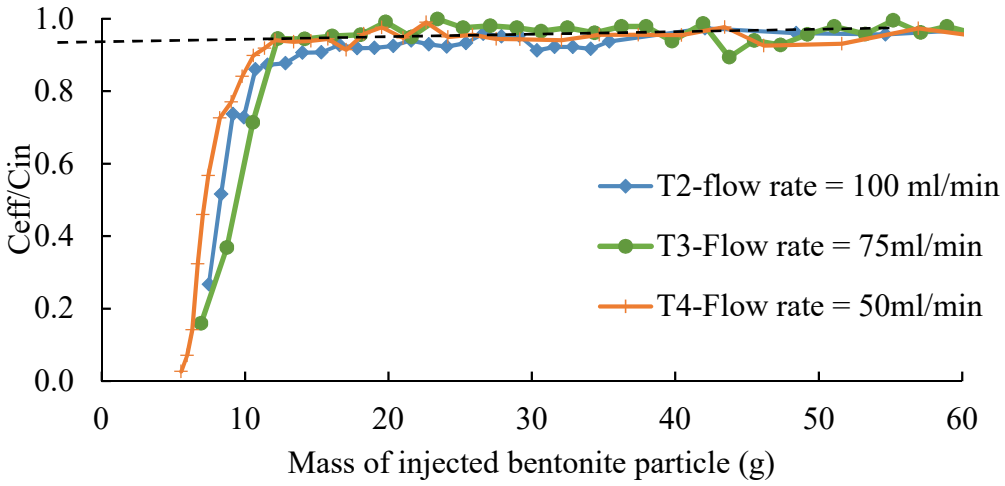

(a)

Figure 8-3: (a) Normalized effluent concentration of 5% bentonite concentration grout for different flow rate

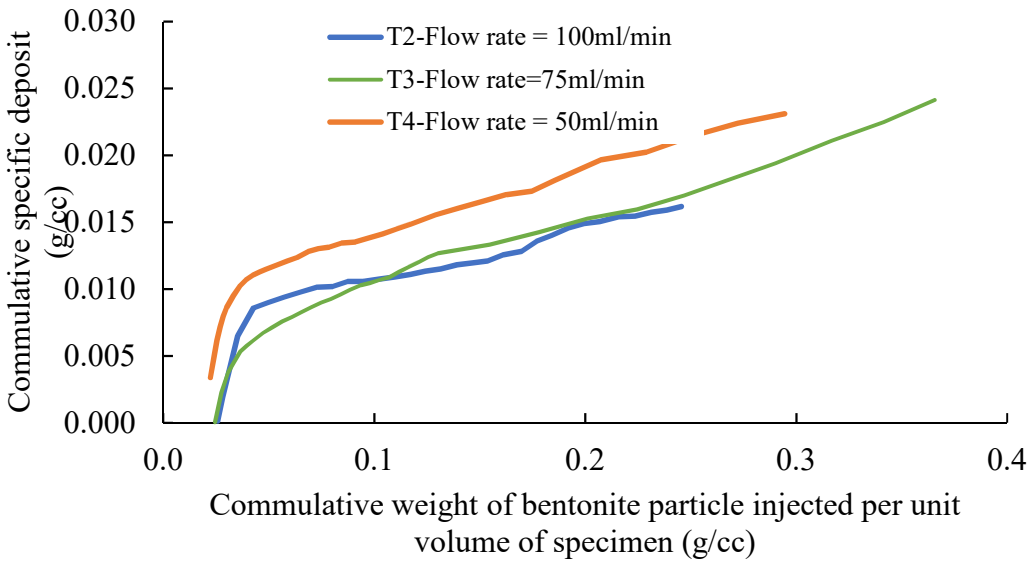

(b)

Figure 8-3: (b) Cumulative specific deposit versus mass of injected bentonite particles

The pulsation in the effluent concentration may be related to variation in the flow rate or the influent concentration (Wong and Mettananda, 2010). The total amount of particle retained is more for slower flow rate for diluted suspension (Figure 8-3(b)). Higher flow rate results in higher hydrodynamic forces and reduce the likelihood of particle retention in the diluted suspension (Baghdlklan et al., 1989). Whereas, Reddi et. al. (2000) negated this theory and mentioned the concept of self-filtration at higher flow rate which is the rearrangement and migration of filter particles and tendency to gradually segregate the fine particles resulting in the reduction of permeability. The results of diluted suspension of 5% bentonite concentration proved the Baghdlklan et al. (1989) theory true whereas the result of concentrated suspension of 10%

bentonite agreed with Reddi et al. (2000) concept. Figure 8-4(a) and Figure 8-4 (b) shows more particle retention for higher flux (100ml/min and 75ml/min) injection of concentrated suspension of 10% bentonite. In experiment T11, the grout injected at high flow rate was stopped earlier due to the buildup of pressure across the specimen beyond the maximum capacity of pump. In experiment T12, Ceff/Cin have reached to asymptotic value of 0.7 before the grout was stopped. The asymptotic value of Ceff/Cin for the flow velocity of 50ml/min is suspected to be more than 0.7 (Figure 8-4) but the flow was stopped before reaching the steady filtration.

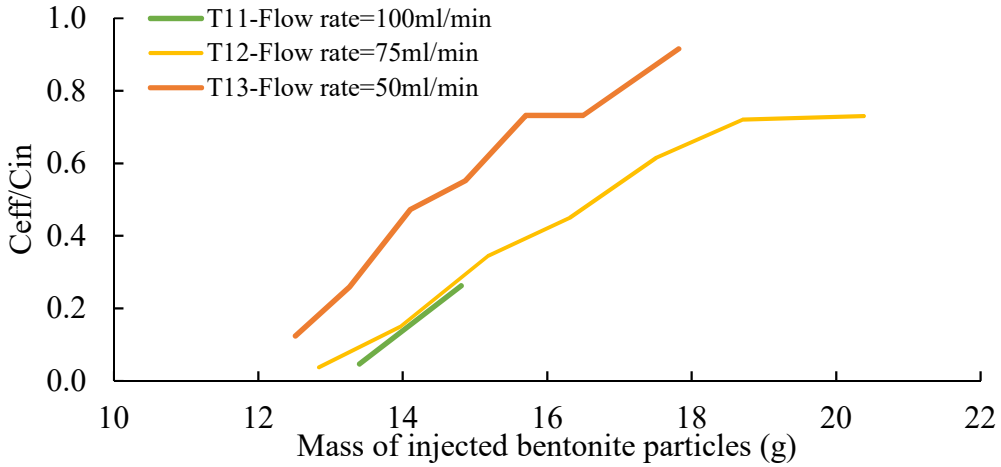

(a)

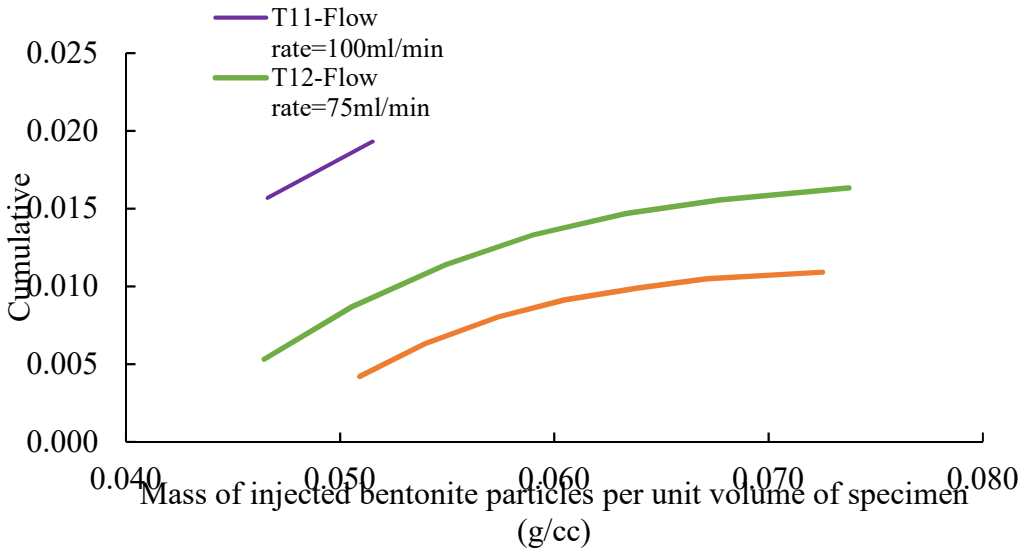

(b)

Figure 8-4 (a) Normalized effluent concentration plot (b) Cumulative specific deposit for the injection of 10% bentonite and 3% SPP suspension grout through Ottawa sand at different flow rate.

8.4.1.2 Effect of bentonite concentration on filtration

Figure 8-5 shows the effect of suspension concertation on the effluent. It indicates that the particle retention depends on the number of suspended particles injected, the amount of particle retained increases with the increase in the concentration of grout. The apparent viscosity increases with the increase in bentonite concentration. Therefore, high pressure head was required to inject thicker suspension (8%B and 7%B) through the reduced pore space and injection stopped due to limitation of the maximum operable pressure of pump which was 690 kPa. Hence, in experiment T6 and T7, the flow of grout was stopped at the injection of 23.18 and 22.23g of bentonite particles respectively due to rheological blocking. The C_{eff}/C_{in} levels off at the value of 0.94 for all the suspension grout eventually.

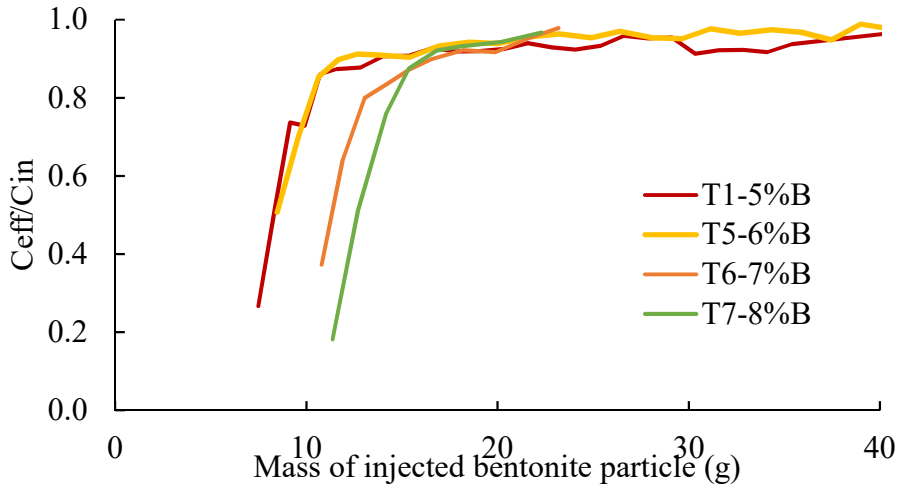

(a)

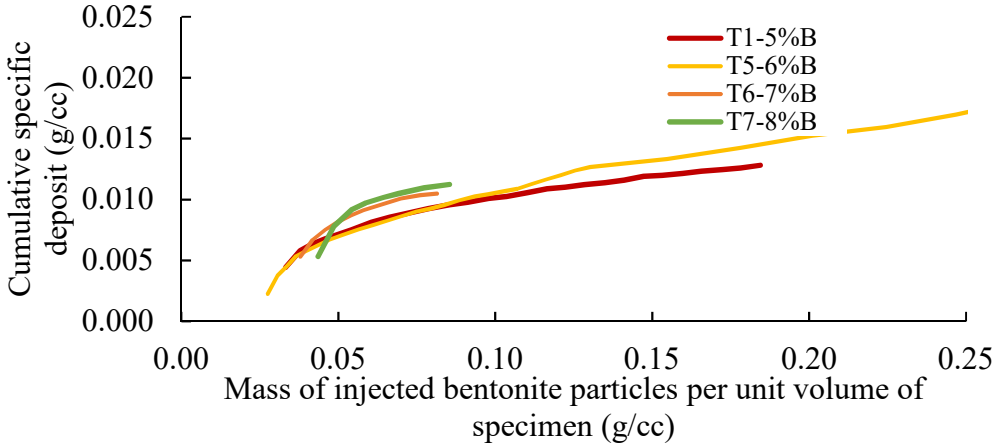

(b)

Figure 8-5: (a) Normalized effluent concertation plot (b) Cumulative specific deposit for different concentration bentonite grout

The number of particles retained is more for higher concentrated suspension for same number of particles injected (Figure 8-5 (b))

8.4.1.3 Effect of Sodium pyrophosphate additives on filtration

Sodium pyrophosphate was used in this study because of its ability to reduce the yield stress and viscosity of bentonite suspension for better penetrability of grout in soils. The addition of SPP controls the rheological blocking by reducing the equilibrium apparent viscosity of grout. It was observed that permeation of 8% bentonite without SPP and with 1%SPP stopped earlier at the total mass of 24g of bentonite particle injection whereas there is successful injection of total mass of 34g of bentonite particles for 8% bentonite with 2%SPP (Figure 8-6 (a)).

Sodium pyrophosphate disperse bentonite particles in the suspension and reduce the likelihood to settle o sand grains. Figure 8-6 (b) shows that the amount of particle retention is more for suspension with no additives.

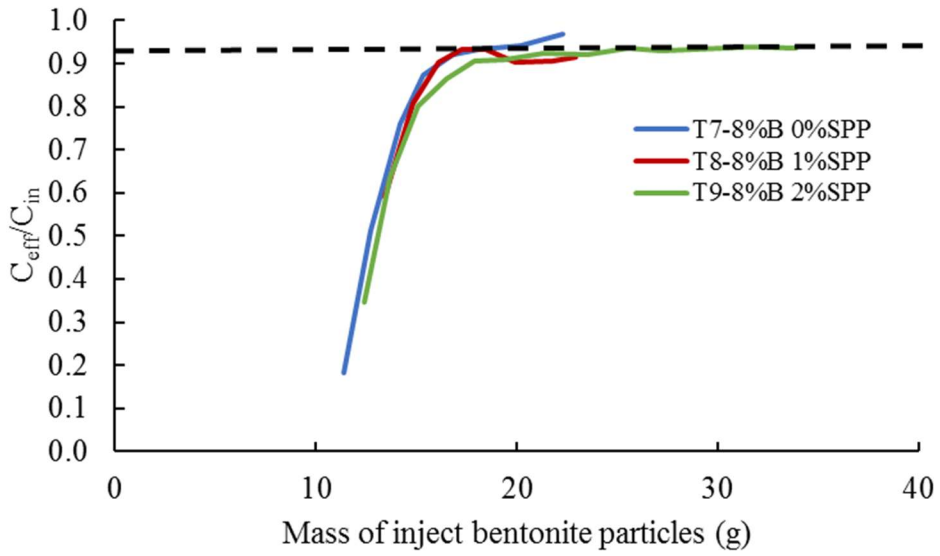

(a)

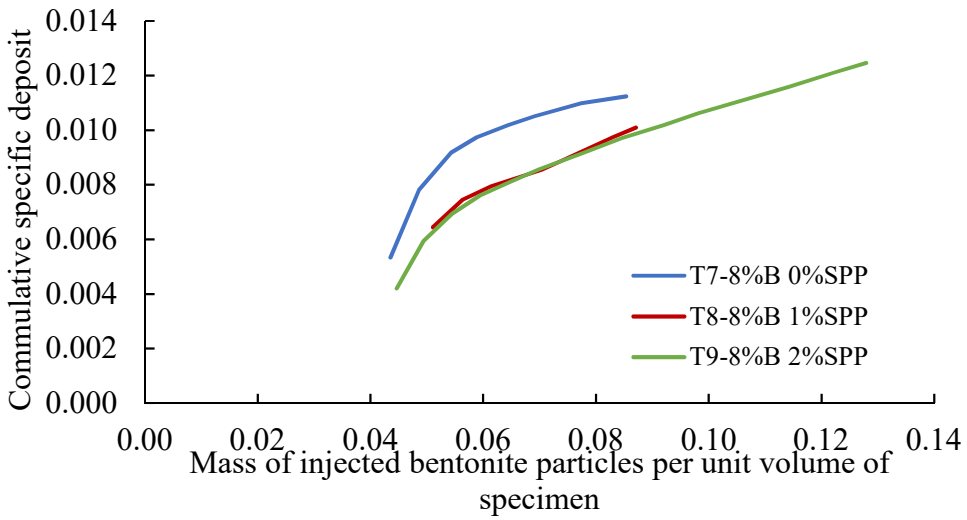

(b)

Figure 8-6: Effect of addition of SPP (sodium pyrophosphate) on the (a) normalized effluent concentration (b) Cumulative specific deposit

8.4.1.4 Effect of grain size distribution of porous media on filtration

Two different soil were used in this study to determine the effect of grain size distribution on particle retention. Smallest pore size of porous media plays a critical role in the particle retention and bridging of pore throat. D_{10} size of mortar soil is 0.07 mm less than that of Ottawa sand (0.25mm). After the injection of certain amount of bentonite particles, pore throat of Mortar soil began to clog and no penetration of grout occurred through soil. The grout flowing through mortar soil experience more resistance. In the experiment T1, grout flow stopped after the injection of 19g whereas in experiment T2, the flow of grout was smooth with total injection of 90g of bentonite particles. Similarly, in the case of permeation of 8% bentonite and 2%SPP suspension grout through Ottawa and Mortar sand. There was no penetration of grout after 4g and 35g of bentonite particles injected through mortar and Ottawa sand respectively. Figure 8-7 (b) shows that number of particles retained is more for same number of particles injected through mortar sand, but flow stopped earlier because of rheological blocking.

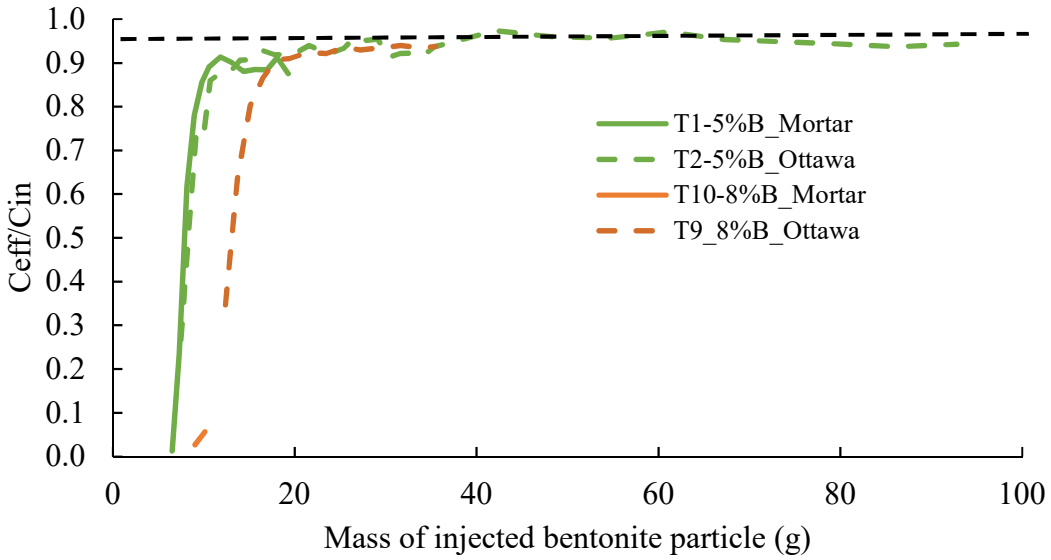

(a)

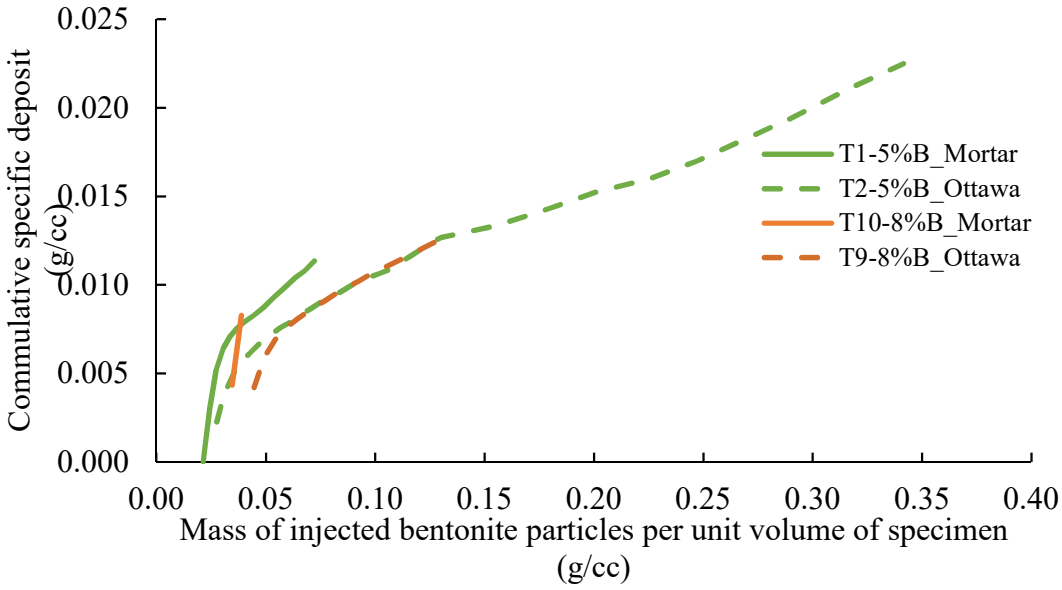

(b)

Figure 8-7: Effect of grain size distribution of porous media on the particle retention

8.4.2 Filtration Coefficient

Filtration coefficient($\lambda(\sigma)$) is the probability of particles to be captured per unit length of trajectory (Herzig et al., 1970) and is assumed to be constant and independent of retained particle concentration for diluted suspensions (Elimelech et al. 1995; Logan2001) in most laboratory tests. In this section, a dependency of filtration coefficient on previously retained particles is studied and a relationship is developed.

In this paper, specific deposit (σ) is expressed as the weight of retained particles per unit volume of porous media and suspension concentration (C) is defined as the ratio of weight of suspended particles to the volume of grout. Equation (8-2) is used to determine the filtration coefficient from the laboratory data and are plotted against the cumulative concentration of previously retained bentonite particles. Figure 8-8 shows that filtration coefficient is a function of previously retained particles. In the early stage of filtration, bentonite particles progressively coated around the sand grains due to Van der Waals and electro-kinetic forces. Later it leads to double layer repulsion and the probability of particles to be retained decreases with increase in the number of particles retained.

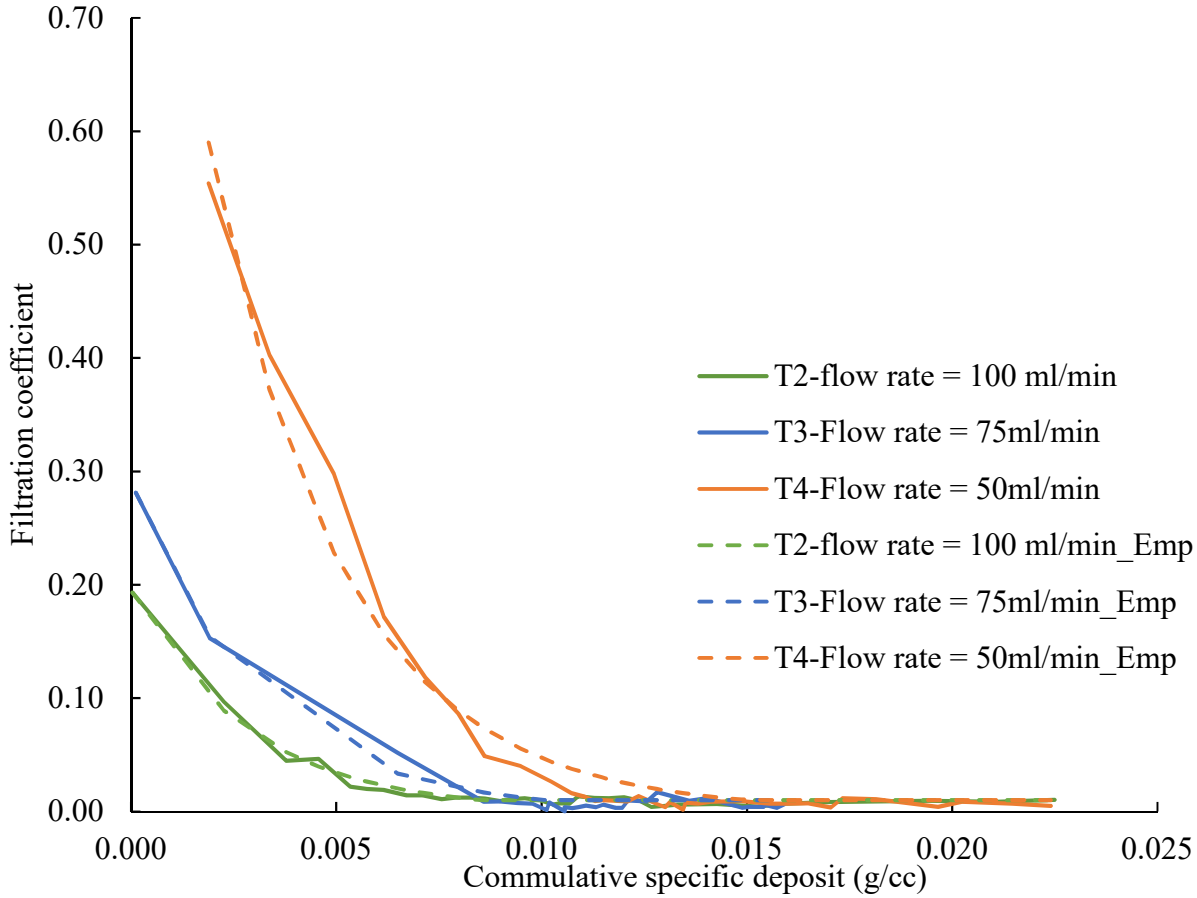

Figure 8-8: Dependency of filtration coefficient on previously retained bentonite particles for the grout flowing at different rate for 5% bentonite grout

The filtration coefficient is more for the smaller flow rate after the similar number of particles retained for diluted suspension as expected. A relationship between filtration coefficient and retained bentonite particles was developed and defined by an empirical equation

(8-3)

$$\lambda(t) = \lambda_0 * \exp(-b * \sum_0^{t-1} \sigma) \text{ if } \lambda(t) < 0.01$$

$$\lambda(t) = 0.01 \; if \; \lambda(t) > 0.01 \tag{8-3}$$

where, λ_0 is the initial filtration coefficient, b is fitting constant, and $\sum \sigma$ is the cumulative specific deposit. Equation (8-3) is a filtration equation for permeation of bentonite suspension grout.

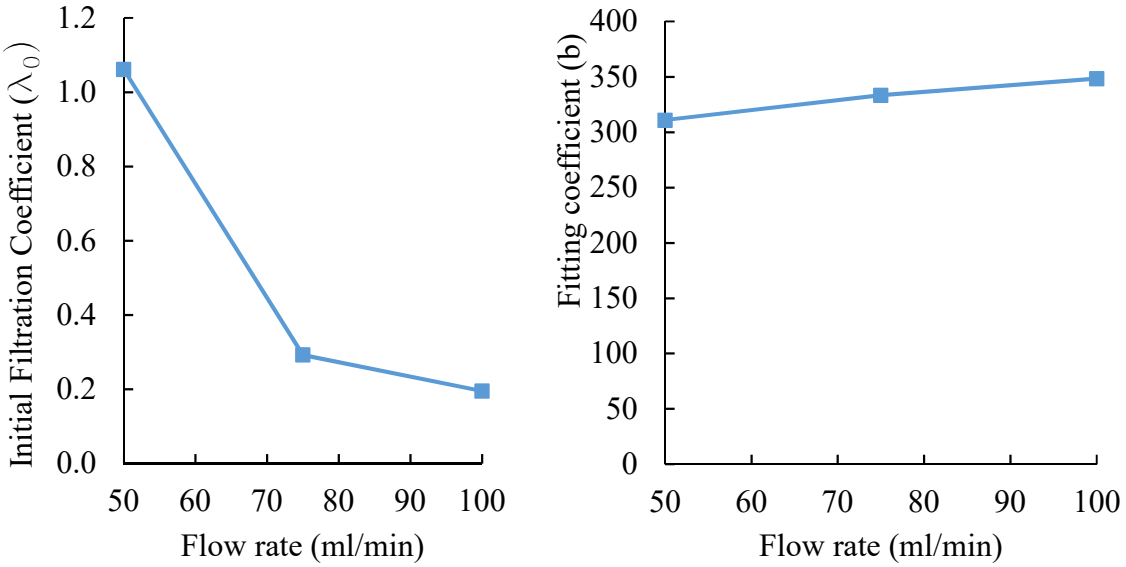

(a) (b)

Figure 8-9: Effect of flow rate on (a) Initial filtration coefficient (b) fitting coefficient for diluted suspension grout of 5% bentonite

The constants of filtration equation (a) initial filtration coefficient (b) fitting coefficient, b; depends on the variables like flow rate, grout concentration, rheology of grout.

Figure 8-9 shows the effect of flow rate on the coefficients of filtration equation for the injection of diluted suspension. The value of initial filtration coefficient decreases with the increase in the flow rate of injection for diluted suspensions as expected whereas it is vice versa for the concentrated suspension (Figure 8-10-b)

Fitting coefficient (b) defines the rate of decrease of filtration coefficient because of the previously retained particles. The larger the value of fitting coefficient (b), faster the rate of declination of filtration coefficient. The declination rate of filtration coefficient is 11 percentage faster for the grout injecting at the flow rate of 100ml/min than at the flow rate of 50ml/min for diluted suspension. Figure 8-10 (A) shows that filtration coefficient of the concentrated grout injecting at high flow rate is more. The proposed filtration equation is fitting well with the laboratory results with r^2 of 0.95 to 0.99 approximately.

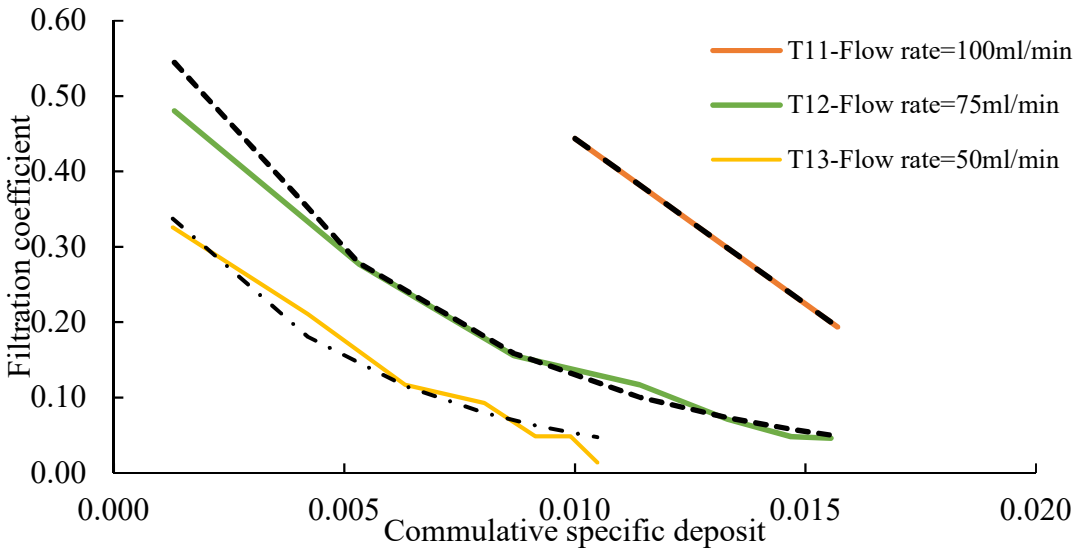

(a)

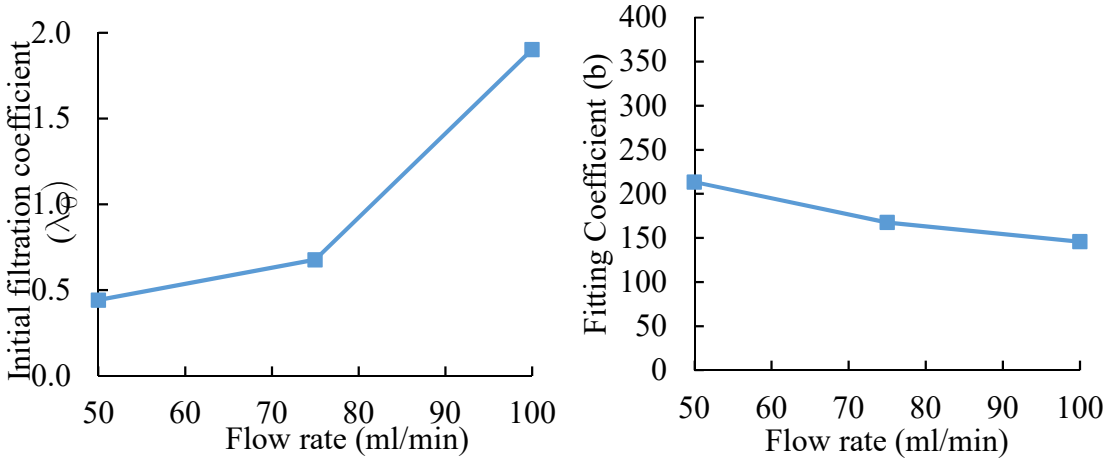

(b)

Figure 8-10: (a) Change in filtration coefficient with particle retention for the concentrated grout (10%B 3%SPP) (b) Effect of flowrate on the filtration equation coefficient

Initial filtration coefficient increases and fitting coefficient decreases with increase in flow rate Figure 8-10 (b). The addition of sodium pyrophosphate(SPP) decreases the apparent viscosity of grout and disperse the bentonite particles in the suspension which decrease the likelihood of particle retention. Therefore, the initial filtration coefficient of grout decreases with the addition of SPP Figure 8-11(b). The fitting coefficient for the grout with additive and no additives has approximately the same value. Hence the declination rate of filtration coefficient with particle retention is same for the similar concentrated grout.

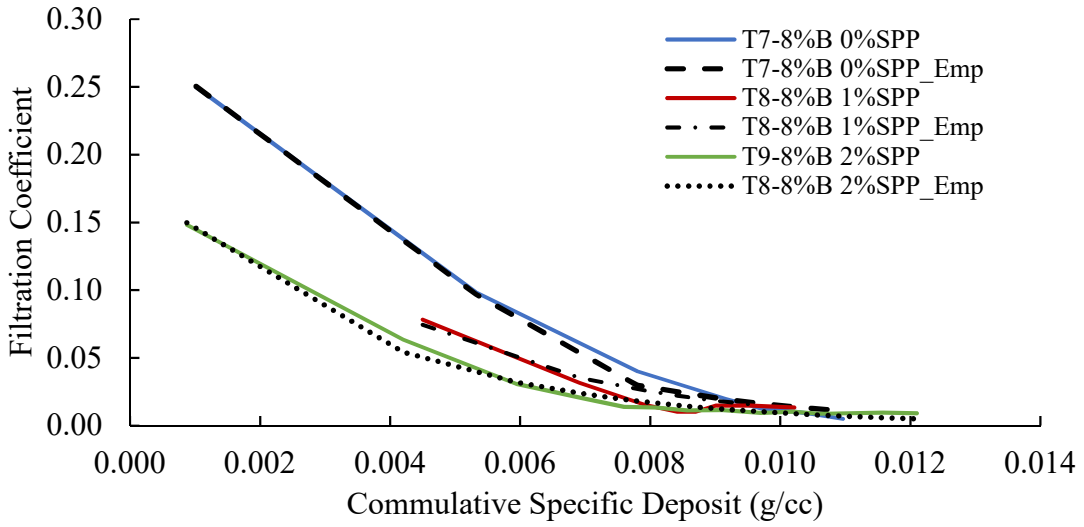

(a)

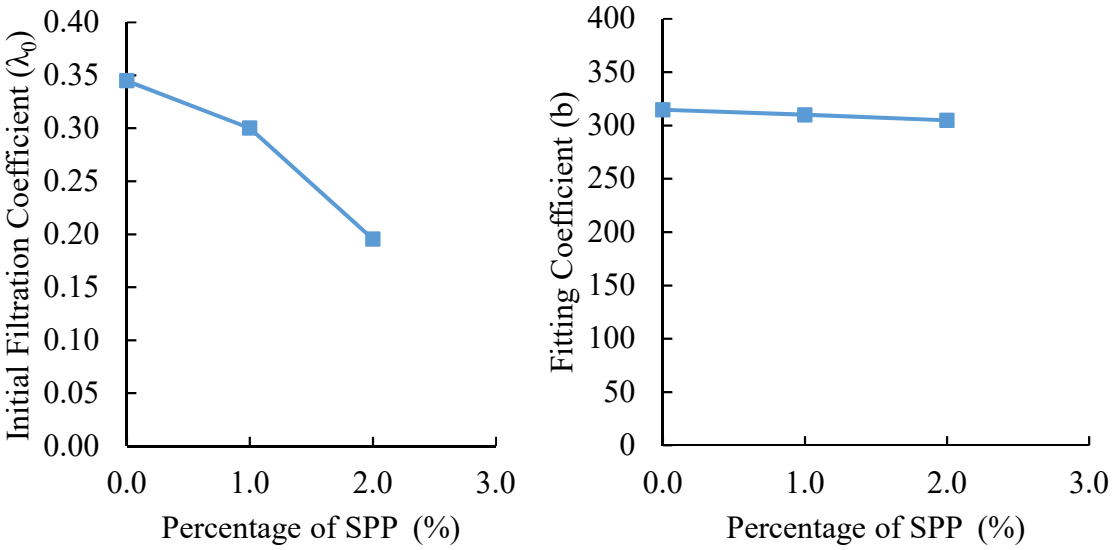

(b)

Figure 8-11: (a) Effect of addition of sodium pyrophosphate (SPP) on the filtration coefficient (b) on the coefficients of filtration equation

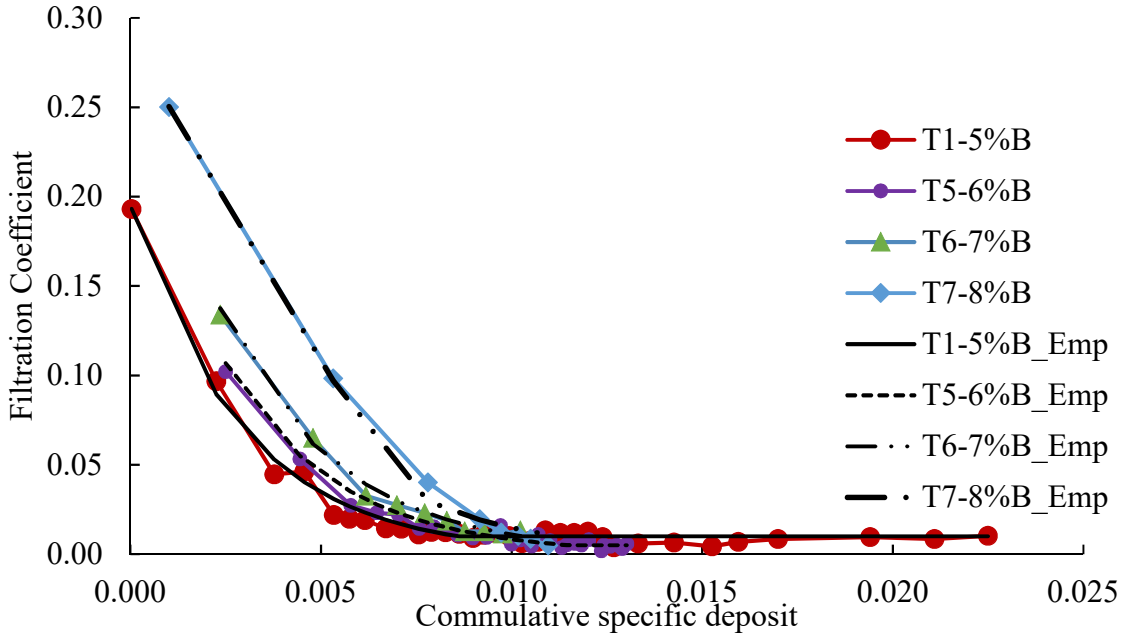

(a)

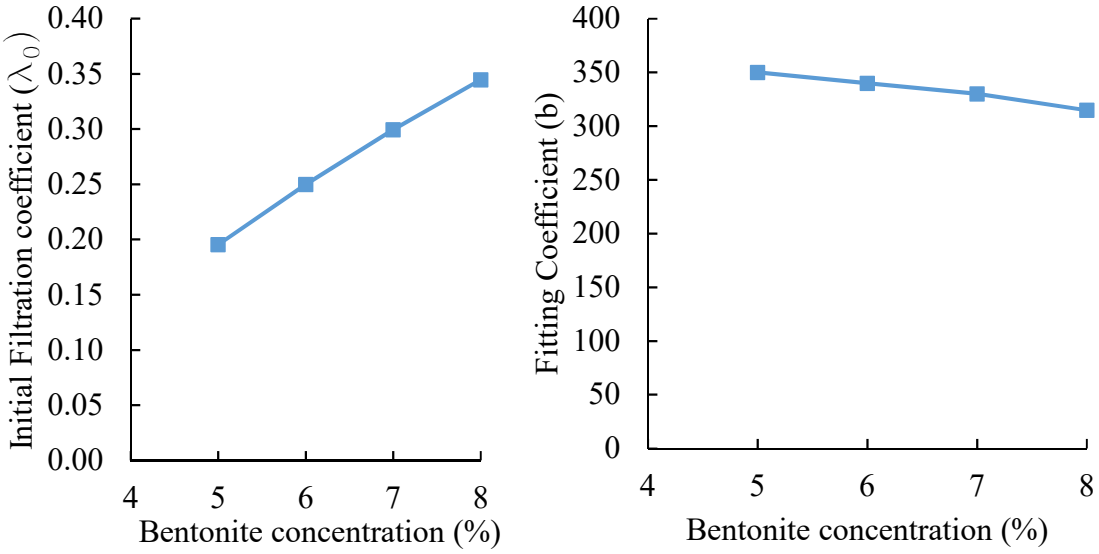

(b)

Figure 8-12: Effect of bentonite concentration on (a) the filtration coefficient (b) the coefficient of filtration equation

The amount of particle retention increases with the increase in the bentonite concentration of suspension grout. Therefore, the value of initial filtration coefficient is linearly increasing with rout concentration. Whereas there is slightly decrease in the value of fitting coefficient with percentage of bentonite particles suspended in grout.

Figure 8-13 shows the effect of the grain size distribution on filtration coefficient. It is found that the probability of particle retention is more for the grout passing through mortar sand because of the smaller pore size (Figure 8-13A). Initial filtration coefficient is more for the grout passing through mortar sand compared to Ottawa sand Figure 8-13 (b).

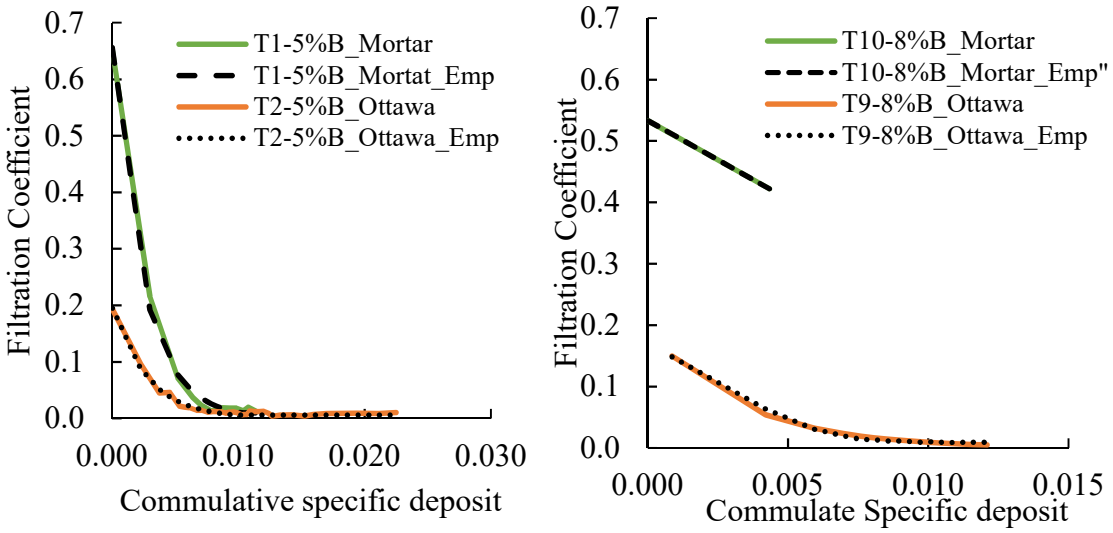

(a)

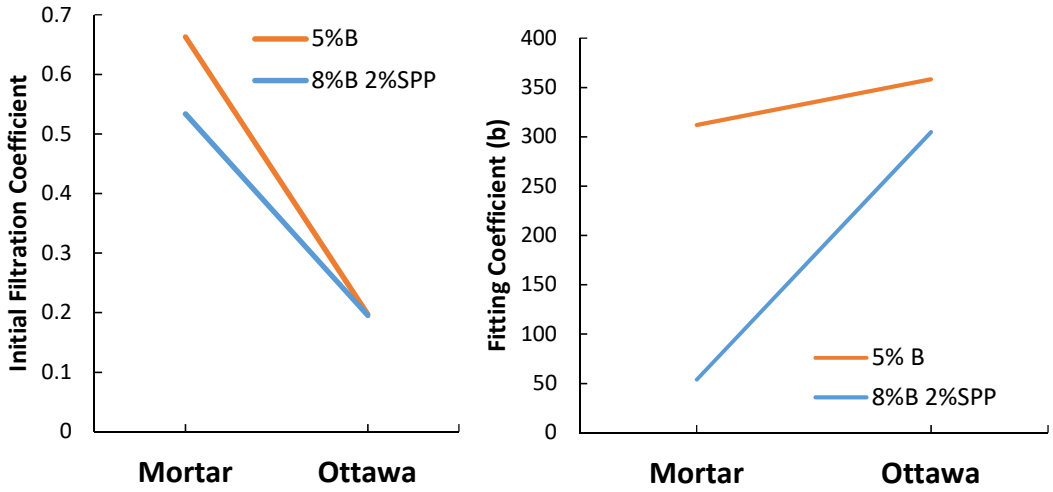

(b)

Figure 8-13: Effect of the pore size of sand on (a) Filtration coefficient (b) coefficient of filtration equation

Particle retention in Mortar sand is controlled by bridging mechanism. Therefore, the declination of filtration coefficient is less for Mortar. The total volume of grout injecting through mortar sand is much lesser compared to that through Ottawa sand because of the restricted grout flow. Figure 8-13A shows that total amount of retained particles is more for Ottawa sand.

8.4.3 Particle Retention rate

As originally proposed by Iwasaki (1937), the rate of particle capture function is usually written as

$$\frac{\partial \sigma}{\partial t} = \lambda u C \tag{8-4}$$

where the filtration coefficient (λ) is determined in the previous section as a function of retained particles and has a dimension of cm^{-1}. C is the concentration of suspended particles, the ratio of weight of bentonite particles to the bulk volume of grout, u is the superficial Darcy velocity. Equation (8-4) is valid for the diluted suspensions. In this section, an effort is made to develop a rate of particle retention function.

The evolution of filtration coefficient (λ) and rate of particle retention $\left(\frac{\partial \sigma}{\partial t}\right)$ was calculated from the laboratory test results during the permeation process. Velocity (u) and concentration of suspension grout (C) are considered constant across the representative size of specimen. Particle retention rate depends on the filtration coefficient and filtration coefficient is the function of

cumulative amount of previously retained particles. Hence the rate of particle retention can be defined as follows

$$(\frac{\partial \sigma}{\partial t})_t = (\lambda(\sigma))_t * u * C \tag{8-5}$$

$$(\frac{\partial \sigma}{\partial t})_t = \lambda_0 * \exp\left(-b * \sum_{0}^{t-1} \sigma\right) * \mathrm{u} * \mathrm{C} \tag{8-6}$$

Equation (8-6) is difficult to solve. Therefore, the rate of particle retention equation was determined using the experimental results. Rate of particle retention was normalized with velocity and concentration and was plotted against the filtration coefficient (Figure 8-14). The equation was determined to best fit the graph.

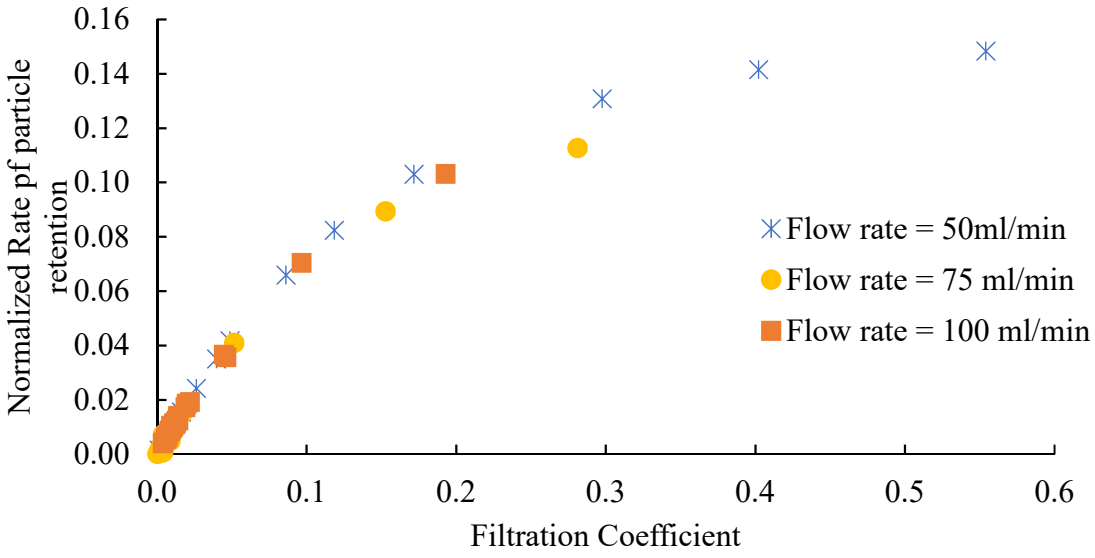

Figure 8-14: Normalized particle retention rate against filtration coefficient for 5% bentonite suspension grout

It was found that the particle retention rate doesn't have a linear relationship with filtration coefficient as proposed by Iwasaki 1937(Figure 8-14).If Figure 8-14 is zoomed for the smaller filtration coefficient, it was found that rate of particle retention rate is directly proportional to filtration coefficient (Figure 8-15)

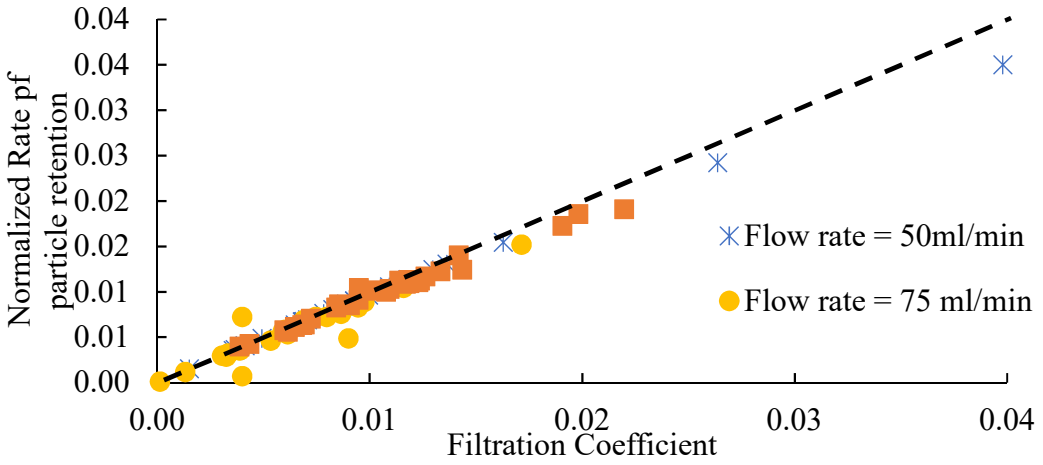

Figure 8-15: Zoomed version of Figure 8-14 shows the validity of Iwasaki proposed relationship for lower range of filtration coefficient

Hence the Iwasaki (1937) relationship for rate of particle capture is valid for the filtration coefficient less than 0.2. The empirical equation determined for defining a relationship between particle retention rate and filtration coefficient for bentonite suspension grout is as follows

$$\frac{\partial \sigma}{\partial t} = \left(\frac{1}{L}\right) * \left(1 - \frac{1}{\exp(\lambda L)}\right) * u * C \qquad (8\text{-}7)$$

where, L is the length of sample.

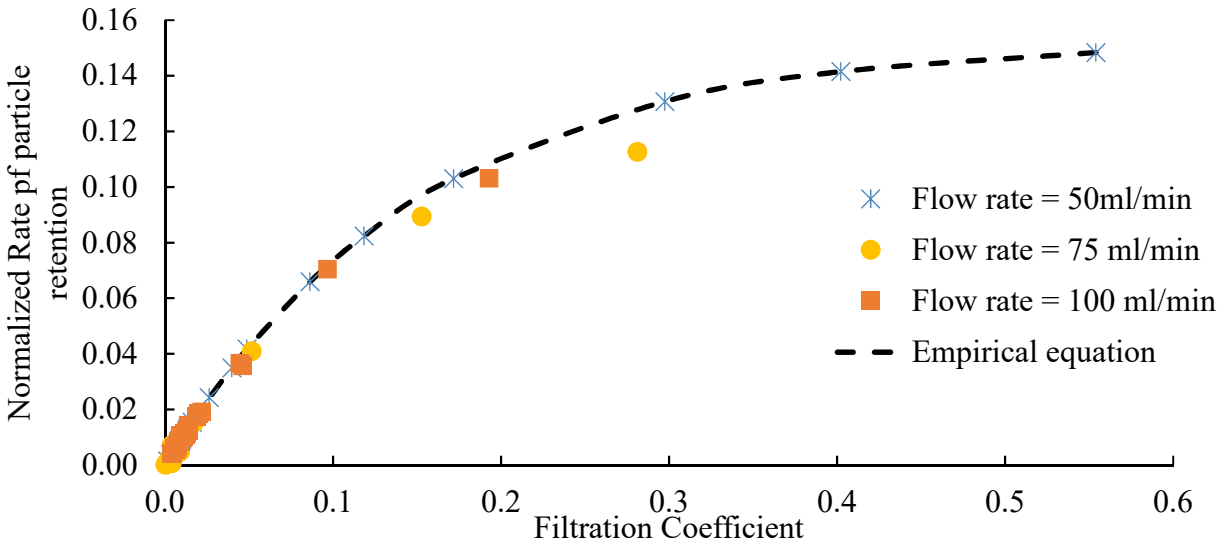

Figure 8-16: Empirical equation for the rate of particle retention as function of filtration coefficient

Equation (8-7) is valid for the large range of filtration coefficient

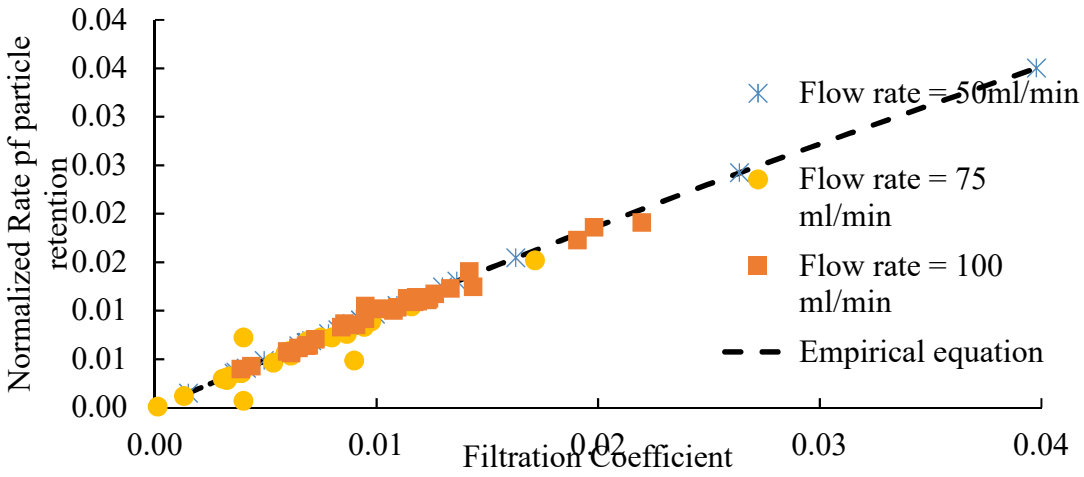

Figure 8-17: Zoomed version of Figure 8-16 to show the validity of empirical equation for broad range of filtration coefficient

8.4.4 Permeability Reduction Function

Sands are prone to accumulation of suspended particles during the grouting process. This cause the reduction in permeability which in turn lead to the limited grout spread. Permeability reduction function is the relationship between the declined permeability and the concentration of retained particles. In this section, permeability reduction function is determined from the results of experimental and theoretical investigation.

The differential pressure increase across the sample caused by gradual particulate clogging was monitored using a differential transducer. The permeability was calculated using Darcy's law with the recorded pressure difference across the sample and flow rate of the pump. The concentration of retained particles is calculated from the difference in the influent and effluent concentrations. The change in porosity of porous media was determined from the hydrated volume of retained bentonite particles. The permeability and porosity are normalized by the initial

permeability and initial porosity. Figure 8-18 shows the reduction in permeability is more than 95 % as grouting proceed.

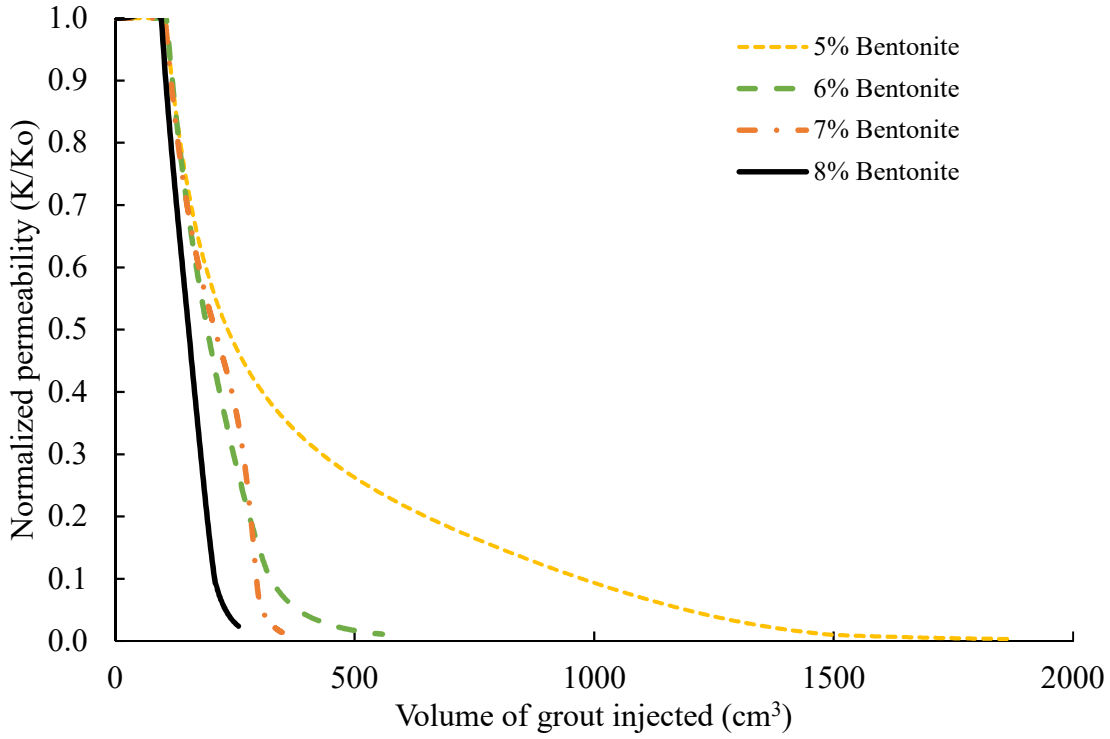

Figure 8-18: Effect of particle concentration on the reduction in permeability of porous media

The semi empirical Kozney-Carman equation is the most famous permeability- porosity relation which is widely used in the field of flow of porous media and is the starting point for many other permeability models. The KC equation which relate permeability to the porosity is

$$k = \frac{n^3}{C * (1 - n^2) * S^2} \tag{8-8}$$

where C= $c\tau^2$ and S are the empirical parameter and specific surface area respectively. Many models considered the change in permeability explicitly depend on the porosity and assumed C, empirical parameter to be constant. The change in the porosity of sand was determined using the Kozney Carman equation from the permeability data (Equation (8-9). It was assumed that there is no effect of filtration on the empirical parameter C and specific surface area S and are constant.

$$\frac{k}{k_o} = \frac{n^3}{(1-n^2)} * \frac{(1-n_0^2)}{n_0^3} \tag{8-9}$$

where k = reduced measured permeability, n is the porosity of porous media, k_0 and n_0 are the initial permeability and porosity of sand. The porosity determined from the Kozney- Carman equation is compared with experimentally measured porosity (n_e).

$$n_e(t) = n_0 - \sum_{n=0}^{t} \sigma \tag{8-10}$$

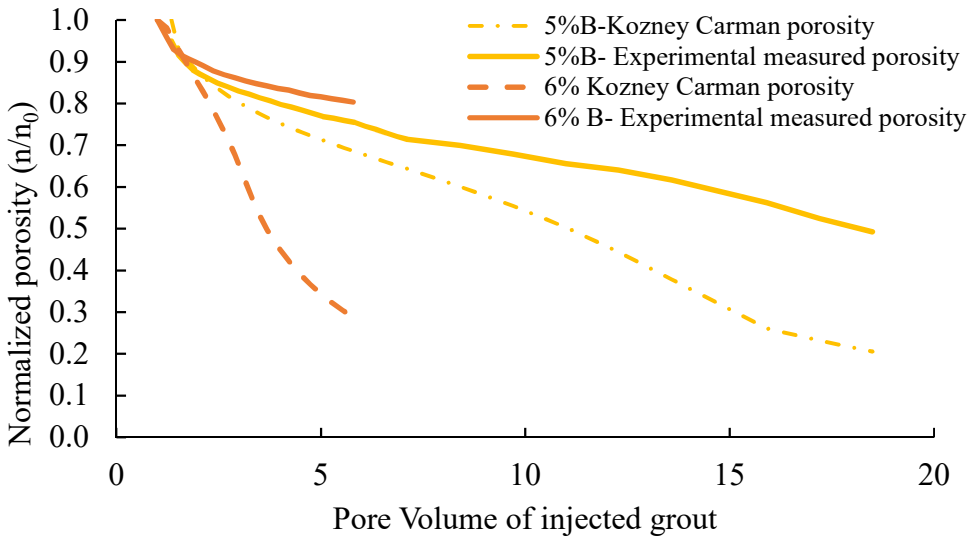

Figure 8-19: Comparison of Kozney Carman interpreted porosity with experimentally measured porosity

Figure 8-19 shows that Kozney Carman overestimated the reduction in porosity and indicated that change in permeability is not solely due to the change in pore space. Particle retention changes the tortuosity and the specific surface as well.

The equation was developed to define the permeability reduction function for the bentonite suspension grouting as a function of reduced porosity and volume of retained bentonite particles.

$$\frac{k(i,j)}{k_0} = k_n(i,j) * k_\sigma(i,j)$$

$$k_n(i,j) = \frac{{n_{i,j}}^3(1-n_0)^2}{{n_0}^3(1-n_{i,j})^2} \quad (8\text{-}11)$$

$$k_\sigma(i,j) = exp(-A * \sum_{i,0}^{i,j} \sigma_{i,j})^B$$

where, ϕ_0 and $\varphi_{i,j}$ are the initial and reduced porosity respectively. $\sum_{i,0}^{i,j} \sigma_{i,j}$ is the cumulative volume of retained particles, A and B being fitting parameters and are determined by the least mean square error between predicted and measured permeability using SOLVER in excel. Normalized permeability was determined using the proposed permeability reduction function and are compared with the experimental and Sharma et al. (2000) results. The permeability reduction function developed by Sharma et al. (2000) is for cement grout and water injection wells.

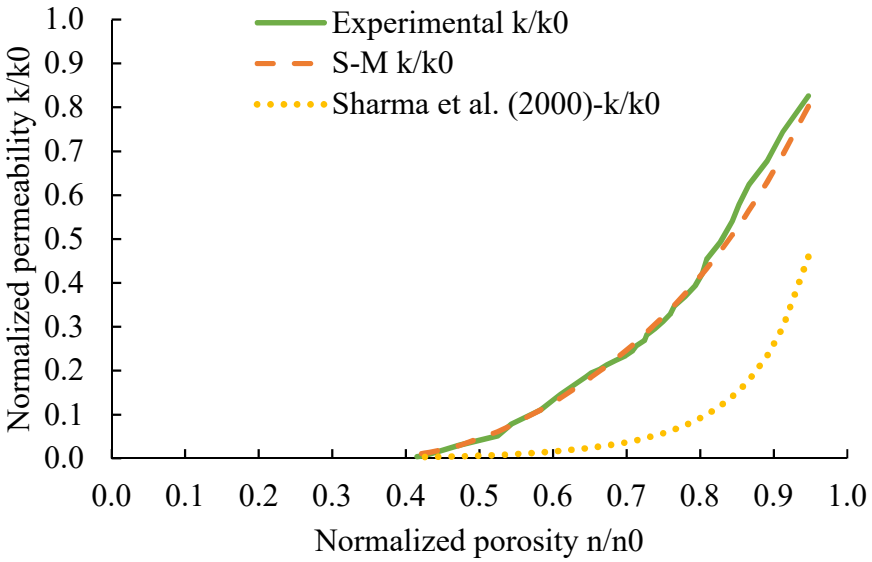

Figure 8-20: Empirically determined normalized permeability using S-M and Sharma et al. (2000) permeability reduction function

It is found that Sharma et al. (2000) overestimate the permeability reduction for bentonite suspension grout. S-K reduction function predicted the reduced permeability close to the experimentally measured permeability with coefficient of determination (r^2) of 0.988 (Figure 8-20)

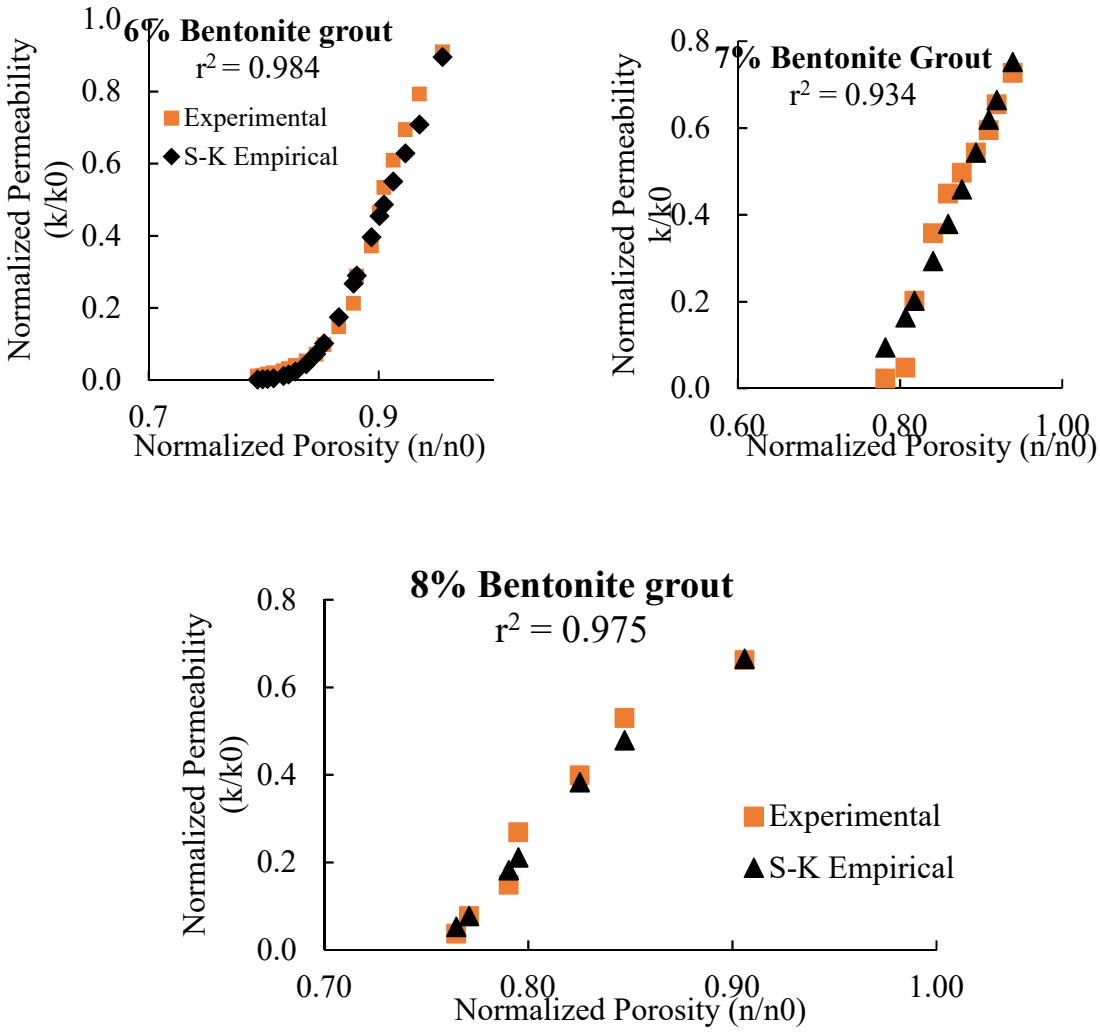

Figure 8-21: Prediction of reduced permeability using S-M permeability reduction function and compared to experimental results

S-K permeability reduction function was used to determine the reduced permeability of different concentration grout and compared to the experimental measured permeability (Figure 8-21). It is found that S-K function is applicable to all concentrated bentonite grout. Predicted reduced permeability fit well with experimentally measured permeability with coefficient of determination (r^2) in range of 0.93-0.99.

8.5 Results and discussion for cement grout

8.5.1 Filtration function for cement grout

This section is divided in three categories (a) Cumulative specific deposit analysis to study the filtration tendency of cement grout (b) determination of filtration coefficient relationship and (c) determination of rate of particle retention empirical equation.

8.5.1.1 Cumulative specific deposit

Figure 8-22 shows that the amount of particle retained is more for low concentrated grout, which is opposite in the case of bentonite grout discussed earlier. Low concentrated cement suspension is unstable and particles got segregated easily and retained on sand grain. Whereas, the high concentrated cement grout of water/cement ratio of 3 are more stable and showed less filtration. The specific deposit of different concentrated grout of water/cement ratio of 3, 5, and 7 are 0.04, 0.048 and 0.063 g/cc respectively after the injection of 100g of cement particles. The particle retention is almost 2 times more for cement grout of water/cement (w/c) of 7 than that of

grout of w/c of 3. Large volume of grout (more than 6 pore volume) was injected through sand to capture the evolution of particle retention.

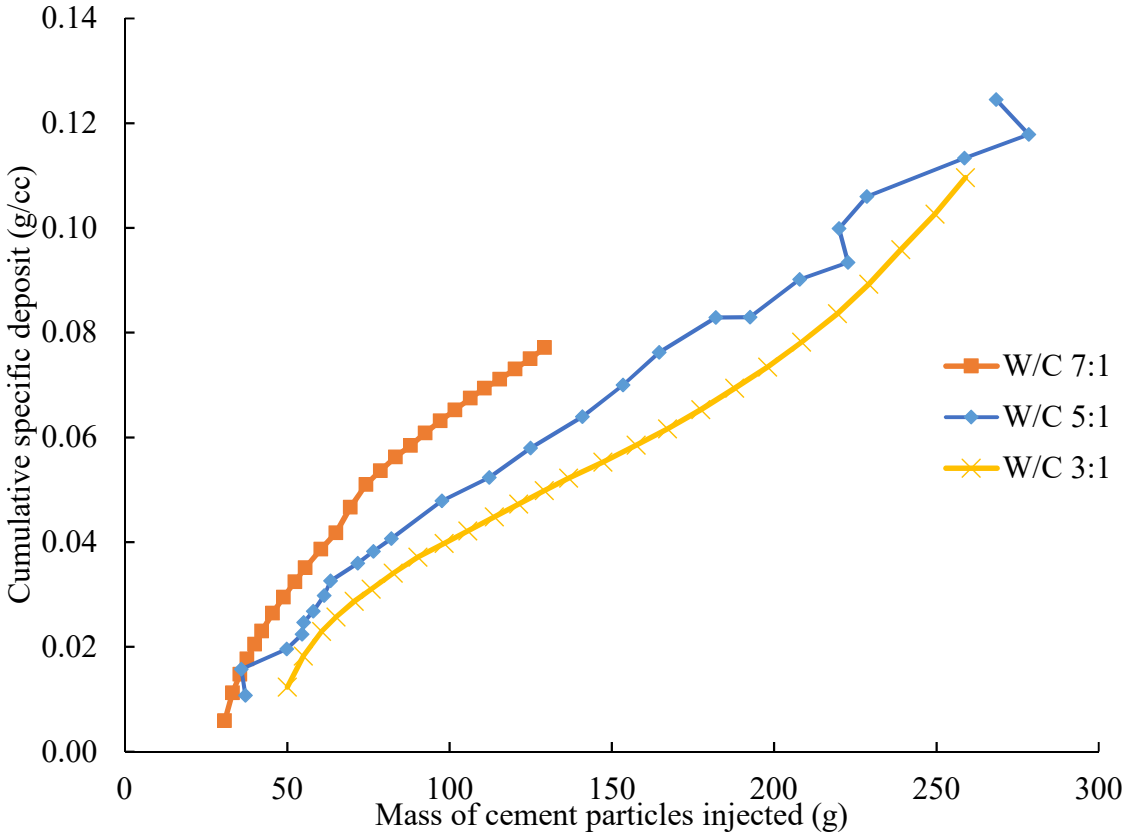

Figure 8-22: Cumulative specific deposit versus the mass of injected particles for different concentration of cement particle

Particle retention haven't reached to the equilibrium state for either of cement grout even after the injection of 10 pore volume. Figure 8-23 shows that addition of superplasticizer reduced the tendency of particle retention on sand grain, similar as observed in static sedimentation test.

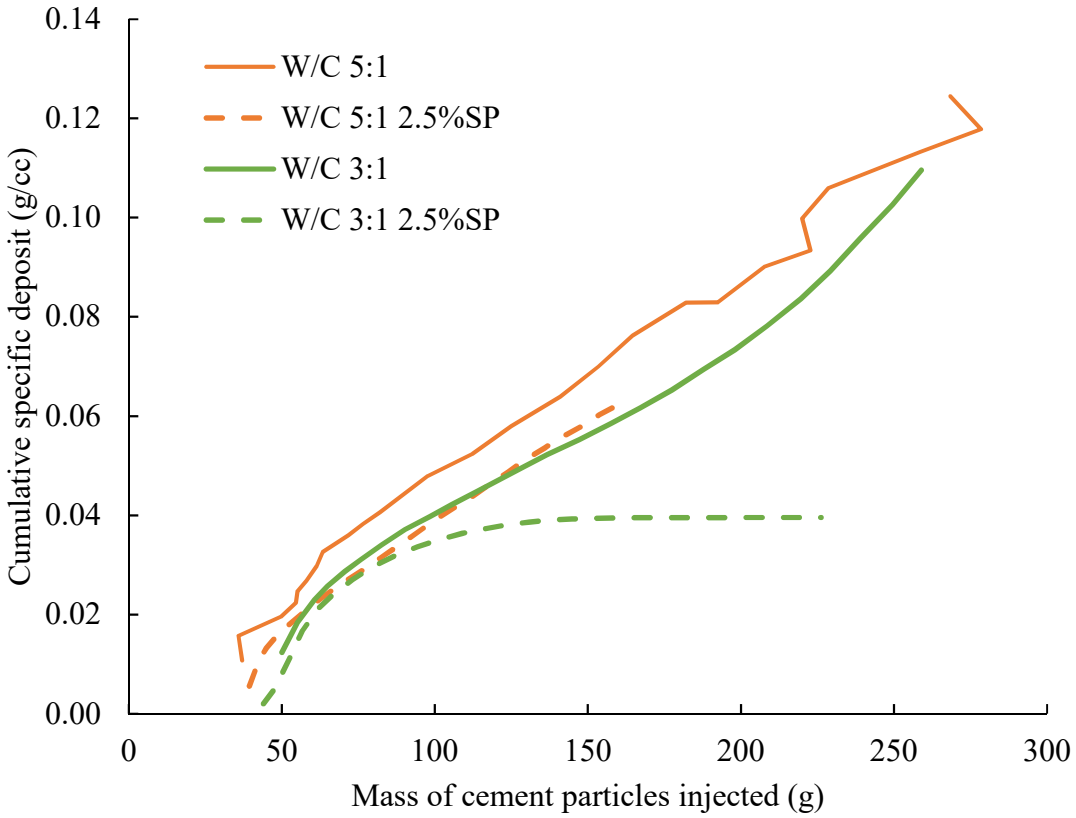

Figure 8-23: Effect of addition of superplasticizer on the particle retention

Cement grout of water/cement ratio of 3 with additives reached to equilibrium state after the deposition of 0.06 g per unit the volume of specimen.

8.5.1.2 Filtration Coefficient

Equation (6.2) is used to determine the filtration coefficient from the effluent concentration data. Filtration coefficient is plotted against the previously retained particle to determine its dependency on the concentration of retained particle (Figure 8-24)

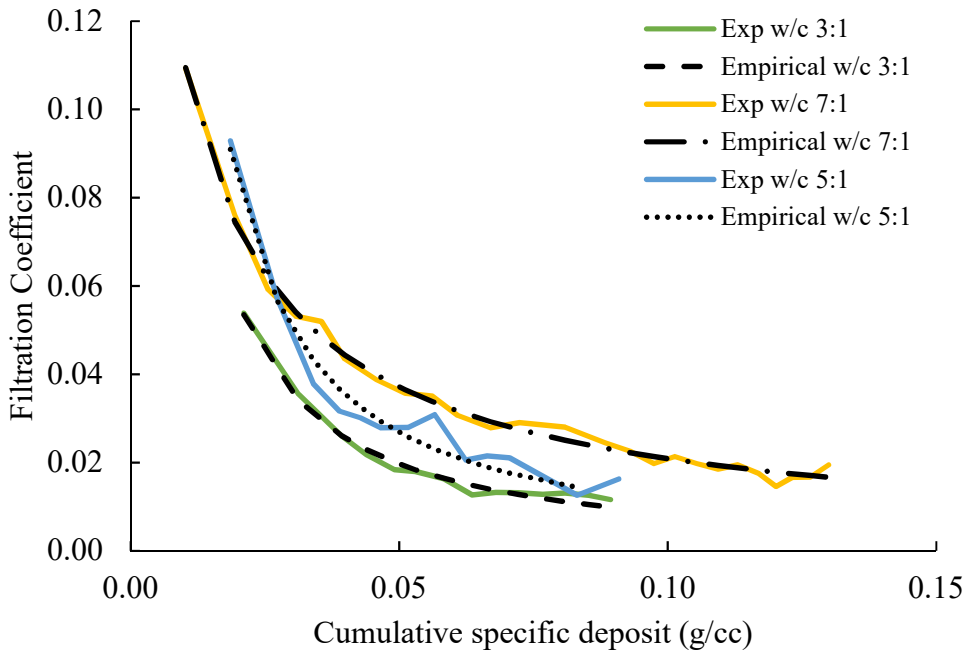

Figure 8-24: Empirical relationship between filtration coefficient and cumulative specific deposit

The filtration coefficient decreases with increase in the concentration of retained particles. Cement particles deposit over pore bodies and pore throats due to mechanical and physiochemical interactions. Particle retention start decreasing since the cement particle covers the sand particle due to particle- particle repulsion forces. The filtration coefficient of concentration cement grout (w/c 3:1) is low comparative to diluted cement grout (w/c 7:1). It was observed that low concentrated grout is unstable and tend to settle faster compared to the high concentrated grout in static sedimentation test. Cement particles of unstable grout has tendency to get separated from the liquid and retained on sand grains due to the pressure filtration (i.e. the loss of water due to injection pressure). An empirical equation was determined to develop a relationship between

filtration coefficient and previously retained particles for the cement grout. A relationship was determined which best fit the experimental results using the SOLVER in excel.

$$\lambda_t = \frac{\lambda_0}{(1 + a * (\sum_0^{t-1} \sigma)^m)} \tag{8-12}$$

where λ_0 is the initial filtration i.e the probability of particle retention at the injection of first pore volume, a and m are fitting coefficient. The filtration coefficient equation is best fitted with experimental results with coefficient of determination (r^2) of 0.92 to 0.98. Therefore, the equation (8-2) well defined the filtration tendency of cement grout during the permeation grouting.

The results of static sedimentation tests concluded that the addition of superplasticizer disperse cement particles and stabilize the grout. Similar result was observed in dynamic filtration test. The addition of superplasticizer decreases the filtration coefficient. (Figure 8-25). Effect of superplasticizer is more significant for the concentrated grout.

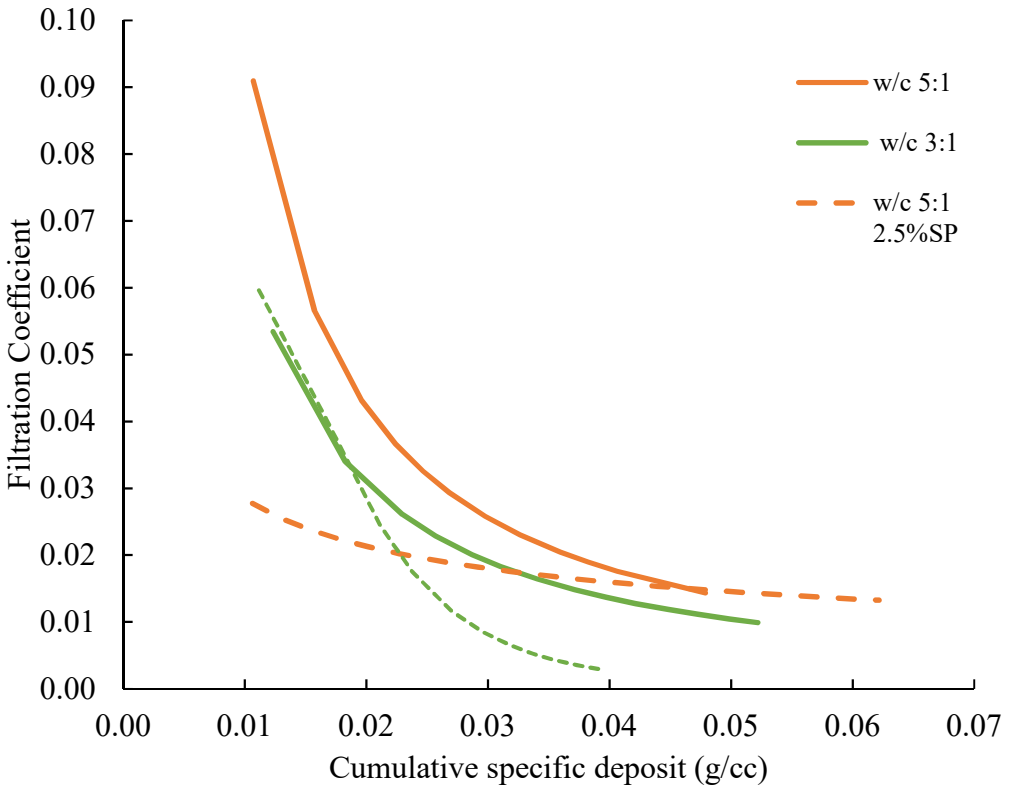

Figure 8-25: Filtration coefficient of cement grout with additives

8.5.1.3 Rate of Particle retention

In this section, a relationship between particle retention rate and filtration is determined experimentally. Normalized particle retention rate is plotted against the experimentally determined filtration coefficient (Figure 8-26)

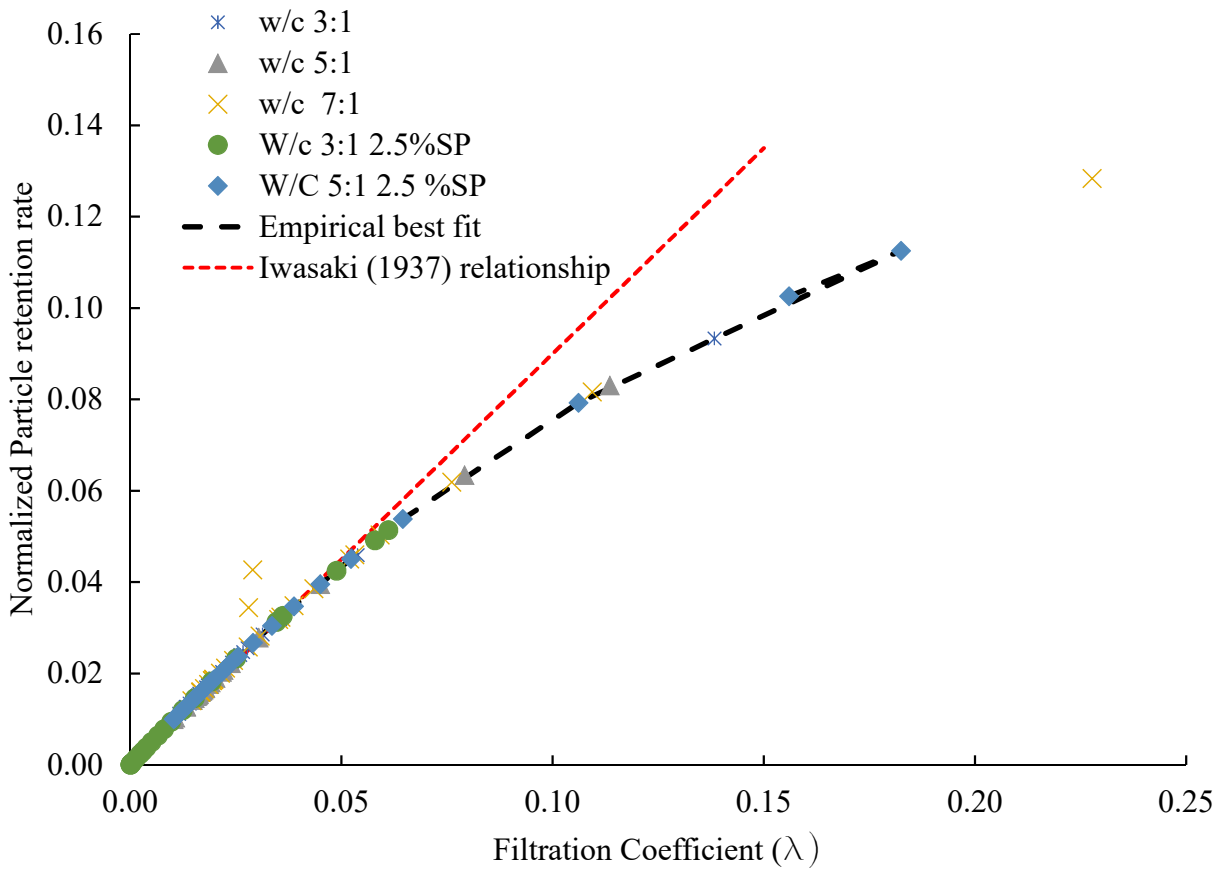

Figure 8-26: A relationship between particle retention rate and filtration coefficient

It is observed that Iwasaki (1937) linear relationship is valid for the filtration coefficient less than 0.05. An empirical equation defining the relationship between filtration coefficient and particle retention rate was determined as follows.

$$\frac{\partial \sigma}{\partial t} = \left(\frac{1}{L}\right) * \left(1 - \frac{1}{\exp(\lambda L)}\right) * u * C \qquad (8\text{-}13)$$

Filtration function is together defined by equation (8-2) and (8-7). Filtration coefficient is function of previously retained particles and particle retention rate depends on the filtration coefficient. Mathematically, this process can be explained as

$$\lambda_t = \frac{\lambda_0}{(1 + a * (\sum_0^{t-1} \sigma)^m)} \tag{8-14}$$

and

$$(\frac{\partial \sigma}{\partial t})_t = \left(\frac{1}{L}\right) * \left(1 - \frac{1}{\exp(\lambda_t L)}\right) * u * C \tag{8-15}$$

8.5.2 Permeability reduction function

The retention of cement particle on sand grains reduce the pore size and the permeability of grout. Saada et al. (2007) modeled the permeability variation by the hyperbolic law that depends on the porosity and concluded that this law is more appropriate than a Kozney Carman law since it can predict high variation of permeability for low variation of porosity. In this section, effort is made to determine the permeability variation as a function of porosity and concentration of retained particles.

The differential pressure was recorded across the specimen during the grout injection. The variation of absolute permeability of medium was measured from the recorded pressure using the Darcy's law. The change in porosity was determined from the effluent concentration data. Detailed

explanation of determining permeability from pressure data and porosity from the effluent concentration data is given in the appendix of Chapter 7.

8.5.2.1 Pressure-time curve

The pressure at the injection point was recorded using the differential pressure transducer connected to the data acquisition system. Figure 8-27 shows the pressure time curves comparing the performance of different w/c ratio grout. Pressure-time curve reflects the flow behavior characteristic of grout through the sand pores. Rheology and filtration simultaneously controls the pressure buildup at the injection point. The inlet grout is always kept in motion under the high-speed mixer to prevent the change in rheology of grout because of thixotropic effect. The speed of mixer is maintained so that there is no segregation of cement particles due to centrifugal force especially for low concentrated grout. Hence the variation of rheology of grout during the injection process can be neglected. Large volume of grout is injected through small sand specimen to study the transient dynamic of filtration. In the process, cement particles retain on the sand grains and pore size and permeability of sand specimen reduces. It changes differential pressure across the specimen for constant flux permeation. The filtration process can be interpreted from the pressure-time curve.

The initial pore pressure measurement (Figure 8-27) reflects that the grout level is rising in the sand specimen and the slope of the pressure-time reflects the viscosity of grout. The viscosity of high concentrated grout (w/c 3:1) is three times more than low concentrated grout (w/c 7:1)

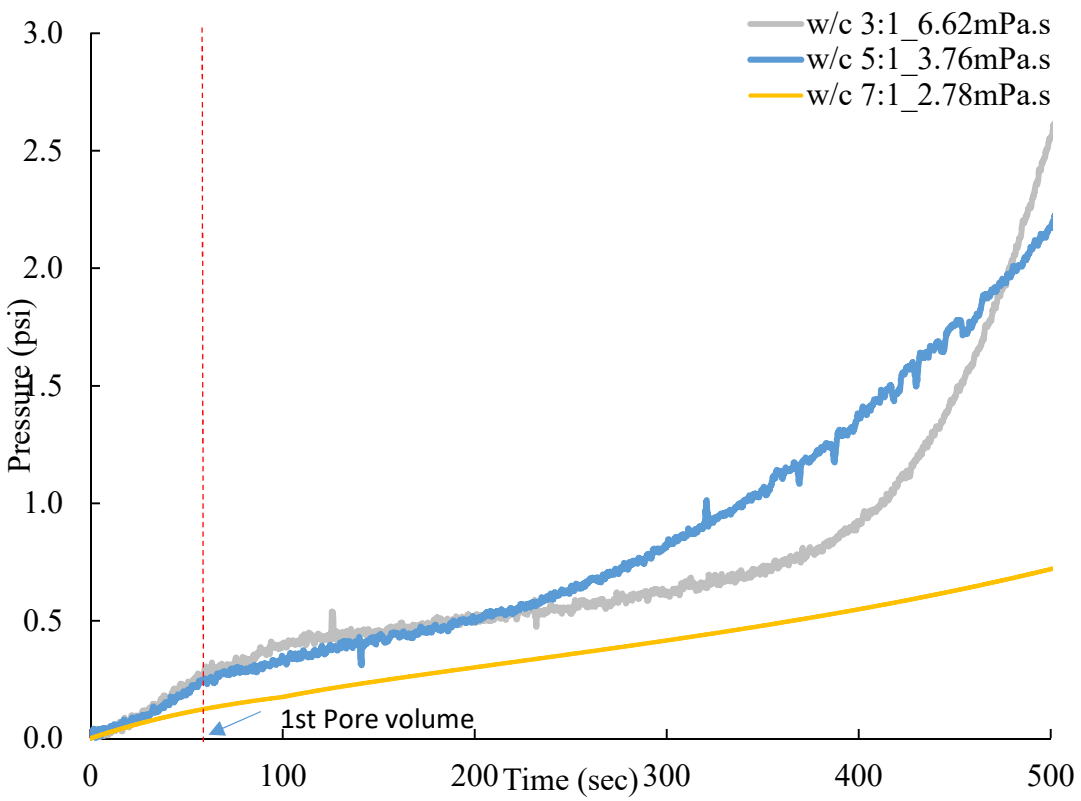

Figure 8-27: The differential pressure recorded across the specimen while injecting the different concentration grout.

Red dashed line shows the injection of first pore volume. The increase in pressure after the first pore volume is due to change in the permeability of medium as a result of filtration. The slope of pressure-time curve is steep for low concentrated grout (w/c 7:1) compared to other grout after the injection of first pore volume. It is concluded that cement particles of low concentrated grout are subjected to more filtration. The pressure at injection point of grout of water/cement ratio of 5 is also increasing at slow rate until time equals to 200s and then increases rapidly afterwards. The change in permeability of sand specimen and viscosity of grout controls the pressure at the

injection. The rate of filtration is faster for cement grout of w/c ratio of 7 compared to w/c ratio of 5 and 3, but the pressure value at the injection point is small due to the apparent viscosity of grout.

The pressure-time slope of grout of w/c ratio of 3 is almost flat after the first pore volume indicates the limited filtration but small change in the pore space/permeability could buildup high pressure for thicker grout. Eventually, the pressure build up rapidly for thicker cement grout after the injection of 5 pore volume. Pressure filtration (i.e. loss of water due to high applied pressure) could be the consequence of the high injection pressure. It is important to keep the injection pressure low to prevent the pressure filtration in later stages. Additives (superplasticizer) are used to lower the apparent viscosity of cement grout and buildup of high pressure at the injection point could be controlled.

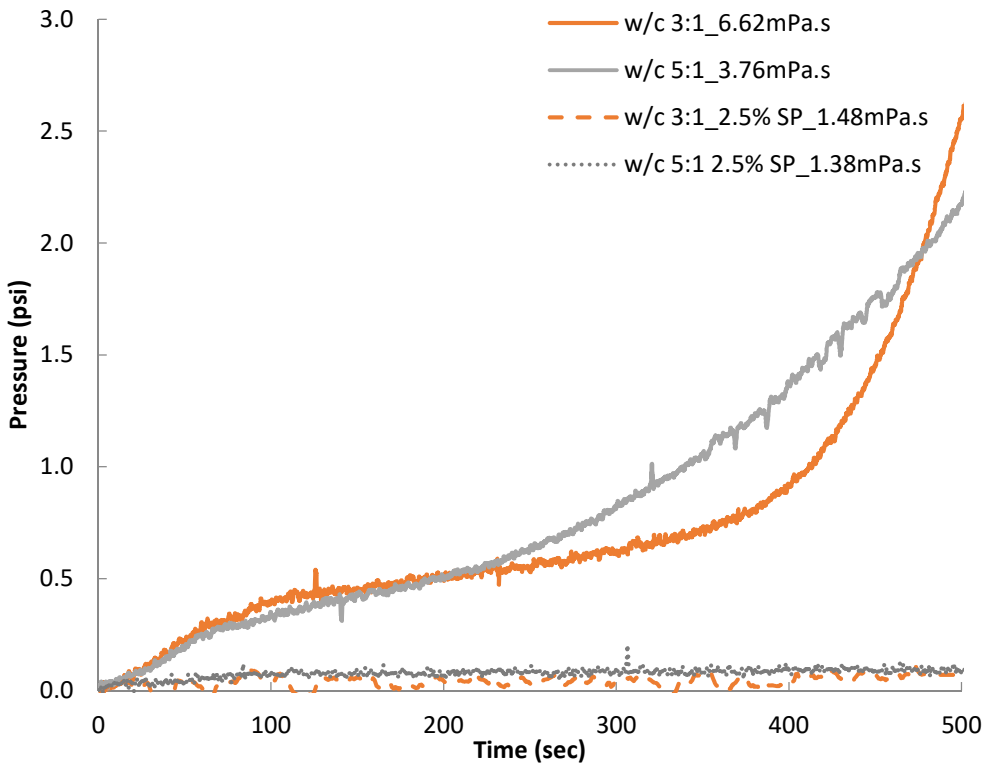

Figure 8-28: Effect of superplasticizer on pressure-time curve

The viscosity of grout decreases almost four times for grout of w/c ratio of 3:1. Therefore, the generated pore pressure for the cement grout with additives is very less compared to grout without additives (Figure 8-28) which allows the deep permeation of grout. More than 10 pore volume of cement grout with additive were permeated without any pressure buildup.

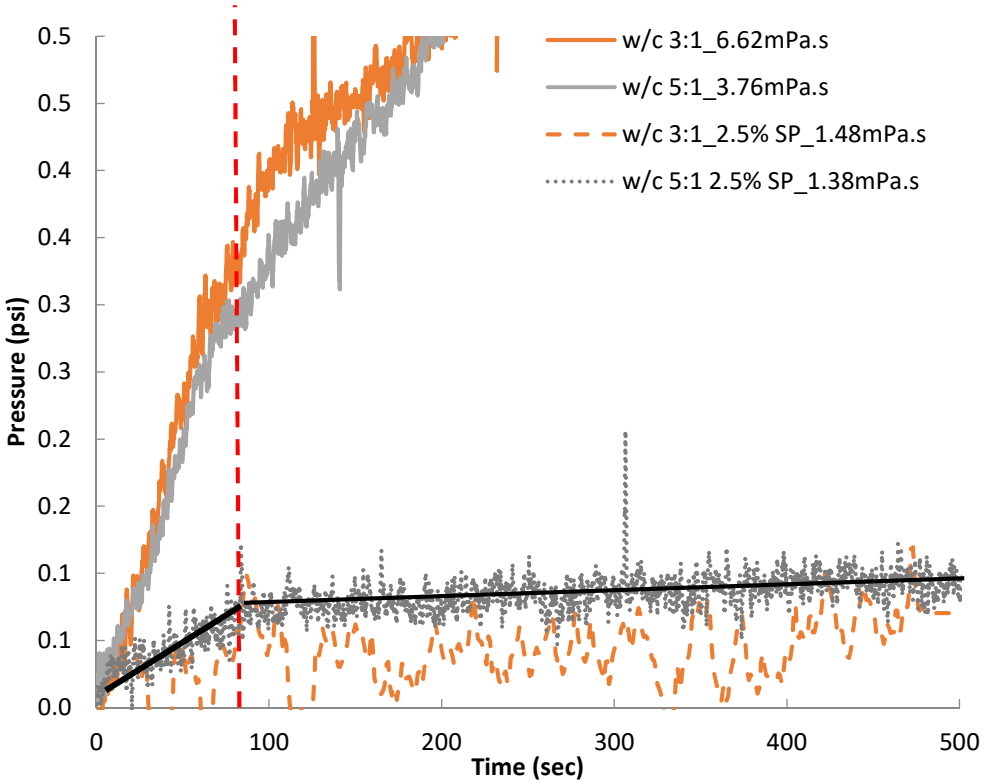

Figure 8-29: Zoomed version of Figure 8-28 to see the pressure buildup of grout with additives.

The initial pore pressure increase due to grout rising in the sand specimen for the injection from bottom to top and it is linear due to constant flux. After the injection of 1 pore volume, slope of pressure-time curve is approximately horizontal, which indicates a limited filtration and almost no change in the permeability of porous media.

8.5.2.2 Effect of filtration on permeability

The temporal variation of absolute permeability of sand specimen was determined from the recorded pressure data using the darcy's law. The change in injection pressure was analyzed in previous section after the injection of large volume of grout through sand specimen. The grout

flowing through sand specimen experience the restricted flow due to particle retention which cause the increase in pore pressure for constant flux injection. The permeability of sand specimen decreases with the number of particles injected.

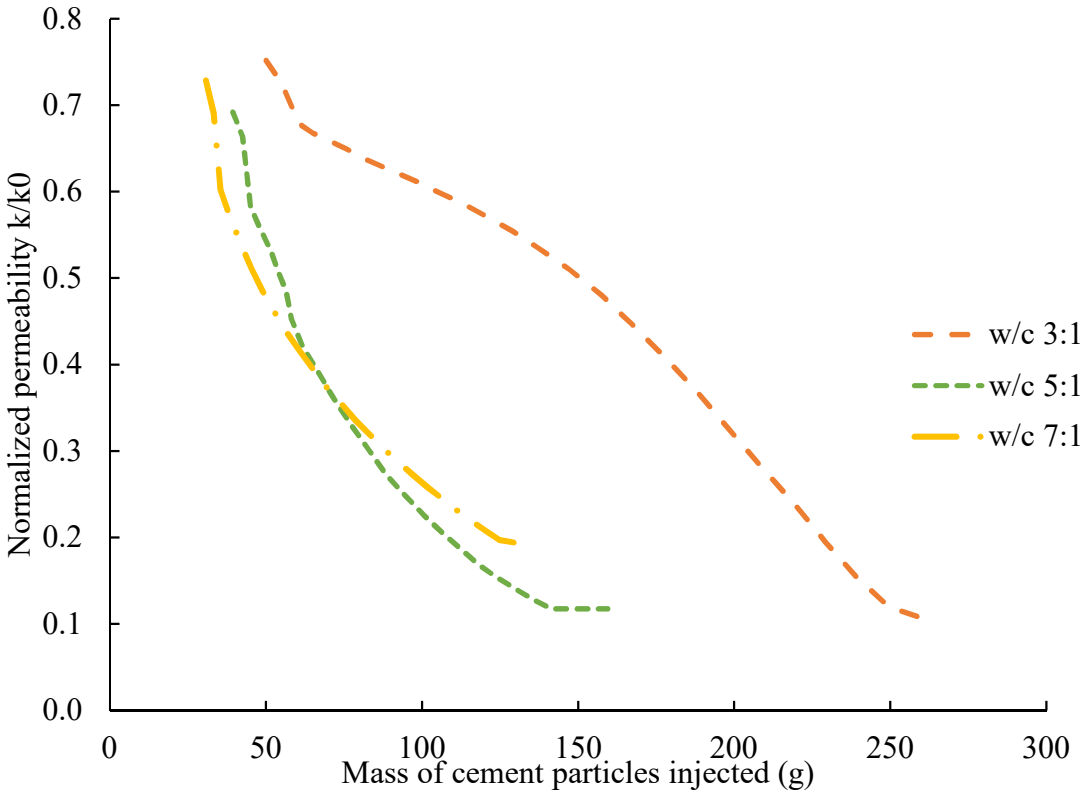

Figure 8-30: Variation in absolute permeability of sand specimen with the mass of cement particles injected

The permeability of sand specimen is normalized with respect to initial permeability. Initial permeability was determined from the pore pressure recorded while flushing it with sand specimen. The reduction in permeability is low for the grout with w/c 3:1 due to less filtration as observed in previous sections as well. The results of effluent concentration and injection pressure are in sync.

The addition of superplasticizer reduces the tendency of cement particles to settle down, Therefore, the reduction in permeability is less than 20% compared to 90% without additives after the injection of 10 pore volume

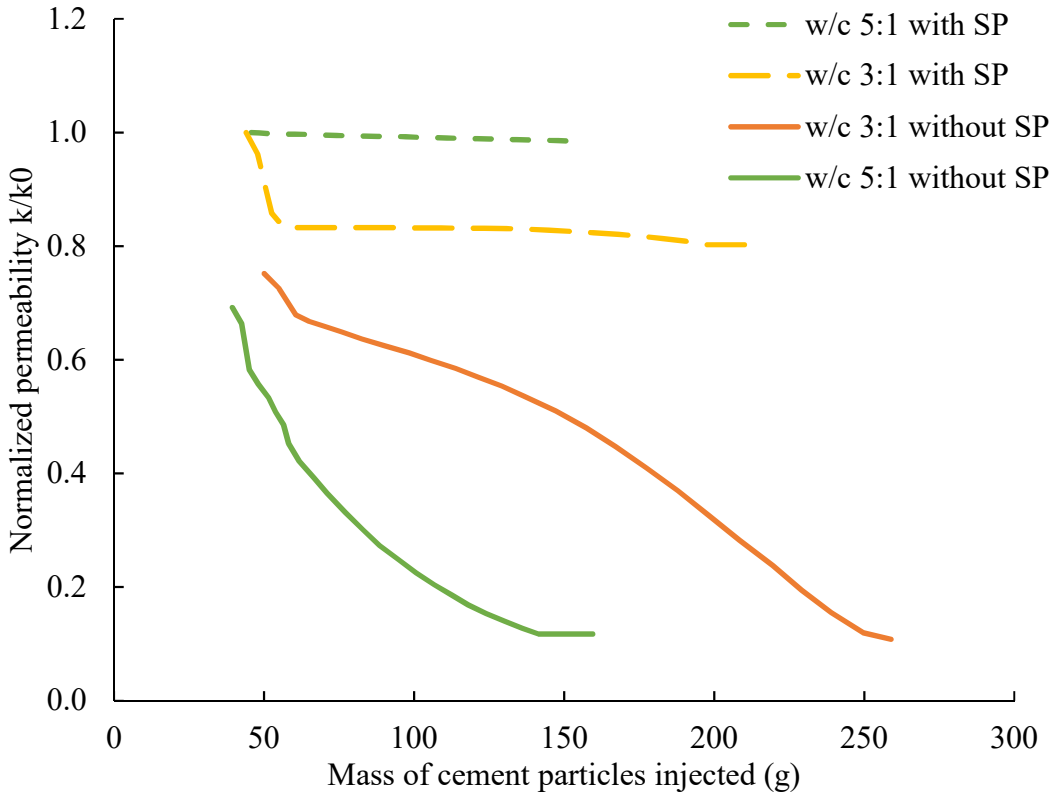

Figure 8-31: Effect of superplasticizer on permeability reduction.

8.5.2.3 Permeability reduction function for cement grout

The most famous permeability- porosity equation is Kozney- Carman equation ((8-16), which is widely used to define the flow through porous media.

$$k = \frac{n^3}{C * (1 - n^2) * S^2} \tag{8-16}$$

The permeability reduction using the Kozney- Carman equation only accounted the change in porosity due to retention whereas Sharma et al. (2000) modified the Kozney-Caman equation and defined the reduction of permeability for water injection wells considering three factors (a) reduced porosity, (b) increased surface area and (c) increased tortuosity.

$$\frac{k}{k_0} = k_{dn} k_{ds} k_{dt} \tag{8-17}$$

where permeability reduction due to reduced porosity of block i at time t = j is

$$k_{dn}(i,j) = \frac{{n_{i,j}}^3 (1 - n_0)^2}{{n_0}^3 (1 - n_{i,j})^2} \tag{8-18}$$

The retained bentonite particles and sand grains are considered as sphere with their entire surface exposed to flow for calculation of reduction in permeability due to increase in surface area

$$k_{ds}(i,j) = \left[\frac{1 + \frac{\sum_{i,0}^{i,j} \sigma_{i,j}}{(1 - n_0)}}{1 + \frac{d_g}{d_p} \frac{\sum_{i,0}^{i,j} \sigma_{i,j}}{(1 - n_0)}} \right]^2 \tag{8-19}$$

where d_g is the size of sand grain, d_p is the size of bentonite particle and σ is the specific deposit.

The reduction in permeability due to tortuosity is

$$k_{dt}(i,j) = \frac{1}{1 + \beta \sum_{i,0}^{i,j} \sigma_{i,j}} \tag{8-20}$$

Where β is damage factor, depends on pore structure.

Saada et al. (2003) and Chupin et al. (2009) modeled the permeability reduction using hyperbolic law for cement grout.

$$k_d(i,j) = \frac{\mathrm{k}_0}{1 + \beta \sum_{i,0}^{i,j} \sigma_{i,j}} \tag{8-21}$$

New permeability reduction function (S-M function) was defined for the bentonite grout in Chapter 7 which is function of reduced porosity and concentration of retained particles.

$$\frac{k(i,j)}{k_0} = k_n(i,j) * k_\sigma(i,j)$$

$$k_n(i,j) = \frac{{n_{i,j}}^3 (1 - n_0)^2}{{n_0}^3 (1 - n_{i,j})^2} \tag{8-22}$$

$$k_\sigma(i,j) = exp(-A * \sum_{i,0}^{i,j} \sigma_{i,j})^B$$

In this section all four empirical relationship (Kozney- Carman, Sharma et al. (2000); Saada et al. (2003) and S-M) are used to evaluate the permeability reduction as function of concentration

of retained particles and determine which of these four permeability reduction function best fit the experimental data ((Figure 8-32). The normalized permeability was plotted against normalized porosity. Permeability decreases wit decrease in porosity but these are not linearly related.

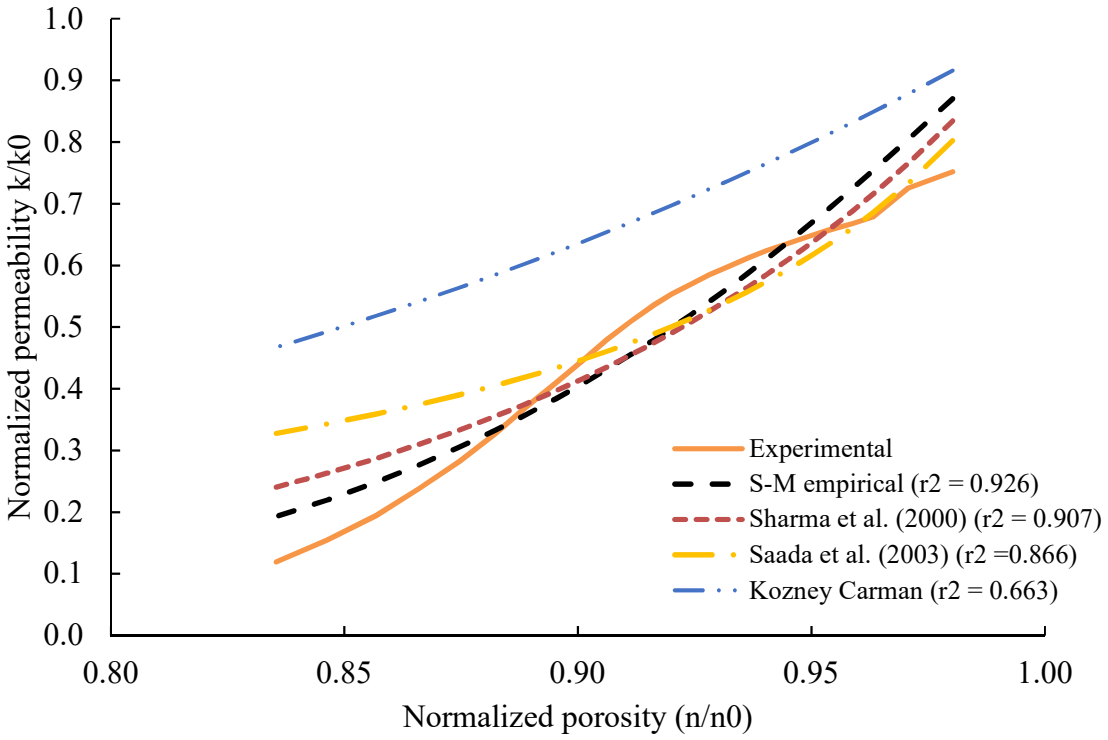

Figure 8-32: Comparison of four different permeability reduction function to best define function for cement grout of w/c 3:1

The permeability due to particle retention is not only the function of change in the porosity. The particle retention also change the tortuosity and specific area which controls the flow in porous media as well. Kozney-Carman equation underestimates the permeability reduction because of filtration. The coefficient of determination for Saada et al. (2003) is 0.866 which indicated that

hyperbolic law is not applicable for the cement grout. This also underestimate the permeability reduction at later stage of filtration when particle started clogging the pore throat and permeability declines at faster rate.

Sharma et al. (2000) captured the permeability reduction due to cement particle retention successfully. The equation predicted the permeability with coefficient of determination (R2) of 0.907. S-M equation developed for bentonite grout also applicable for cement grout. Similar results are observed for cement grout of w/c/ of 5:1

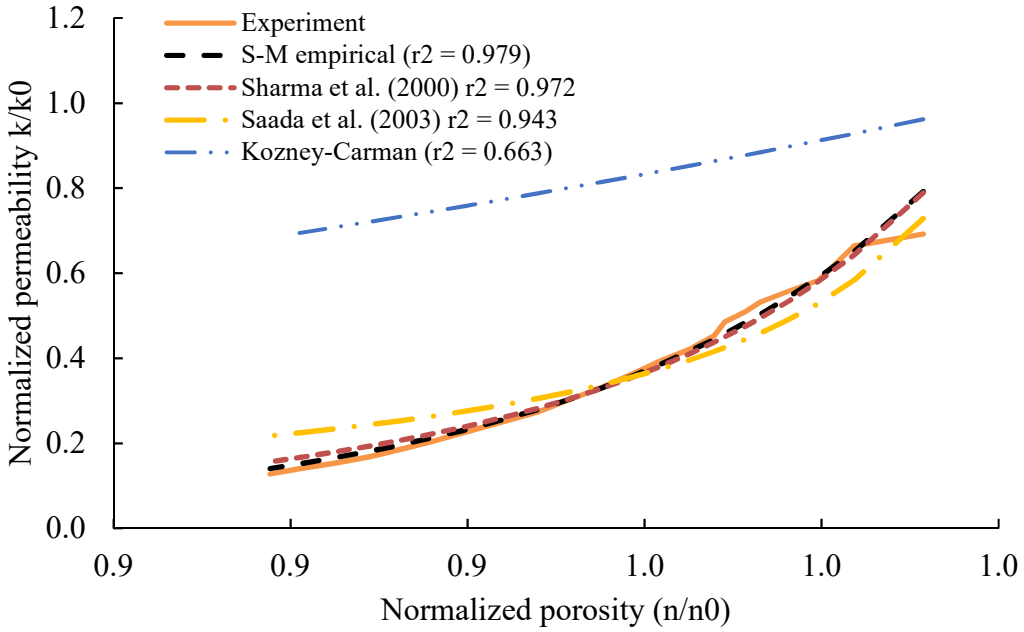

Figure 8-33: Comparison of four different permeability reduction function to best define function for cement grout of w/c 5:1

8.6 Improvisation of Filtration Model

In Chapter 7, filtration model is developed. The Iwasaki (1937) and Ives (1965) filtration and permeability reduction function were modified to best fit the permeation experimental results for bentonite grout. In this section, filtration functions determined in this chapter are used in mathematical modeling to determine if these functions define the bentonite grout permeation. The performance of grouting can be predicted independently with the knowledge of these functions.

8.6.1 Filtration model for bentonite grout

The filtration and permeability reduction function of bentonite grout (Equation (8-3), (8-6) and (8-11)) is used in the numerical filtration model discussed in Chapter 7.

Filtration model gives the better fit to pressure time curve compared to Model 5 (mentioned in Chapter 5). Filtration parameters (λ_0 , b) and permeability reduction parameters (A, B) are determined by fitting the simulated pressure time curves to experimentally measured pore pressure. The simulated pore pressure is close to the measured one with r^2 of 0.99 (Figure 8-34). The model was verified similarly by comparing the predicted bentonite content profile to the measured data. It was found that filtration did better job in capturing the bentonite distribution along the injection length.

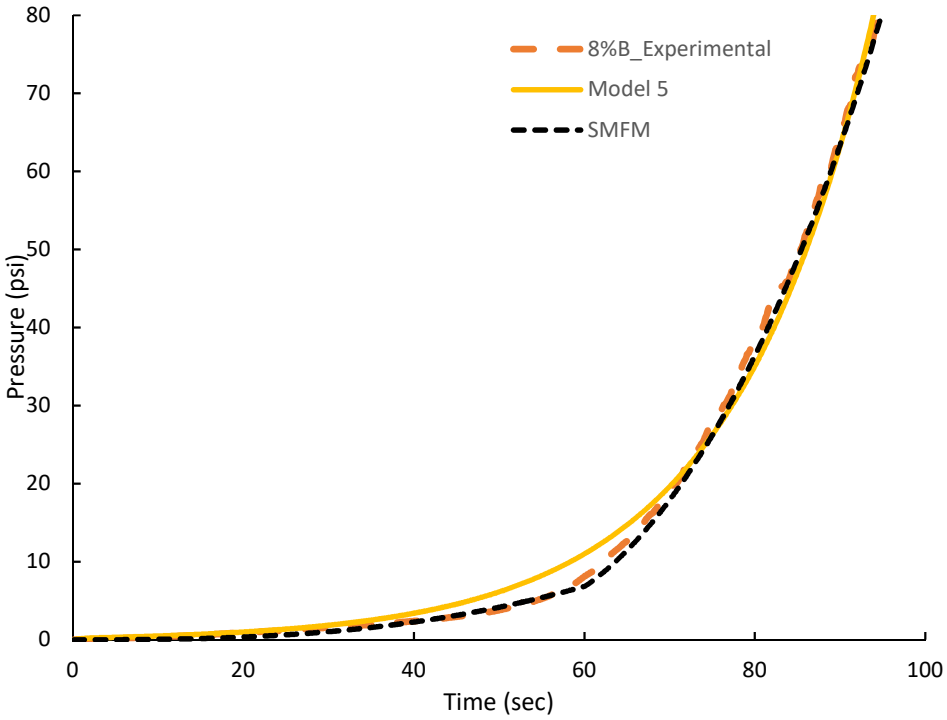

Figure 8-34: Comparison of Model 5 and proposed filtration functions

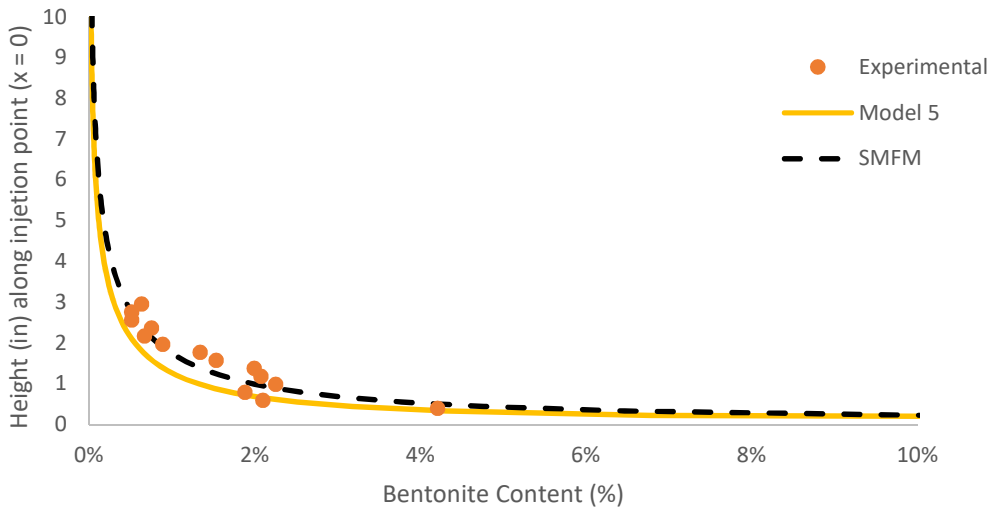

Figure 8-35: Comparison of predicted bentonite content profile using Model 5 filtration function and proposed filtration model to the experimentally measured data

8.6.2 Filtration model for cement grout

In this section, a theoritical model of cement suspension flow in granular porous media considering the particle filtration is presented. The filtration function and intrinsic permeability evolution determined in previous section are used to develop a mathematical model. The equations of this model are solved analytically in the one-dimensional case. It could be implemented easily in situations where no analytical solution is available. Finally, the predictions of the model are compared to the results of a grout injection test on a long column of sand.

The pore pressure at the injection point was predicted using the filtration model and compared with the experimentally recorded pore pressure data. It was found that filtration model with the determined filtration function and permeability reduction function could be used to

simulate the flow of cement grout through granular soils. Simulated pore pressure-time curves closely fit the measured pressure time curve with coefficient of determination (r^2) of 0.971 to 1.00 (Figure 8-36).

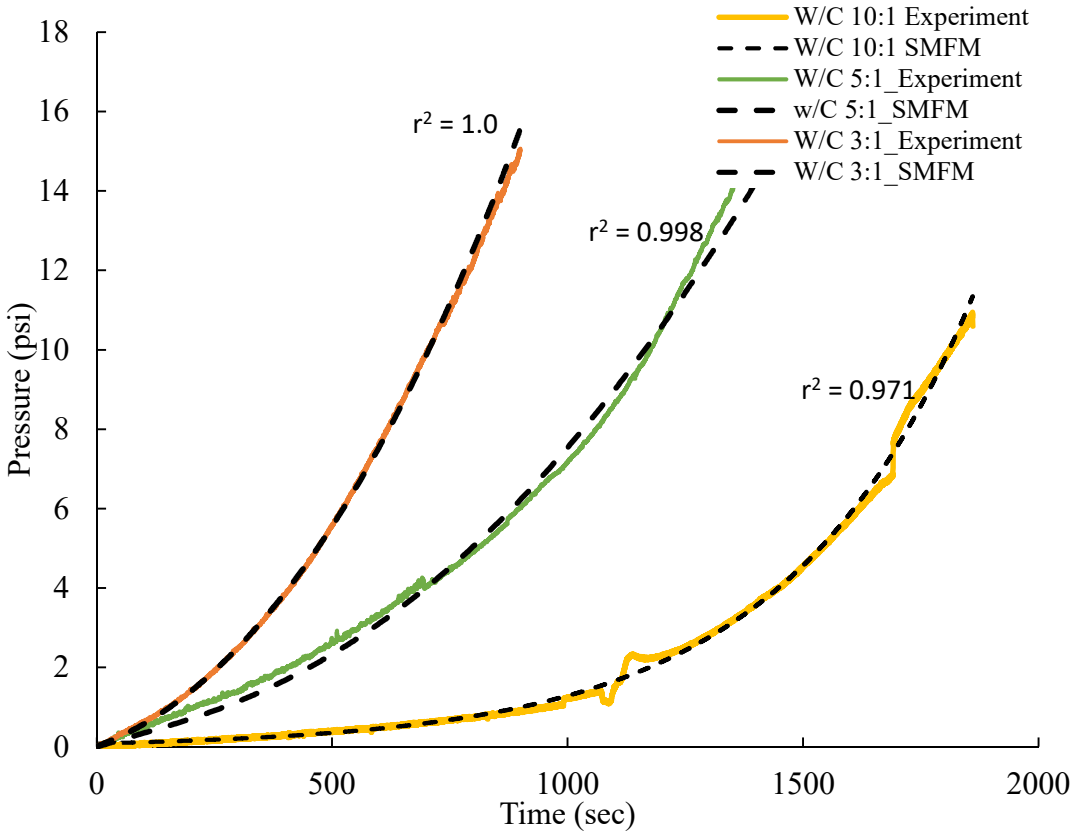

Figure 8-36: Measured (experiment) and predicted (SMFM) pressure time curve

Figure 8-37 shows the reduction in the permeability of sand column section closest to the injection point due to particle retention. It was found that low concentrated grout is unstable and

have tendency of more filtration comparative to stable concentrated grout. The reduction in the permeability of the diluted suspension grout of water cement ratio of 10 is at early stage of grouting which indicates the quick filtration and unstable grout. Similar observation was made from the static sedimentation and filtration test.

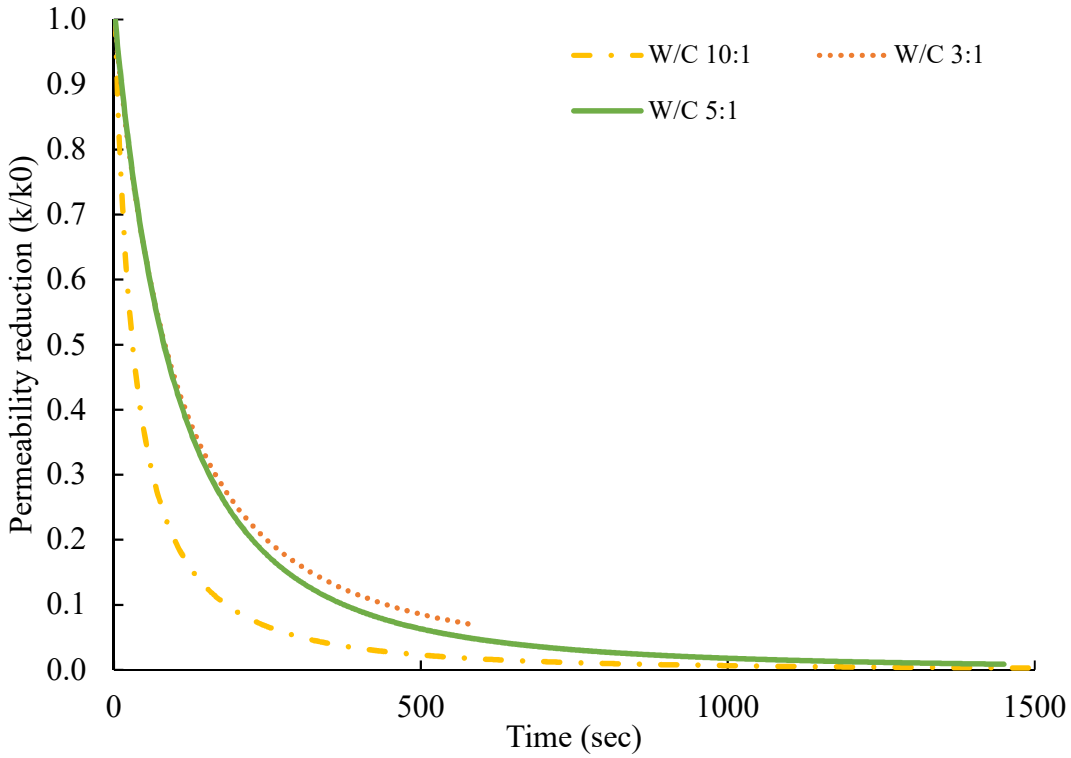

Figure 8-37: permeability reduction due to filtration predicted by filtration model (SMFM)

The amount of cement particle distribution can be determined from the filtration model which could be useful to determine the post grouting performance. The strength of grouted specimen depends on the amount of cement particles. In the previous chapters, it was noticed that unconfined compression strength of the grouted specimen was decreasing along the permeation

depth due to filtration (Figure 8-38). Figure 8-38 shows that the number of particles retained are more at the injection point and the number of cement particles decrease as move away from injection point.

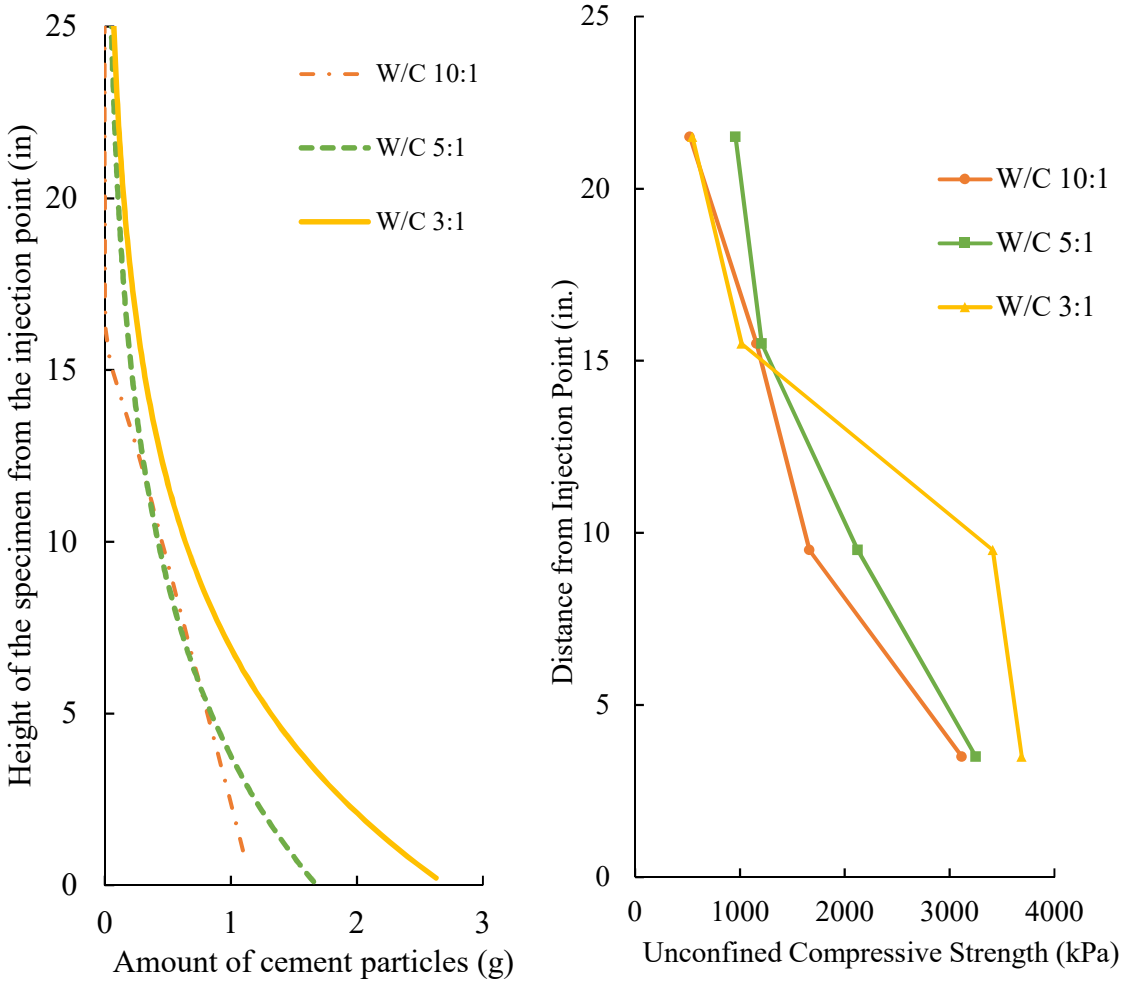

Figure 8-38: The amount of particle retained along the length of sand column

2 ft. long grouted sand column was dissected into four specimens of 6 ft. height and unconfined compression strength was determined for each. The total number of cement particles

in each 6ft. specimen is determined and plotted against the unconfined compression strength to develop a relationship (Figure 8-39)

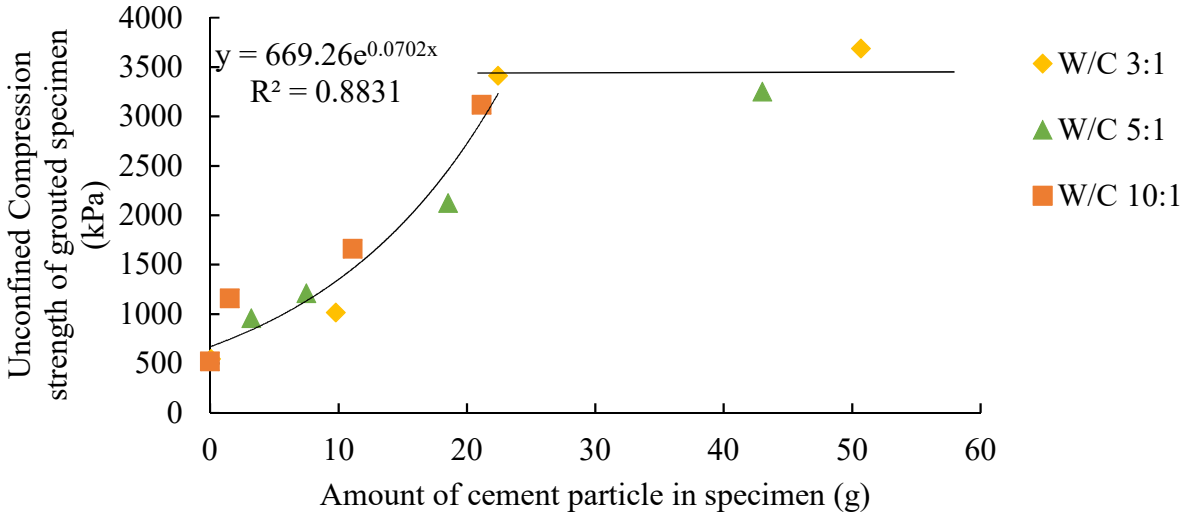

Figure 8-39: The relationship between the unconfined compression strength and amount of cement particles in the grouted specimen

8.7 Conclusion

The one-dimensional filtration tests were conducted on the small sand column specimen to determine the elementary filtration parameters which were used in modeling the flow of suspension grout through porous media. Different concentration grouts were used with and without additive to determine the factors affecting the filtration. Filtration parameters determined in this chapter are (a) filtration coefficient (b) reduced permeability. Filtration coefficient is the probability of particle retention on the grain and it decreases with the increase in the concentration of retained particles. Higher the filtration coefficient, larger the number of particles filtered.

Following are the factors influencing the filtration coefficient:

1. Filtration coefficient decreases with the increase of the concentration of previously retained suspension particles on sand grains.

2. In diluted suspension, the likelihood of particle retention decreases with increase in flow rate due to higher hydrodynamic forces whereas it is vice versa for the concentrated suspensions. Particle retention is more for higher flow rate due to self-filtration.

3. The retention of bentonite particles is faster for the concentrated suspension. Whereas, the concentrated cement grout with low water/cement ratio are more stable and less susceptible to retain on sand grains.

4. The addition of SPP disperse the bentonite particles in suspension and reduce its likelihood to settle down and retain on sand grains because of more Brownian motion. Similarly, addition of super plasticizer stabilizes the cement grout and lead to less filtration.

5. Grout flow is limited through the smaller pore size due to pore clogging. Though the number of retained particles is same for the identical volume of grout injected through Ottawa and Mortar sand, but the resistance to the grout flow is more for Mortar sand due to smaller pore size.

Filtration mechanism can be defined as circular dependency process, where the retention of particles depends on the probability of particle retention i.e filtration coefficient and filtration coefficient depends on the previously retained particles. The empirical equation was developed to

define the dependency of filtration coefficient on previously retained particle. Fitting parameters were determined by fitting the numerical results to the experimental results. The second equation was developed two determine the rate of particle retention as a function of filtration coefficient. Two equations combined are known as filtration function.

The recorded differential pressure across the specimen was used to determine the change in permeability of specimen as a function of reduced porosity and volume of retained particles. The predicted normalized permeability plot against the reduced porosity fitted well with the experimentally measured permeability plot with the coefficient of determination (r^2) of 0.93 to 0.99. Later, the permeability reduction function and the filtration function developed in this study were used in numerical filtration model developed in Chapter 7 and it was found that simulated pore pressure is very close to experimentally measured pressure (r2 = 0.98-0.99) for different concentration grout. Hence numerical filtration model with the proposed filtration parameters could be used to determine the performance of permeation grouting of suspension grout for large scale.

8.8 Appendix of the analysis of filtration test results

In this section, outputs of filtration test are evaluated.

q = Injection Flow rate

A = Cross sectional area of specimen

L = Length of specimen

μ_g = Viscosity of grout

ρ_g= density of grout

μ_w = Viscosity of water

ρ_w= density of water

n_0 = initial porosity of specimen

dt = time step

(a) Preparation of 500 g of grout of bentonite concentration (B) of 8% and sodium pyrophosphate (SPP) of 2%.

Total weight of grout (W_g) = 500g

Weight of bentonite in grout (W_b)= 8% of 500g = 40g

Weight of SPP in grout = 2% of weight of bentonite = 0.02 x 40 g = 0.8 g

Weight of water = (500 – 40 – 0.8) g = 459.2 g

(b) Concentration of Influent

Specific gravity of bentonite (δ_B) = 2.65

Density of grout = $\delta_g = \frac{\delta_B}{B+(1-B)\delta_B} = \frac{2.65}{0.08 \quad (1-0.08)*2.65} = 1.05\ g/cc$

Concentration of influent (C_{in})= $\frac{Weight\ of\ Bentonite\ particle}{Volume\ of\ grout} = \frac{W_B * \delta_g}{Wg} = B * \delta_g$

$$C_{in} = 0.08 * 1.05 = 0.0842\ g/ml$$

(c) Concentration of Effluent

Effluent is collected at intervals of Δt in cans and kept in the oven for 24 hours to determine the weight of bentonite particle (W_{bo}) in effluent.

Concentration of Effluent (C_{eff}) for time Δt $\quad (C_{eff})_t = (\frac{(W_{bo})}{V_g})_t = \frac{W_{bo}}{q*\Delta t}$ g/ml

(d) Volume of retained particles

Bulk factor of bentonite particle in aqueous media = 8ml/g

Hence, the density of hydrated bentonite particle in pore space (δ_{hb}) = 0.125 g/cc

Volume of bentonite particle retained in interval of Δt $(V_D)_t = \frac{W_{bo}}{\delta_{hb}}$

(e) Specific Deposit

Specific deposit (σ) is the volumetric concentration of particles in deposition (Volume of particles retained divided by the total volume of sample (V)

$$\sigma_t = \frac{(V_D)_t}{V}$$

(f) Filtration coefficient

Filtration coefficient was calculated using the experimental results and plotted against the specific deposit to develop the filtration function.

$$\lambda_t = \frac{1}{L}\ln(\frac{C_{in}}{(C_{eff})_t})$$

(g) Change in porosity

Porosity of porous media change with the deposition of particles. New porosity after interval Δt

$$n_{t+1} = n_0 - \sum_{1}^{t} \sigma_t$$

(h) Absolute permeability from pressure data

Injection velocity = $V = \frac{q}{A*n_0}$

Length of specimen grouted in one time step= dx = V*dt

Total time steps to inject one pore volume of grout (M) = $\frac{L}{dx}$

Differential pressure across the specimen for t = N*dt where N<M

$$P_t = \frac{V * Ndx * \mu_g}{k_t * \rho_g * g} + \frac{V * (L - Ndx) * \mu_w}{k_0 * \rho_w * g} + \rho_g * g * Ndx + \rho_w * g * (L - Ndx)$$

Hence the permeability of grouted specimen before the injection of one pore volume of grout

$$k_t = \frac{V * Ndx * \mu_g}{(P_t - \frac{V * (L - Ndx) * \mu_w}{k_0 * \rho_w * g} + \rho_g * g * Ndx + \rho_w * g * (L - Ndx)) * \rho_g * g}$$

Differential pressure across the specimen for t = N*dt where N>M

$$P_t = \frac{V * L * \mu_g}{k_t * \rho_g * g} + \rho_g * g * L$$

Hence the permeability of grouted specimen after the injection of more than one pore volume of grout

$$k_t = \frac{V * \mathrm{L} * \mu_g}{(P_t - \rho_g * g * L) * \rho_g * g}$$

Permeability reduction function was determined using the measured absolute permeability, reduced porosity and volume of retained particles.

CHAPTER 9 CONCLUSION AND FUTURE WORK

9.1 Introduction

The grouting community has mostly consisted of practitioners and grouting success depends on the expertise of the "men in the trenches" rather than design. The main objective of this study is to investigate the flow of suspension grout (bentonite or cement) through the granular soil and to engineer the "smart" grout for site-specific application by balancing its rheological and filtration properties.

This chapter summarizes the key findings from this study. The rheological properties of the modified bentonite and cement suspensions, their permeation through granular soil and mechanism of particle deposition were investigated based on the extensive experimental and numerical studies. Also, two simple, inexpensive and quick methods to determine the unsaturated hydraulic conductivity of sand and to evaluate the homogeneity of sand column prepared in the laboratory were developed.

Based on these findings, this research will make a significant contribution to understanding 1) the rheological properties of suspension grouts with and without additives, 2) the flow behavior of suspension grout through granular soil, 3) the factors affecting the pressure at injection point for constant flux permeation, 4) the mechanism of suspended particle deposition 5) the physical change in pore space and permeability of granular soil due to filtration and its effect on the groutability 6) filtration model to predict the performance of permeation grouting, 7) the simple method to determine the unsaturated hydraulic conductivity of long sand column prepared in laboratory and its homogeneity.

In addition, the following practical contribution will be drawn from this research: 1) developing a site specific engineered grout to maximize the effective grouting 2) developing an empirical correlation for predicting the pressure at injection point to control the hydrofracturing or disturbance to the existing structure during the constant flux permeation grouting, 3) change in rate of suspended particle deposition and pore space due to filtration which controls the grout spread 4) filtration model to better predict the groutability, injection depth and stability of grout, 5) the distribution of suspended particles along the injection length to evaluate the post-grouting stability, 6) the determination of local porosity distribution along the specimen height prepared in the laboratory

9.2 Conclusion

The research focused on 1) the determination of unsaturated hydraulic conductivity of sand and the evaluation of homogeneity of prepared sand column in laboratory, 2) measuring the rheological properties of the various engineered suspension grout over time, 3) investigating the parameters affecting the flow of the bentonite/cement suspensions through granular soils, 4) determining the filtration and permeability reduction function to model the numerical model for prediction of injection depth. Based on the extensive laboratory and numerical studies, the following conclusions were drawn:

(1) A simple method is proposed to determine the unsaturated hydraulic properties of sandy soil using a combination of experimental testing and inverse numerical modeling. An unsaturated sandy soil specimen is subjected to a multistage constant flux flushing while recording pressure buildup at the base of the specimen. The experimental protocol is then simulated using Hydrus 1D, and the unsaturated hydraulic parameters were estimated using two optimization

techniques (Levenberg-Marquardt and Shuffled complex evolution). Predicted van Genuchten parameters are in the reasonable range of parameters obtained using the conventional hanging column test. The spatial and temporal changes in volumetric moisture contents have been achieved by combining the Hydrus 1D modeling with pressure measurements at the base of the sand column, without the need to install additional sensors along the height of the specimen. Despite the simplicity of the experimental testing procedure for the SEM method, it allows for testing properties of materials with very low suction, which wouldn't have been possible with the hanging column test procedure.

(2) A non-invasive, simple and quick RPR method is developed to determine the local porosity distribution of the laboratory prepared specimen. Dry pluvial soil column flushed with water from bottom to top at constant flux and pressure was recorded at the injection point. The theory behind this paper is that the increase in pressure and seepage velocity is the function of pore space through which water is flowing. RPR method is based on Darcy's law and Kozney Carman equation. The relative standard deviation was used to define the deviation of pore space within the specimen from the average value and found to be approximately 6-8%. The average local porosity of the assembled specimen was measured lower than the mean porosity determined by the conventional W-H method which was expected due to the disturbance caused in preparing the subsequent layers. The advantage of RPR method is to identify the local porosity distribution of the similar specimen which can be used future for any geotechnical experiments.

(3) The addition of a small amount of sodium pyrophosphate (SPP) was found to significantly reduce the yield stress and apparent viscosity of bentonite suspensions. However, this

reduction tends to converge after the threshold percentage of (SPP). It was concluded that small percentage of SPP (1-4%) are effective to improve the mobility of bentonite suspension grout effectively.

(4) The reduced yield stress and apparent viscosity of bentonite suspension gradually recover with time. The concentrated specimen produces a lower degree of increase in the yield stress (low thixotropic ratio) and apparent viscosity comparative to the diluted suspension. Similarly, the suspension with a significant percentage of SPP has a high thixotropic ratio. The concentrated suspension has already the constrained Brownian motion, so there is less scope of gaining yield stress and apparent viscosity. The addition of SPP reduced the inter-aggregate bonds (3-D network) and showed a high degree of Brownian motion. Therefore, the concentrated suspensions with SPP show higher thixotropic ratio compared to unmodified bentonite suspensions.

(5) Cement grout was found as shear thinning material; the apparent viscosity decreases with increase in shear rate. The viscosity of grout is inversely proportional to the water/cement ratio. Superplasticizer stabilizes the grout by dispersing the cement particles i.e. particles that have joined to form agglomerates are separated and decreases the apparent viscosity. Stability of grout was determined using the sedimentation tests. The addition of superplasticizer and 1% bentonite by weight reduce the cement particle sedimentation hence increase the stability of grout.

(6) One dimensional permeation tests were performed to determine the factors (rheology and filtration parameters) affecting the permeation grouting. 2 ft long column are permeated with various bentonite concentration (modified and unmodified) from the base of the column at

constant flux rate and pore pressure was recorded at the injection point with time. The grouted specimen was left for few days to let the grout recover its strength and then bentonite content distribution was determined along the specimen height.

Following conclusions are made from permeation tests of bentonite suspension grout:

- The pore pressure at the injection point is a good indicator of the permeation depth and filtration. The increase in pore pressure should be linear with time if there is no filtration. Whereas in the case of bentonite suspension permeation; the increase in pore pressure was not linear, it increases non-linearly at a slow rate in the beginning and then increases exponentially because of change in pore space and grout rheology due to filtration.

- The addition of SPP improves the permeation depth. The suspension grout with low apparent viscosity tends to go deeper in sand column.

- The penetration depth of grout with same apparent viscosity depends on the concentration of grout. Bentonite particles of concentrated grout have higher tendency to retain on sand grains due to less hydrodynamic forces.

- Bentonite particles of grout permeated at higher flow rate have a tendency to intersect the grain boundaries and collect on sand grains and more filtration, which leads to less penetration depth.

- Three types of sand of different grain size distribution were used to determine the effect of Normalized effective grain size (D_{10}/d_{95}) on filtration and permeation depth. Larger the (D_{10}/d_{95}), deeper the penetration depth.

- Constant flux permeation results were compared with constant pressure permeation tests mentioned in Mohtar et al. (2015). Penetration length is more for grout injecting at constant flux for the same bentonite grout and granular soil. The difference in penetration length is more significant for larger water to bentonite ratio (W/B).

- The empirical formula is developed to determine the pressure- time curve for constant flux bentonite permeation grouting as a function of the rheology of grout (apparent equilibrium viscosity), the particle size of soil and bentonite particle and flow rate. This empirical equation can be used in industries to anticipate the pressure buildup while injection and volume of grout needed to inject before reaching the pressure limit.

Following conclusions are made from permeation tests of cement suspension grout:

- Microfine cement was used for this study, and the pressure-time curves were used to analyze their groutability.

- The permeation test results conclude that there are various factors like size of hydrated cement particle, rheology of grout and stability of grout affect the permeation grouting

- The unconfined compression test determines the strength of grouted samples. After three days of setting. 2 ft grouted sand column was dissected into four sections. The strength data shows the non-uniform permeation of grout. The strength of section closer

to injection point is higher than those further due to filtration. Cement grout with superplasticizer gives uniform unconfined compression strength throughout the sand column indicates no filtration. Whereas strength of sections permeated with cement–bentonite grout decreases as going away from the injection point. It is found that addition of 1%bentonite to cement grout has reduced the filtration, but because of increase in viscosity, there was an increase in pressure build up and decrease in permeation depth.

(7) A simple experimental test was developed to investigate the factors affecting the filtration of bentonite particles. The mechanism of particle retention during the grouting process was studied by observing the concentration of effluent. Filtration coefficient is the probability of particle retention on the grain, and it decreases with the increase in the concentration of retained particles. Higher the filtration coefficient, larger the number of particles filtered.

Following are the factors influencing the filtration coefficient for bentonite suspension grout:

- In diluted suspension, the likelihood of particle retention decrease with increase in flow rate due to higher hydrodynamic forces whereas it is vice versa for the concentrated suspensions. Particle retention is more for higher flow rate due to self-filtration.

- An increase in concentration led to faster retention of bentonite particles.

- The addition of SPP disperse the bentonite particles in suspension and reduce its likelihood to settle down and retain on sand grains.

- The smaller pore size limits grout flow due to pore clogging. Though the number of retained particles is same for the equal volume of grout injected through Ottawa and Mortar sand.

Following are the results of filtration test for cement suspension grout:

- Low concentrated cement suspensions are unstable, and particles got segregated easily and retained on sand grain. Whereas, the high concentrated cement grout of water/cement ratio of 3 are more stable and showed less filtration.

- The addition of superplasticizer reduced the tendency of particle retention on sand grain, similar as observed in static sedimentation test.

- Similar as bentonite suspension, the filtration coefficient decreases with increase in the concentration of previously retained particles. Cement particles deposit over pore bodies and pore throats due to mechanical and physicochemical interactions. Particle retention starts decreasing since the cement particle covers the sand particle due to particle- particle repulsion forces.

- The filtration coefficient of concentration cement grout (w/c 3:1) is low comparative to diluted cement grout (w/c 7:1). The addition of superplasticizer decreases the filtration coefficient. Effect of superplasticizer is more significant for the concentrated grout.

8) Filtration mechanism can be defined as circular dependency process, where the retention of particles depends on the probability of particle retention, i.e., filtration coefficient and filtration coefficient depends on the previously retained particles. The empirical equation was developed

to define the dependency of filtration coefficient on the previously retained particle. Fitting parameters were determined by fitting the numerical results to the experimental data. The second equation was developed to determine the rate of particle retention as a function of filtration coefficient. Two equations combined are known as filtration function.

9) The recorded differential pressure across the specimen was used to determine the change in permeability of specimen as a function of reduced porosity and volume of retained particles. A simple function named as S-M permeability reduction function was developed for bentonite suspension. Whereas, Sharma et al. (2000) permeability reduction function were found suitable for cement grout.

10) The permeability reduction and the filtration coefficient empirical function determined in this study were used to develop the filtration model to simulate the flow of suspension grout through the granular soil. The novelty of the filtration model is that it accounts for the change in rheology of grout and the porosity and permeability of the porous medium as a function of the retention of particles. The proposed filtration model was compared with other seven other filtration model using different filtration coefficient relationship and permeability reduction function. The simulated and experimentally measures pore pressure at the injection point are in great agreement with the r^2 value of 0.99 for both bentonite and cement suspension. Fitting filtration parameters and formation damage parameters are determined using by fitting the simulated pore pressure to the experimental pore pressure. Bentonite content profile along the height of the sand column determined numerically using the proposed filtration model was similar to that obtained from the experimental results from the post-permeation analysis. This model can simulate the flow of suspension grout through porous media by balancing the

rheology and filtration properties. This model is developed for 1 D injection application hence valid for the permeation grouting in confined area.

9.3 Future scope

This dissertation showed the possibility to predict the flow of suspension grout through granular soil considering the spatial and temporal variation in grout rheology and pore space of soil due to particle retention during the grouting. Permeability depth and the distribution of grout along the injection length can be predicted to evaluate the performance of permeation grouting. The proposed model applies to design the "smart" engineered grout for known site conditions.

Filtration and permeability reduction function are defined as an empirically to explain the mechanics of filtration mathematically. The empirical relationships have the fitting parameters (filtration parameter and formation damage parameter) which are determined by the inverse technique. The dependency of filtration and formation damage parameters on the known grout and porous media property is not studied in this dissertation and recommended for future research work. The proposed filtration model will be capable of predicting the groutability and selecting the suitable grout for the known site condition.

The permeation tests and the numerical solution proposed in this study are for one-dimensional injection. The propagation of one-dimensional flow can be correlated to the 3-dimensional flow which is assimilated to field condition. In the field, Tube-a-Manchette is used as injection method, and the grout propagation from a point source is typically modeled as spherical or ellipsoidal. 3D projection of proposed filtration model is possible by converting the volume of grout injected in the radius of grouted field, which is not studied in this dissertation and is

recommended to study further in future. This research could help in designing the grouting process by determining the spacing between injection point.

This work was focused on laboratory tests (small scale), the full-scale grout propagation could not be captured in this study. Hence, large-scale tests are recommended to actual field application for a) the effect of heterogeneity in the field on the preferential grout propagation b) determination of the spacing of the injection point.

REFERENCES

Bedrikovetsky, P.G., Marchesin, D., Shecaira, F., Serra, A.L., Resende, E. (2001), "Characterization of deep bed filtration system from laboratory pressure drop measurements," J. Petrol. Sci. Eng. **64**(3), 167–177.

Abend, S. and Lagaly, G. (2000), "Sol-gel transitions of bentonite dispersions," Applied Clay Science, 16, 201-227.

Abichou, T., Benson, C.H., and Edil, T. B. (2002), "Micro-Structure and Hydraulic Conductivity of Simulated Sand-Bentonite Mixtures" Clays and Clay Minerals, Vol. 50, No. 5, 537–545.

Abrams, A. (1977), "Mud design to minimize rock impairment due to particle invasion," J. Pet. Technol. 29(May), 586–592

Aitchison,G.D; and Richards, B.G. (1965) Abroad-scale study of moisture conditions in pavement subgrades throughout Australia. In: Moisture in soils beneath covered areas. Butterworths, Australia, pp 198– 204

Al-Abduwani, F.A.H. (2005), "Investigation into the injectivity decline due to produced water re-injection under fracturing conditions," Ph.D. Thesis, TU Delft, Netherlands

Al-Abduwani, F.A.H., Farajzadeh, R., Van den Broek,W.M.G.T., and Currie, P.K. (2004),"Utilizing static filtration experiments to test existing filtration theories for conformance," In: Second Produced Water Workshop. Aberdeen, UK

Amin, M.H.G., Hall, L.D., Chorley, R.J. and Richards, K.S. (1998), "Infiltration into soils, with particular reference to its visualization and measurement by magnetic resonance imaging (MRI)," Progress in Physical Geography, 22, 135-165.

Amirtharajah, A. (1988). ''Some theoretical and conceptual views of filtration.'' J. Am. Water Works Assn., (December), 36–46.

Anderson, B. Roskrow The channel tunnel story CRC Press, Boca Raton, FL (2003)

Anderson, S.H., Peyton, R.L. and Gantzer, C.J. (1990), "Evaluation of constructed and natural soil macropores using X-ray computed tomography," Geoderma, 46:13-29.

Ayoubian, A. and Robertson, P. K. (1998), "Void ratio redistribution in undrained triaxial extension tests on Ottawa sand," Canadian Geotechnical Journal, Vol. 35, pp. 351-359

Baghdlklan, S. Y., Sharma, M. M., and Handy, L. L. (1989). ''Flow of clay suspensions through porous media.'' SPE Reservoir Engrg., (May), 213–220.

Barkman, J.H., Davidson, D.H. (1972), "Measuring water quality and predicting well impairment," J. Pet. Technol. **24** (July), 865–873.

Bedrikovetsky, P.G., Tran, K., Broek, W.M.G.T. Van den, Marchesin, D., Rezende, E., Siqueira, A., Serra, A.L., Shecaira, F. (2003), "Damage characterization of deep bed filtration from pressure measurements," J. SPE PF **3**, 119–128

Bell, F.G., (1993). Engineering Treatment of Soils. E&FN Spon, London.

Benson, C.H. and Bosscher, P.J. (1999) Time-domain reflectometry (TDR) in geotechnics: a review, nondestructive and automated testing for soil and rock properties. ASTM SPT 1350(Eds. W.A. Marrand C.E. Fairhurst), ASTM, West Conshohochen,PA.

Berggren, L. The Oslofjord subsea tunnel, a case record Proceedings of the International Symposium on Ground Freezing and Frost Action in Soils, A.A. Balkema, Louvain-La-Neuve, Belgium (2000), pp. 267–272

Berryman, J. G., and Blair, S. C. (1986), "Use of Digital Image Analysis to Estimate Fluid Permeability of Porous Material: Application of Two-Point Correlation Functions," Journal of Applied Physics, Vol. 60, No.6, pp. 1930-1938.

Bhatia, S. K., and Soliman, A. E. (1990), "Frequency Distribution of Void Ratio of Granular Material Determined by an Image Analyzer," Soils and Foundations, Vol. 30, No. 1, pp. 1-16.

Bohne, K., Nitsche, C., and Leij, Feike J. (1992). "Requirement and use of indirect method for estimation the hydraulic functions of unsaturated soils." Proc. Int. Workshop, Indirect methods for estimating in hydraulic properties of unsaturated soils: 359-368.

Bremen, R. (1997). The use of additives in cement grouts. The Int. J. Hydropower Dams 4: 71–76.

Burwell E.B., (1958), “Cement, clay grouting of foundations: Practice of the corps of engineering,” J. Soil Mech. Foundation Div., ASCE 84, 1551/1-1551/22.

Cardiff, M., W. Barrash, P. K. Kitanidis, B. Malama, A. Revil, S. Straface, and E. Rizzo (2009). "A potential-based inversion of unconfined steadystate hydraulic tomography." Ground Water **47(2)**( ): 259-270.

Chauveteau G., Nabzar L. and Coste J.P. (1998), “Physics and modeling of permeability damage induced by particle deposition” SPE 39463, International Symposium on Formation Damage Control, Lafayette, Louisiana, USA, February 18-19.

Chiu, T.-F., Shackelford, C.D. (1998). " Unsaturated hydraulic conductivity of compacted sandkaolin mixtures." Journal of Geotechnical and Geoenvironmental Engineering 120(2): 160-170.

Cho, G.C., Lee, J.S., Santamarina, J.C. (2004), “Spatial variability in soils: high-resolution assessment with electrical need probe,” J. Geotech. & Geoenvir. Engrg., ASCE, 130(8), 843-850.

Christodoulou, D. N., Markou, I. N., & Papadopoulos, B. K. (2014). Penetrability of microfine cement grouts: Experimental investigation and fuzzy regression modeling.Canadian Geotechnical Journal, 52(7), 868-882. doi:10.1139/cgj-2013-0297

Clarke, J.P. (2008), “Investigation of time-dependent rheological behavior of sodium pyrophosphate–bentonite suspensions,” Thesis, Purdue University, West Lafayette, IN

Cui YJ, T. A., Loiseau C, Delage P. (2008). "Determining the unsaturated hydraulic conductivity of a compacted sand-bentonite mixture under constant-volume and free-swell conditions." Physics and Chemistry of the Earth Parts A/B/C 33: S462-S471.

Dane, J. H., and Hruska, S. (1983). "In situ determination of soil hydraulic properties during drainage." Soil Sci. Soc. Am. J. **47**: 619-624.

Davidson, D.H. (1979), “Invasion and impairment of formations by particles,” In :54th Annual Fall Technical Conference and Exhibition, 23–26 September, Paper SPE 8210. Society of Petroleum Engineers, Las Vegas

Dong, X., and Wang, Y. H. (2005), “EM-Wave based Characterizations of Local Void Ratios in Soils,” GSP 138 Site Characterization and Modeling, Geo-Frontiers Congress 2005, Austin, pp. 1-8.

Duan, Q., Sorooshian, S., and Gupta, V. (1992). "Effective and Efficient Global Optimization for Conceptual Rainfall-Runoff Models " Water Resour. Res. 28(4)(April): 1015-1031.

Dullien, F.A.L. (1982), “Porous Media. Fluid Transport and Pore Structure,” Academic Press, San Diego.

Dupla, J. C., Canou, J. and Gouvenot, D. (2004), “An advanced experimental set-up for studying a monodirectional grout injection process” Ground Improvement, 8, No. 3,91-99.

Durner, W. (1992). "Predicting the unsaturated hydraulic conductivity using multi-porosity water retention curves." In: van Genuchten, M. Th., F. J. Leij, and L. J. Lund (eds.), Proc. Int. Workshop, Indirect Methods for Estimating the Hydraulic Properties of Unsaturated Soils: 185-201.

Durner, W., Schultze, B. Zurmuhl, T. (1999). "State-of-the-art in Inverse modeling of Inflow/Outflow Experiments." Proc. Int. Workshop on Characterization and Measurement of the Hydraulic Properties of Unsaturated Porous Media

Eching, S. O., and Hopmans, J. W. (1993). "Optimizaion of Hydraulic Functions from Transient outflow and Soil water pressure Data." Soil Sci. Soc. Am. J. **57**: 1167-1175.

El Mohtar, C. S., Bobet, A., Santagata, M.C., Drnevich, V.P., Johnston C. (2013) “Liquefaction Mitigation using Bentonite Suspensions,” Journal of Geotechnical and Geoenvironmental Engineering, ASCE, Vol. 139, No. 8, p.p. 1369–1380, 2013.

El Mohtar, C.S., Clarke, C., Bobet, A., Santagata, M., Drnevich, V., and Johnston, C. (2008) "Cyclic Response of Sand with Thixotropic Pore Fluid," ASCE Geotechnical Special Publication GSP-181: Geotechnical Earthquake Engineering and Soil Dynamics Conference IV, GEESD IV, May 18-22, 2008.

Elimelech, G., Gregory, J., Jia, X.,Williams, R.A, (1995), “Particle Deposition and Aggregation,” Butterworth-Heinemann, USA

Eriksson, M., Stille, H., and Andersson, J.(2000), “Numerical calculations for Prediction of grout spread with account for Filtration and varying aperture”, Tunneling and Underground Space Technology, Vol. 15, No. 4, pp 353-364, 2000.

Eylander, J.G.R. (1988), “Suspended solids specifications for water injection from coreflood tests,” SPE Reserv. Eng.(December), 1287–1300

Frost, J. D. & Jang, D. (2000). “Evolution of sand microstructure during shear.” J. Geotech. & Geoenvir. Engrg., ASCE, 126(2), 116-130.

Gardner, W. R. (1958). "Some steady-state solutions of the unsaturated moisture flow equation with application to evaporation from a water table." Soil Sci. **85**: 228-232.

Ghanbarian-Alavijeh, B., Liaghat, A., Guan-Hua, H., and Van Genuchten, M.Th. (2010). "Estimation of the van Genuchten soil water retention properties from Soil Textural Data." Pedosphere **20(4)**: 456-465.

Ghidaglia C, De Arcangelis L, Hinch J, Guazzelli E. Transition in particle capture in deep bed filtration. PhysicalReview 1996; 53(4):R3028–R3031.

Goh, R., Leong, Y.K., and Lehane, B. (2011), “Bentonite slurries—zeta potential, yield stress, adsorbed additive and time-dependent behavior,” Rheologica Acta (2011) 50:29–38 DOI 10.1007/s00397-010-0498-x

Grabe, J., Henke, S., Kinzler, S. and Pucker, T. (2010), “ Inverse determination of soil density and stress state using dispersion wave measurements and cone penetration tests in a non-layered soil,” Soil Dynamics and Earthquake Engineering 30(6):481-489

Haines, W. B., (1930), “The Hysteresis Effect in Capillary Properties and the Modes of Moisture Distribution Associated Therewith,” J. Agric. Sci., Vol. 20, pp. 97–116.

Håkansson, U., Hässler, L., & Stille, H. (1992). Rheological properties of microfine cement grouts. Tunnelling and Underground Space Technology Incorporating Trenchless Technology Research, 7(4), 453-458. doi:10.1016/0886-7798(92)90076-T

Haug, M.D., and Wong, L.C. (1992), “Impact of molding water content on hydraulic conductivity of compacted sand bentonite,” Canadian Geotechnical Journal, 29(2): 253–262. doi:10.1139/t92-029.

Hedberg, S. A., Knight, R.J., MacKay, A. L., and Whittall, K. P. (1993), "The use of nuclear magnetic resonance for studying and detecting hydrocarbon contaminants in porous rocks," Water Resour. Res., 29(4), 1163–1170, doi:10.1029/92WR02540

Heertjes, P.M., and Lerk, C. F. (1967), "The functioning of deep bed filters," Trans. Inst. Chem, Eng., 45, 129-145

Henn, R. W., & Soule, N. C. (2010). Ultrafine cement in pressure grouting. Reston, Va: American Society of Civil Engineers.

Herzig, J. P., Leclerc, D.M. and Goff, P. Le., (1970), "Flow of Suspension through Porous media," Flow through porous media symposium VOL 62 NO. 5, 9-35.

Hjelmås, T.A., Bakke, S., Hilde, T. Vik, E.A. and Grüner, H. (1996), "Produced Water Re-Injection: Experiences from Performance Measurements on Ula in the North Sea," SPE 35874, presented at the International Conference on Health, Safety and the Environment, New Orleans, Louisiana, 9-12 June.

Ibrahim, A. A., and Kagawa, T. (1991), "Microscopic Measurement of Sand Fabric from Cyclic Tests Causing Liquefaction," Geotechnical Testing Journal, Vol. 14, No. 4, pp. 371-382.

Incecik, M., Ceran, I., (1995). Cement grouting model tests. Bulletin of The Istanbul Technical University of Istanbul, 48, 305-317.

Ives, 1987, "Filtration of clay suspensions through sand," Clay Minerals, 22, pp 49-61.

Ives, K.J., and Pienvichitr, V. (1965), "Kinetics of the filtration of dilute suspensions",Chem. Eng. Sci., 20, 965-973.

Iwasaki, T. (1937), "Some notes on sand filtration", J.Am.Water Works Ass., 29 (10), 1591-1602.

Kuo, C.Y. and Frost, J.D., (1996), "Uniformity evaluation of cohesionless specimens using digital image analysis," Journal of Geotechnical Engineering, 122(5), pp 390-396.

Ladd, R. S. (1974), "Specimen Preparation and Liquefaction of Sands, "Journal of Geotechnical Engineering, ASCE, Vol. 100, No. GT 10, pp. 1180-1184.

Lee J, and Koplik J. (2001), “Network model for deep bed filtration,” Physics of Fluids 2001; 13(5):1076–1086.

Lee, K. M., Shen, C. K., Leung, H. K. & Mitchell, J. K. (1999), “Effects of placement method on the geotechnical behavior of hydraulic fill sands,” J. Geotech. & Geoenvir. Engrg., ASCE, 125(10), 832-846.

Likos, W. J., and Yao, Jun (2014). "Effects of constraints on van Genuchten parameters for modeling Soil-Wate Characteristic Curves." Journal of Geotechnical and Geoenvironmental Engineering.

Liu, J., and Neretnieks, I., 2006, “Physical and chemical stability of the bentonite buffer,” SKB Rapport R-06-103, ISSN 1402-3091.

Liu, S., T.-C. J. Yeh, and R. Gardiner (2002). " Effectiveness of hydraulic tomography: Sandbox experiments." Water Resour. Res. **38(4)**: 1034.

Liu, X., W A. Illman, A. J. Craig, J. Zhu, and T.-J. Yeh (2007). " Laboratory sandbox validation of transient hydraulic tomography." Water Resour. Res. **43**.

Logan, J.D. (2001), “Transport Modeling in Hydrogeochemical Systems,” Springer

Mackie RI. Rapid gravity filtration towards a deeper understanding. Filtration and Separation 1989; 26:32–35.

Maghous, S., Saada, Z., Canou, L., Dormieux, L., and Dupla, J.C., (2007), “A model for in situ grouting with account for particle filtration” Computers and Geotechnics, 34, 164-174.

Marquardt, D. W. (1963). "An Algorithm for least-squares estimation of nonlinear parameters." SIAM J. Appl. Math. **11**: 431-441.

McDowell-Boyer, L.M., Hunt, J.R., Sitar, N. (1986), “Particle transport through porous media” Water Resour. Res. **22**(13), 1901–1921

Mitchell, J.K. (1981), “Soil Improvement State-of-the-Art,” In: Proceedings of the 10th International Conference of Soil Mechanics and Foundation Engineering, ICSMFE, Vol. 4, pp 509-565.

Moghdasi, J., Jamialahmadi, M., Muller-Steinhagen, H., Sharif, A., Izadpanah, M.R. (2002), "Formation damage in Iranian oil fields," In: SPE International Symposium and Exhibition on FormationDamage Control. 20–21 February, Paper SPE 73781. Society of Petroleum Engineers, Lafayette, Louisiana

Moghdasi, J., Muller-Steinhagen, H., Jamialahmadi, M., and Sharif, A.(2004), "Theoretical and experimental study of particle movement and deposition in porous media during water injection," J. Petrol. Sci. Eng. **43**, 163–181

Mollamahmutoğlu, M., & Avci, E. (2014). Ultrafine portland cement grouting performance with or without additives. KSCE Journal of Civil Engineering, 19(7), 2041-2050. doi:10.1007/s12205-014-1445-7

Mualem, Y. (1976). "A new model for predicting the hydraulic conductivity of unsaturated porous media." Water Resour. Res. **12**: 513-522.

Mulilis, J. P., Seed, H. B., Chan, C. K., Mitchell, J. K., and Arulanandan, K. (1977), "Effect of Sample Preparation on Sand Liquefaction," Journal of Geotechnical Engineering, ASCE, Vol.103, No. GT2, pp. 91-108.

Naudts, W., Landry, E., Hooey, S., & Naudts, A (2003). Additives and Admixtures in Cement-Based Grouts. (pp. 1180-1191) doi:10.1061/40663 66

Nikiforov AI, Nikan'shin DP. Simulation of transfer of solid particles by a filtration flow. Journal of Engineering Physics and Thermophysics 1998; 71(6):933–938.

Oda, M. (1972), "Initial Fabrics and Their Relations to Mechanical Properties of Granular Material," Soils and Foundations, Vol. 12, No. 1, pp. 17-36.

Oda, M. (1976), "Fabrics and Their Effects on the Deformation Behavior of Sand," Special Issue, Department of Foundation Engineering, Faculty of Engineering, Saitama University, Japan.

Palmström, A.(1994), "The challenge of subsea tunneling Tunneling and Underground Space Technology", 9 (2) (1994), pp. 145–150

Pang, S., and Sharma, M.M. (1994), "A model for predicting injectivity decline in water injection wells," In: 69th Annual Technical Conference and Exhibition. New Orleans. Society of Petroleum Engineers. SPE 28489

Payatakes AC, Tien C, Turian RM. (1973),"A new model for granular porous media: Part I. Model formulation," AIChE Journal 1973; 19(1):58–67.

Payatakes, A.S., Rajagopalan, R., and Tien, C.(1974), "Application of porous medium models to the study of deep bed fitration." Can. J. Chem. Eng. **52**, December 1974

Peyton, R.L., Haeffner, B.A., Anderson, S.H. and Gantzer, C.J. (1992), "Applying X-ray CT to measure macropore diameters in undisturbed soil cores" In A.R. Mermut and L.D. Norton (Editors), Digitization, Processing and Quantitative Interpretation of Image Analysis in Soil Science and Related Areas. Geoderma, 53: 329-340.

Reddi, L.N., Ming, X., Hajra, M. G., and Lee, I.M. (2000), "Permeability reduction of soil filter due to physical clogging," Journal of Geotechnical and Geoenvironmental Engineering, 236, March 2000.

Rege SD, Fogler HS.(1988), "A network model for deep bed filtration of solid particles and emulsion drops," AIChE Journal 1988; 34(11):1761–1772.

Roque, C., Chauveteau, G.A., Thibault, G., Bouteca, M. (1995), "Mechanisms of formation damage by retention of particles suspended in injection water" In: SPE paper 30110

Rosquoët, F., Alexis, A., Khelidj, A., & Phelipot, A. (2003). Experimental study of cement grout. Cement and Concrete Research, 33(5), 713-722. doi:10.1016/S0008-8846(02)01036-0

Rostami Barani HR, Lashkaripour GL, Ghafoori M (2014), "Predictive permeability model of faults in crystalline rocks; verification by Joint Hydraulic factor (JH) obtained from water pressure tests," J Earth Syst Sci 123(6):1325–1334

Rugg, D.A., Yoon, J.S., Hwang, H. and El Mohtar, C. S. (2011), "Undrained Shearing Properties of Sand Permeated with a Bentonite Suspension for Static Liquefaction Mitigation," ASCE Geotechnical Special Publications GSP-211, Geofrontiers: Advances in Geotechnical Engineering, p.p. 677-686, Dallas, TX, March 13-16, 2011.

Scheffler, G. A., and Plagge, R. (2011). "Application of instantaneous profile measurement of moisture content and moisture potential in porous materials." Materials and Structures **44**: 1517-1536.

Schwarz LG (1997), " Roles of rheology and chemical filtration on injectability of microfine cement grouts," Ph.D. Thesis, Northwestern University, U.S.A., 1997.

Sharma, M.M., Pang S., Wennberg, K.E., and Morgenthaler, L.N. (2000), "Injection decline in Water-Injection Wells: An Offshore Gulf of Mexico Case sudy," SPE Prod. & Facilities 15 (1), February

Sharma,M.M., and Yortsos, Y.C.(1987), "A network model for deep bed filtration processes," AIChE J. **33**(10), 1644–1652. doi:10.1002/aic.690331008

Šimůnek, J., van Genuchten M. Th. and Šejna, M. (2012). "HYDRUS: Model Use, Calibration, and Validation." American Society of Agricultural and Biological Engineers **55(4)**: 1261-1274.

Smart, E., Leng, X., and Bai, X. (1992), "Image Analysis of Soil Microstructure," Proceedings, International Conference on Geotechnics and Computer, Paris, France, pp. 905-912.

Soueid Ahmed, A., Jardani, A., Revil, A., and Dupont, J.P. (2014). "Hydraulic conductivity field characterization from the joint inversion of hydraulic heads and self-potential data." Water Resour. Res. **50**: 3502-3522.

Stein, P. C. (1940), ''A study of the theory of rapid filtration of water through sand,'' DSc dissertation, Massachusettes Institute of Technology, Cambridge, Mass.

Straface, S., T.-J. Yeh, J. Zhu, S. Troisi, and C. H. Lee (2007). "Sequential aquifer tests at a well field, Montalto Uffugo Scalo, Italy." Water Resour. Res. **43**: W07432.

Tan, O., Zaimoglu, A. S., Hinislioglu, S., & Altun, S. (2005). Taguchi approach for optimization of the bleeding on cement-based grouts. Tunnelling and Underground Space Technology Incorporating Trenchless Technology Research,20(2), 167-173. doi:10.1016/j.tust.2004.08.004

Tarafdar S, Dey A, Gupta BS. A multiple state stochastic model for deep-bed filtration. Chemical Engineering and Technology 1992; 15(1):44–50.

Tobiason, J. E., and O'Melia, C. R. (1988), ''Physicochemical aspects of particle removal in depth filtration.'' J. Am. Water Works Assn., 80(12), 54–64.

Todd, A.C., Brown, J., Noorkami, M and Tweedie, J.A., (1979), “Review of permeability damage studies and related North Sea water injection.' SPE 7883.

van Dam J.C., S., J. N. M., and Droogers, P. (1994). "Inverse Method to determine soil hydraulic functions from Multistep Outflow experiments." Soil Sci. Soc. Am. J. **58**: 647-652.

van Genuchten, M. T. (1980). "A closed form equation for predicting the Hydrauclic conductivity of unsaturated soils." Soil Sci. Soc. Am. J. **44(5)**(September-October).

van Oort, E., van Velzen, J.F.G., and Leerlooijer, K. (1993), ‘‘Impairment by Suspended Solids Invasion Testing and Prediction,’’ SPEPF, August, 178; Trans., AIME, **295**.

Veerapen, J.P., Nicot, B., and Chauveteau, G.A.(2001), “In-depth permeability damage by particle deposition at high flow rates,” In: SPE paper 68962

Vetter, O.J., Kandarpa, V., Stratton, M., Veith, E. (1987), “Particle invasion into porous medium and related injectivity problems,” In: SPE International Symposium on Oilfield Chemistry, Paper SPE 16255, pp. 101–120. Society of Petroleum Engineers, San Antonio, TX

Wennberg, K.I., and Sharma, M.M. (1997), “Determination of the filtration coefficient and the transition time for water injection wells,” In: Society of Petroleum Engineers. SPE 38181

White, J., Zardava, K., Nayagum D., and Powrie W. (2015). "Functional relationships for the estimation of van Genuchten parameter values in landfill processes models." Waste Management **38**: 222-231.

Yeh, T.-C. J., M. Jin, and S. Hanna (1996). "An iterative stochastic inverse approach: Conditional effective transmissivity and head fields." Water Resour. Res. **32(1)**: 85-92.

Yeh, W. W.-G. (1986). "Review of parameter identification procedures in groundwater hydrology: The inverse problem." Water Resour. Res. **22**: 95-108.

Yoon, J. and El Mohtar, C. S. (2013), “Groutability of granular soils using sodium pyrophosphate modified bentonite suspensions,” Tunneling and Underground Space Technology, Vol. 37 p.p. 135–145, 2013

Zachmann, D. W., P. C. DuChateau, and A. Klute (1982). "Simultaneous approximation of water capacity and soil hydraulic conductivity by parameter identification." Soil Sci. **134**: 157-163.

Zebovitz S, Krizek RJ, Atmatzidis DK. Injection of fine sands with very fine cement grout. Journal of Geotechnical Engineering 1989; 115(12):1717–1733

Zhang, J., and T.-C. J. Yeh (1997). "An iterative geostatistical inverse method for steady flow in the vadose zone." Water Resour. Res. **33(1)**: 63-71.

Zurmühl, T. (1996). "Evaluation of different boundary conditions for independent determination of hydraulic parameters using outflow methods." In: DuChateau P. and J. Gottlieb (eds), Parameter Identification and Inverse Problems in Hydrology, Geology and Ecology. Water Science and Technology Libary **23**: 165-184.